

Mott Transition and
Quantum Critical Metamagnetism
on
Compressible Lattices

Inaugural-Dissertation

zur

Erlangung des Doktorgrades

der Mathematisch-Naturwissenschaftlichen Fakultät

der Universität zu Köln

vorgelegt von

Mario Zacharias

aus Bochum



2013

Berichterstatter: Priv.-Doz. Dr. Markus Garst
Prof. Dr. Achim Rosch

Tag der mündlichen Prüfung: 02.07.2013

Abstract

Solid state phase transitions, which are amenable to pressure, generically, have an intrinsic coupling of the order parameter to the elastic degrees of freedom. The applied pressure primarily affects the lattice by varying the lattice spacing which, in turn, modifies the coupling constants of the critical degrees of freedom. Therefore, a coupling of the strain to the order parameter can strongly affect the phase transition. In this Thesis we investigate this influence on the finite temperature critical point of the Mott metal-insulator transition and the zero temperature quantum critical metamagnetic endpoint.

The universality class of the Mott endpoint is a topic which is still under debate. In this Thesis, we show that the nature of the Mott transition is drastically changed when interacting with a compressible lattice. The expected Ising criticality of the electronic system is preempted by an isostructural instability. Due to long ranged shear forces, in the vicinity of the critical endpoint an elastic Landau regime emerges, where the system shows mean-field behavior. The smoking gun criterion to detect the elastic Landau regime is the breakdown of Hooke's law, i.e., a non-linear stress-strain relation. Furthermore, the specific heat coefficient exhibits a finite mean field jump at the transition. For the family of organic salts κ -(BEDT-TTF)₂X, we determine the extent of the elastic Landau regime as $\Delta T^* \approx 2.5$ K and $\Delta p^* \approx 50$ bar based on thermal expansion experiments [1, 2].

In the second part, we investigate the quantum critical endpoint of itinerant metamagnets. Recently, it was suggested that quantum critical metamagnetism is a generic feature in itinerant ferromagnets [3] such as UCoAl [4] and UGe₂ [5, 6]. Within the framework of spin fluctuation theory, we determine the free energy and its temperature dependence, obtained by fluctuation renormalizations, and deduce the critical thermodynamics. Importantly, the compressibility shows the same behavior as the susceptibility which, by definition, diverges at a metamagnetic transition. Therefore, the metamagnetic quantum critical endpoint is intrinsically unstable towards an isostructural transition.

This isostructural transition preempts the metamagnetic quantum critical endpoint and the elastic degrees of freedom crucially alter the critical thermodynamics. Most importantly, at the critical field we obtain for lowest but finite temperatures a

regime of critical elasticity which is characterized by unusual power laws of the thermodynamic quantities. Whereas the thermal expansion has a much stronger temperature divergence for fields close to the critical field, the specific heat divergence is cut off upon entering this regime. As a consequence, the Grüneisen parameter diverges with an unusual high power of temperature.

Kurzzusammenfassung

Druckabhängige Phasenübergänge in Festkörpern sind stets an die elastischen Freiheitsgrade des Gitters gekoppelt. Der angelegte Druck wirkt auf das Gitter, indem der Gitterabstand verändert wird, was wiederum die Wechselwirkung der kritischen Freiheitsgrade beeinflusst. Daher kann eine Kopplung zwischen Gitterspannung und Ordnungsparameter den Phasenübergang stark beeinflussen. In dieser Arbeit betrachten wir die Auswirkung einer solchen Kopplung auf den Mott Metall-Isolator Übergang, der bei endlichen Temperaturen stattfindet, sowie den quantenkritischen metamagnetischen Endpunkt bei $T = 0$.

Die Frage nach der Universalitätsklasse des kritischen Endpunktes des Mott-Übergangs ist noch immer nicht abschließend geklärt. In dieser Arbeit zeigen wir, dass der Charakter des Mott-Übergangs sich drastisch ändert, wenn man Wechselwirkungen mit einem kompressiblen Gitter in Betracht zieht. Dem erwarteten Ising-kritischen Verhalten des elektronischen Systems kommt ein isostruktureller Phasenübergang zuvor. Auf Grund von langreichweitigen Scherkräften im Kristall bildet sich in der unmittelbaren Nähe des kritischen Punktes ein elastisches Landau-Regime, in dem das System Mean-Field Verhalten zeigt. Dieses elastische Landau-Regime kann eindeutig durch die Verletzung des Hooke'schen Gesetzes identifiziert werden, das einen linearen Zusammenhang zwischen der mechanischen Spannung und der resultierenden Ausdehnung voraussagt. Des Weiteren springt die spezifische Wärme Mean-Field-artig am Übergang. Basierend auf Messungen der thermischen Ausdehnung [1, 2], können wir für die Familie organischer Salze κ -(BEDT-TTF)₂X die Ausmaße des elastischen Landau-Regimes abschätzen und erhalten $\Delta T^* \approx 2.5$ K und $\Delta p^* \approx 50$ bar.

Im zweiten Teil der Arbeit untersuchen wir den quantenkritischen Endpunkt von itineranten Metamagneten. Kürzlich wurde darauf hingewiesen [3], dass dieser ganz allgemein in itineranten Ferromagneten wie UCoAl [4] und UGe₂ [5, 6] auftritt. Im Rahmen der Spin-Fluktuationstheorie bestimmen wir die Temperaturabhängigkeit der freien Energie und folgern die kritischen thermodynamischen Eigenschaften. Bemerkenswerterweise ist die Kompressibilität proportional zur Suszeptibilität, welche am metamagnetischen Übergang divergiert. Daher der metamagnetische quantenkritische Endpunkt intrinsisch instabil gegenüber einem isostrukturellen Übergang.

Dieser isostrukturelle Phasenübergang kommt dem metamagnetischen quantenkritischen Endpunkt zuvor und die elastischen Freiheitsgrade verändern entscheidend die Thermodynamik. Insbesondere finden wir am kritische Magnetfeld bei tiefsten aber endlichen Temperaturen einen Regime der kritischen Elastizität das durch ungewöhnliche Potenzgesetze der kritischen thermodynamischen Größen charakterisiert ist. Während die thermische Ausdehnung nahe des quantenkritischen Endpunktes stärker als üblich mit fallender Temperatur divergiert, wird die Divergenz der spezifischen Wärme abgeschnitten. Daraus resultiert eine erstaunlich hohe Divergenz des Grüneisenparameters als Funktion der Temperatur.

Contents

1	Introduction	1
2	Elasticity	3
2.1	Continuous Elasticity Theory	4
2.1.1	Displacement and the Strain Tensor	4
2.1.2	The Stress Tensor	5
2.1.3	The Free Energy	7
2.1.4	The Elastic Modulus Tensor	8
2.2	Crystal Elasticity	10
2.2.1	Crystal Structure	11
2.2.2	Effective Potential of Displacements	12
2.2.3	Phonons	14
2.2.4	Continuum Limit	15
2.3	Phonon Field Integral	21
3	Elasticity in Critical Systems	25
3.1	Landau Theory and Elasticity	26
3.1.1	Symmetry and Strain	26
3.1.2	Coupling to the Order Parameter	28
3.2	Ising Theory	29
3.2.1	Quadratic Coupling	29
3.2.2	Microscopics of the Quadratic Coupling	31
3.2.3	Bilinear Coupling	37
3.3	Classification by Cowley	39
4	Mott-Transition on Compressible Lattices	43
4.1	Mott Metal-Insulator Transition	44
4.1.1	Basic Concepts	45
4.1.2	Universality Class	48
4.1.3	The Ising Field Theory	50
4.2	Coupling to the Lattice	53

4.3	Free Energy	54
4.3.1	Perturbative Solution	55
4.3.2	Non-Perturbative Solution	57
4.3.3	Behavior Around the Former Endpoint	59
4.4	Thermodynamics	60
4.4.1	Specific Heat Coefficient	61
4.4.2	Thermal expansion	63
4.4.3	Compressibility	64
4.5	Experimental Relevance	65
4.5.1	The κ -(BEDT-TTF) ₂ X Family	66
4.5.2	Vanadium Sesquioxide V ₂ O ₃	72
4.6	Summary and Discussion	73
5	Quantum Critical Metamagnets	77
5.1	Metamagnetism	78
5.1.1	Mean-Field Theory	78
5.1.2	Experiments	80
5.2	Spin-Fluctuation Theory	82
5.2.1	Wegner-Houghton Equation	84
5.2.2	Effective Metamagnetic Potential	85
5.3	Free Energy	87
5.3.1	Linear Regime	87
5.3.2	Non-Linear Regime	90
5.3.3	Free Energy Density	91
5.4	Thermodynamics	93
5.4.1	Susceptibility, Magnetostriction and Compressibility	94
5.4.2	Thermal Expansion, Temperature Derivative of the Magnetization	96
5.4.3	Specific Heat Coefficient	98
5.4.4	Grüneisen Parameters	100
5.5	Summary	101
6	Compressible Quantum Critical Metamagnetism	103
6.1	Elastic Coupling	104
6.2	Phonons	105
6.2.1	Neutron Scattering Intensity	106
6.2.2	Parameter Renormalization Due To Phonons	108
6.3	Free Energy	111
6.3.1	First Order Transition	112
6.3.2	Quantum Endpoint	117

6.4	Thermodynamics	119
6.4.1	Susceptibility, Compressibility and Magnetostriction	119
6.4.2	Thermal Expansion, Temperature Derivative of the Magnetization	122
6.4.3	Specific Heat Coefficient	124
6.4.4	Grüneisen Parameters	126
6.5	Estimate for $\text{Sr}_3\text{Ru}_2\text{O}_7$	126
6.6	Summary	128
7	Summary	131
A	Symmetry Classes of the Elastic Constant Matrix	133
A.1	Triclinic System	133
A.2	Monoclinic System	134
A.3	Orthorhombic System	134
A.4	Trigonal System	135
A.5	Tetragonal System	136
A.6	Hexagonal System	136
A.7	Cubic System	137
B	Irreducible Representations of the Strain Tensor	139
C	Effective Action due to Phonons	141
	Bibliography	151
	Acknowledgments	158
	Erklärung	161
	Teilpublikationen	161
	Lebenslauf	162

Chapter 1

Introduction

Phase transitions, where a system drastically changes its properties, are one of the most interesting phenomena in nature. Melting and solidification, magnetic or metal-insulator transitions are not only of interest for physicists in their ambition to understand and explain nature and its phenomena, but also yield amazing innovations in technical respects.

In recent years, physicists became interested in phase transitions happening at absolute zero temperature, where the ground state of a system changes as function of a non-thermal parameter. As thermal fluctuations are completely frozen out, such a quantum phase transition is solely driven by quantum fluctuations. Although the transition itself is not observable due to the inaccessibility of zero temperatures, its existence is far from being a pure academic curiosity. Thermal fluctuations, acting on the peculiar ground state of the transition point, yield an unusual behavior of thermodynamic quantities up to relatively high temperatures.

In solid state theory, phase transitions of, for instance, electronic degrees of freedom do not take place in the vacuum but on top of an underlying lattice of atoms. In many cases, this lattice is considered to be completely rigid. However, this is, of course, only a simplification. Instead, the lattice can be deformed and, thus, has elastic degrees of freedom which are, generically, coupled to the critical degrees of freedom. The influence of elastic couplings on the nature of a phase transition is the subject of this thesis.

Although, the theory of elastic deformations is a long studied issue dating back to the 17th century, nowadays this topic is no longer part of the common curriculum of physics. Therefore, the first two chapters are devoted to an introduction to this subject and an overview of preceding work considering critical systems on compressible lattices.

In particular, Chap. 2 is intended to introduce the reader to the concepts and nomenclature of elasticity, where we distinguish between elasticity in continuous systems and in crystals. Classical, i.e., finite temperature phase transitions on com-

pressible lattices were the subject of intensive studies already in the 60's and 70's of the 20th century, which we discuss in Chap. 3.

After these introductory chapters, we consider a particular finite temperature phase transition, namely the Mott metal-insulator transition which is an electronic transition due to strong correlation effects. We will see in Chap. 4 how the coupling to the elastic degrees of freedom changes the nature of this phase transition. In particular, it may help to solve the long standing discussion about the universality class of the Mott transition. To be specific, we will consider two different materials, the organic transfer salt κ -(BEDT-TTF)₂X and chromium doped V₂O₃, both being subject of current investigations, and we connect our theoretical results to experimental findings. In particular, for κ -(BEDT-TTF)₂X we are able to estimate the temperature and pressure range on which the effects of the elastic coupling are observable, and find them to be well within experimental accessibility.

Having discussed the influence on classical finite temperature phase transitions, we turn to the topic of a quantum phase transition. In particular, we will focus on the special situation of a second-order critical endpoint which is driven to zero temperature by some non-thermal parameter. Metamagnetism, i.e., a sudden increase of the magnetization at some finite applied magnetic field, provides a way to such a quantum critical point without any symmetry breaking.

In Chap. 5, we will first discuss the quantum critical metamagnetism in absence of an elastic coupling. By means of functional renormalization group techniques, we obtain the fluctuation-induced temperature-dependence of the free energy and deduce the critical thermodynamics of the bare metamagnetic system. Due to a coupling to the lattice, the diverging susceptibility induces a crystal softening and yields an isostructural phase transition.

This elastic effects are considered in Chap. 6, where we investigate the influence of the phonons and the macroscopic strain on the quantum critical metamagnetism. We will show that, on the one hand, the intensity pattern of neutron scattering experiments, measuring the magnetic structure, is changed by the phonons. On the other hand, apart from a parameter renormalization their effect on the critical behavior is only due to sub-leading terms. This is because of the different energy scales of the ballistic phonons and the metamagnetic quasi-particles, i.e., the metamagnons, which are subject to Landau damping.

The macroscopic strain will, however, give rise to a qualitative change of the critical free energy. In particular, we find a regime with Fermi-liquid-like features at the critical field, h_c , below a finite temperature scale $T_{Fl} > 0$. This leads in the vicinity of the quantum critical point to strong deviations from the bare metamagnetic critical properties. The specific heat coefficient, for instance, which diverges upon approaching the quantum critical point, approaches a constant in presence of a magnetoelastic coupling.

Chapter 2

Elasticity

The theory of elastic deformations of solids is a subject dating back to the very beginning of the investigation of mechanical systems. Since elastic stability is a crucial aspect of any kind of construction work, people were very early interested in this field of mechanics.

The first publication concerning elastic systems was Robert Hooke's *De Potentia Restituiva* in 1678, nine years before Newton's *Principia*. In this work, Hooke found the law named after him stating that the force restoring equilibrium is proportional to the deviation from the equilibrium position. This law is the foundation of general elasticity theory. In the following, many famous physicists and mathematicians worked on this field, including Leibniz, Bernoulli, Euler and Cauchy.

The focus of these scientists was on homogeneous bodies, as those were used in constructions. With the appearance of the modern solid state theory at the end of the 19th century, people started to think also about crystal elasticity. Since in crystals translational invariance is broken down to a subset of discrete lattice vectors, a continuum description is not adequate to explain all effects. For instance, the existence of optical phonon branches is completely determined by the microscopic crystal structure.

In this chapter, we first give the basic notions of continuous elasticity theory in Sec. 2.1. Thereafter, in Sec. 2.2, we discuss the basics of crystal elasticity, i.e., the consequences and effects of the crystal structure. We will also make a connection to the continuous description and its limits of applicability.

Since we will investigate the elastic properties of systems close to a phase transition, we are especially interested in the fluctuation modes of elastic systems, i.e., the phonons. Therefore, these lattice waves are considered in some detail. In particular, we will give a brief deduction of the field theoretical description of the elastic degrees of freedom in Sec. 2.3.

For further details on elasticity the reader may be referred to Refs. [7–10] or Refs. [11, 12], approaching the subject in terms of ultrasonic measurements.

2.1 Continuous Elasticity Theory

In this section we will first consider homogeneous bodies, which can be described in a continuum theory. This is the limit in which elasticity theory was first investigated, as experiments were done on springs or wooden beams. In the following, the basic concepts are introduced, along the lines of Ref. [7].

2.1.1 Displacement and the Strain Tensor

Applying forces to a solid yields deformations of the structure, which means that a volume element centered at $\mathbf{r} = (x_1, x_2, x_3)$ in some arbitrary chosen coordinate system is shifted to the position \mathbf{r}' . The local displacement is the difference between initial and final position, $\mathbf{u} = \mathbf{r}' - \mathbf{r}$, and the distortions of all volume elements of the body define the vector field of displacement, which is given as

$$\mathbf{u}(\mathbf{r}) = \mathbf{r}'(\mathbf{r}) - \mathbf{r}. \quad (2.1)$$

Since the counteracting force restoring equilibrium depends on the mutual distance of the constituents, we have to consider the transformation of small length scales $dl^2 = (\mathbf{r}_1 - \mathbf{r}_2)^2$ upon deformations. With the abbreviation $d\mathbf{r} = \mathbf{r}_1 - \mathbf{r}_2$, the distorted distance is given by $dl'^2 = (d\mathbf{r} + \mathbf{u}(\mathbf{r}_1) - \mathbf{u}(\mathbf{r}_2))^2$. Assuming that the displacement field is smooth, we may linearize

$$\mathbf{u}(\mathbf{r}_1) - \mathbf{u}(\mathbf{r}_2) \approx \frac{\partial \mathbf{u}(\mathbf{r}_1)}{\partial x_i} (\mathbf{r}_1 - \mathbf{r}_2)_i. \quad (2.2)$$

Here and in the following we applied the Einstein summation convention where over every index is summed which appears more than once in a term. In the linearized approximation, the deformed distance reads as

$$\begin{aligned} dl'^2 &= dx_i dx_i + 2 \frac{\partial u_i(\mathbf{r}_1)}{\partial x_k} dx_i dx_k + \frac{\partial u_i(\mathbf{r}_1)}{\partial x_k} \frac{\partial u_i(\mathbf{r}_1)}{\partial x_l} dx_l dx_k \\ &= dx_i dx_i + \left(\frac{\partial u_i(\mathbf{r}_1)}{\partial x_k} + \frac{\partial u_k(\mathbf{r}_1)}{\partial x_i} + \frac{1}{2} \frac{\partial u_l(\mathbf{r}_1)}{\partial x_i} \frac{\partial u_l(\mathbf{r}_1)}{\partial x_k} \right) dx_i dx_k, \end{aligned} \quad (2.3)$$

where we relabeled the summation indices in the second line. The last line may for notational convenience be written as $dl'^2 = dl^2 + 2u_{ik}(\mathbf{r}_1) dx_i dx_k$. The tensor u_{ik} is called the strain tensor and follows from Eq. (2.3) as

$$u_{ik} = \frac{1}{2} \left(\frac{\partial u_i}{\partial x_k} + \frac{\partial u_k}{\partial x_i} + \frac{\partial u_l}{\partial x_i} \frac{\partial u_l}{\partial x_k} \right). \quad (2.4)$$

Apparently, the strain tensor is symmetric, $u_{ik} = u_{ki}$, which implies that it can be diagonalized at any given point. Such a diagonalization defines a local orthonormal system, given by the principal axes of $u_{ik}(\mathbf{r})$.

Transforming to this local coordinate system, $\mathbf{r} \rightarrow \tilde{\mathbf{r}}$, the distance is given as

$$dl'^2 = (1 + 2\tilde{u}_{ii})d\tilde{x}_i^2. \quad (2.5)$$

Thus, at any point, we can decompose the strain tensor such that the change of a length element is given as a dilation or compression along three mutually perpendicular directions. The length change along a principal axis is $d\tilde{x}'_i = \sqrt{1 + \tilde{u}_{ii}}d\tilde{x}_i$. Importantly, one has to keep in mind, that the diagonalization of the strain tensor can only be done locally, i.e., the principal axes at one point, \mathbf{r}_1 , are in generally different from the ones at another point, \mathbf{r}_2 .

In rigid bodies the change in distances due to the deformation is, in general, small compared to the distance in the undeformed body, $|dx'_i - dx_i|/dx_i \ll 1$. Since the strain tensor describes the relative changes in lengths, all its components are small quantities, $u_{ij} \ll 1$. Additionally, we assume the displacement vector, $\mathbf{u}(\mathbf{r})$, to be also a small quantity. As we will see later, due to long range shear forces this is not a strong restriction, as small strains do imply small displacements. Exceptions are, of course, first order structural transitions of a crystal.

Given that the displacement is small, we can neglect the last term in Eq. (2.4) and the strain tensor for small deformations is given by

$$u_{ik} = \frac{1}{2} \left(\frac{\partial u_i}{\partial x_k} + \frac{\partial u_k}{\partial x_i} \right). \quad (2.6)$$

The change in distances implies, of course, also a change of the infinitesimal volume element, dV' . In the local coordinate system defined by the principal axes, it reads as $dV' = \prod_{i=1}^d d\tilde{x}'_i \approx dV (1 + \tilde{u}_{ii})$, where we neglected higher order terms of the strain. As the trace is invariant under orthogonal transformations, we may write

$$\frac{dV' - dV}{dV} = u_{ii}(\mathbf{r}), \quad (2.7)$$

i.e., the relative change of the volume element centered at \mathbf{r} is given by the trace of the strain tensor.

2.1.2 The Stress Tensor

In absence of any external force, the constituents of the body under consideration are fixed to a position determined by the thermal equilibrium condition. Deforming it by applying a force, drives the constituents out of their equilibrium position and an internal counteracting force builds up which is called the internal stress. We will in the following assume that the molecular forces are very short ranged which is valid in many cases. It does not apply to ionic crystals where deformations lead to

the formation of macroscopic electric fields as, for instance, in piezoelectric crystals. However, we will not consider this case.

The total force on an arbitrary volume of the deformed body, V' , can be calculated by integrating over all forces, \mathbf{F} , per unit volume: $\mathbf{F}_{\text{tot}} = \int \mathbf{F} dV'$. Considering the smallness of the deformations, we may substitute the deformed coordinate system by the original one, as the difference is of sub-leading order.

Since all internal forces of this volume have to add up to zero, the total force on the volume is determined by the forces applied to the surface of the volume, and, thus, we can rewrite the volume integral as a surface integral. For every component of the force, Gauss's theorem implies then the existence of a rank 2 tensor determining the force components by

$$F_i = \frac{\partial \sigma_{ik}}{\partial x_k}. \quad (2.8)$$

This tensor, σ , is called the stress tensor with which one can rewrite the volume integral as a surface integral

$$\int_V F_i dV = \int_V \frac{\partial \sigma_{ik}}{\partial x_k} dV = \int_{\partial V} \sigma_{ik} df_k, \quad (2.9)$$

where df denotes the surface vector pointing outwards of the volume.

The components of the stress tensor, σ_{ik} , give the total force component F_i on the surface perpendicular to the x_k -axes. Thus, for instance, the normal force on the xy -plane is given by σ_{zz} , whereas σ_{zx} and σ_{zy} , account for tangential forces on this plane. These off-diagonal components are called shear stress and move surfaces relative to each other. The surface integral in Eq. (2.9) describes the force exerted on the volume under consideration and due to Newton the same force with an opposite sign is exerted by the volume element on the surrounding.

Of particular interest is hydrostatic pressure, i.e., uniform compression from all sides, as it is easy to apply it in pressure cells. In this case, the pressure p yields a force on every surface element, df_i , given by $F_i = -p df_i$, pointing inside the volumes. Comparison with Eq. (2.9), yields $\sigma_{ik} = -p \delta_{ki}$, thus, no shear forces arise.

Let us consider, the moments, $M_{ik} = \int F_i x_k - F_k x_i dV$, of the applied force. Substituting Eq. (2.8) and partial integration yields

$$M_{ik} = \int_{\partial V} (\sigma_{il} x_k - \sigma_{kl} x_i) df_l - \int_V (\sigma_{ik} - \sigma_{ki}) dV. \quad (2.10)$$

Due to the equilibrium condition the moments have to be a surface integral only, thus, the second term has to vanish. This gives rise to the important symmetry relation

$$\sigma_{ik} = \sigma_{ki}. \quad (2.11)$$

In equilibrium, all external forces are balanced by the internal stress. In particular, if external forces are absent, we have $F_i = 0$, i.e.,

$$\partial\sigma_{ik}/\partial x_k = 0. \quad (2.12)$$

which is the equilibrium condition.

2.1.3 The Free Energy

In the following, we will consider only elastic deformations, i.e., deformations which disappear if the acting forces are removed. Additionally, we will assume that the deformation is adiabatic such that the deformed body is in equilibrium at any time and the processes are thermodynamically reversible.

The change in the internal energy, \mathcal{E} , relative to a unit volume due to an infinitesimal deformation is given by the acquired heat, TdS and the work, dW , due to the internal stresses

$$d\mathcal{E} = TdS - dW. \quad (2.13)$$

Considering a small displacement, δu , of an already deformed body, the work is given by the volume integral of the force multiplied by the displacement

$$W = \int_V F_i \delta u_i dV. \quad (2.14)$$

Replacing the force by the definition of the strain tensor, Eq. (2.9), and integrating by parts, we obtain

$$W = \int_{\partial V} \sigma_{ik} \delta u_i df_k - \int_V \sigma_{ik} \frac{\partial \delta u_i}{\partial x_k} dV. \quad (2.15)$$

If we consider the thermodynamic limit, $V \rightarrow \infty$, we may assume that the body is not deformed at the surface. Then, the stress vanishes at the surface, i.e., $\sigma_{ik} = 0$ in the first integral. Thus, we are only left with the second term which due to the symmetry of the stress tensor can be rewritten as

$$W = - \int_V \sigma_{ik} \frac{1}{2} \left(\frac{\partial \delta u_i}{\partial x_k} + \frac{\partial \delta u_k}{\partial x_i} \right) dV = - \int_V \sigma_{ik} \delta u_{ik} dV, \quad (2.16)$$

Therefore, the work per unit volume can be read off as

$$dW = -\sigma_{ik} du_{ik}. \quad (2.17)$$

In particular, for hydrostatic pressure, $\sigma_{ik} = -p \delta_{ik}$, the work per unit volume is given by $dW = p du_{ii}$. As mentioned above, the trace of the strain tensor determines

the relative volume change, Eq. (2.7). Therefore, as we consider the unit volume, we obtain the familiar form $dW = p dV$.

The independent variables of the energy density, \mathcal{E} , are the strains, u_{ik} , and the entropy S . The stress is determined by differentiation with respect to the strains

$$\sigma_{ik} = \partial\mathcal{E}/\partial u_{ik}. \quad (2.18)$$

Since it is more convenient to take the temperature rather than the entropy as an independent variable, we switch to a grand canonical ensemble. The thermodynamic potential, the free energy, \mathcal{F} , is defined as $\mathcal{F} = \mathcal{E} - TS$, thus, an infinitesimal deformation changes the free energy as

$$d\mathcal{F} = -S dT + \sigma_{ik} du_{ik}. \quad (2.19)$$

The stress is still determined analogous to Eq. (2.18), i.e., by a derivative with respect to the strain tensor.

2.1.4 The Elastic Modulus Tensor

As the deformations are small, we may expand the free energy in the strain. In absence of external forces the body is undeformed, $u_{ik} = 0$, and due to the equilibrium condition the stress vanishes also, $\sigma_{ik} = 0$. From Eq. (2.18) follows that the free energy has no term linear in the strain. Therefore, the free energy density reads to lowest order as

$$\mathcal{F} = \mathcal{F}_0 + \frac{1}{2} C_{ijkl} u_{ij} u_{kl}. \quad (2.20)$$

The temperature dependent constant \mathcal{F}_0 will be neglected in the following.

To obtain a scalar quantity from two strain tensors, we had to introduce the rank 4 tensor C_{ijkl} , which is called the elastic modulus tensor. It has 81 components which, however, are not completely independent of each other due to the symmetries of the theory. Since the free energy has to be invariant under the exchange of the index pairs (ij) and (kl) , the same has to be true for the elastic modulus tensor. Furthermore, the strain tensor is symmetric with respect to exchange of its indices, i.e., $(i \leftrightarrow j)$ and $(k \leftrightarrow l)$, thus, the elastic modulus tensor has to have the same symmetry. Taken together, we have the general symmetry properties

$$C_{ijkl} = C_{jikl} = C_{ijlk} = C_{klij}, \quad (2.21)$$

and we are left with a total number of 21 independent components.

As the elastic stress tensor is the thermodynamically conjugated quantity to the strain tensor, see Eq. (2.18), it follows immediately that it is determined by

$$\sigma_{ij} = C_{ijkl} u_{kl}. \quad (2.22)$$

This linear stress-strain relation is the generalization of Hooke's law that the force restoring equilibrium is proportional to the deviation from the equilibrium position. Inversion of this relation, $u_{ij} = D_{ijkl} \sigma_{kl}$, defines the compliance tensor D_{ijkl} . From Eq. (2.18) we also deduce that if we consider external stress applied to the body, we have to add a source term to the free energy yielding

$$\mathcal{F} = \frac{1}{2} C_{ijkl} u_{ij} u_{kl} + u_{ij} \sigma_{ij}. \quad (2.23)$$

Due to the symmetries, it is not necessary to keep track of all indices, but only of combinations. Therefore, the Voigt notation (see Ref. [13]) is often used, which contracts the indices of the stress tensor, $\sigma_{ij} \rightarrow \sigma_{\rho}^V$ and the strain tensor, $u_{ij} \rightarrow u_{\rho}^V$, as well as the corresponding index pairs of the elastic constant matrix, $C_{ijkl} \rightarrow C_{\rho\lambda}^V$. The canonical identification is determined by the rule

$$\rho = \begin{cases} i & \text{for } i = j \\ 9 - i - j & \text{for } i \neq j \end{cases}. \quad (2.24)$$

Thus, the elastic modulus tensor is arranged in a six-by-six matrix which reads as

$$C^V = \left(\begin{array}{ccc|ccc} C_{1111} & C_{1122} & C_{1133} & C_{1123} & C_{1113} & C_{1112} \\ C_{1122} & C_{2222} & C_{2233} & C_{2223} & C_{2213} & C_{2212} \\ C_{1133} & C_{2233} & C_{3333} & C_{3323} & C_{3313} & C_{3312} \\ \hline C_{1123} & C_{2223} & C_{3323} & C_{2323} & C_{2313} & C_{2312} \\ C_{1113} & C_{2213} & C_{3313} & C_{2313} & C_{1313} & C_{1312} \\ C_{1112} & C_{2212} & C_{3312} & C_{2312} & C_{1312} & C_{1212} \end{array} \right). \quad (2.25)$$

Similarly, the stress tensor in Voigt notation is a six dimensional vector reading as $\sigma^V = (\sigma_{11}, \sigma_{22}, \sigma_{33}, \sigma_{23}, \sigma_{13}, \sigma_{12})^T$. Concerning the strain tensor, one has to be careful to preserve the correct tensor products. This is done by multiplying the off-diagonal components by a factor of two, yielding the strain in Voigt notation as $u^V = (u_{11}, u_{22}, u_{33}, 2u_{23}, 2u_{13}, 2u_{12})^T$. Note, that other conventions may distribute this factor in different ways.

It is important to keep in mind that this mapping is only a notational simplification and still the tensors transform under a coordinate change according to their natural rank. The strain tensor transforms like a matrix rather than a vector and the elastic constant matrix remains a tensor of rank 4. For a detailed discussion of the mapping to the compact representation, the reader may be referred to Ref. [14]. In the following, we will skip the superscript V to indicate the Voigt notation. Instead, Arabic indices take values $i \in \{1, 2, 3\}$ and Greek indices run from 1 to 6.

In absence of external strains the free energy, Eq. (2.23), reads as

$$\mathcal{F} = \frac{1}{2} C_{\rho\lambda} u_\rho u_\lambda, \quad (2.26)$$

and it is, thus, a quadratic form in a six-dimensional vector space. For the system to be stable under elastic fluctuations, the matrix $C_{\rho\lambda}$ has to be positive definite. As known from linear algebra, this is true if and only if all principal minors, are positive, i.e.,

$$C_{11} > 0, \quad \begin{vmatrix} C_{11} & C_{12} \\ C_{12} & C_{22} \end{vmatrix} > 0, \quad \dots, \quad \det C > 0, \quad (2.27)$$

which are the conditions of stability.

Isotropic bodies are of particular simplicity. The free energy is then given by the only two quadratic invariants the strain tensor can form, namely its squared trace and the trace of its square

$$\mathcal{F} = \frac{1}{2} \lambda u_{ii}^2 + \mu u_{ij} u_{ji}. \quad (2.28)$$

The constants $\lambda = C_{12}$ and $\mu = C_{44}$ are called the Lamè coefficients.

In Eq. (2.7), we have seen that the trace of the strain tensor yields the volume change. We therefore may separate the trace of the strain tensor

$$u_{ij} = u_{kk} + \bar{u}_{ij} = u_{kk} + \left(u_{ij} - \frac{1}{3} \delta_{ij} u_{kk} \right) \quad (2.29)$$

which yields the free energy

$$\mathcal{F} = \frac{1}{2} K u_{ii}^2 + \mu \bar{u}_{ij}^2, \quad (2.30)$$

The first term describes the free energy due to a pure hydrostatic compression, i.e., a volume change where the shape of the body is preserved. Therefore the constant $K = \lambda + \frac{2}{3}\mu$ is called the bulk modulus. The second term on the other hand, only accounts for deformations which alter the shape of the body and preserves the volume. This is called a pure shear strain, and μ is, correspondingly, called the shear modulus. Stability under elastic fluctuations requires both constants to be positive.

2.2 Crystal Elasticity

The previous considerations were valid for elastic deformations of rigid bodies which can be described in a continuum theory. However, solid state theory mainly focuses on crystal systems where the constituents of the body, i.e., the atoms, are arranged on a periodic lattice. The distance between the atomic positions is usually much

larger than the typical deformations, thus, a continuous description is oversimplified. In particular, we have an invariance under a discrete set of translations and, depending on the crystal symmetry, may have also other discrete symmetries such as rotations by certain angles. These microscopic details of the solid will show their signatures also in macroscopic quantities, as they must have the same symmetries.

2.2.1 Crystal Structure

A perfect crystal is characterized by a Bravais lattice, which is a periodic structure build up from three lattice vectors, \mathbf{a}_i . Every site of the Bravais lattice can be reached from any other site by a vector

$$\mathbf{R}_n = n_i \mathbf{a}_i, \quad (2.31)$$

where $n = (n_1, n_2, n_3)$ is a three tuple of integer numbers.

On every lattice site a primitive lattice cell is centered, the so-called Wigner-Seitz cell, which is given by

$$V_W = \left\{ \mathbf{x} \in \mathbb{R}^3 \mid |\mathbf{x}| \leq |\mathbf{x} - \mathbf{R}_n| \forall n \neq (0, 0, 0) \right\}, \quad (2.32)$$

where the origin is placed at the Bravais lattice point. Therefore, the periodic array of primitive cells fills the whole space.

For simple lattices, every cell is occupied by one atom of the same sort positioned in the center of the cell. For more complex materials, a number of N atoms are arranged in the cell forming the basis of the crystal. The position of the m -th atom with respect to the cell center is given by some constant vector, \mathbf{x}_m , which has to be within the Wigner-Seitz cell. Therefore, adapting the notation of Ref. [15], the position of every atom of a crystal can be written as

$$\mathbf{r}_{[m]}^n = \mathbf{R}_n + \mathbf{x}_m \quad \text{with} \quad \mathbf{x}_m \in V_W. \quad (2.33)$$

From the basis vectors, \mathbf{a}_j , one obtains another set of vectors, \mathbf{b}_i , by the condition $\mathbf{b}_i \cdot \mathbf{a}_j = 2\pi \delta_{ij}$. These vectors are called the reciprocal vectors and have the form

$$\mathbf{b}_i = \frac{\pi \epsilon_{ijk}}{\det(\mathbf{a}_1, \mathbf{a}_2, \mathbf{a}_3)} (\mathbf{a}_j \times \mathbf{a}_k), \quad (2.34)$$

where ϵ_{ijk} denotes the Levi-Civita symbol. Similar to the lattice vectors, the reciprocal vectors span a lattice, where every point is connected to any other point by a vector

$$\mathbf{G}_h = h_i \mathbf{b}_i \quad \text{with} \quad h_i \in \mathbb{Z}. \quad (2.35)$$

This lattice is called the reciprocal Bravais lattice, and the corresponding Wigner-Seitz cell in reciprocal space is called the first Brillouin zone.

The translational invariance with respect to the lattice vectors \mathbf{R}_n , will be reflected in any physical quantity, $\psi(\mathbf{r}) = \psi(\mathbf{r} + \mathbf{R}_n)$. Thus, we may represent it in a Fourier series,

$$\psi(\mathbf{r}) = \frac{1}{|V_W|} \sum_{\mathbf{G}_h} \psi(\mathbf{G}_h) e^{i\mathbf{G}_h \cdot \mathbf{r}}, \quad (2.36)$$

where the summation runs over the reciprocal lattice vectors due to their very definition. On the other hand, if a function is only defined on the lattice points, $\psi(\mathbf{R}_n)$, assuming periodic boundary conditions we can write down the Fourier series as

$$\psi(\mathbf{R}_n) = \frac{1}{|V_W|} \sum_{\mathbf{q} \in 1.\text{BZ}} \psi(\mathbf{q}) e^{i\mathbf{q} \cdot \mathbf{R}_n}. \quad (2.37)$$

The summation runs only over the momenta within the first Brillouin zone since every other vector, \mathbf{q}' , may be written as $\mathbf{q}' = \mathbf{q} + \mathbf{G}_h$, where \mathbf{q} is again from the first Brillouin zone. Since by definition $\mathbf{G}_l \cdot \mathbf{R}_n = 2\pi m$ with an integer m , the exponential is one, and, thus, vectors from outside the first Brillouin zone give no further contribution.

2.2.2 Effective Potential of Displacements

Considering a deformation of a crystal, we can split the displacement of the atoms from their equilibrium position, $\mathbf{r}_{[m]}^{[n]}$, in a microscopic and a macroscopic part. The local displacement, $\mathbf{u}_{[m]}^{[n]}$, describes a microscopic position shift

$$\tilde{\mathbf{r}}_{[m]}^{[n]} = \mathbf{r}_{[m]}^{[n]} + \mathbf{u}_{[m]}^{[n]}. \quad (2.38)$$

For a finite crystal volume, V , we assume a vanishing displacement of the surface atoms. In the thermodynamic limit, $V \rightarrow \infty$, this boundary condition has no influence on any properties of the bulk.

Macroscopic distortions are described by a matrix E , such that the final position of an atom is determined by

$$\mathbf{r}'_{[m]}^{[n]} = (\mathbb{1} + E) (\mathbf{r}_{[m]}^{[n]} + \mathbf{u}_{[m]}^{[n]}). \quad (2.39)$$

Macroscopic rotations of the whole crystal are irrelevant for physical quantities. Since those are given by the antisymmetric part of the matrix, E , we may assume it to be symmetric. Note that we have a certain gauge freedom namely the choice of the origin, $\mathbf{r}_{[m]}^{[n]} = 0$.

We will consider only local displacements, $\mathbf{u}_{[m]}^{[n]}$, which are small with respect to the interatomic distance, and likewise, the components of the macroscopic distortion tensor, E_{ij} , are assumed to be small compared with unity. In this limit, we may linearize the total displacement to

$$\tilde{\mathbf{u}}_{[m]}^{[n]} = \mathbf{r}'_{[m]}^{[n]} - \mathbf{r}_{[m]}^{[n]} = E \cdot \mathbf{r}_{[m]}^{[n]} + \mathbf{u}_{[m]}^{[n]}. \quad (2.40)$$

The interaction between the atoms of the lattice is described by some potential, $V(\{\mathbf{r}'_{[m]}^{[n]}\})$, left unspecified for the moment. The Hamiltonian of such a system reads as

$$\mathcal{H} = \frac{1}{2M_m} \mathbf{p}'_{[m]}^{[n]\dagger} \cdot \mathbf{p}'_{[m]}^{[n]} + V(\{\mathbf{r}'_{[m]}^{[n]}\}), \quad (2.41)$$

with $\mathbf{p}'_{[m]}^{[n]}$ being the canonically conjugated momenta to $\mathbf{r}'_{[m]}^{[n]}$. We may expand the potential in the displacement of the atoms from their position in the undeformed lattice, $\mathbf{r}_{[m]}^{[n]}$. This yields in the harmonic approximation the effective potential

$$V_{\text{eff}}(\{\tilde{\mathbf{u}}_{[m]}^{[n]}\}) \approx V(\{\mathbf{r}_{[m]}^{[n]}\}) + \Psi_{[m]i}^{[n]} \tilde{u}_{[m]i}^{[n]} + \frac{1}{2} \Phi_{[m m']ij}^{[n n']} \tilde{u}_{[m]i}^{[n]} \tilde{u}_{[m']j}^{[n']} + \dots \quad (2.42)$$

$$\Psi_{[m]i}^{[n]} = \frac{\partial V(\{\mathbf{r}_{[m]}^{[n]}\})}{\partial r_{[m]i}^{[n]}}, \quad \Phi_{[m m']ij}^{[n n']} = \frac{\partial^2 V(\{\mathbf{r}_{[m]}^{[n]}\})}{\partial r_{[m]i}^{[n]} \partial r_{[m']j}^{[n']}}. \quad (2.43)$$

As the first term is an overall constant, we will neglect it in the following. Due to the system being in equilibrium the second term has to vanish and the matrix $\Phi_{[m m']ij}^{[n n']}$ has to be positive definite. Furthermore, $\tilde{\Phi}_{[m m']ij}^{[n n']}$ is symmetric with respect to the exchange $(n, m, i) \leftrightarrow (n', m', j)$.

A constant displacement, $\tilde{u}_{[m]i}^{[n]} = u_i$, corresponding to a global translation, will not yield a change in energy. Therefore, we find the identity

$$\sum_{\substack{n, n' \\ m, m'}} \Phi_{[m m']ij}^{[n n']} = 0. \quad (2.44)$$

Similar, if we consider a constant displacement on top of a homogeneous deformation, $\tilde{u}_{[m]i}^{[n]} = E_{ij} r_{[m]j}^{[n]} + u_i$, the change in energy, again, will not depend on the global translation. Using the sum rule Eq. (2.44), the effective potential, Eq. (2.42), leaves us with a term linear in u_i . Since this term has to vanish for an arbitrary deformation, E_{jl} , we obtain another sum rule

$$\sum_{\substack{n, n' \\ m, m'}} \Phi_{[m m']ij}^{[n n']} r_{[m]l}^{[n]} = 0. \quad (2.45)$$

Considering an infinite volume or, equivalently, periodic boundary conditions we do not have to care about boundary effects and the periodicity of the crystal

lattice has also to be reflected by the symmetry of the effective potential, i.e., by the symmetry of the matrix $\Phi_{[m m']}^{[n n']}$. Therefore, the dependence on the Bravais lattice indices, n and n' , can only be due to the difference of the lattice vectors,

$$\Phi_{[m m']}^{[n n']}_{ij} = \Phi_{mi, m'j}(\mathbf{R}_n - \mathbf{R}_{n'}) =: \Phi_{[m m']}^{[n-n']}_{ij}. \quad (2.46)$$

In this case Eq. (2.44) even holds if we drop the summation over n' .

The above stated symmetries simplify even further if the atoms interact with central forces only, i.e., $V(\{\mathbf{r}'^{[n]}\}) = V(\{|\mathbf{r}'^{[n]} - \mathbf{r}'^{[n']}\})$. As the distance between two atoms is can be indicated by the differences of the indices, we have

$$\Phi_{[m m']}^{[n-n']}_{ij} = \Phi_{[m-m']}^{[n-n']}_{ij} = \Phi_{[m-m']}^{[n-n']}_{ji}. \quad (2.47)$$

The sum rule Eq. (2.44) does then take the form

$$\sum_{n,m} \Phi_{[m m']}^{[n n']}_{ij} = 0, \quad (2.44a)$$

whereas Eq. (2.45) is not an independent sum rule but follows directly from Eq. (2.44a).

2.2.3 Phonons

Let us consider the local displacement, $\mathbf{u}_{[m]}^{[n]}$, which is compatible with the periodic boundaries of the crystal, and neglect macroscopic deformations for the moment. Due to the lattice periodicity, we can diagonalize $\Phi_{[m m']}^{[n n']}$ with respect to the lattice indices n, n' by the matrix $C_{\mathbf{q}\mathbf{R}_n} = V^{-1/2} e^{i\mathbf{q}\cdot\mathbf{R}_n}$, where the momenta, \mathbf{q} , are from the first Brillouin zone. In other words, the system of harmonic oscillators splits into decoupled sectors of different \mathbf{q} . Thus, if a crystal in d dimensions has N atoms per unit cell, we are left with $d \times N$ coupled harmonic oscillators

$$\mathcal{H} = \frac{1}{2} \sum_{\mathbf{q}} \left[\frac{1}{M_m} p_{[m]i}^{[\mathbf{q}]\dagger} p_{[m]i}^{[\mathbf{q}]} + u_{[m]i}^{\dagger[\mathbf{q}]} \Phi_{[m m']}^{[\mathbf{q}]}_{ij} u_{[m']j}^{[\mathbf{q}]} \right], \quad (2.48)$$

with the Fourier components of the displacement and interaction kernel

$$\mathbf{u}_{[m]}^{[\mathbf{q}]} = \sum_{\mathbf{R}_n} C_{\mathbf{q}\mathbf{R}_n} \mathbf{u}_{[m]}^{[n]} \quad , \quad \Phi_{[m m']}^{[\mathbf{q}]}_{i,j} = \sum_{\mathbf{R}_n} C_{\mathbf{q}\mathbf{R}_n} \Phi_{[m m']}^{[n]}_{i,j} \quad (2.49)$$

and the canonically conjugated momenta $\mathbf{p}_{[m]}^{[\mathbf{q}]}$ of the displacement.

The solutions of this Hamiltonian are the different phonon branches, labeled by the index α , which have eigenvalues, i.e., dispersions, $\omega_{\mathbf{q}\alpha}$. The eigenvalue equation can be written as

$$M_m \omega_{\mathbf{q}\alpha}^2 u_{[m]i}^{[\mathbf{q}]} e^{i\mathbf{q}\cdot\mathbf{R}_n} = \sum_{n',m'} \Phi_{[m m']}^{[n-n']}_{ij} u_{[m']j}^{[\mathbf{q}]} e^{i\mathbf{q}\cdot\mathbf{R}_{n'}}. \quad (2.50)$$

One possible configuration is given by a displacement in some arbitrary but fixed direction, say x_i , which is constant throughout the unit cell, i.e., all atoms in the unit cell oscillate in phase, and only atoms in different unit cells have a finite phase difference. Such a displacement is independent of the index m , $u_{[m]}^{[n]} = u_{[-]}^{[n]}$. For these phonons, we find the eigenvalue problem

$$M_m \omega_{\mathbf{q}\alpha}^2 u_{[-]}^{[\mathbf{q}]_i} e^{i\mathbf{q}\mathbf{R}_n} = \sum_{n',m'} \Phi_{[mm']}^{[n-n']_{ii}} u_{[-]}^{[\mathbf{q}]_i} e^{i\mathbf{q}\mathbf{R}_{n'}}. \quad (2.51)$$

In the long wavelength limit, we can expand this equation in small momenta and compare the respective orders. Considering central interaction forces only, we obtain to zeroth order

$$M_m \omega_{\mathbf{q}\alpha}^2 |_{\mathbf{q}=0} = \sum_{n',m'} \Phi_{[mm']}^{[n-n']_{ii}} = 0, \quad (2.52)$$

due to Eq. (2.44a), which implies $\omega_{\mathbf{q}\alpha} |_{\mathbf{q}=0} = 0$, i.e., a vanishing dispersion for zero momentum. This is reasonable, since the limit $\mathbf{q} \rightarrow 0$ corresponds to a vanishing phase difference between the unit cells and, thus, leads to a constant shift of all atoms of the crystal, i.e., a global translation, which does not cost any energy.

In first order, the left hand side is zero, due to the vanishing $\omega_{\mathbf{q}\alpha} |_{\mathbf{q}=0}$. Hence, the right hand side has also to vanish, and the expansion yields another symmetry of the effective potential

$$\sum_{n',m'} \Phi_{[mm']}^{[n-n']_{ii}} (\mathbf{R}_n - \mathbf{R}_{n'}) = 0. \quad (2.53)$$

Finally, the first non-vanishing term appears in second order and reads as

$$M_m \left(\nabla_{\mathbf{q}} \omega_{\mathbf{q}\alpha} |_{\mathbf{q}=0} \cdot \mathbf{q} \right)^2 = -\frac{1}{2} \sum_{\mathbf{R},m'} \Phi_{[mm']}^{[n-n']_{ii}} (\mathbf{q} \cdot \mathbf{R}_{n-n'})^2. \quad (2.54)$$

Therefore, the dispersion of this particular mode has to be linear, $\omega \sim q$. Since one of these modes exists per dimension, we have at least d branches with a linear dispersion for small q . These branches are called the acoustic phonons, as they are responsible for carrying sound through a crystal. The remaining $d(N-1)$ phonon branches have, in general, a non-vanishing dispersion in the limit $\mathbf{q} \rightarrow 0$. These branches are called the optical phonons as they can often be excited by electromagnetic fields.

2.2.4 Continuum Limit

The description in the previous section was quite general and captures all energy and wavelength ranges. However, we are mainly interested in low energies and long wavelength fluctuations. Therefore, we may neglect the structure of the unit cell

and switch to a continuum theory. The limit is performed by omitting the index m and describing the lattice by continuous position vectors, \mathbf{r} , of a volume element with a mass density ρ . The total displacement, Eq. (2.40) then takes the form

$$\tilde{\mathbf{u}}(\mathbf{r}) \approx E \cdot \mathbf{r} + \mathbf{u}(\mathbf{r}). \quad (2.55)$$

The relevant degrees of freedom are the 6 independent components of the matrix E and the three components of the local displacement field, \mathbf{u} .

Let us assume that the interaction of the atoms is only due to central forces, $V(\mathbf{r}_1, \mathbf{r}_2) = V(\mathbf{r}_1 - \mathbf{r}_2)$. The expansion of the potential, Eq. (2.42), is then given by

$$V_{\text{eff}} = \frac{1}{2} \int d\mathbf{r}_1 d\mathbf{r}_2 \tilde{u}_i(\mathbf{r}_1) \Phi_{ij}(\mathbf{r}_1 - \mathbf{r}_2) \tilde{u}_j(\mathbf{r}_2). \quad (2.56)$$

In the long wavelength limit, we assume that the displacement field changes only slowly in space and, furthermore, the interaction is assumed to be only short ranged. Hence, we may expand the displacement around the mean position, $\mathbf{R} = (\mathbf{r}_1 + \mathbf{r}_2)/2$, in the mutual distance $\bar{\mathbf{r}} = \mathbf{r}_1 - \mathbf{r}_2$. Using $\Phi_{ik}(\bar{\mathbf{r}}) = \Phi_{ki}(\bar{\mathbf{r}})$ for central forces and the continuous version of the sum rule, Eq. (2.44a), we obtain

$$V_{\text{eff}} = \frac{1}{2} \int d\mathbf{R} \frac{\partial \tilde{u}_i(\mathbf{R})}{\partial r_j} C_{ijkl} \frac{\partial \tilde{u}_k(\mathbf{R})}{\partial r_l} \quad (2.57)$$

$$C_{ijkl} = -\frac{1}{2} \int d\bar{\mathbf{r}} \bar{r}_j \Phi_{ik}(\bar{\mathbf{r}}) \bar{r}_l. \quad (2.58)$$

Notably, as we integrated by parts, we omitted a surface term which is valid if we, for instance, have periodic boundary conditions for \mathbf{u} .

The rank four tensor C_{ijkl} is the elastic modulus tensor already introduced in Sec. 2.1.4. Since the macroscopic distortion, E_{ij} , is a symmetric matrix, the tensor C_{ijkl} has also to be symmetric within its first and second index pair. Furthermore, it has also to be invariant with respect to exchange of the two pairs. Thus, we have the relations $C_{ijkl} = C_{jikl} = C_{ijlk}$, see Eq. (2.21), and a total number of 21 independent elastic moduli. Due to the symmetry of C , we may also symmetrize the derivative of the microscopic displacement yielding the strain tensor, u_{ij} , as defined in Eq. (2.4) and the potential reads as

$$V_{\text{eff}} = \frac{1}{2} \int d\mathbf{r} \tilde{u}_{ij}(\mathbf{r}) C_{ijkl} \tilde{u}_{kl}(\mathbf{r}). \quad (2.59)$$

Substituting the decomposition (2.55) into Eq. (2.59), we note that the terms which mix the microscopic displacement, u_i , and the macroscopic distortion, E_{ij} , are total derivatives. Thus, a partial integration yields only boundary terms proportional to $\int n_j u_i(\mathbf{r}) dS$. Demanding periodic boundary conditions for \mathbf{u} , those terms vanish and we are left with

$$V_{\text{eff}} = \frac{1}{2} \int d\mathbf{r} u_{ij}(\mathbf{r}) C_{ijkl} u_{kl}(\mathbf{r}) + E_{ij} C_{ijkl} E_{kl}, \quad (2.60)$$

i.e., the macroscopic distortion and the microscopic displacement are decoupled.

Concerning the elastic modulus tensor, Eq. (2.58) implies also invariance under exchanging $i \leftrightarrow k$ and $j \leftrightarrow l$, respectively, such that the tensor is fully symmetric in all its indices. In Voigt notation, these additional symmetries yield

$$\begin{aligned} C_{23} &= C_{44}, & C_{13} &= C_{55}, & C_{12} &= C_{66}, \\ C_{14} &= C_{56}, & C_{25} &= C_{46}, & C_{36} &= C_{45}, \end{aligned}$$

which are called the Cauchy relations and reduce the number of independent elastic moduli to a total number of 15.

These relations are, however, in physical systems not fulfilled in general. They originate from the assumption that the atoms interact with central forces only which is in general not valid. For instance, in covalent crystals the interaction between the atoms is mediated by the valence electrons which are in general in anisotropic orbitals. In ionic crystals, on the other hand, a deformation of the ions yields a polarization giving rise to a surface charge, which has a macroscopic electric field. The shape of the field depends on the geometry of the probe itself and, thus, has no unique thermodynamic limit. The Cauchy relations are, however, approximately fulfilled, if every atom is a center of inversion symmetry, since then no macroscopic field will arise.

As we consider crystals having a lattice structure with certain symmetries, these must also be reflected by the elastic modulus tensor. This yields additional restrictions reducing the number of independent components. As it turns out, the 32 crystallographic point groups give rise to 9 different symmetry classes of the elastic modulus tensor which are discussed in App. A.

Cubic systems have the highest symmetry which leads to strong simplifications. The elastic constant matrix for cubic systems reads in Voigt notation as

$$C = \left(\begin{array}{ccc|ccc} C_{11} & C_{12} & C_{12} & & & \\ C_{12} & C_{11} & C_{12} & & 0 & \\ C_{12} & C_{12} & C_{11} & & & \\ \hline & & & C_{44} & 0 & 0 \\ & & & & C_{44} & 0 \\ & 0 & & & & C_{44} \end{array} \right), \quad (2.61)$$

having only three different elastic moduli, C_{11} , C_{12} and C_{44} .

In the special case that the three remaining moduli fulfill the relation

$$C_{11} - C_{12} - 2C_{44} = 0, \quad (2.62)$$

the expansion of the elastic potential for cubic crystals results in only two terms, namely the squared trace and the trace of the square of the strain tensor. This is the same as for isotropic bodies, as we have seen in Sec. 2.1.4. Thus, we conclude

that a cubic crystal with the above relation of its elastic constants, Eq. (2.62), can be considered as being completely isotropic with respect to the elastic degrees of freedom. The bulk modulus reads as $K = C_{11} - \frac{4}{3}C_{44} = C_{11} - \frac{2}{3}(C_{11} - C_{12})$, whereas the shear modulus is given by $\mu = C_{44}$.

Let us consider the dynamics of the lattice which follows from the equations of motion for the strain, E , and the phonons, \mathbf{u} . Of course, in the long wavelength limit, we will only deal with the acoustic phonons. However, due to the dispersion relation those are the low energy excitations and, thus, of particular interest.

Adding a time dependence of the displacement field, we have also to integrate over the time to obtain the energy. The total kinetic energy due to the atomic motion of a crystal of volume V is, thus, given by

$$T_{\text{el}} = \int_V dt d\mathbf{r} \frac{\rho}{2} \dot{\tilde{u}}_i(\mathbf{r}, t) \dot{\tilde{u}}_i(\mathbf{r}, t), \quad (2.63)$$

whereas the potential energy is given by Eq. (2.60) with an additional time dependence of the field. Since the integral over the microscopic strain vanishes we may rewrite it conveniently to

$$V_{\text{el}} = \int_V dt d\mathbf{r} \tilde{u}_{ij}(\mathbf{r}, t) C_{ijkl} \tilde{u}_{kl}(\mathbf{r}, t). \quad (2.64)$$

To obtain the equations of motion for the macroscopic distortion and the microscopic strain we have to vary the atomic displacement as, $\delta \tilde{u}_i = \delta \tilde{u}_i + \delta E_{ij} r_j$. The resulting change of the action is to linear order given by

$$\begin{aligned} \delta \mathcal{S} = & \int_V dt d\mathbf{r} \rho [(\partial_t \delta u_i(\mathbf{r}, t)) \dot{\tilde{u}}_i(\mathbf{r}, t) + (\partial_t \delta E_{ij}(t)) r_j \dot{\tilde{u}}_i(\mathbf{r}, t)] \\ & - \int_V dt d\mathbf{r} [(\partial_j \delta u_i(\mathbf{r})) C_{ijkl} \tilde{u}_{kl}(\mathbf{r}) + \delta E_{ij} C_{ijkl} \tilde{u}_{kl}(\mathbf{r})]. \end{aligned} \quad (2.65)$$

After a partial integration and sorting by the variations, δu_i and δE_{ij} , we obtain

$$\begin{aligned} \delta \mathcal{S} = & - \int dt \int_V d\mathbf{r} \partial_j [\delta u_i(\mathbf{r}, t) C_{ijkl} \tilde{u}_{kl}(\mathbf{r}, t)] \\ & - \int dt \int_V d\mathbf{r} \delta u_i(\mathbf{r}, t) [\rho \ddot{\tilde{u}}_i(\mathbf{r}, t) - \partial_j (C_{ijkl} \tilde{u}_{kl}(\mathbf{r}, t))] \\ & - \int dt \delta E_{ij}(t) \int_V d\mathbf{r} [r_j \ddot{\tilde{u}}_i(\mathbf{r}, t) + C_{ijkl} \tilde{u}_{kl}(\mathbf{r}, t)] \end{aligned} \quad (2.66)$$

The first term is a boundary term which can be rewritten by substituting the strain tensor, $\sigma_{ij} = C_{ijkl} \tilde{u}_{kl}$, as

$$\int dt \int_{\partial V} dS n_j \sigma_{ij}(\mathbf{r}, t) \delta u_i(\mathbf{r}, t), \quad (2.67)$$

where \mathbf{n} is the vector normal to the surface. As the energy change has to vanish irrespectively of the particular variation the integrands have to be zero. Therefore, the first and second line of Eq. (2.66) leaves us with two sets of equations, namely

$$n_j \sigma_{ij}(\mathbf{r}, t) \Big|_{\partial V} = 0 \quad (2.68)$$

$$\rho \left(\ddot{u}_i(\mathbf{r}, t) + \ddot{E}_{ik}(t) r_k \right) = \partial_j \sigma_{ij}(\mathbf{r}, t). \quad (2.69)$$

We may multiply Eq. (2.69) by r_s and integrate the resulting equation over the volume. Integrating the right hand side by parts and using the boundary condition, Eq. (2.68), we obtain by relabeling the summation indices

$$\rho \int_V d\mathbf{r} \left(r_j \ddot{u}_i(\mathbf{r}, t) + r_j \ddot{E}_{ik}(t) r_k \right) = - \int_V d\mathbf{r} \sigma_{ij}(\mathbf{r}, t) \quad (2.70)$$

which is exactly the equation of motion following from the third line of Eq. (2.66).

Thus, we obtain six independent equations of motion for the six independent strain components, \tilde{u}_{ij} . Since a decomposition of the total strain is always a matter of choice, we cannot expect more than these. However, for the particular decomposition into the macroscopic and the microscopic part, we also require the local displacement to have a vanishing zero-momentum component which yields an additional set of three equations. Altogether we obtain the nine equations

$$\rho \left(\ddot{u}_i(\mathbf{r}, t) + \ddot{E}_{ik}(t) r_k \right) = C_{ijkl} \partial_j \partial_k u_l(\mathbf{r}, t) \quad (2.71a)$$

$$n_j C_{ijkl} \partial_k u_l(\mathbf{r}, t) \Big|_{\partial V} = -C_{ijkl} n_j E_{kl} \quad (2.71b)$$

$$\int_V d\mathbf{r} u_i(\mathbf{r}, t) = 0 \quad (2.71c)$$

of which the first three, Eqs. (2.71a), are local equations, and the remaining six, Eqs. (2.71b) and (2.71c), are global. This corresponds to the three local degrees of freedom, $u_i(\mathbf{r}, t)$ and the six global degrees of freedom, $E_{ij}(t)$.

Apparently, the macroscopic and microscopic strain are not independent from each other. Furthermore, especially the Eqs. (2.71b) are defined only on the surface of the crystal including the surface normals, \mathbf{n} . Therefore, the solution of the equation of motions depends on the actual shape of the crystal and can not be obtained in general. However, Eqs. (2.71a-c) define the crystal motion for a given geometry.

Let us consider for simplicity the situation of a static macroscopic deformation, $\ddot{E}_{ij} = 0$. Then, Eq. (2.71a) depends only on the microscopic displacement as

$$\rho \ddot{u}_i(\mathbf{r}, t) = C_{ijkl} \partial_j \partial_k u_l(\mathbf{r}, t). \quad (2.72)$$

The macroscopic deformation does however still enter through the boundary conditions, Eqs. (2.71b). A Fourier transformation of Eq. (2.72) in space and time yields the eigenvalue equation

$$\rho \omega^2 u_i(\mathbf{q}, \omega) = D_{il}(\mathbf{q}) u_l(\mathbf{q}, \omega), \quad (2.73)$$

$$D_{il}(\mathbf{q}) = C_{ijkl} q_j q_k \quad (2.74)$$

where we introduced the dynamical matrix, D . The solution of this eigenvalue equation yields three modes with a linear dispersion corresponding to the three acoustic phonon branches. As mentioned above, the optical phonon branches are not captured in the long wavelength approximation since they depend on the microscopic structure of the unit cell, which was neglected.

For isotropic systems, we always have a longitudinal solution, where the displacement and the vector of propagation, \mathbf{q} , are parallel, and two transversal solutions with $\mathbf{u} \perp \mathbf{q}$. In non-isotropic lattices, this is only true for certain directions of the propagation vector, and, in general, the phonons have both, longitudinal and transversal character.

For a cubic lattice, for instance, the elastic modulus tensor is given in Cartesian coordinates by Eq. (2.61). We may switch to the basis of longitudinal and transversal phonons, $\mathbf{u} = (u_L, u_1, u_2)$, with

$$u_L(\mathbf{q}) = \mathbf{u}(\mathbf{q}) \cdot \hat{\mathbf{q}} \quad , \quad u_\lambda(\mathbf{q}) = \mathbf{u}(\mathbf{q}) \cdot \mathbf{e}_\lambda(\hat{\mathbf{q}}).$$

The vectors of polarization obey the symmetry relation, $\mathbf{e}_\lambda(-\hat{\mathbf{q}}) = -\mathbf{e}_\lambda(\hat{\mathbf{q}})$ and are orthogonal to each other, $\hat{\mathbf{q}} \cdot \mathbf{e}_\lambda(\hat{\mathbf{q}}) = 0$ and $\mathbf{e}_\lambda(\hat{\mathbf{q}}) \cdot \mathbf{e}_{\lambda'}(\hat{\mathbf{q}}) = \delta_{\lambda\lambda'}$.

However, the dynamic matrix, D mixes longitudinal and transversal phonons, such that they are only eigenvectors for certain propagation directions. As the cubic anisotropy is measured by the deviation of the combination $\delta = C_{11} - C_{12} - 2C_{44}$ from zero, we may decompose the dynamical matrix into an isotropic and an anisotropic part, $D = D_{\text{iso}} + \delta D_{\text{an}}$. The respective matrices read as

$$D_{\text{iso}} = |q|^2 \begin{bmatrix} C_{11} & 0 & 0 \\ 0 & C_{44} & 0 \\ 0 & 0 & C_{44} \end{bmatrix}, \quad D_{\text{an}} = |q|^2 \begin{bmatrix} -1 + \sum \hat{q}_i^4 & \sum \hat{q}_i^3 \mathbf{e}_{1,i} & \sum \hat{q}_i^3 \mathbf{e}_{2,i} \\ \sum \hat{q}_i^3 \mathbf{e}_{1,i} & \sum \hat{q}_i^2 \mathbf{e}_{1,i}^2 & \sum \hat{q}_i^2 \mathbf{e}_{1,i} \mathbf{e}_{2,i} \\ \sum \hat{q}_i^3 \mathbf{e}_{2,i} & \sum \hat{q}_i^2 \mathbf{e}_{1,i} \mathbf{e}_{2,i} & \sum \hat{q}_i^2 \mathbf{e}_{2,i}^2 \end{bmatrix}. \quad (2.75)$$

The off-diagonal elements vanish exactly for propagation along the highest symmetry directions, which are along the cubic axes, $\langle 1, 0, 0 \rangle$, along the face diagonals, $\langle 1, 1, 0 \rangle$, and along the space diagonals, $\langle 1, 1, 1 \rangle$. For these directions one obtains the respective sound velocities

$$\begin{aligned} \langle 1, 0, 0 \rangle: \quad \rho v_L^2 &= C_{11}, & \rho v_1^2 &= C_{44}, & \rho v_2^2 &= C_{44} \\ \langle 1, 1, 0 \rangle: \quad \rho v_L^2 &= \frac{1}{2}(C_{11} + C_{12} + 2C_{44}), & \rho v_1^2 &= \frac{1}{2}(C_{11} - C_{12}), & \rho v_2^2 &= C_{44} \\ \langle 1, 1, 1 \rangle: \quad \rho v_L^2 &= \frac{1}{3}(C_{11} + 2C_{12} + 4C_{44}), & \rho v_1^2 &= \frac{1}{3}(C_{11} - C_{12} + C_{44}), & \rho v_2^2 &= \rho v_1^2 \end{aligned}$$

As mentioned, in the isotropic case, $\delta = 0$, the longitudinal and transversal basis are eigenvectors for every propagation direction.

To conclude the considerations about the lattice dynamics, we may ask what happens if we allow for slow dynamic deformations. In this case, the macroscopic

strain tensor acts as a perturbation of the phonon solution derived above. As mentioned above, for a given crystal shape we may still solve the equation of motions, for instance by a Green's function approach, at least numerical.

However, since phonons describe coherent harmonic oscillations of the lattice atoms with periodic boundary conditions, we can not expect a phonon-like solution for a non-static boundary. Due to the dynamic macroscopic distortion the crystal changes its shape with time and, thus, simple phonon modes are destroyed.

2.3 Phonon Field Integral

In Chap. 6, we want to describe the acoustic phonons within a quantum field theory. Thus, we need the action for the displacement given in momentum space by

$$\mathcal{S}_{\text{el}}[u] = \frac{1}{2} \sum_{\mathbf{q}, \omega_n} u_i(\mathbf{q}, \omega_n) (D^{-1})_{il}(\mathbf{q}, \omega_n) u_l(\mathbf{q}, \omega_n), \quad (2.76)$$

where $D^{-1}(\mathbf{q}, \omega_n)$ is the inverse Green's function. In principle, it is determined by the equations of motion, however, as there are different formulations of the phonon field integral, we will, in the following, deduce it for the notation used in this Thesis. For simplicity, we consider the zero temperature phonon Green's function from which the finite temperature propagator follows by substituting the continuous frequencies, ω , by discrete Matsubara frequencies, $\omega_n = 2\pi n/T$ with n being integer. In doing so, we follow Ref. [16].

As a first step, we obtain the operator for the displacement field and its canonically conjugated operator. Considering the local displacement field, $\mathbf{u}(\mathbf{r}, t)$, we can Fourier transform it for finite momenta, $\mathbf{q} \neq 0$, yielding

$$\mathbf{u}(\mathbf{r}, t) = \frac{1}{\sqrt{V}} \sum_{\mathbf{q}, \alpha} \mathbf{e}_\alpha(\mathbf{q}) \left(u_\alpha(\mathbf{q}) e^{i(\mathbf{q}\cdot\mathbf{r} - \omega_{\mathbf{q}\alpha} t)} + u_\alpha^\dagger(\mathbf{q}) e^{-i(\mathbf{q}\cdot\mathbf{r} - \omega_{\mathbf{q}\alpha} t)} \right) \quad (2.77)$$

Here, the $\omega_{\mathbf{q}\alpha}$ are the eigenenergies obtained by the condition of a vanishing determinant of the dynamical matrix, Eq. (2.74). The corresponding normalized eigenvectors, i.e., the polarization vectors, \mathbf{e}_α , are orthogonal to each other and obey the symmetry relation $\mathbf{e}_\alpha(-\mathbf{q}) = -\mathbf{e}_\alpha(\mathbf{q})$. Finally, as the displacement is a real quantity, the amplitudes obey the relation $u_\alpha^\dagger(\mathbf{q}) = -u_\alpha(-\mathbf{q})$.

The momentum of the displacement at a certain point, \mathbf{r} , is given by $\rho \dot{\mathbf{u}}(\mathbf{r}, t)$. In order to quantize the theory, we have to replace the displacement field and its momentum by operators, for notational convenience denoted by the same labels, which have to obey the canonical commutation relation

$$[\rho \dot{u}_i(\mathbf{r}, t), u_j(\mathbf{r}', t)] = -i \delta_{ij} \delta(\mathbf{r} - \mathbf{r}'). \quad (2.78)$$

Substituting Eq. (2.77) in Eq. (2.78), where we also replace the functions $u_\alpha(\mathbf{q})$ by operators denoted by the same letters, the commutator reads as

$$\begin{aligned} \frac{\rho}{V} \sum_{\substack{\mathbf{q}, \mathbf{q}' \\ \alpha, \alpha'}} \mathbf{e}_{\alpha,i}(\mathbf{q}) \mathbf{e}_{\alpha',j}(\mathbf{q}') (-i\omega_{\mathbf{q}\alpha}) \left\{ \begin{aligned} & \left[u_\alpha(\mathbf{q}), u_{\alpha'}(\mathbf{q}') \right] e^{i[\mathbf{q}\cdot\mathbf{r} + \mathbf{q}'\cdot\mathbf{r}' - t(\omega_{\mathbf{q}\alpha} + \omega_{\mathbf{q}'\alpha'})]} \\ & + \left[u_\alpha(\mathbf{q}), u_{\alpha'}^\dagger(\mathbf{q}') \right] e^{i[\mathbf{q}\cdot\mathbf{r} - \mathbf{q}'\cdot\mathbf{r}' - t(\omega_{\mathbf{q}\alpha} - \omega_{\mathbf{q}'\alpha'})]} \\ & - \left[u_\alpha^\dagger(\mathbf{q}), u_{\alpha'}(\mathbf{q}') \right] e^{-i[\mathbf{q}\cdot\mathbf{r} - \mathbf{q}'\cdot\mathbf{r}' - t(\omega_{\mathbf{q}\alpha} - \omega_{\mathbf{q}'\alpha'})]} \\ & - \left[u_\alpha^\dagger(\mathbf{q}), u_{\alpha'}^\dagger(\mathbf{q}') \right] e^{-i[\mathbf{q}\cdot\mathbf{r} + \mathbf{q}'\cdot\mathbf{r}' - t(\omega_{\mathbf{q}\alpha} + \omega_{\mathbf{q}'\alpha'})]} \end{aligned} \right\}. \end{aligned} \quad (2.79)$$

Eq. (2.78) is satisfied if the u_α obey the commutation relations

$$\begin{aligned} \left[u_\alpha(\mathbf{q}), u_{\alpha'}(\mathbf{q}') \right] &= \left[u_\alpha^\dagger(\mathbf{q}), u_{\alpha'}^\dagger(\mathbf{q}') \right] = 0 \\ \left[u_\alpha(\mathbf{q}), u_{\alpha'}^\dagger(\mathbf{q}') \right] &= (2\rho\omega_{\mathbf{q}\alpha})^{-1} \delta_{\alpha,\alpha'} \delta_{\mathbf{q},\mathbf{q}'}. \end{aligned} \quad (2.80)$$

Thus, we may define new operators, $b_{\alpha,\mathbf{q}} = \sqrt{2\rho\omega_{\mathbf{q}\alpha}} u_\alpha(\mathbf{q})$, which obey the canonical commutation relations for annihilation and creation operators. The elements of the Green's function, D_{ij} , follows from the zero temperature expectation value

$$D_{il}(\mathbf{r}, t; \mathbf{r}', t') = -i \left\langle T_t \left(u_i(\mathbf{r}, t), u_l^\dagger(\mathbf{r}', t') \right) \right\rangle, \quad (2.81)$$

where T_t denotes the time ordering operator. In evaluating the zero temperature expectation value, one has to keep in mind that no phonons exist in the ground state. Thus, for the expectation values of the square of the operators $b_{\alpha,\mathbf{q}}$ we obtain $\langle b_{\alpha,\mathbf{q}}^\dagger b_{\alpha',\mathbf{q}'} \rangle = 0$ and $\langle b_{\alpha,\mathbf{q}} b_{\alpha',\mathbf{q}'}^\dagger \rangle = \delta_{\alpha,\alpha'} \delta_{\mathbf{q},\mathbf{q}'}$ and, therefore, Eq. (2.81) becomes

$$D_{il}(\mathbf{r}, t; \mathbf{r}', t') = -\frac{i}{V} \sum_{\mathbf{q}\alpha} \frac{1}{2\rho\omega_{\mathbf{q}\alpha}} e_{\alpha,i} e_{\alpha,l} \begin{cases} e^{i\mathbf{q}\cdot(\mathbf{r}-\mathbf{r}')} e^{-i\omega_{\mathbf{q}\alpha}(t-t')} & t > t' \\ e^{-i\mathbf{q}\cdot(\mathbf{r}-\mathbf{r}')} e^{i\omega_{\mathbf{q}\alpha}(t-t')} & t < t' \end{cases}. \quad (2.82)$$

Due to the symmetry of the polarization vectors, $\mathbf{e}_\alpha(\mathbf{q})$, and the fact that the eigenenergies do not depend on the sign of the respective momentum, $\omega_{-\mathbf{q}\alpha} = \omega_{\mathbf{q}\alpha}$, we may relabel $\mathbf{q} \rightarrow -\mathbf{q}$ in the second case. Thus, the phonon propagator in real space and time reads as

$$D_{il}(\mathbf{r}, t; \mathbf{r}', t') = \frac{1}{V} \sum_{\mathbf{q}} \left[\sum_{\alpha} \frac{1}{2i\rho\omega_{\mathbf{q}\alpha}} e_{\alpha,i} e_{\alpha,l} e^{-i \operatorname{sgn}(t-t') \omega_{\mathbf{q}\alpha}(t-t')} \right] e^{i\mathbf{q}\cdot(\mathbf{r}-\mathbf{r}')} \quad (2.83)$$

$$= \frac{1}{V} \sum_{\mathbf{q}} D(\mathbf{q}, t-t') e^{i\mathbf{q}\cdot(\mathbf{r}-\mathbf{r}')}. \quad (2.84)$$

Calculating the Fourier transformation in time, $\int_{-\infty}^{\infty} D(\mathbf{q}, \tau) e^{-i\omega\tau} d\tau$, we have to take care of the sign of $\tau = t - t'$, and, therefore, we have to calculate the integrals $\int_0^{\infty} e^{-i\tau(\omega_{\mathbf{q}\alpha} \pm \omega)} d\tau$. This is done by a regularization, $\omega \rightarrow \omega \mp i\epsilon$, where the limit $\epsilon \rightarrow 0$ is taken in the end.

The solution reads as

$$D_{il}(\mathbf{q}, \omega) = \sum_{\alpha} \frac{1}{2\rho\omega_{\mathbf{q}\alpha}} e_{\alpha,i} e_{\alpha,l} \left(\frac{1}{\omega - \omega_{\mathbf{q}\alpha} + i\epsilon} - \frac{1}{\omega + \omega_{\mathbf{q}\alpha} - i\epsilon} \right) \quad (2.85)$$

$$= \frac{1}{\rho} \sum_{\alpha} e_{\alpha,i} \frac{1}{\omega^2 - \omega_{\mathbf{q}\alpha}^2 + i\epsilon} e_{\alpha,l}. \quad (2.86)$$

Now, we have an expression for the propagator $D(\mathbf{q}, \omega) = U \cdot \text{diag}(d_{\alpha}) \cdot U^T$, where U is the matrix of eigenvectors \mathbf{e}_{α} . The elements of the inverse matrix are given by

$$D^{-1}(\mathbf{q}, \omega)_{il} = U_{i\alpha} d_{\alpha}^{-1} U_{l\alpha} = \sum_{\alpha} e_{\alpha,i} \rho (\omega^2 - \omega_{\mathbf{q}\alpha}^2 + i\epsilon) e_{\alpha,l} \quad (2.87)$$

$$= \rho \omega^2 \delta_{il} - C_{ijkl} q_j q_k, \quad (2.88)$$

where the frequency has to be taken infinitesimal above the real axis. Switching to the imaginary time formalism, i.e., introducing Matsubara frequencies, we have to replace $\omega \rightarrow -i\omega_n$.

Chapter 3

Elasticity in Critical Systems

The influence of a compressible lattice on phase transitions is a widely studied field, nevertheless, the elastic degrees of freedom still yield interesting and surprising physics. In particular, as discussed in the following, at a structural phase transition the speed of sound does generally not vanish but stays finite due to long-ranged interactions. This result, although long known, is yet surprising when translated in the language of critical theories. It implies that such a structural phase transition is a symmetry breaking transition without soft modes. Consequently, second order structural transitions show mean field behavior.

In this chapter, we will review the studies of classical critical systems on compressible lattices, i.e., the coupling of critical degrees of freedom to the strain and its fluctuations. We will focus on couplings which are non-perturbative in the sense that they alter the critical behavior drastically. In particular, second order transitions may be driven to first order or inherit the elastic mean field behavior.

In Sec. 3.1, we will discuss the Landau theory for elastically coupled phase transitions in general, focusing on the possible couplings between the critical and the elastic degrees of freedom. As we will see, the symmetry of the crystal yields restraints in that respect. For a more detailed presentation of strain-order parameter coupling at, in particular, structural phase transitions, the reader may be referred to Refs. [17, 18].

Thereafter, in Sec. 3.2, we focus on a specific model, namely the classical Ising model, which is by far the best studied critical theory. In particular, we discuss the effect of the quadratic and the bilinear coupling of the order parameter to the strain field. The calculations presented there follow Refs. [19, 20].

Finally, in Sec. 3.3, we review the most complete study on structural phase transitions, done by Cowley [21]. He studied the strain tensor for all types of crystal symmetry classes, and characterized the resulting phase transition. For other kinds of phase transitions in crystals, where a bilinear elastic coupling between order parameter and the strain is allowed, this discussion carries over.

3.1 Landau Theory and Elasticity

At a second order phase transition, the symmetry of the system changes spontaneously from a high symmetry state to a low symmetry state. In order to describe such phase transitions, Landau introduced the concept of a macroscopic order parameter, ϕ , which is zero in the high symmetry phase and has a finite value in the other phase [22].

Although this description is valid only for second order transitions, it is still applicable for nearly continuous first order transitions. In particular, this implies that Landau theory may be used to describe the behavior in the vicinity of a second order critical endpoint.

In its original form, Landau theory is a mean field theory, neglecting fluctuations, which is for second order transitions only correct in dimensions above the so-called upper critical dimension, d_+ . This dimension depends on the character of the fluctuations, and, thus, on the universality class of the transition. For the incompressible Ising model, for instance, this upper critical dimension is $d_+ = 4$. Below this dimension, fluctuations of the order parameter become important and lead to deviations from mean field behavior, thus, being responsible for the characteristics of thermodynamic quantities.

Solid state phase transitions, which are amenable to pressure, have, generically, an intrinsic coupling of the order parameter to the elastic degrees of freedom. The applied pressure primarily affects the lattice by varying the lattice spacing. This, in turn, modifies the coupling constants of the critical degrees of freedom, and, thus, a finite strain also influences the critical behavior. In order to study the extent of this influence, we first have to ask, how the order parameter and the strain can couple, an issue which is intimately related to the symmetries of the crystal.

3.1.1 Symmetry and Strain

The interactions between some order parameter and the crystal lattice, of course, obey the symmetries of this lattice which are characterized by a number of transformations under which the lattice is invariant. These symmetry operations form a group, namely one of the 32 crystallographic point groups, and, as such, can be analyzed in the context of group theory. For an introduction to group theory and its application in physics, the reader may be referred to Ref. [23].

According to group theory, every point group consists of several irreducible representations, such that every group element can be written as a sum of the irreducible representations. Since elasticity deals with a tensor of rank two, the strain tensor, not all of the irreducible representations are important for our concerns. For instance, a full inversion, mapping every coordinate on its negative, does not affect the strain tensor as $E_{-\alpha,-\beta} = E_{\alpha,\beta}$, due to the transformation rules for tensors.

As a simple example, let us consider a cubic crystal, for which the strain tensor splits into three irreducible representations, namely a singlet, A, a doublet, E, and a triplet, T₂. The basis vectors of the irreducible representations are given as

$$\begin{aligned} \text{A:} \quad \epsilon_1 &= \frac{1}{\sqrt{3}}(E_{xx} + E_{yy} + E_{zz}), \\ \text{E:} \quad \epsilon_2 &= \frac{1}{\sqrt{2}}(E_{xx} - E_{yy}), \\ &\quad \epsilon_3 = \frac{1}{\sqrt{6}}(2E_{zz} - E_{xx} - E_{yy}) \\ \text{T}_2: \quad \epsilon_4 &= E_{yz}, \quad \epsilon_5 = E_{xz}, \quad \epsilon_6 = E_{xy}. \end{aligned}$$

The singlet corresponds to an isostructural volume change since it is the trace of the strain tensor. The doublet is an expansion along one of the cubic axis and a compression of the other axes such that the total volume is preserved, whereas the triplet describes pure shear. The elastic constant tensor, given in Eq. (2.61) in Voigt notation, is in this basis diagonal, reading

$$C = \left(\begin{array}{ccc|ccc} C_{11} + 2C_{12} & 0 & 0 & & & \\ 0 & C_{11} - C_{12} & 0 & & & \\ 0 & 0 & C_{11} - C_{12} & & & \\ \hline & & & C_{44} & 0 & 0 \\ & & & & C_{44} & 0 \\ & & & & & C_{44} \end{array} \right). \quad (3.1)$$

A full classification of the irreducible representations of the strain tensor for each of the point groups, taken from Ref. [21], can be found in App. B.

In general, a Landau theory is an analytic expansion, which for the strain tensor can be formulated in terms of the irreducible representations. In every order of the expansion, we sum over all possible invariants which can be formed from combinations of the irreducible representations. In second order, denoting the basis vectors of an irreducible representation Γ by $\epsilon_{\Gamma,i}$, we simply have

$$\mathcal{V}_\epsilon = \frac{1}{2} \sum_{\Gamma,i} C_\Gamma \epsilon_{\Gamma,i}^2 \quad (3.2)$$

where the C_Γ are the corresponding eigenvalues of the elastic constant matrix.

However, in higher order, the expansion is more complicated, as the symmetry of a representation may not allow invariants of a certain order. In Sec. 3.3 the question of the existence of a third order invariant of a given irreducible representations will become particularly important.

On the other hand, in higher orders, more than one invariant may exist. In fourth order, for instance, a doublet, $\epsilon_E = (\epsilon_{E,1}, \epsilon_{E,2})$, has two invariants, namely $(\epsilon_{E,1}^2 + \epsilon_{E,2}^2)^2$ and $\epsilon_{E,1}^4 + \epsilon_{E,2}^4$. Finally, combinations of invariants are, of course, also invariant under transformations, and, therefore, in fourth order, all strain components are

coupled to each other. Neglecting such couplings, the Landau theory, e.g., for a singlet, ϵ_A , is given by

$$\mathcal{V}_\epsilon = \frac{1}{2}C_A\epsilon_A^2 - U_A^{(3)}\epsilon_A^3 + U_A^{(4)}\epsilon_A^4 + \dots \quad (3.3)$$

and symmetry now dictates which of the prefactors, $U^{(n)}$, can be different from zero.

3.1.2 Coupling to the Order Parameter

As mentioned before, phase transitions are described by an order parameter, ϕ , which can also be classified in terms of the irreducible representations of the symmetry group. The order parameter may be a scalar, e.g., the magnetization in systems with an easy axis anisotropy, a vector as, for instance, the polarization vector in ferroelectrics or some higher order tensor.

A coupling term between order parameter and strain has to be an invariant as well, thus, the possible coupling terms are restricted. In the cubic case, for instance, the singlet, A, transforms as a scalar and, hence, can only couple to another scalar quantity, thus, if the order parameter is a vector, it has to enter the coupling term quadratically. In return, if the order parameter is a scalar, only a singlet, A, can couple bilinear to it, whereas couplings to doublets or triplets only appear in second order in the strain and are, thus, much weaker affected by the ordering.

To lowest order, only one of the irreducible representations of the strain, say ϵ_A , will be strongly affected by the order parameter. For a scalar order parameter, ϕ , expansion of the interaction potential to lowest order then yields

$$\mathcal{V}_c = -\gamma_1\epsilon_A\phi - \gamma_2\epsilon_A\phi^2. \quad (3.4)$$

In the following, we restrict ourselves to the discussion of these two terms. In principle, it would be sufficient to consider the bilinear coupling, i.e., the first term in Eq. 3.4, as it the most relevant term. However, due to the symmetries of the high temperature phase, the coupling may have to be invariant under the transformation, $\phi \rightarrow -\phi$, i.e., an Ising symmetry. In this case a bilinear coupling to the strain is not allowed and the next order term has to be considered, namely the quadratic coupling.

Finally, the part of the Landau theory describing the ordering itself is organized in ascending orders of invariants of the order parameter. Similar as for the strain, there may be more than one n^{th} -order invariant which, in principle, have different coefficients and over which is summed. Also, not all invariants necessarily exist. For scalar order parameters, the expansion reads as

$$\mathcal{V}_\phi = -h\phi + \frac{r}{2}\phi^2 + \frac{v}{3!}\phi^3 + \frac{u}{4!}\phi^4 + \dots \quad (3.5)$$

In case of a negative fourth order coefficient, one has to take higher orders into account. The cubic term can, for scalar order parameters, always be absorbed by a shift, $\phi \rightarrow \phi - \frac{v}{u}$.

The coefficients of the expansion are supposed to be only weakly temperature dependent and are, in fact, treated as constants, apart from the quadratic coefficient, r , which vanishes at the critical temperature. In the vicinity of the critical point, we may expand it to first order, obtaining $r = a(T - T_c)$, where T_c denotes the critical temperature.

3.2 Ising Theory

The theory outlined above is quite general. To be more specific, we will consider in the following the critical Ising system as it is, on the one hand, one of the most important and, at the same time, one of the simplest models. It is characterized by a scalar order parameter, ϕ , which, in the original formulation of critical spin systems, denotes the magnetization. Therefore, in absence of a magnetic field, h , i.e., if the system is symmetric under time reversal, it is Ising symmetric. The Landau functional, Eq. (3.5), is, thus, organized in even powers of ϕ and reads up to fourth order as

$$\mathcal{V}_{\text{Ising}} = -h_0 \phi + \frac{r_0}{2} \phi^2 + \frac{u_0}{4!} \phi^4. \quad (3.6)$$

The magnetic field, h_0 , breaks the time inversion symmetry, therefore, the linear coupling to the field is allowed and acts as a source term.

Due to the Ising symmetry at zero field, only a quadratic coupling to the strain is allowed. However, we may also consider a line of first order phase transitions terminating in a second order critical point. As mentioned above, close to the endpoint, such a system has only a weak first order transition and can, thus, be described within a Landau theory. The Ising symmetry is then an emergent symmetry as it strictly exists only at the critical endpoint, therefore also a bilinear coupling to the lattice degrees of freedom is allowed. In the following, we will discuss both couplings in more detail.

3.2.1 Quadratic Coupling

The first considerations of the Ising model on compressible lattices dates back to Rice [24] in 1954. Based on thermodynamic arguments, he pointed out that the compressibility becomes negative close to the transition point whenever the specific heat at constant pressure diverges. Since this is a physically unstable situation, the system exhibits a first order transition before the critical temperature is reached.

Only shortly after, Domb [25] gave a very short argument for a first order transition of the compressible Ising model. He assumed a volume dependence of the spin-spin interaction, $J(v)$. Since the volume change is, for cubic systems, given by the strain singlet, A , we indeed identify this coupling to be a quadratic coupling effect. Writing the free energy as

$$F = T\Psi\left(\frac{J(v)}{T}\right), \quad (3.7)$$

the specific heat at constant volume follows as

$$C_v = T\frac{\partial^2 F}{\partial T^2} = \left(\frac{J(v)}{T}\right)^2 \Psi''\left(\frac{J(v)}{T}\right). \quad (3.8)$$

A divergence of the specific heat, thus, implies a divergence of Ψ'' at the critical temperature. The inverse compressibility can be obtained by differentiating the free energy twice with respect to the volume, and thus reads as

$$\frac{\partial P}{\partial v} = -\frac{\partial^2 F}{\partial v^2} = J''(v)\Psi'\left(\frac{J(v)}{T}\right) + \frac{J'(v)^2}{T}\Psi''\left(\frac{J(v)}{T}\right). \quad (3.9)$$

The first term is finite since $J(v)$ is assumed to be a smooth function and the first derivative of Ψ describes the pressure, which does not diverge at the transition. Therefore, the second term of the inverse compressibility becomes dominant before the Curie point is reached. Since this would imply that a smaller volume yields a lower pressure, the system becomes unstable. As in the van der Waals gas, a Maxwell construction yields a first order transition before the Curie point is reached. Although this argument is based only on a volume dependence of J , further work by Mattis and Schultz [26] came to the same result

In terms of the Ising critical exponents, a diverging specific heat translates to a positive critical exponent α . According to the scaling relations the specific heat exponent is connected to the dimensionality as $\alpha = 2 - \nu d$, where ν is the correlation length exponent. Therefore, this kind of elastic coupling yields a preemptive first order transition and is, thus, non-perturbative for dimensions $\nu d < 2$. For a quantum phase transition the same criterion applies, with the dimension replaced by the effective dimension of the quantum theory, $d_{\text{eff}} = d + z$, where z is the dynamical exponent, see Ref. [27].

These results were obtained for constant pressures, whereas for a constant volume Ising criticality is still obtained. However, Fisher [28] assumed that the “real” underlying phase transition happens at constant pressures and, starting from that assumption, studied how the system behaves for a constant volume. By means of an RG analysis, he found a second order phase transition with so-called Fisher-renormalized critical exponents, for instance $\alpha_F = \alpha/(1 - \alpha)$.

The first to consider the microscopics of the quadratic coupling were Larkin and Pikin [19], see also [20, 29] for a more comprehensive presentation. They considered an isotropic crystal at constant pressure and, importantly, took spatial fluctuations of the order parameter as well as of the elastic degrees of freedom into account. Similar considerations were made by Sak [30], and subsequent publications [31, 32].

Bergman and Halperin [33] considered for the first time not only elastically isotropic systems but also cubic lattices. By means of an RG analysis for the order parameter and the elastic field, they found also a first order transition at constant pressures. At constant volume, a second order transition with Fisher-renormalized exponents was found for isotropic crystals, however, only if the surface atoms were fixed. For the cubic symmetry, a microscopic instability preempted this transition independent of the boundary conditions.

3.2.2 Microscopics of the Quadratic Coupling

In the following, the microscopic analysis of Larkin and Pikin [19] is reviewed along the lines of the very pedagogical review of Dünweg [20].

According to Eq. (2.55), the total displacement is split into a macroscopic deformation and a microscopic displacement vector, $\tilde{u}_i(\mathbf{r}) = E_{ij}r_j + u_i(\mathbf{r})$, from which the strain tensor in Fourier expansion follows as

$$\tilde{u}_{ij}(\mathbf{r}) = E_{ij} + \frac{i}{2} \sum_{\alpha, \mathbf{q} \neq 0} u_{\alpha}(\mathbf{q}) [q_j e_{\alpha, i}(\mathbf{q}) + q_i e_{\alpha, j}(\mathbf{q})] e^{i\mathbf{q}\cdot\mathbf{r}}, \quad (3.10)$$

where we chose for convenience the longitudinal-transversal basis, \mathbf{e}_{α} , with $\mathbf{e}_0 = \hat{\mathbf{q}}$.

We want to determine the free energy, i.e., the logarithm of the partition function, of the elastically coupled Ising system in the framework of a classical field theory. The partition function is given by the functional integral over all degrees of freedom of the weights, $\exp[-\beta \mathcal{H}]$, where \mathcal{H} is the Hamiltonian of the system.

The potential per unit volume of the elastic system in terms of the strain tensor is given by Eq. (2.30), yielding the elastic Hamiltonian per volume

$$\frac{1}{V} \mathcal{H}_{\text{el}} = \frac{1}{V} \int d\mathbf{r} \frac{K}{2} (u_{ii}(\mathbf{r}) + E_{ii})^2 + \mu (\bar{u}_{ij}(\mathbf{r}) + \bar{E}_{ij})^2 - \sigma_{ij} E_{ij} \quad (3.11)$$

$$= \frac{K}{2} E^2 + \mu \bar{E}_{ij} \bar{E}_{ij} - pE - (\sigma_{ij} - p\delta_{ij}) \bar{E}_{ij} \quad (3.12)$$

$$+ \frac{1}{2} \left(K + \frac{4}{3}\mu \right) \sum_{\mathbf{q} \neq 0} q^2 |u_L(\mathbf{q})|^2 + \frac{\mu}{2} \sum_{\alpha=1}^2 \sum_{\mathbf{q} \neq 0} q^2 |u_{\alpha}(\mathbf{q})|^2.$$

In the second line, we used the orthogonality relations for the polarization vectors, \mathbf{e}_{α} , and the Fourier basis, $e^{i\mathbf{q}\cdot\mathbf{r}}$. The quantities \bar{u} and \bar{E} , again, denote the respective trace-free parts and the hydrostatic pressure $p = -\sigma_{ii}/3$ was introduced.

Importantly, Larkin and Pikin [19] noticed that there is an apparent difference between the modes with $\mathbf{k} = 0$ and the ones with a finite momentum, as they are governed by different moduli. In particular, for a finite shear modulus, $\mu > 0$, the macroscopic volume change E has the smaller modulus.

The Ising Hamiltonian for the spatially varying order parameter, $\phi(\mathbf{r})$, follows from the potential, Eq. (3.6), as

$$\mathcal{H}_0 = \int d\mathbf{r} \left[\frac{r_0}{2} \phi(\mathbf{r})^2 + \frac{1}{2} (\nabla \phi(\mathbf{r}))^2 + \frac{u_0}{4!} \phi(\mathbf{r})^4 - h \phi(\mathbf{r}) \right], \quad (3.13)$$

by adding a gradient term and integration over the sample. The quadratic coupling of the Ising to the elastic degrees of freedom reads as

$$\mathcal{H}_c = \lambda \int d\mathbf{r} \phi(\mathbf{r})^2 (E_{ii} + u_{ii}(\mathbf{r})) = \lambda \int d\mathbf{r} \left[E + i \sum_{\mathbf{q} \neq 0} q u_L(\mathbf{q}) e^{i\mathbf{q} \cdot \mathbf{r}} \right] \phi(\mathbf{r})^2. \quad (3.14)$$

The free energy is, thus, obtained by functional integration over the microscopic displacement and the order parameter field, $\mathcal{D}u_\alpha(\mathbf{q})$ and $\mathcal{D}\phi(\mathbf{r})$, and simple integrations over the macroscopic strain,

$$\mathcal{F} = -T \ln \int dE_{ij} \mathcal{D}u_\alpha(\mathbf{q}) \mathcal{D}\phi(\mathbf{r}) \exp[-\beta (\mathcal{H}_0 + \mathcal{H}_{el} + \mathcal{H}_c)]. \quad (3.15)$$

Holding the volume constant yields the constraint $E = E_{ii} = 0$, whereas for constant pressures the integration is unrestricted.

We can perform the functional integration over the transversal phonons since they are not coupled to the order parameter, ϕ , but enter only quadratic in the Hamiltonian. Similar, the macroscopic pure shear, \bar{E}_{ij} , is decoupled and upon completing the square in \mathcal{H}_{el} we can also integrate out these degrees of freedom yielding only a non-critical contribution, $\mathcal{F}_0(p, T)$, which will be neglected in the following.

Integration over the longitudinal phonons, also requires to complete the square

$$\begin{aligned} & \frac{V}{2} \left(K + \frac{4}{3}\mu \right) \sum_{\mathbf{q} \neq 0} \left[q^2 |u_L(\mathbf{q})|^2 - \frac{2i\lambda}{V \left(K + \frac{4}{3}\mu \right)} q u_L(\mathbf{q}) \int d\mathbf{r} e^{i\mathbf{q} \cdot \mathbf{r}} \phi(\mathbf{r})^2 \right] \\ &= \frac{V}{2} \left(K + \frac{4}{3}\mu \right) \sum_{\mathbf{q} \neq 0} \left[q u_L(\mathbf{q}) - \frac{i\lambda}{V \left(K + \frac{4}{3}\mu \right)} \int d\mathbf{r} \phi(\mathbf{r})^2 e^{i\mathbf{q} \cdot \mathbf{r}} \right]^2 \\ &+ \frac{\lambda^2}{2V \left(K + \frac{4}{3}\mu \right)} \sum_{\mathbf{q} \neq 0} \int d\mathbf{r} d\mathbf{r}' \phi(\mathbf{r})^2 \phi(\mathbf{r}')^2 e^{i\mathbf{q} \cdot (\mathbf{r} + \mathbf{r}')}. \end{aligned} \quad (3.16)$$

The term in the last line resembles the fourth order Ising term if we add the zero momentum mode, therefore, we obtain

$$\frac{1}{V} \sum_{\mathbf{q} \neq 0} \int d\mathbf{r} d\mathbf{r}' \phi(\mathbf{r})^2 \phi(\mathbf{r}')^2 e^{i\mathbf{q} \cdot (\mathbf{r} + \mathbf{r}')} = \int d\mathbf{r} \phi(\mathbf{r})^4 - \frac{1}{V} \left[\int d\mathbf{r} \phi(\mathbf{r})^2 \right]^2. \quad (3.17)$$

Finally, considering the macroscopic mode, E , we have to decide whether we describe the system at a constant volume or at constant pressure. In the former case the macroscopic volume change is zero, $E = 0$, and we, thus, end up with the Hamiltonian

$$\mathcal{H} = \int d\mathbf{r} \left[\frac{r_0}{2} \phi(\mathbf{r})^2 + \frac{1}{2} (\nabla \phi(\mathbf{r}))^2 + \frac{u}{4!} \phi(\mathbf{r})^4 - h_0 \phi(\mathbf{r}) \right] - \frac{J_v}{2V} \left[\int d\mathbf{r} \phi(\mathbf{r})^2 \right]^2, \quad (3.18)$$

with a repulsive infinitely long-ranged interaction, J_v , and a renormalized quartic interaction, u , which read as

$$u = u_0 - \frac{4!}{2} \lambda^2 \left(K + \frac{4}{3} \mu \right)^{-1} \quad \text{and} \quad J_v = -\frac{\lambda^2}{K + \frac{4}{3} \mu}. \quad (3.19)$$

On the other hand, if we allow for volume fluctuations, i.e., if we consider constant pressures, we have to integrate over E . Thus, upon completing the square,

$$V \left(\frac{K}{2} E^2 - pE \right) + \lambda E \int d\mathbf{r} \phi(\mathbf{r})^2 = V \frac{K}{2} \left[E - \frac{p}{K} + \frac{\lambda}{VK} \int d\mathbf{r} \phi(\mathbf{r})^2 \right]^2 - \frac{p^2}{2K} + \frac{\lambda p}{K} \int d\mathbf{r} \phi(\mathbf{r})^2 - \frac{\lambda^2}{2K} \frac{1}{V} \left[\int d\mathbf{r} \phi(\mathbf{r})^2 \right]^2, \quad (3.20)$$

integration over E corresponds to dropping of the first term.

Concerning the second line, the first term can be absorbed into the non-critical contribution of the free energy, $\mathcal{F}_0(p, T)$, whereas the second term leads to a renormalization of the quadratic coefficient, r_0 . The last term can be absorbed into a renormalization of the long-ranged interaction constant in Eq. (3.18), yielding J_p . Thus, the Hamiltonian takes the same form as in the case of volume having the renormalized constants

$$r = r_0 - \frac{\lambda p}{K}, \quad u = u_0 - 4! \frac{\lambda^2}{2 \left(K + \frac{4}{3} \mu \right)} \quad \text{and} \quad J_p = \lambda^2 \left(\frac{1}{K} - \frac{1}{K + \frac{4}{3} \mu} \right). \quad (3.21)$$

The renormalization of the quadratic coefficient, r , renders the critical temperature to be pressure dependent, thus, turning the phase transition amenable to pressure tuning. Importantly, the long-ranged interaction J_p , is now positive, supporting the ordering, due to the difference of the elastic moduli or the volume fluctuations and the finite momentum fluctuations. Thus, the cases of constant volume and constant pressure are distinguished by the sign of the long-ranged interaction.

Furthermore, the quartic interaction gets a negative renormalization which may drive it to negative values. Thus, we have to distinguish between a strong elastic coupling, where $u < 0$ and a weak elastic coupling, $u > 0$.

Weak Coupling

If the coupling is not large enough to drive the quartic interaction term negative, Eq. (3.18) is the usual Ising Hamiltonian, with an additional infinitely long-ranged interaction, $J_{p/v}$. To treat this last term, for constant pressures, $J_p > 0$, a Gaussian integration yields

$$\exp \left\{ \frac{\beta J_p}{2V} \left[\int d\mathbf{r} \phi(\mathbf{r})^2 \right]^2 \right\} = \sqrt{\frac{2\pi\beta J_p}{V}} \int dz \exp \left\{ -\frac{V}{2\beta J_p} z^2 - z \int d\mathbf{r} \phi(\mathbf{r})^2 \right\}.$$

The second term of the exponent yields another renormalization of the quadratic coupling constant. Denoting the free energy density of the bare Ising model by $f_0(r)$, the functional integration over the order parameter field, ϕ , yields the critical part of the free energy,

$$\mathcal{F}_{\text{crit}} = -T \log \int dz \exp \left\{ -\beta V f_0 \left(r + z \frac{2}{\beta} \right) - V \frac{z^2}{2\beta J_p} \right\}. \quad (3.22)$$

Since the exponent is proportional to the volume, V , we may obtain the full free energy by a saddle point approximation,

$$\partial_z \left(\beta f_0 \left(r + z \frac{2}{\beta} \right) + \frac{z^2}{2\beta J_p} \right) \stackrel{!}{=} 0, \quad (3.23)$$

which becomes exact in the thermodynamic limit. Furthermore, the Ising free energy is given in terms of the specific heat exponent, α , as $f_0(x) = -A|x|^{2-\alpha}$, with the critical amplitude $A > 0$. Therefore, we obtain the equation

$$g(x) := 8J_p A(2 - \alpha) |x|^{1-\alpha} \operatorname{sgn} x \stackrel{!}{=} x - r. \quad (3.24)$$

The qualitative solution can be obtained by the intersection of the graphs of both sides, as depicted in Fig. 3.1.

The right hand side of Eq. (3.24) is just a straight line which due to the temperature dependence of $r \sim T - T_0$ gets shifted upwards for decreasing temperatures and vice versa. The behavior of the function $g(x)$ depends on the specific heat exponent. For the Ising model, it is $\alpha \geq 0$ in any dimension, therefore, it is a convex function for negative x and concave for positive x . However, as the above analysis carries over to other theories as, for instance, the Heisenberg model, we may also consider the case $\alpha < 0$, in which case the behavior of $g(x)$ is the other way round.

Since there is in general more than one solution to this equation, we have to consider the respective stability, which is determined by the second derivative of the exponent in Eq. (3.22) to be negative, i.e.,

$$8J_p A(2 - \alpha)(1 - \alpha) |x|^{-\alpha} > 1, \quad (3.25)$$

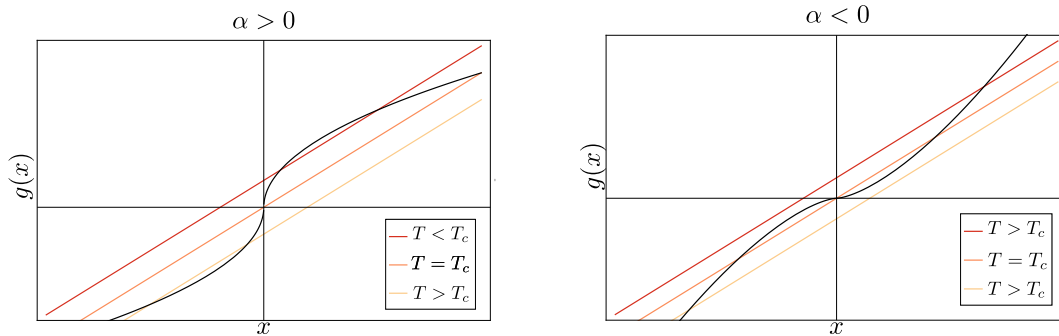


Fig. 3.1: Graphical solution of Eq. (3.24) for the critical exponents $\alpha > 0$ (left panel) and $\alpha < 0$ (right panel). The straight lines correspond to the right hand side of Eq. (3.24), and are shifted by temperature.

Therefore, the first derivative, $g(x)$, has to be flatter than the straight line. From Fig. 3.1, we see that for $\alpha > 0$ the outer solutions are the stable solutions and, thus, the order parameter jumps upon crossing the phase transition, i.e., it is of first order.

In contrast, for $\alpha < 0$, only the inner solution is stable. Thus, the order parameter varies continuously and the system has a second order phase transition. The critical free energy is a function of x rather than of $r \sim T - T_c$, however, since close to the critical point we obtain $g(x) \sim x$, the critical exponents are unchanged.

Apparently, Fig. 3.1 suggests that, apart from temperatures close to the critical value, $r = 0$, no stable solution exists at all. However, the previously neglected non-critical contributions become important here. The specific heat has to be finite and positive at the critical point, $x = 0$. Its critical part is proportional to $g'(x)$ and vanishes at the transition. Therefore, the non-critical part of the specific heat at the transition has to be positive, yielding an additional linear term to the function $g(x)$. This counteracts the shift of the straight lines in Fig. 3.1, giving rise to stable solutions.

As this linear term dominates in the vicinity of the critical point, we, thus, obtain $x \sim r$. This implies that the critical theory for constant pressures and $\alpha < 0$ has on a compressible lattice the same critical exponents as the bare model.

For the experimentally less relevant scenario of constant volume, the interaction parameter J_v is negative, however one may still perform a complex Gaussian integral,

$$\exp \left\{ -\frac{\beta |J_v|}{2V} \left[\int d\mathbf{r} \phi(\mathbf{r})^2 \right]^2 \right\} = \sqrt{\frac{2\pi\beta |J_v|}{V}} \int dv \exp \left\{ -\frac{V}{2\beta |J_v|} v^2 - iv \int d\mathbf{r} \phi(\mathbf{r})^2 \right\}, \quad (3.26)$$

and, similarly, integrate out the order parameter yielding the functional

$$\mathcal{F}_{\text{crit}} = \log \int dv \exp \left\{ -\beta V f_0 \left(r + iv \frac{2}{\beta} \right) - \frac{V}{2\beta |J_v|} v^2 \right\}. \quad (3.27)$$

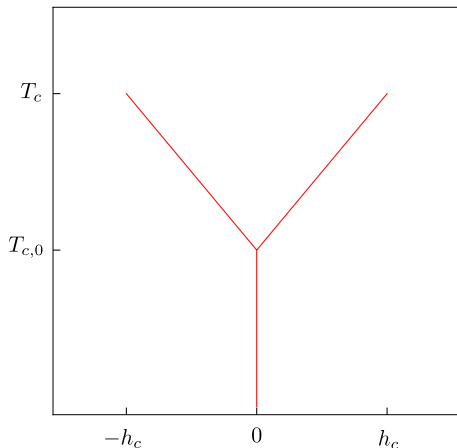


Fig. 3.2: Phase diagram for the case of strong elastic coupling. At the critical point of the bare model, $(0, T_{c,0})$, a triple point is obtained, from which two first order transition lines for finite magnetic fields emerge. The transition lines terminate in a second order critical endpoint at $(\pm h_c, T_c)$

Although, due to the complex argument, the interpretation of minimizing a free energy is no longer valid, we may nevertheless perform a saddle point approximation, which, in this case, yields only a sign change of the function $g(y)$,

$$-8 |J_v| A(2 - \alpha) |x|^{1-\alpha} \operatorname{sgn} x \stackrel{!}{=} x - r. \quad (3.28)$$

Thus, the graph of $g(x)$, depicted in Fig. 3.1, is mirrored at the y -axis and it exists always one unique solution, implying a second order phase transition.

For $\alpha < 0$, the function $g(x) - x$ is approximately linear close to the critical point. Therefore, it is $x \sim r$ and the system has Ising critical exponents. On the other hand, for $\alpha > 0$, we find that $r = x - g(x) \sim |x|^{1-\alpha}$ is non-linear and, hence, we obtain the Fisher-renormalized exponent $\alpha_F = \alpha/(1 - \alpha)$.

Strong Coupling

For a sufficiently large coupling constant, λ , the quartic term, u , is driven negative, and we have to expand the Ising potential to the sixth order for stability. Therefore, at zero magnetic field, we obtain a first order transition as function of temperature, where the order parameter jumps from zero at high temperatures to some finite value, $\phi = \phi_{\pm}$. For constant pressures the volume will jump at the same point due to the elastic coupling.

If we take the magnetic field into account, we see that for temperatures below the critical endpoint, the magnetization jumps at $h = 0$ from the positive minimum, ϕ_+ , to the negative minimum of the free energy, ϕ_- . Above the critical temperature, the system is in a disordered phase at zero field. However, the potential still has two local minima at a finite magnetization, one of which gets stabilized by applying a magnetic field. Therefore, the endpoint, $(h = 0, T_{c,0})$, is a tricritical point, from which two lines of first order phase transition emerge in the (h, T) -plane for positive and negative fields, as depicted in Fig. 3.2.

On the other hand, for high temperatures, the influence of the quartic term gets washed out, such that the first order phase transition at finite fields becomes a crossover. Therefore, these transition lines have to terminate in a second order critical endpoint, $(\pm h_c, T_c)$. At the critical endpoint, we can, again, set up a Landau theory, however, due to the finite field and magnetization, the Ising symmetry is only an emergent theory at the endpoint. Thus, odd terms in the order parameter are allowed, yielding a bilinear strain coupling which is discussed in the next section.

3.2.3 Bilinear Coupling

If away from the critical point the Ising symmetry is broken, odd powers of the order parameter are in general allowed. Shifting the order parameter such that the cubic term vanishes and neglecting terms beyond fourth order, we have the same Ising Hamiltonian as before. However, a bilinear coupling of the order parameter to the strain does now exist which reads as

$$\mathcal{H}_c = \lambda \int d\mathbf{r} \phi(\mathbf{r}) \tilde{u}_{ii}(\mathbf{r}), \quad (3.29)$$

and will dominate the thermodynamics at the transition.

The first to consider the implications of such a linear coupling were Levanyuk and Sobyenin [34]. They investigated the phase transition of ferroelectrics where a linear coupling to the strain is allowed if the paraphase above the ferroelectric transition is already piezoelectric. For simplifications, they neglected crystal anisotropies for the elastic Hamiltonian, but considered a non-isotropic coupling to the ferroelectric order parameter. With this approximation, they obtained a preemptive mean field transition with a finite jump in the specific heat, a result which was also obtained by Villain [35]. Similar, Wagner and Horner [36] considered the liquid-gas transition of hydrogen dissolved in metals. They also found mean field behavior arising from a long-ranged interaction due to the elastic coupling and, furthermore, an isotropic volume change at the transition.

Let us consider the bilinear elastic coupling of a classical Ising transition on the same theoretical grounds as the quadratic coupling in the previous section. The free energy is, again, given by the field integral Eq. (3.15). After a Fourier transformation, the coupling term reads as

$$\mathcal{H}_c = \lambda \phi_0 E + i\lambda \sum_{\mathbf{q} \neq 0} |q| \phi(\mathbf{q})^* u_L(\mathbf{q}), \quad (3.30)$$

Thus, the macroscopic strain couples to the zero momentum mode only, whereas the finite momentum modes couple to the longitudinal phonons. As in the quadratic case, we may, again, integrate out the transversal phonons and the pure shear strains, which yields only a non-critical additive term to the free energy.

Completing the squares for the macroscopic volume change, E , and the longitudinal phonons we end up with

$$\begin{aligned} \mathcal{H} = & \frac{VK}{2} \left(E + \frac{\lambda\phi_0 - p}{K} \right)^2 + \frac{V}{2} \left(K + \frac{4}{3}\mu \right) \sum_{\mathbf{q} \neq 0} \left| q u_L(\mathbf{q}) - \frac{i\lambda}{K + 4\mu/3} \phi(\mathbf{q}) \right|^2 \\ & + \int d\mathbf{r} \left[-h\phi(\mathbf{r}) + \frac{r}{2}\phi(\mathbf{r})^2 + \frac{1}{2}(\nabla\phi(\mathbf{r}))^2 + \frac{u_0}{4!}\phi(\mathbf{r})^4 \right] - \frac{J_p V}{2} \phi_0^2. \end{aligned} \quad (3.31)$$

The longitudinal phonons can be integrated out and the second line, again, denotes a renormalized Ising model, which captures all fluctuation effects, with a infinitely long range “interaction” on top. The renormalized parameters and the interaction constant, J_p , are given by

$$h = h_0 - \frac{\lambda p}{K}, \quad r = r_0 - \frac{\lambda^2}{K + 4\mu/3} \quad \text{and} \quad J_p = \lambda^2 \left(\frac{1}{K} - \frac{1}{K + \frac{4}{3}\mu} \right). \quad (3.32)$$

Note that for the bilinear coupling the critical magnetic field, $H_c = H - h$, becomes pressure dependent and is to lowest order linear in p . The renormalization of the quadratic coefficient is negative and, hence, corresponds to a shift of the critical temperature to higher values, thus, the bare Ising transition gets preempted.

The distinction between the ensemble at constant pressure and the one with a constant volume is again given by the sign of the long-ranged interaction. For constant pressure, we again integrate out the macroscopic volume change, i.e., we may skip the first term of Eq. (3.31). Instead, for constant volume, it is $E = 0$, and the first term in Eq. (3.31) drives, again, the long-ranged interaction repulsive, yielding $J_v = -\frac{\lambda^2}{K + \frac{4}{3}\mu}$. Integrating out the finite momentum components of the order parameter we obtain

$$\begin{aligned} \mathcal{F} = & -T \ln \int d\phi_0 \mathcal{D}\phi_{\mathbf{q} \neq 0} \exp \{-\beta\mathcal{H}\} \\ = & -T \ln \int d\phi_0 \exp \left\{ -\beta V \left(f_0(T, \phi_0) - \frac{J_{p/v}}{2} \phi_0^2 \right) \right\}, \end{aligned} \quad (3.33)$$

where the second line serves as a definition of the function f_0 .

For temperatures above the critical temperature of the bare Ising model, the free energy and, thus, also f_0 are analytic, hence, we may write down a Landau expansion

$$f_0(T, \phi_0) = -H(h, T) \phi_0 + \frac{a(h, T)}{2} \phi_0^2 + \frac{b(h, T)}{4!} \phi_0^4. \quad (3.34)$$

Therefore, for a constant pressure, $J_p > 0$, we obtain a mean field like critical point, at a critical temperature given by

$$a(h, T_c) = J_p. \quad (3.35)$$

Considering the experimentally less relevant scenario of a fixed volume, the long range interaction constant, J_v , is negative and, therefore, suppresses order, $\phi_0 \neq 0$. Consequently, Eq. (3.35) has no solution in its range of applicability, thus, the critical temperature of the bare Ising model can be reached. However, since the long range interactions favors the zero magnetization state, $\phi_0 = 0$, critical fluctuations become suppressed yielding mean field behavior. On a technical level, this can be shown by finite size scaling arguments, see Ref. [20].

3.3 Classification by Cowley

The bilinear coupling is always non-perturbative because the strain directly follows the order parameter and vice versa. On the basis of a pure mean field theory for an arbitrary symmetry, minimization of the general potential with respect to the strain multiplet yields

$$-\lambda \phi = C_{\Gamma} \epsilon_{\Gamma}, \quad (3.36)$$

and both quantities are in a sense equivalent, Thus, the critical theory can be analyzed in terms of the strain field, independent of the underlying type of phase transition. For such systems, a detailed analysis for all crystal symmetry classes was performed by Cowley [21], which will be discussed in the following.

As discussed in Sec. 2.2.4, a structural instability arises if one of the eigenvalues of the elastic constant matrix C_{Γ} vanishes. In this case, the crystal distorts to another structure whose symmetry is determined by the corresponding irreducible representation of the strain.

In contrast to other phase transitions, the corresponding fluctuations, i.e., the elastic waves, are not governed by the same interaction kernel than the macroscopic order parameter, as we already saw in the isotropic case. Rather than by the elastic constant matrix, they are obtained by the dynamical matrix, $D_{ik} = C_{ijkl} \hat{q}_j \hat{q}_l$, see Eq. (2.73). The eigenvalues of D , and therefore the dispersions of the phonons, depend on the direction of propagation. We obtain three eigenvalues, and three eigenvectors, i.e., phonon polarizations, \mathbf{u} , for each propagation direction, \mathbf{u} . In general, these eigenvalues are, of course, different from the eigenvalues of the elastic constant matrix.

From these considerations follows that at a structural instability the speed of sound may stay finite, which is a well known fact. It is, nevertheless, surprising when thinking about it in the framework of critical theories, where this statement implies that it is a symmetry breaking phase transition without any soft modes. This peculiarity stems from the fact that the order parameter is related to the macroscopic strain tensor which has 6 independent degrees of freedom. The long

wave length fluctuations, however, are the acoustic waves of the crystal which have only three components. Thus, in some sense, they have to be linear combinations of the strain components and so are their eigenvalues, i.e., their mass.

Considering for instance a cubic crystal, the strain tensor E splits into the three irreducible representations A, E and T_2 , as discussed in Sec. 3.1.1. The dynamical matrix for the fluctuations, on the other hand, can be written as

$$D_{ik} = \left(\frac{1}{3}(C_A - C_E) + C_T \right) q_i q_k + \left(C_T |q|^2 + (C_E - 2C_T) q_i^2 \right) \delta_{ik} \quad (3.37)$$

For the propagation along the (100) direction, one eigenvector of the dynamical matrix is the longitudinal phonon, \mathbf{u}_L , having an eigenvalue $C_{11} = \frac{1}{3}C_A + \frac{2}{3}C_E$. Thus, it is a linear combination of the singlet and doublet strains,

$$\mathbf{u}_L \cong \sqrt{\frac{1}{3}}A_1 + \sqrt{\frac{2}{3}}E \quad (3.38)$$

The transversal phonons, on the other hand, have the eigenvalue $C_{44} = C_T$, i.e., of the triplet, T.

At a phase transition, one has, thus, to determine whether or not elastic waves with frequencies solely given by the vanishing eigenvalue of the elastic constant matrix exist. For elastically non-isotropic systems there are in principle three different possibilities which Cowley termed type 0, I and II and are discussed in following.

First of all, instabilities of type 0 have no critical phonons, as, for instance, an instability of the singlet, A in the cubic case. The singlet has the full cubic symmetry, whereas any wave vector, \mathbf{q} , necessarily breaks some of the symmetries. Thus, at a phase transition, the fluctuations are always gapped and will only appear on length scales comparable to the sample size. In the thermodynamic limit, $V \rightarrow \infty$, the transition, hence, becomes mean field like.

If, on the other hand, the eigenvalue of the doublet, E, vanishes, it exists a one-dimensional subspace of phonon modes which become soft. Such a situation is denoted as behavior of type I. These soft phonons with an eigenvalue C_E propagate on a face diagonal, e.g., in the direction [110]. Their polarization vector lies on the same face but perpendicular to the propagation vector, i.e., $[\bar{1}\bar{1}0]$.

Finally at instabilities of type II, there is a whole plane of soft propagation directions, \mathbf{q} . In cubic crystals this happens if C_T becomes small, i.e., for a triplet instability. We then find that transverse waves polarized along one of the cubic axis of the crystal all have the eigenvalue $C_{44} = C_T$.

In isotropic crystals, the soft phonons cannot break this isotropy, which leaves two possibilities. Either, there are no soft acoustic waves close to the instability at all, which is the case for the single eigenvalue C_{11} , corresponding to an isotropic volume change. The other case is a melting process, where soft phonons for every

direction. Obviously the isotropy is preserved and the soft propagation vectors span the whole three dimensional momentum space. Consequently, Cowley denotes these instabilities with respect to the eigenvalue C_{44} as type III. The classification of the behavior of the elastic fluctuations for all 32 crystallographic point groups, as done by Cowley [21], is summarized in App. B.

To analyze the nature of the respective phase transition, Cowley [21], further on, investigated for which symmetries a cubic invariant of the irreducible representations of the strain exists. In presence of a third order invariant, Landau theory yields a first order transition, at least for doublet and triplet representations. Notably, in case of a very small cubic term, fluctuations may still become large, though not divergent.

For singlets, a proper rescaling of the order parameter cancels the cubic term. Upon fine-tuning one can also drive the linear and the quadratic term to zero and, thus, obtains a critical point in phase space where the transition may be still of second order. However, as it turns out, all singlet instabilities, where symmetry allows a cubic term, are of type 0, and, therefore, this classical critical endpoint shows always mean field behavior.

If there is no cubic invariant of the strain tensor, the respective phase transition is, in case of a positive quartic term, of second order. This happens for the strain singlets of orthogonal crystals and some of the singlets as well as the doublet of tetragonal crystals. For these cases, the influence of the elastic fluctuations, i.e., acoustic waves of type I or type II, have to be taken into account which was done by means of renormalization group techniques.

As a result, the singlets of orthorhombic and the tetragonal crystals show, again, mean field behavior. The flow equations concerning the doublet of tetragonal crystals were intractable, however, Cowley argues that they, most likely, yield a first order transition.

In conclusion, all structural transitions are either of first order or a classical, i.e., mean field like, second order transition. If an order parameter of some other symmetry breaking phase transition and the strain are coupled bilinear, the two order parameters directly follow each other. Thus, the latter phase transition will also become a first order transition or mean field like.

Chapter 4

Mott-Transition on Compressible Lattices

As it was summarized in Chap. 3, the nature of a phase transition may be dramatically changed by the influence of the elastic degrees of freedom. Pressure couples to the lattice degrees of freedom, by changing the distance between neighboring sites. This in turn affects the electronic interactions as the overlap between wave functions depends on their distance. In combination with the non-linear tensorial structure of crystal elasticity this may lead to non-perturbative effects changing the whole nature of an electronic phase transition.

In this chapter we will investigate the influence of the elastic lattice on a particular phase transition at finite temperatures, namely the pressure driven Mott metal-insulator transition. The Mott transition is a well studied electronic phase transition and a paradigm for strongly correlated systems in condensed matter physics. For systems with exactly one electrons per site, i.e., at half filling, the ratio of the strength of the Coulomb repulsion to the kinetic energy of the single electrons determines their mobility. As the Coulomb repulsion grows the electrons avoid each other and at half filling, eventually, freeze out, such that the conductivity vanishes. A brief recapitulation of the basic concepts of the electronic Mott metal-insulator transition is given in Sec. 4.1.1

In particular, the nature of the critical endpoint of the first order Mott transition is subject of a long-standing discussion. As we will review in Sec. 4.1.2, theoretical work suggests that the Mott transition belongs to the Ising universality class, however, experimental observations seem to contradict this statement.

In this chapter, we will argue, that these observations may be explained by the coupling to the elastic degrees of freedom. Assuming that the bare electronic Mott transition indeed belongs to the Ising universality class, we find that the Mott transition on compressible lattices, i.e., in every solid state realization, does not show Ising critical, but rather mean field behavior in the vicinity of the endpoint.

The mean field behavior is a result of a non-perturbative bilinear coupling between the electronic and the elastic degrees of freedom which is specified in Sec. 4.2. In the following Sec. 4.3, we will derive an expression for the free energy of the elastically coupled Mott transition and discuss the resulting features of the thermodynamic quantities (Sec. 4.4).

This work is mainly motivated by Refs. [1, 2], where the thermodynamics of an organic salt of the series κ -(BEDT-TTF)₂X were investigated. The Mott transition in these compounds can be tuned by pressure and the members of this series are at ambient pressures located at different points of the phase diagram. Thus, they have different pressure distances to the critical endpoint and are good candidates to investigate the elastic influence on the critical behavior of the phase transition. In Sec. 4.5, we, therefore, address the quantitative implications of the elastic coupling on these compounds. In particular, we estimate the range of the so-called non-perturbative regime in the phase diagram, where the coupling to the lattice changes the nature of the critical point. Furthermore, based on fits obtained by Bartosch et al. [2], we show how the thermodynamics quantitatively change.

Additionally, we consider another well studied example for pressure driven Mott transitions, namely the chromium doped V₂O₃, which shows in experiments hardly any indications of Ising critical behavior. We will show, that this observation can be explained by critical elasticity and propose further experiments to substantiate this explanation

Large parts of this chapter we have published in Ref. [37].

4.1 Mott Metal-Insulator Transition

With the concept of Bloch's band theory of electrons in solids [38], the distinction between metals and insulators was made according to the band filling. In metals at least one band is only partially filled i.e., the Fermi energy lies within an electron band, whereas insulators have no states at the Fermi energy, having only completely filled or empty bands. The band theory relies on the assumption that the electron-electron interactions are very weak, which due to the screening of the Coulomb interaction is often the case.

However, with the discovery of the insulating behavior of many transition metal oxides with partially filled *d*-bands [39], this classification became questionable, as they should be good metals according to the band picture. Following suggestions by Peirels, Mott argued that strong electron interactions might be the reason for the insulating behavior [40]. This metal-insulator transition, subsequently named Mott transition, became one of the outstanding examples of strongly correlated electron systems, a field which since then developed into one of the most exciting branches in condensed matter theory. In the following, we will introduce the basic concepts

of the Mott transition. For further studies, the reader may be referred to the very detailed review of Imada et al. [41].

4.1.1 Basic Concepts

The basic idea of the mechanism at play in a Mott insulator can be understood from a seemingly simple model, namely the Hubbard model [42]. For details of its derivation see for instance Rev. [43]. The Hubbard model is a simplified lattice fermion model where the Hamiltonian is given by

$$H = - \sum_{i,j,\sigma} t_{ij} \left(c_{i,\sigma}^\dagger c_{j,\sigma} + \text{h.c.} \right) + U \sum_i n_{i,\uparrow} n_{i,\downarrow}. \quad (4.1)$$

The first term accounts for hopping of electrons with spin σ from one site, j , to another site, i , which yields a gain in kinetic energy of t_{ij} . The hopping amplitude is determined as the expectation value of the kinetic energy when hopping from an atomic Wannier orbitals centered at site i , $\phi_{i,\sigma}(\mathbf{r})$, to another one centered at site j ,

$$t_{ij} = \int d\mathbf{r} \phi_{i,\sigma}^*(\mathbf{r}) \left[\frac{\nabla^2}{2m} - \sum_l V_{\text{lat}}(\mathbf{R}_l - \mathbf{r}) \right] \phi_{j,\sigma}(\mathbf{r}). \quad (4.2)$$

where $V_{\text{lat}}(\mathbf{R}_l - \mathbf{r})$ accounts for the lattice potential due to the ion at site \mathbf{R}_l .

As, for instance, the d -electrons are strongly localized at the positions of the ions, the overlap between Wannier orbitals centered at distant sites is very small such that it is sufficient to taken only hopping between nearest neighbors into account. Additionally, depending on the lattice structure, the hopping amplitude often only weakly depends on the site indices and is, therefore, simplified to $t_{ij} = t$ for nearest neighbors and $t_{ij} = 0$ otherwise.

The second term accounts for the Coulomb repulsion which is simplified to a local on-site interaction; a doubly occupied site costs an energy U , which is given as

$$U = \int d\mathbf{r} d\mathbf{r}' \phi_{i,\sigma}^*(\mathbf{r}) \phi_{i,\sigma}(\mathbf{r}) \frac{e^2}{|\mathbf{r} - \mathbf{r}'|} \phi_{i,\bar{\sigma}}^*(\mathbf{r}') \phi_{i,\bar{\sigma}}(\mathbf{r}'). \quad (4.3)$$

This model is clearly oversimplified as it, for example, takes only one localized electron orbital per ion into account, whereas especially in the transition metals the d -electrons have an orbital degeneracy. Despite the simplifications, the Hubbard model describes very well the low-energy properties of many systems. This is because often only few or even just one band cross the Fermi level and are, thus, relevant for low-energy excitations. However, multiband-effects strongly renormalize the actual value for the parameters t and U .

The behavior of the system depends on the relative strength of both terms and on the filling. For small on-site repulsion $t \gg U$ the electrons move freely through

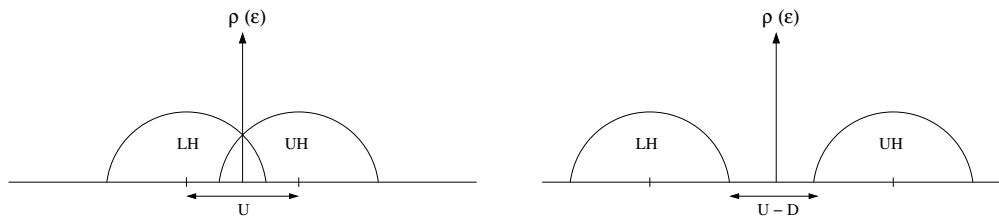


Fig. 4.1: Density of states in the Hubbard approximation. The lower (LH) and upper Hubbard band (UH) cross the Fermi energy in the metallic phase, thus allowing for a finite conductivity (left). For $U > U_c$, the two Hubbard bands are separated by an energy $U - D$ where D is the non-interacting bandwidth.

the system, which, therefore is metallic. In the opposite limit, $t \ll U$, double occupancies are strongly suppressed, thus, if there is one electron per site, i.e., at exactly half filling, the electrons are strongly localized forming an insulator. These two phases are separated by a phase transition at a critical value $U = U_c$.

Despite its apparent simplicity, there is no exact solution of the Hubbard model and the nature of the transition from the metallic to the insulating phase is hard to determine. In his original work [42], Hubbard analyzed it by starting from the atomic limit, $t = 0$, applying perturbation theory. This ansatz results in a spectral function which consists of two bands, the so-called upper Hubbard band, corresponding to the doubly occupied sites, and lower Hubbard band, corresponding to the empty sites, see Fig. 4.1. They have a distance from the Fermi energy of $(U - D)/2$ where $D \sim t$ is the non-interacting bandwidth. Upon increasing t , the two bands approach each other until they cross the Fermi energy, thus we get a continuous transition from the insulating to the metallic phase.

Although this analysis does predict the Mott transition, there are important features which are not captured in this approach. First of all, it does not recover a metal with Fermi liquid properties. Furthermore, it identifies the finite temperature Mott transition as a continuous phase transition, although it is actually a first order transition. Additionally, experimentally a very large effective mass of the quasiparticles in the metallic phase was found close to the transition, which would correspond to a sharp peak in the density of states at the Fermi level.

These effects could be explained by the dynamical mean field theory (DMFT), ([44–46]), which becomes exact in the limit of infinite coordination number. It shows that the density of states not only develops two peaks corresponding to the upper and lower Hubbard band, but also a very pronounced peak emerges at the Fermi energy, the so-called Kondo resonance (see Fig. 4.2). When approaching the Mott transition, spectral weight is transferred from the Fermi energy to the Hubbard bands and the peak becomes sharper. This yields a large effective mass, which grows inversely with the weight of the peak, for the quasiparticles at the Fermi energy.

The DMFT results also identify the finite temperature Mott transition as a first order phase transition. The transition line is surrounded by a coexistence regime

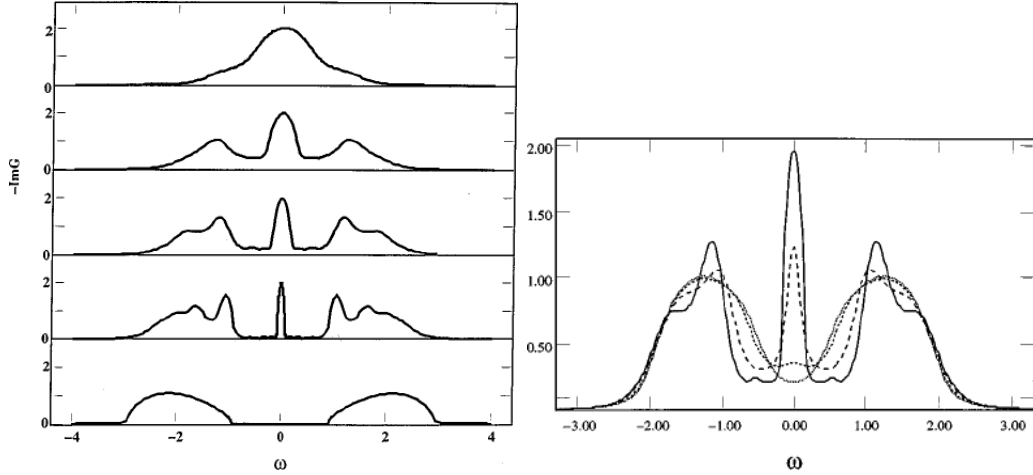


Fig. 4.2: Local spectral density $\pi D\rho(\omega) = -\text{Im} G$ close to the Mott transition for $T = 0$ and increasing U (left; top to bottom) and for increasing temperature (right; full, dashed, short-dashed, dotted) obtained by DMFT (taken from Ref. [47]). In both cases, two peaks emerge above and below the Fermi energy, $\omega = 0$, as predicted by perturbation theory. Exactly at the Fermi energy a sharp quasiparticle peak (also called Kondo resonance) prevails until the Mott insulating phase is entered.

$U_{c1}(T) < U < U_{c2}(T)$ between which a metastable minimum of the free energy exists. Approaching zero temperature the transition line terminates in U_{c2} . Here, the quantum phase transition is somewhat peculiar, in the sense that the transition has some continuous aspects, but the gap between upper and lower Hubbard band opens abruptly, yielding a non-critical spectrum.

However, the DMFT results does not reflect the real physics at lowest temperatures since Mott insulators often develop an antiferromagnetic ordering. The latter is already captured by the Hubbard model Eq. (4.1). At half filling, the charge degrees of freedom are in the limit $U \gg t$ completely frozen out, since on every site sits exactly one electron. If neighboring sites have the same spin orientation, also the spin degrees of freedom are frozen out, whereas for an antiferromagnetic ordering there is the possibility of virtual hopping depicted in Fig. 4.3, where two neighboring electrons exchange places.

This effect is explained by second order perturbation theory in the parameter t/U . Let us consider a simple two-site system which is in the antiferromagnetically aligned spin state $|\psi\rangle = |\uparrow\rangle_1 |\downarrow\rangle_2$ and has an energy of $E_0 = 0$. The hopping term of the Hubbard model is an off-diagonal term, changing the spin state, for instance, to $|\psi'\rangle = |0\rangle_1 |\uparrow\downarrow\rangle_2$, which has an energy $E_1 = U$. Therefore, in second order perturbation theory, we obtain an energy gain, ΔE , by such a virtual hopping process which is

$$\Delta E = \frac{\left| \langle \uparrow \rangle_1 \langle \downarrow \rangle_2 t c_{1,\uparrow}^\dagger c_{2,\downarrow} | 0 \rangle_1 |\uparrow\downarrow\rangle_2 \right|^2}{E_0 - E_n} = -\frac{t^2}{U}. \quad (4.4)$$

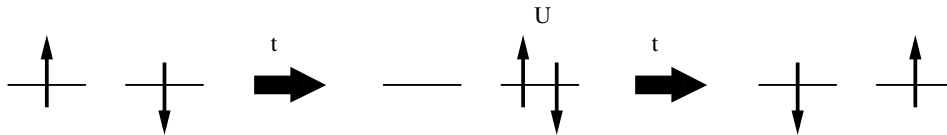


Fig. 4.3: Schematical picture of a virtual hopping process. For antiferromagnetically aligned spins, one spin electron can hop on the neighboring site giving an energy t . This doubly occupied site costs an energy U and decays in the final state with again one electron per site releasing an energy t . Upon this process the spins on the two lattice sites may have been flipped, thus the spin degrees of freedom are not frozen out.

In contrast, for ferromagnetically ordered spins we obtain $\Delta E = 0$ since double occupancies are forbidden due to the Pauli principle. Taking into account, that the above hopping process may also happen in the other direction, i.e., with an unoccupied site $|0\rangle_2$, and with or without a spin flip we conclude that the effective spin dynamics are governed by an antiferromagnetic Heisenberg Hamiltonian

$$H = J \sum_{\langle ij \rangle} \mathbf{S}_i \cdot \mathbf{S}_j, \quad \text{with } J = \frac{4t^2}{U}. \quad (4.5)$$

As plain DMFT is a local theory, such non-local magnetic ordering effects cannot be captured, though it is included in more sophisticated DMFT-schemes.

In Fig. 4.4 we show the phase diagram for V_2O_3 which becomes a Mott insulator for negative pressure achieved for instance by chemical doping with chromium. As mentioned above, the compound is antiferromagnetic at low temperatures. Above the Néel temperature and for low pressures the system is in a Mott insulating state. Increasing pressure, the hopping amplitude grows and the system eventually becomes metallic. These two phases are separated by a line of first order transitions.

4.1.2 Universality Class

As no symmetry is broken at a Mott transition, one may avoid the first order transition at high temperatures, giving rise to a second order critical endpoint at (T_c, U_c) which terminates the line of first order transitions, see Fig. 4.4. Above this endpoint only a crossover between the metallic and the insulating phase exists. The nature of this critical endpoint and its universality is a long-standing discussion.

The phase diagram of the pressure tuned Mott transition has apparent similarities to the liquid-gas transition. First of all, it is a pressure tuned, finite temperature phase transition, terminating in a critical endpoint. Secondly, the order parameter at the endpoint of the liquid-gas transition is the relative density and similarly one could think of the order parameter of the Mott transition as the density of doubly-occupied sites. As the liquid-gas endpoint is known to belong to the Ising universality class, the same may be true for the Mott transition.

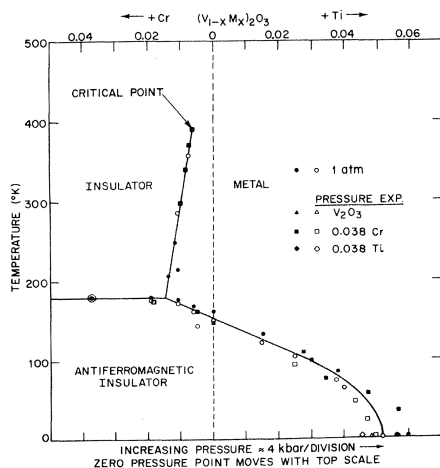


Fig. 4.4: Phase diagram for the Mott metal-insulator transition for V_2O_3 (from Ref. [48]). The metallic and the Mott insulating phase are separated by a first order transition line. As no symmetry is broken at the transition, one can circumvent this transition at higher temperatures. Thus, the transition line terminates at a second order critical endpoint.

These theoretical considerations were substantiated by Castellani et al. [49] who by symmetry arguments mapped the Hubbard model onto the so-called Blume-Emery-Griffiths Hamiltonian (BEG) which describes the λ -transition of a He^4 - He^3 -mixture [50]. The BEG model belongs indeed to the universality class of the Ising model, however, the mapping is not precise but yields an extra term. About twenty years later an Ising-like Landau functional for the Mott transition was constructed by DMFT calculations [51], a result which later was supported by further work adding spatial fluctuations to the DMFT calculation [52]. Also a two-step density-matrix renormalization group study found 2D Ising critical behavior [53].

Experimentally, however, contradictory observations were made. For instance, chromium doped V_2O_3 , one of the best studied Mott insulators, was investigated by conduction measurements [54]. The critical exponents obtained by this measurement were for large pressure and temperature ranges found to agree with mean field exponents rather than with Ising critical exponents. Only at very small distances from the endpoint a deviation, interpreted as a crossover to 3D Ising critical behavior, was found.

Similar conduction measurements on an organic quasi-two dimensional salt of the κ -(BEDT-TTF) $_2X$ family yielded a set of critical exponents $(\delta, \beta, \gamma) = (2, 1, 1)$ [55] which is different from the ones of the 2D and 3D Ising universality class as well as from the mean field exponents. Furthermore, they did not even match any set of critical exponents of a related universality class, such as the Heisenberg or the XY-model, though they obeyed scaling relations. Therefore, it was interpreted as the discovery of a new universality class.

Papanikolaou et al. [56] did, however, explain these exponents within Ising criticality. They argued that the measured conductance, G , is not a direct measurement of the order parameter of the transition, but it has the general form

$$G = G_0 + f_m \langle m \rangle + f_\epsilon \langle \epsilon \rangle. \quad (4.6)$$

The second term is proportional to the order parameter, m , whereas the third term is given by the energy density, ϵ . The relative magnitude of f_ϵ and f_m determines a crossover from an energy dominated regime to an order parameter dominated regime. For $f_\epsilon \gg f_m$ indeed the order parameter determines the conductivity at long length scales, $G - G_0 \sim \langle m \rangle$, but at short length scales we have $G - G_0 \sim \langle \epsilon \rangle$.

In terms of the critical exponents of the order parameter, $\langle m \rangle \sim |T - T^c|^\beta$, and the specific heat, $C \sim \partial_T \epsilon \sim |T - T^c|^{-\alpha}$, this implies

$$G - G_0 \sim \langle m \rangle^{-(\alpha-1)/\beta}. \quad (4.7)$$

The following conversion of the measured conductivity exponents indeed recovered the critical exponents of the 2D Ising universality class. Later dilatometric data on the same compound [1] could also be fitted to the 2D Ising free energy [2].

In summary, there are indications that the Mott transition belongs to the Ising universality class. However, there are also contradictory experimental results, therefore the question of the nature of the critical endpoint is not yet conclusively answered.

4.1.3 The Ising Field Theory

To describe the finite temperature Mott transition close to the critical endpoint, we would like to write down a Landau functional. As discussed in Sec. 4.1.2, the theoretical considerations as well as some experimental results suggest that the Mott transition belongs to the Ising universality class. Therefore, we will start from the assumption, that the bare Mott transition is indeed described by an Ising theory. The contradictory behavior seen in experiments on V_2O_3 Ref. [54] will be addressed in Sec. 4.5.

The order parameter, ϕ , in which the Landau functional is formulated may, as explained, be viewed as the density of the doubly occupied sites. More precise, it is associated with the amplitude of the quasiparticle peak, as discussed in Ref. [51]. There are two relevant perturbations in the Ising model, namely the reduced temperature, $\Delta T = (T - T_c)/T_c$, where T_c denotes the critical temperature, and the magnetic field H . Close to the critical point where the magnetization is small and only long wavelength fluctuations are important, the effective field theory for the Ising model is given as

$$S[\phi] = \int d^d \mathbf{r} \left\{ \frac{1}{2} (\partial \phi)^2 + \frac{r}{2} \phi^2 - \tilde{h} \phi + \frac{u}{4!} \phi^4 \right\}. \quad (4.8)$$

The parameters r and \tilde{h} are the deviations from the critical point

$$r = C_r \Delta T (1 + \mathcal{O}(\Delta T, H^2)) \quad \text{and} \quad \tilde{h} = C_H H (1 + \mathcal{O}(\Delta T, H^2)), \quad (4.9)$$

where the positive constants C_r and C_H are non-universal and depend on the microscopic model. The quartic interaction, u , is also a non-universal constant and higher order interactions are neglected as they are irrelevant in the RG-sense.

	α $C \sim \Delta T ^{-\alpha}$	β $\phi \sim \Delta T ^\beta$	γ $\chi \sim \Delta T ^{-\gamma}$	δ $\phi \sim h ^{1/\delta}$	η $C(\mathbf{r}) \sim \mathbf{r} ^{2-d-\eta}$	ν $\xi \sim \Delta T ^{-\nu}$
D=2	0	$\frac{1}{8}$	$\frac{7}{4}$	15	$\frac{1}{4}$	1
D=3	0.11	0.33	1.24	4.789	0.036	0.63
mean field	0	$\frac{1}{2}$	1	3		$\frac{1}{2}$

Tab. 4.1: Critical exponents of the Ising universality class for two and three dimensions as well as the mean field values taken from Ref [57]. The mean field exponents and the ones for $D = 2$ are exact, whereas the exponents in three dimensions are determined numerically.

According to the scaling hypothesis, the singular part of the free energy, f_{sing} , can be described by a single homogeneous function, g , which controls the thermodynamic properties of the critical point,

$$f_{\text{sing}}(\Delta T, \tilde{h}) = \Delta T^{2-\alpha} g \left(\Delta T |\tilde{h}|^{(\delta-1)/(\gamma\delta)} \right). \quad (4.10)$$

The exponents α , γ and δ are the critical exponents of the universality class which for the Ising class are given in Tab. 4.1.

Since our work was motivated by measurements of the Mott transition in the compound κ -(BEDT-TTF)₂X which is a quasi-2D material, we will focus in the following mainly on the 2D Ising model. Belavin, Polyakov and Zamolodchikov proposed in two seminal papers [58, 59] the full conformal invariance of the 2D Ising theory, which could explain many phenomena. This was only recently proven mathematically rigorously for some observables by Chelkak and Smirnov [60].

The analytic properties of the singular part of the free energy, f_{sing} , were analyzed in great detail by Fonseca and Zamolodchikov [61]. It is formulated in terms of the temperature, $\tau = C_\tau \Delta T (1 + \mathcal{O}(\Delta T, H^2))$, and the magnetic field, $h = C_h H (1 + \mathcal{O}(\Delta T, H^2))$. Since C_τ and C_h are again positive constants depending on the microscopic details, τ and h are proportional to r and \tilde{h} . The singular part of the free energy in two dimensions is given by

$$f_{\text{sing}}(\tau, h) = \frac{\tau^2}{8\pi} \log \tau^2 + |h|^{16/15} \Phi \left(\tau |h|^{-8/15} \right), \quad (4.11)$$

where the asymptotic behavior of the universal scaling function, Φ , was obtained as

$$\Phi(x) = \begin{cases} -c_1 x^{-7/4} + c_2 x^{-22/4} & , \quad x \gg 1 \quad \text{(I)} \\ -\tilde{c}_1 (-x)^{1/8} - \tilde{c}_2 (-x)^{-7/4} & , \quad -x \gg 1 \quad \text{(II)} \\ -\frac{x^2}{8\pi} \log x^2 - \phi_0 + \phi_1 x + \phi_2 x^2 & , \quad |x| \ll 1 \quad \text{(III)} \end{cases}. \quad (4.12)$$

by Fonseca and Zamolodchikov [61] and the roman numbers in parenthesis refer to the regions in the (h, τ) -space depicted in Fig. 4.5.

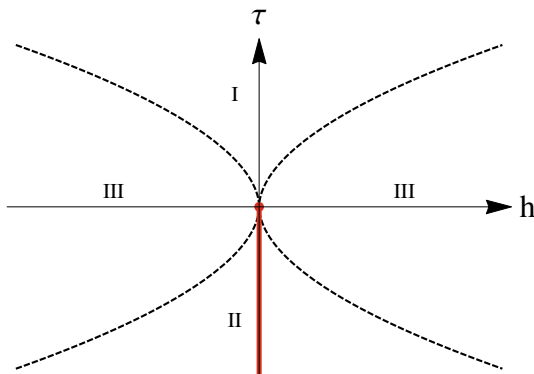


Fig. 4.5: Crossover lines of the Ising critical free energy function. The red line indicates the first order transition which terminates at the critical endpoint at $(\tau, h) = (0, 0)$.

The numerical value of the constants appearing in Eq. (4.12) were also calculated with high precision in Ref. [61] and are approximately given by

$$c_1 = 1.845, \quad c_2 = 8.334, \quad \tilde{c}_1 = 1.358, \quad \tilde{c}_2 = 0.049 \quad (4.13)$$

$$\phi_0 \approx 1.198, \quad \phi_1 \approx 0.319, \quad \phi_2 \approx 0.111.$$

The two relevant parameters for the Hubbard model at half filling are the reduced temperature, ΔT , and the ratio of kinetic to potential energy, t/U , which is driven by pressure. As there is no exact mapping of the Hubbard to the Ising model, one has to assume that, in principle, both contribute to the temperature-like parameter τ as well as to the field-like parameter, h .

However, the direction of the τ -axis in the (T, p) -phase diagram is determined by the tangent of the first order transition line at the critical endpoint. This implies that in case of a low temperature critical endpoint, the parameter τ is, in principal, given by the temperature which may be seen by the Clausius-Clapeyron relation. The latter states that the slope of the line of first order transitions is given by the ratio of the volume change and the entropy change

$$\frac{\partial T_c}{\partial p} \sim \frac{\Delta V}{\Delta S}. \quad (4.14)$$

At a pressure driven first order transition, the volume necessarily jumps yielding a finite ΔV . On the other hand, according to the Nernst theorem, the entropy approaches a constant at zero temperature, i.e., $\Delta S \rightarrow 0$. As a result, the derivative diverges and the first order transition line emerges vertical from the zero temperature axis. For small critical temperatures the finite curvature due to the finite temperatures, will only be a sub-leading effect and we may approximate $\tau \sim \Delta T$. As seen in Fig. 4.4, the transition line for V_2O_3 terminates at the critical endpoint with a finite slope and by linearization one may obtain the local $\tau(T, p)$ -axis. Notably the $h(T, p)$ -axis is in general not perpendicular to it.

4.2 Coupling to the Lattice

Pressure tuning of the Mott transition necessarily implies a coupling of the electronic degrees of freedom to the underlying lattice. As one applies pressure to the crystal, the lattice sites get closer together, which in turn allows for a larger overlap of the electronic wave functions, resulting in a larger hopping amplitude t . Thus, to understand the pressure driven Mott transition, it is important to investigate the coupling between the electronic and the elastic degrees of freedom.

As discussed in Chap. 2, the potential of the elastic system is given in terms of the strain tensor $u_{ij}(\mathbf{r})$ by

$$\mathcal{V}_{\text{el}} = u_{ij}(\mathbf{r}) C_{ijkl} u_{kl}(\mathbf{r}) + u_{ij}(\mathbf{r}) \sigma_{ij}(\mathbf{r}), \quad (4.15)$$

where σ_{ij} accounts for the external macroscopic stress and C_{ijkl} is the elastic constant matrix.

In lowest order the coupling to the electronic degrees of freedom will be linear in the strain tensor. The order parameter field, ϕ , can couple both, linearly and quadratically to the strain, since the Ising symmetry is only an emergent symmetry at the critical endpoint. Thus, the interaction is given by

$$\mathcal{L}_{\text{int}}[\phi, u_{ij}] = -\tilde{\gamma}_{1,ij} u_{ij} \phi + \frac{1}{2} \tilde{\gamma}_{2,ij} u_{ij} \phi^2, \quad (4.16)$$

with a certain set of coupling constants $\tilde{\gamma}_{1,ij}$ and $\tilde{\gamma}_{2,ij}$. The respective relevance of these two terms can be obtained by comparing them to the terms of the Ising theory, Eq. (4.8). We identify the bilinear term as the most important coupling since the elastic degrees of freedom act as an additional magnetic field, $\delta\tilde{h}$, in the Ising theory which is the most relevant parameter. The quadratic coupling, on the other hand, yields a shift in $r \sim T - T_c$ and, thus, gives a renormalization of the critical temperature. Additionally, it induces non-local interactions of the order parameter, $r(\mathbf{q}) \sim u_{i,j}(\mathbf{q})$, which are not considered in the following.

We may also take the different point of view and consider the effect of the electronic degrees of freedom on the elastic system. In second order perturbation theory, the bilinear term yields a renormalization of the elastic tensor proportional to $\delta C_{ijkl} \sim \langle \phi \phi \rangle \sim \chi$. Since, this renormalization corresponds to the susceptibility, χ , which close to the critical endpoint inevitably diverges, at least one of the elastic moduli is driven to zero at some finite $\Delta T > 0$. This, as explained in Chap. 3, leads to a crystal softening which induces a structural transition preempting the Mott transition. In turn the structural transition will trigger the metal-insulator transition. This shift of the transition temperature was also pointed out in Ref. [62].

The acoustic modes, on the other hand, are not governed by the elastic moduli itself but rather by the dynamical matrix $M_{il} = \sum_{jk} C_{ijkl} \mathbf{q}_j \mathbf{q}_k$ depending on the

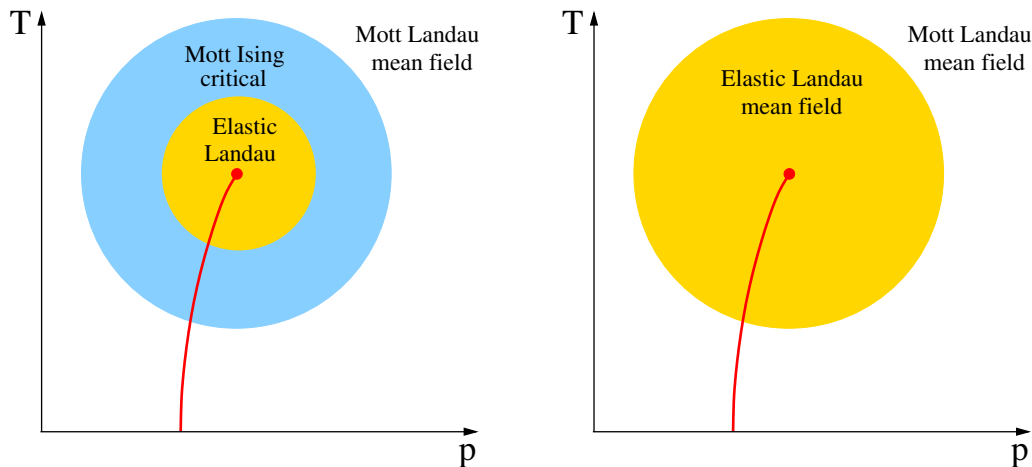


Fig. 4.6: Depending on the extent of the elastic Landau critical regime there are two possible scenarios of the Mott transition. Either, as depicted on the left hand side, the system undergoes first a crossover from the Mott-Landau regime where it shows mean field behavior to the Ising critical regime. Only closer to the endpoint the system has a second crossover to the elastic Landau regime where mean field behavior is recovered. If the elastic Landau regime is much larger, there may be no Ising critical region at all and only a single crossover from the Mott-Landau to the elastic Landau critical regime occurs.

vector of propagation, \mathbf{q} , of the acoustic mode. Its eigenvalues will soften at a lattice instability but, in general, remain finite due to the finite shear moduli. Consequently, the structural transition can be described within standard Landau mean-field theory as the acoustic modes remain non-critical. Thus, we can neglect the latter in the following and consider only the macroscopic strain, E_{ij} , determined by

$$\frac{1}{V} \int \mathcal{V}_{\text{el}} + \mathcal{L}_{\text{int}} \, \mathbf{dr} = E_{ij} C_{ijkl} E_{kl} + E_{ij} \bar{\sigma}_{ij} + \tilde{\gamma}_{1,ij} E_{ij} \phi + \tilde{\gamma}_{2,ij} E_{ij} \phi^2, \quad (4.17)$$

where $\bar{\sigma}_{ij}$ denotes the spatial average of the stress tensor.

4.3 Free Energy

As mentioned in Sec. 4.1.3, we assume that the bare Mott transition shows Ising critical behavior. This is of course only true within a finite region around the critical point where interaction effects are strong, i.e., if the resulting mass renormalization is much larger than the bare mass, $r \ll u (\langle \phi^2 \rangle - \langle \phi^2 \rangle_0)$. Here, $\langle \phi^2 \rangle_0$ captures some cutoff-dependent renormalizations of the interaction constant, u . If this so-called Ginzburg criterion is violated, the system displays mean field behavior. As we will explicate below, in the vicinity of the Mott-endpoint on a compressible lattice the system does not show Ising critical behavior due to the elastic coupling. Depending on the strength of the elastic coupling, there are two possible scenarios as depicted in Fig. 4.6. For strong elastic couplings, the regime of critical elasticity may be so

large, that Ising critical behavior will not develop at all. For weak elastic couplings, Ising criticality can be observed around the endpoint and the elastic coupling will affect the system only at much smaller distances from the endpoint. In the following analysis, we assume the latter scenario.

The singular part of the free energy of the bare electronic system is then given by Eq. (4.11) depending on the two parameters $\tau = r C_\tau / C_r$ and $h = \tilde{h} C_h / C_H$. On the other hand, we have seen that the interaction with the elastic degrees of freedom yields a renormalization of the electronic parameters, $\delta\tilde{h} = \tilde{\gamma}_{1,ij} E_{ij}$ and $\delta r = \tilde{\gamma}_{2,ij} E_{ij}$. Thus, denoting $\gamma_{2,ij} = \tilde{\gamma}_{2,ij} C_\tau / C_r$ and $\gamma_{1,ij} = \tilde{\gamma}_{1,ij} C_h / C_H$ we may substitute parameters of the bare Mott transition, τ and h_0 , in the argument of the electronic free energy by the elastically renormalized values and obtain the effective elastic potential

$$V(E_{ij}) = E_{ij} C_{ijkl} E_{kl} + E_{ij} \bar{\sigma}_{ij} + f_{\text{sing}}(\tau + \gamma_{2,ij} E_{ij}, h_0 + \gamma_{1,ij} E_{ij}), \quad (4.18)$$

To obtain the free energy density of the coupled system, we have to minimize Eq. (4.18) with respect to the macroscopic strain fields.

Due to the bilinear coupling, only singlets of the irreducible representation of the crystal group couple to the Mott degrees of freedom as discussed in Sec. 3.1. In the following, we will, for simplicity, only consider the strongest coupled singlet, E which becomes critical first. The corresponding potential Eq. (4.18) reads as

$$V(E) = \frac{K_0}{2} E^2 - p E + f_0 f_{\text{sing}}(\tau + \gamma_2 E, h_0 + \gamma_1 E), \quad (4.19)$$

with K_0 being the bare eigenvalue of the elastic constant matrix which corresponds to the strain E . Furthermore, we consider hydrostatic pressure $\bar{\sigma}_{ij} = -p \delta_{ij}$ and assume that it has a finite overlap with E . As f_{sing} is a dimensionless quantity, we have to take a non-universal scale factor f_0 into account to get the right units. For simplicity, it is set to one in the following, which corresponds to measuring the bulk modulus, K_0 , and the pressure, p , on a scale set by f_0 .

4.3.1 Perturbative Solution

To obtain the macroscopic strain field E we have to minimize the potential Eq. (4.19). Sufficiently far from the Mott endpoint, the fluctuations originating from the Ising theory are weak. Thus, we can minimize the potential Eq. (4.19), perturbatively in the elastic couplings, γ_1 and γ_2 , by expanding the singular part of the free energy. To lowest order the solution is simply given by $E = p/K_0$ and, hence, the free energy density of the system is obtained as

$$\mathcal{F}_{\text{pert}} = -\frac{p^2}{2K_0} + f_{\text{sing}}\left(\tau + \gamma_2 \frac{p}{K_0}, h_0 + \gamma_1 \frac{p}{K_0}\right). \quad (4.20)$$

Hence, the elastic coupling leads to a pressure dependence of the arguments of the singular part of the Ising free energy. Thereby, the elastic coupling, Eq. (4.16), makes the Mott transition amenable to pressure tuning, i.e., we can control the distance to the critical endpoint with p . In particular, the dependence of the arguments on the pressure is linear which is the assumption made in Ref. [2].

The critical point is identified by the condition that the arguments of the function f_{sing} have to vanish which leads to $p_{c,0} = -h_0 K_0/\gamma_1$ and $\tau_{c,0} = \gamma_2 h_0/\gamma_1$. Defining the quantities $t_0 = \tau - \tau_{c,0}$ and $\tilde{p} = \gamma_1 (p - p_{c,0})/K_0$, Eq. (4.20) takes the form

$$\mathcal{F}_{\text{pert}} = -\frac{K_0}{2\gamma_1^2}(\tilde{p} - h_0)^2 + f_{\text{sing}}\left(t_0 + \frac{\gamma_2}{\gamma_1}\tilde{p}, \tilde{p}\right) \quad (4.21)$$

Therefore, we see, that as a consequence of the finite quadratic coupling, the two arguments of the Ising free energy are not independent of each other, i.e., in the (p, T) -phase diagram they do not draw a 90° angle. However, one has also to keep in mind that in principle h_0 is temperature dependent and thus also $p_{c,0}$ is not a constant.

As argued above, the elastic coupling to the field-like argument of the Ising free energy is more important than to the temperature one. Thus, we may for simplicity consider the limit $\gamma_2 \rightarrow 0$. The free energy follows from Eqs. (4.11) and (4.12) as

$$\mathcal{F}_{\text{pert}} = -\frac{K_0}{2\gamma_1^2}(\tilde{p} - h_0)^2 + \begin{cases} \frac{1}{8\pi} t_0^2 \log t_0^2 - c_1 \tilde{p}^2 t_0^{-\frac{7}{4}} + c_2 \tilde{p}^4 t_0^{-\frac{11}{2}}, & \text{(I)} \\ \frac{1}{8\pi} t_0^2 \log t_0^2 - \tilde{c}_1 |\tilde{p}| |t_0|^{\frac{1}{8}} - \tilde{c}_2 \tilde{p}^2 |t_0|^{-\frac{7}{4}}, & \text{(II)} \\ \frac{1}{8\pi} t_0^2 \log |\tilde{p}|^{\frac{16}{15}} - \phi_0 |\tilde{p}|^{\frac{16}{15}} + \phi_1 |\tilde{p}|^{\frac{8}{15}} t_0, & \text{(III)} \end{cases} \quad (4.22)$$

The roman numbers again refer to Fig. 4.5 identifying the h -axis with \tilde{p} and τ with t_0 , and denote the high temperature (I), low temperature (II) and the large pressure regime (III).

Upon approaching the critical endpoint, the fluctuations become stronger and, thus, such a perturbative treatment is no longer valid. This becomes most obvious when setting $\gamma_2 = 0$ and approaching the critical point from high temperatures. There, the Ising free energy adds a term $\delta\mathcal{V} = -c_1 (h_0 + \gamma_1 E)^2 t_0^{-7/4}$ to the elastic potential. Importantly, this contribution diverges as t_0 is driven to zero, and, hence, causes a sign change of the quadratic term of the potential at some finite value of τ , i.e., above the critical point identified by the perturbative approach. Thus, as already mentioned, the critical point is preempted by an isostructural transition, which in turn will trigger the Mott transition and determines the critical endpoint of the Mott transition on a compressible lattice. Notably, this does not depend on the sign of the elastic interaction, γ_1 .

4.3.2 Non-Perturbative Solution

Close to the critical endpoint of the elastic Mott transition, the diverging singular part of the Ising free energy density cannot be treated as a small perturbation of the elastic potential. Since, the argument of the function f_{sing} are small but finite, $(\tau + \gamma_2 E, h_0 + \gamma_1 E) \neq (0, 0)$, we may expand the potential Eq. (4.19) in a Taylor series up to fourth order. For convenience, we expand in $\epsilon = E - \bar{E}(\tau, h_0)$ where $\bar{E}(\tau, h_0)$ is chosen such that the third order term of the expansion vanishes. With the shifted variables $t = \tau + \gamma_2 \bar{E}$ and $h = h_0 + \gamma_1 \bar{E}$ the resulting potential in the non-perturbative regime reads up to constant terms as

$$\mathcal{V}_{\text{non}} = f_{\text{sing}}(t, h) - (p - p_c) \epsilon + \frac{K(t)}{2} \epsilon^2 + \frac{u(t)}{4!} \epsilon^4. \quad (4.23)$$

The quartic interaction, $u(t)$, is a superposition of all fourth-order derivatives of $f_{\text{sing}}(t, h)$, and the critical pressure takes the form $p_c = K_0 \bar{E} + \gamma_1 \partial_h f_{\text{sing}}(t, h) + \gamma_2 \partial_t f_{\text{sing}}(t, h)$. Most important is, however, the renormalization of the effective bulk modulus, $K(t)$ due to the second order derivatives of $f_{\text{sing}}(t, h)$

$$K(t) = K_0 - \gamma_1^2 \chi_{hh} - 2\gamma_1 \gamma_2 \chi_{ht} - \gamma_2^2 \chi_{tt}, \quad (4.24)$$

where we introduced the generalized susceptibilities $\chi_{\alpha\beta} = -\partial_\alpha \partial_\beta f_{\text{sing}}(t, h)$. When the critical endpoint of the uncoupled system is approached, χ_{hh} necessarily diverges. At some finite value $(t_c, h_c) \neq (0, 0)$, where the Taylor expansion is well defined, the effective bulk modulus is driven to zero. Thus, we see that the Mott-Ising endpoint is preempted by an isostructural transition at (t_c, p_c) . Importantly, the critical endpoint of the compressible system is mean-field like since the Ising singularities at $(t, h) = (0, 0)$ are avoided. Also note that this happens for any finite value of γ_1 , independent of its magnitude.

To minimize Eq. (4.23) one may first rescale the strain as $\epsilon = \epsilon \bar{p} / |K(t)|$ where we set $\bar{p} = p - p_c$. The conditional equation for ϵ reads then as

$$-1 + \epsilon \left(\text{sgn } K(t) + \frac{1}{3!} \frac{|\bar{p}|^2 u(t)}{|K(t)|^3} \epsilon^2 \right) = 0. \quad (4.25)$$

The magnitude of the ratio $|\bar{p}|^2 u(t) / |K(t)|^3$ and the sign of the effective bulk modulus, $K(t)$, discriminate the three different regimes, depicted in Fig. 4.7:

For large pressures, $|\bar{p}|^2 u(t) \gg |K(t)|^3$ the solution is independent of the sign of $K(t)$ and reads as

$$\epsilon_c = \text{sign}(\bar{p}) \left[\left(\frac{6|\bar{p}|}{u(t)} \right)^{1/3} - K(t) \left(\frac{4}{3|\bar{p}|u(t)^2} \right)^{1/3} \right], \quad (4.26)$$

In particular, at the critical value $K(t) = 0$ we obtain $\epsilon \sim |\bar{p}|^{1/\delta}$ with the Landau mean field exponent $\delta = 3$ for the stress-strain relation. Importantly, this

non-perturbative relation is a clear violation of Hooke's law which states a linear dependence of ϵ on the pressure. This power law is the smoking gun criterion for the identification of critical elasticity.

In the opposite limit of small pressures, $|\bar{p}|^2 u(t) \ll |K(t)|^3$, it is important whether the temperature is above or below t_c . If the bulk modulus, $K(t)$, is positive, the solution is simply

$$\epsilon_a = \frac{\bar{p}}{K(t)}, \quad (4.27)$$

resembling the perturbative regime for large temperatures, as $K(t)$ converges to K_0 with increasing temperatures. Below the endpoint, however, we have to keep the cubic term in Eq. (4.25) to obtain the global minimum of the potential given by

$$\epsilon_b = \text{sgn}(\bar{p}) \left[\sqrt{\frac{-6K(t)}{u(t)}} + \frac{|\bar{p}|}{2|K(t)|} \right]. \quad (4.28)$$

Thus, tuning through $\bar{p} = 0$ the volume jumps about $2\sqrt{-6K(t)/u(t)}$ into the coexisting but previously metastable local minimum of the potential, characteristic for a first order isostructural transition. At the crossover to the large pressure regime, (c), this metastable minimum ceases to exist.

An important question is, on what scales this elastic Ising mean field regime arises in the phase diagram. The pressure range can be estimated by comparing the perturbative and the non-perturbative volume change, i.e., at which pressure the deviation from Hooks law arises. In the rescaled variables the perturbative solution is given as $\epsilon_{\text{pert}} = (\bar{p} + p_c - K_0 \bar{E})/K_0 \approx \bar{p}/K_0$ where the last approximation holds in zeroth order of the elastic couplings. Now, comparing this with Eq. (4.26) we obtain for the extent of the non-perturbative region

$$\bar{p}^* = \left(\frac{6K_0^3}{u} \right)^{1/2}. \quad (4.29)$$

The temperature scale of the non-perturbative regime may be defined by the difference between the critical temperature, t_c , and the perturbatively calculated one.

For simplicity, we set $\gamma_2 = 0$ for the remainder of the analysis. Since it is $t > 0$ around the endpoint, the Ising free energy is evaluated in regime I of Fig. 4.5, having the form

$$f_{\text{sing}}(t, h + \gamma_1 \epsilon) = \frac{t^2}{8\pi} \log t^2 - c_1 t^{-7/4} |h + \gamma_1 \epsilon|^2 + c_2 t^{-22/4} |h + \gamma_1 \epsilon|^4. \quad (4.30)$$

Thus, the condition of a vanishing third order term translates to $h = 0$ implying $\bar{E} = -h_0/\gamma_1$. The critical pressure follows as $p_c = K_0 h_0/\gamma_1$ and the fourth order interaction is given as $u(t) = 4! \gamma_1^4 c_2 t^{-22/4}$. The renormalized bulk modulus is

$$K(t) = K_0 - 2\gamma_1^2 c_1 t^{-7/4}, \quad (4.31)$$

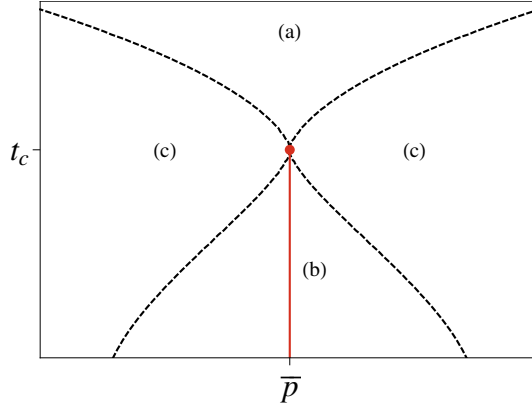


Fig. 4.7: Schematic phase diagram of the elastically coupled Mott transition around the critical endpoint. The dashed lines separate the three different regimes denoted by (a), (b) and (c). The high temperature regime (a) approaches the perturbative linear solution. The high pressure regime (c) is characterized by a non-linear strain-stress relation with the mean-field exponent $\delta = 3$. In the coexistence regime (b) there is a line of first order transitions (red), where the volume jumps. It ends in the elastic Mott endpoint (p_c, t_c) which is mean-field like, due to the fluctuations being cut off.

defining the critical temperature by the condition $K(t_c) = 0$, therefore, we obtain $t_c = (2\gamma_1^2/K_0)^{4/7}$. Expanding $K(t)$ around the critical temperature to first order yields $K(t) \approx \frac{7}{2}\gamma_1^2 c_1(t - t_c) \sim (t - t_c)$, according to a mean field theory.

Taking all together, and denoting $x = K^3/(|\bar{p}|^2 u)$, we obtain the free energy to be up to constants

$$\mathcal{F}_{\text{non}} = \frac{t^2}{8\pi} \log t^2 + \begin{cases} -\frac{|\bar{p}|^2}{2K(t)} & x \gg 0 \quad (a) \\ -\frac{3K(t)^2}{2u(t)} - |\bar{p}| \sqrt{\frac{6|K(t)|}{u(t)}} - \frac{|\bar{p}|^2}{4K(t)} & -x \gg 0 \quad (b) \\ -\frac{3}{4} \left[\frac{6|\bar{p}|^4}{u(t)} \right]^{1/3} + \frac{K(t)}{2} \left[\frac{6|\bar{p}|}{u(t)} \right]^{2/3} & x \ll 0 \quad (c) \end{cases} \quad (4.32)$$

The range of the non-perturbative regime, Eq. (4.29), is $\bar{p}^* = \bar{p}_I(t_c)/\sqrt{2c_2/c_1}$ where $\bar{p}_I(t_c)$ denotes the crossover line from region I to region III at the critical temperature in Fig. 4.5.

4.3.3 Behavior Around the Former Endpoint

For completeness, we consider the behavior around the point which the perturbative analysis identifies as the critical point of the pressure tuned Mott transition. According to Sec. 4.3.1, this point is given by $(\tau_{c,0}, p_{c,0}) = (\gamma_2 h_0/\gamma_1, -h_0 K_0/\gamma_1)$, thus, the potential becomes up to constants

$$\mathcal{V}(\epsilon) = \frac{K_0}{2} \delta E^2 - (p - p_{c,0}) \delta E + f_{\text{sing}}(t_0 + \gamma_2 \delta E, \gamma_1 \delta E), \quad (4.33)$$

where we defined $\delta E = E - p_{c,0}/K_0$ and set $t_0 = \tau - \tau_{c,0}$.

Depending on the relative magnitude of the elastic coupling parameters, the singular part of the Ising free energy has to be evaluated either in region II (for $|\gamma_2| \gg |\gamma_1|$) or in region III ($|\gamma_1| \gg |\gamma_2|$) of Fig. 4.5.

Neglecting, again, the coupling γ_2 , we can identify t_0 with t from Sec. 4.3.2 and, furthermore, δE and $p_{c,0}$ equal ϵ and p_c , respectively. Obviously, because of the bilinear coupling term, ϵ is always finite at $t = 0$, such that there is a surrounding region with $|\gamma_1 \epsilon|^{8/15} \gg t$. Thus, the Ising part of the free energy has to be evaluated in regime III and the potential Eq. (4.19) becomes to lowest order in t

$$\mathcal{V}(\epsilon) = \frac{K_0}{2} \epsilon^2 - \bar{p} \epsilon - \phi_0 |\gamma_1 \epsilon|^{16/15} + \phi_1 t |\gamma_1 \epsilon|^{8/15}. \quad (4.34)$$

Rescaling $\epsilon = x \bar{p} / K_0$ leads at $t = 0$ to the the following equation determining the macroscopic volume change, ϵ

$$\mathcal{V}(x) = x - 1 - \mu |x|^{1/15} \operatorname{sgn} x, \quad (4.35)$$

where we set $\mu = \frac{16}{15} \phi_0 |\gamma_1|^{16/15} |\bar{p}|^{-14/15} K_0^{-1/15}$.

For large μ , which corresponds to low pressures, the potential is minimized by $x = \mu^{15/14} + \frac{15}{14}$ leading to

$$\epsilon = \left(\frac{16\phi_0}{15K_0} \right)^{15/14} \gamma_1^{16/14} \operatorname{sgn}(\bar{p}) + \frac{15}{14} \frac{\bar{p}}{K_0}, \quad \text{for } \bar{p}^{14} K_0 \ll 0. \quad (4.36)$$

Hence, we obtain a jump of the macroscopic volume change $\Delta\epsilon \propto K_0^{-15/14}$ as we cross the zero pressure axis, ($\bar{p}=0$), characteristic for a first order transition.

For small μ , i.e., higher pressures, the solution is given by $1 + \mu$, corresponding to a volume change of

$$\epsilon = \frac{\bar{p}}{K_0} + \operatorname{sgn}(\bar{p}) \frac{16\phi_0}{15} \left(\frac{\gamma_1^{16} |\bar{p}|}{K_0^{16}} \right)^{1/15} \quad \text{for } \bar{p}^{14} K_0 \gg 1, \quad (4.37)$$

resembling the perturbative result for large pressures. Fig. 4.8 summarizes the different regimes close to the critical endpoint.

4.4 Thermodynamics

From the free energy one can calculate thermodynamic quantities such as the specific heat coefficient, $\gamma \sim -\partial_T^2 \mathcal{F}$, the thermal expansion, $\alpha \sim \partial_T \partial_p \mathcal{F}_{\text{pert}}$, and the compressibility, $\kappa \sim -\partial_p^2 \mathcal{F}$.

Clearly, the thermodynamic quantities calculated in the non-perturbative regime will differ from those calculated in the perturbative regime. At the critical point determined by the perturbative solution, the Ising free energy becomes singular,

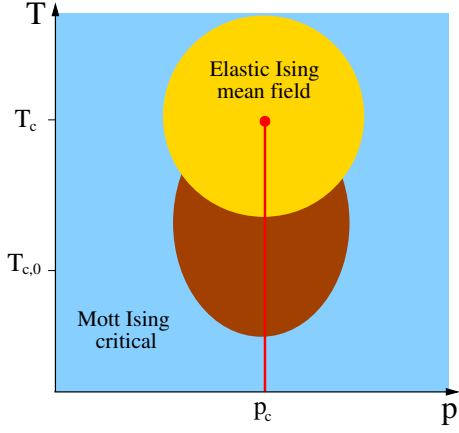


Fig. 4.8: Different regimes of the Mott endpoint on compressible lattices. Close to the endpoint at T_c , elastic criticality is obtained (yellow), whereas further away the Ising critical behavior of the Mott transition is recovered (blue). Around the perturbatively estimated endpoint, $T_{c,0}$ (brown), the behavior is neither Ising critical nor mean field. Far away from the endpoint, the fluctuations become weak and one obtains Mott mean field behavior which is not shown here.

thus, yielding divergences in thermodynamics. In the non-perturbative regime, in contrast, the Ising free energy is non-singular, therefore, we expect that at least some divergences are cut-off at the elastic Mott transition.

In order to focus on the important effects, we will again consider the limit of a vanishing quadratic coupling, $\gamma_2 = 0$, in the following. As mentioned in Sec. 4.3.3, in this case we can identify $t = t_0$ and $p_c = p_{c,0}$. Furthermore, to lowest order, we can assume t to be linear in temperature, $t = (T - T_{c,0})/T_0$, where $T_{c,0}$ denotes the perturbatively calculated critical temperature and T_0 is some non-universal temperature scale. As a further simplification, we will assume h_0 to be temperature independent since for small critical temperatures it only weakly depends on T . This is due to the Clausius Clapeyron relation as explained in Sec. 4.1.3.

In the perturbative regime, the free energy is given in terms of the parameter $\tilde{p} = \gamma_1(p - p_{c,0})/K_0$. Thus, we deduce

$$\begin{aligned} \partial_T \mathcal{F}_{\text{pert}}(t, \tilde{p}) &= \frac{1}{T_0} \frac{\partial \mathcal{F}_{\text{pert}}(t, \tilde{p})}{\partial t} \Big|_{\tilde{p}=\tilde{p}\gamma_1/K_0} \quad , \quad \partial_T \mathcal{F}_{\text{non}}(t, \tilde{p}) = \frac{1}{T_0} \frac{\partial \mathcal{F}_{\text{non}}(t, \tilde{p})}{\partial t} \\ \partial_p \mathcal{F}_{\text{pert}}(t, \tilde{p}) &= \frac{\gamma_1}{K_0} \frac{\partial \mathcal{F}_{\text{pert}}(t, \tilde{p})}{\partial \tilde{p}} \Big|_{\tilde{p}=\tilde{p}\gamma_1/K_0} \quad , \quad \partial_p \mathcal{F}_{\text{non}}(t, \tilde{p}) = \frac{1}{T_0} \frac{\partial \mathcal{F}_{\text{non}}(t, \tilde{p})}{\partial t} . \end{aligned}$$

Additionally, we reintroduce the free energy scale f_0 , which enters linear in $K(t) - K_0$ and $u(t)$. In the following, one has to keep in mind, that while the perturbatively calculated critical point lies at $(t, \tilde{p}) = (0, 0)$, the (actual) non-perturbative endpoint is at a finite temperature, t_c .

4.4.1 Specific Heat Coefficient

The specific heat coefficient in the perturbative regime is given by

$$\gamma_{\text{pert}} = - \frac{f_0}{T_0^2} \frac{\partial^2 f_{\text{sing}}(t, h)}{\partial t^2} \Big|_{h=\gamma_1 \tilde{p}/K_0} . \quad (4.38)$$

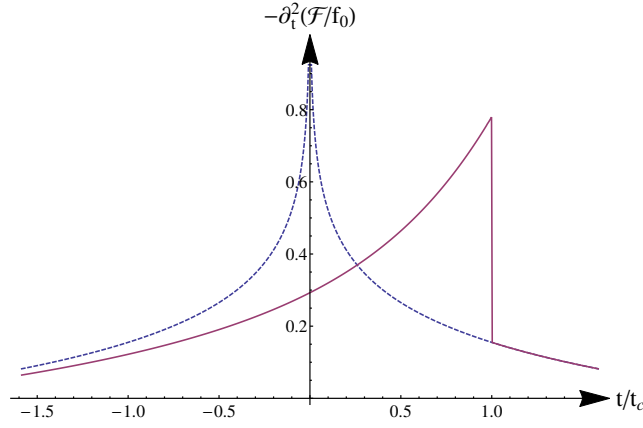


Fig. 4.9: Specific heat at $p = p_c$ as a function of temperature. From the perturbative calculation one expects a logarithmic divergence (dashed curve) at the critical temperature, $t_{c,0} = 0$. However, in the non-perturbative regime it exhibits a pure mean field jump at the critical temperature $t_c > 0$ (solid curve). Thus, due to the linear Mott-elastic coupling the Ising singularity is preempted by a mean field like transition.

Approaching the critical point from high or low temperatures at low pressures, i.e., from regime I or II, respectively, the specific heat coefficient, thus, reads as

$$\frac{T_0^2}{f_0} \gamma_{\text{pert}} = \begin{cases} -\frac{1}{4\pi}(\log t^2 + 3) + \frac{77}{16} c_1 \frac{\gamma_1^2}{K_0^2} \bar{p}^2 t^{-15/4} & \text{(I)} \\ -\frac{1}{4\pi}(\log t^2 + 3) - \frac{7}{64} \tilde{c}_2 \frac{\gamma_1}{K_0} |\bar{p}| t^{-15/8} & \text{(II)} \end{cases}. \quad (4.39)$$

For vanishing pressure, \bar{p} , the specific heat diverges logarithmically upon approaching the critical point at $t = 0$ in agreement with the critical exponent $\alpha = 0$ for the 2D Ising universality class. In the non-perturbative regime, we get above the critical temperature, t_c

$$\frac{T_0^2}{f_0} \gamma_{\text{non}} = -\frac{1}{4\pi}(\log t^2 + 3) + \frac{\bar{p}^2}{2} \left(2 \frac{(K')^2}{K^3} - \frac{K''}{K^2} \right) \quad \text{in (a)}, \quad (4.40)$$

which also yields a critical exponent $\alpha = 0$, since this is the mean field value. Lowering the temperature, one enters region (b) where the effective bulk modulus becomes negative. Close to the critical point the specific heat coefficient at $\bar{p} = 0$ and in leading order of $K(t)$ is given by

$$\begin{aligned} \frac{T_0^2}{f_0} \gamma_{\text{non}} &= -\frac{1}{4\pi}(\log t^2 + 3) + \frac{147}{16} \frac{(K_0 - K(t))^2}{u(t)t^2} + \frac{693}{16} \frac{K(t)(K_0 - K(t))}{u(t)t^2} \quad \text{in (b)} \\ &= -\frac{1}{4\pi}(\log t^2 + 3) + \frac{49c_1^2}{32c_2} + \frac{231}{64c_2\gamma_1^2} K(t)t^{7/4}. \end{aligned} \quad (4.41)$$

Hence, lowering the temperature at the critical pressure, the specific heat diverges logarithmically until the critical temperature $T_c = T_{c,0} + T_0 t_c$ is reached. At this temperature, the divergence is cut off and the specific heat has a jump of the size of $\Delta\gamma = f_0 49c_1^2/(32c_2T_0^2) \approx 0.63 f_0/T_0^2$, showing mean field behavior.

Notably, this jump is universal, in the sense, that it does not depend on the magnitude of the elastic coupling constant, γ_1 or the critical temperature. Of course, this is no longer true if anharmonic effects, $\sim u_0\epsilon^4$, are included in the bare elastic potential. Similarly, switching on the quadratic interaction γ_2 or taking temperature effects of the field, h_0 , into account would lead to a finite slope of γ as function of T . Instead, the jump would occur along some curved trace in the (T, \bar{p}) -diagram, however, the logarithmic divergence would still be cut off.

Below T_c , the specific heat coefficient decreases and asymptotically resembles the perturbative result. In Fig. 4.9 the specific heat at the critical temperature, calculated numerically with the exact function f_{sing} , is shown. The blue, dashed curve is calculated perturbatively by setting $F = \mathcal{V}(E = p/K_0)$, while the red curve gives the exact non-perturbative result, which was obtained by numerical minimization of the full potential Eq. (4.19).

For temperatures close to the critical temperature and large pressures, i.e., in regime III, the perturbative calculation gives for the specific heat coefficient

$$\frac{T_0^2}{f_0} \gamma_{\text{pert}} = -\frac{1}{4\pi} \log \left| \frac{\gamma_1 \bar{p}}{K_0} \right|^{16/15} - 2\phi_2 \quad (\text{III}), \quad (4.42)$$

i.e., also a logarithmic divergence as function of pressure. When entering the non-perturbative regime, the logarithmic divergence has to be cut off since one has no longer to evaluate the function f_{sing} in region III but rather in region I. Close to $t = t_c$ in lowest order of the effective bulk modulus and pressure, we obtain

$$\begin{aligned} \frac{T_0^2}{f_0} \gamma_{\text{non}} &= -\frac{1}{4\pi} (\log t^2 + 3) - \frac{147}{8} \frac{(K_0 - K(t))^2}{t^2 u(t)} \left(1 + \frac{5}{9} K(t) \left(\frac{6}{\bar{p}^2 u(t)} \right)^{1/3} \right) \\ &= -\frac{1}{4\pi} (\log t^2 + 3) - \frac{49 c_1^2}{16 c_2} \left(1 + \frac{5}{9} K(t) \left(\frac{1}{4 \gamma_1^4 c_2 \bar{p}^2} \right)^{1/3} t^{11/6} \right) \quad \text{in (c)}. \end{aligned} \quad (4.43)$$

Hence, the specific heat saturates at a value $\frac{1}{4\pi} (\log t_c^2 + 3) - (49 c_1^2)/(16 c_2)$.

4.4.2 Thermal expansion

The thermal expansion is given by the mixed derivative with respect to t and p ,

$$\alpha_{\text{pert}} = \frac{f_0 \gamma_1}{T_0 K_0} \frac{\partial^2 f_{\text{sing}}(t, h)}{\partial t \partial h} \Big|_{h=\gamma_1 \bar{p}/K_0}. \quad (4.44)$$

As the potential is an even function of the pressure, the thermal expansion is an odd function of \bar{p} . For the perturbative solution, we obtain for smallest pressures

$$\frac{T_0}{f_0} \alpha_{\text{pert}} = \frac{7}{2} \frac{\gamma_1^2}{K_0^2} c_1 t^{-11/4} \bar{p} \quad (\text{I}), \quad (4.45)$$

$$\frac{T_0}{f_0} \alpha_{\text{pert}} = \frac{1}{8} \frac{\gamma_1}{K_0} \tilde{c}_1 |t|^{-7/8} \text{sgn } \bar{p} \quad (\text{II}). \quad (4.46)$$

As argued above, the $\text{sgn}(\bar{p})$ yields the right symmetry concerning the pressure axis. For vanishing pressure, the thermal expansion is zero above the transition, whereas it has a finite value below the critical point. Being the mixed derivative with respect to pressure and temperature, one can identify the thermal expansion as the derivative of the elastic order parameter, $\epsilon = \partial_p \mathcal{F}$, with respect to temperature. The order parameter scales as $\epsilon \sim |t|^\beta$, from which we deduce $\alpha \sim |t|^{\beta-1}$. Hence, we can identify the critical exponent $\beta = 1/8$, which agrees with the critical exponent of the Ising class.

In the non-perturbative regime, on the other hand, approaching the critical point from high temperatures we have

$$\frac{T_0}{f_0} \alpha_{\text{non}} = \bar{p} \frac{K'(t)}{K(t)^2} \quad \text{in (a)}, \quad (4.47)$$

again recovering asymptotically the perturbative result for $K(t) \approx K_0$, i.e., far from the critical point. Below the critical point, we obtain

$$\frac{T_0}{f_0} \alpha_{\text{non}} = -\frac{1}{2} \sqrt{\frac{6|K(t)|}{u(t)}} \left(\frac{K'(t)}{|K(t)|} - \frac{u'(t)}{u(t)} \right) \text{sgn } p \quad \text{in (b)}, \quad (4.48)$$

diverging as $\alpha_{\text{non}} \propto |K(t)|^{-1/2} \propto |t - t_c|^{-1/2}$, hence, we can identify the critical exponent $\beta = 1/2$ in agreement with mean field behavior.

Lowering the pressure at $K(t) = 0$, the perturbative result states a divergence according to

$$\frac{T_0}{f_0} \alpha_{\text{pert}} = |\gamma_1 \bar{p}|^{-7/15} \left[\frac{8\phi_1}{15} + \frac{4}{15\pi} \frac{t}{|\gamma_1 \bar{p}|^{8/15}} \right] \text{sgn } p \quad \text{(III)}, \quad (4.49)$$

whereas the non-perturbative calculation yields a crossover to

$$\frac{T_0}{f_0} \alpha_{\text{non}} = K'(t) \left(\frac{4}{3p u(t)^2} \right)^{1/3} \text{sgn } p \quad \text{in (c)}. \quad (4.50)$$

4.4.3 Compressibility

The compressibility in the perturbative regime consists of two contributions, namely

$$\kappa = \frac{1}{K_0} - f_0 \left(\frac{\gamma_1}{K_0} \right)^2 \left. \frac{\partial^2 f_{\text{cr}}(t, h)}{\partial h^2} \right|_{h=\gamma_1 \bar{p}/K_0}. \quad (4.51)$$

The first term is the constant lattice contribution which is also present in the bare elastic system and will be not considered in the following. Concerning the critical part, $\kappa_{\text{pert,c}} = \kappa_{\text{pert}} - 1/K_0$, it follows as

$$\frac{1}{f_0} \kappa_{\text{pert,c}} = 2c_1 \frac{\gamma_1^2}{K_0^2} t^{-7/4} \quad \text{(I)}, \quad (4.52)$$

$$\frac{1}{f_0} \kappa_{\text{pert,c}} = 2\tilde{c}_2 \frac{\gamma_1^2}{K_0^2} t^{-7/4} \quad \text{(II)}, \quad (4.53)$$

and diverges, apart from the different coefficients, symmetrically as $|t|^{-7/4}$ above and below the critical point.

In the non-perturbative regime above (a) and below (b) the critical point, we obtain the compressibility to be

$$\frac{1}{f_0} \kappa_{\text{non}} = \frac{1}{K(t)} \quad \text{in (a),} \quad (4.54)$$

$$\frac{1}{f_0} \kappa_{\text{non}} = \frac{1}{2K(t)} \quad \text{in (b).} \quad (4.55)$$

Thus, a perturbative expansion for large temperatures resembles the previous result of the perturbative solution $\frac{1}{f_0} \kappa_{\text{non}} \approx \frac{1}{K_0} + 2\gamma_1^2 c_1 t^{-7/4} / K_0^2$. Close to the elastic Mott transition, however, the compressibility diverges with the inverse power of the renormalized bulk modulus $\chi \sim K(t)^{-1} \sim (T - T_c)^{-1}$. When tuning through the critical point, the compressibility obeys the mean field ratio $\kappa_{\text{non}}^{\text{a}} / \kappa_{\text{non}}^{\text{b}} = 2$. Asymptotically, it does not exactly reproduce the perturbative result, Eq. (4.53), which is, however, not surprising. It is due to the finite range of validity of the Taylor expansion of f_{sing} close to the critical point, which necessarily breaks down when this function changes its behavior, i.e., ultimately when $t < 0$.

Considering the compressibility at the critical temperature for finite pressures, we see that the perturbative calculation yields

$$\frac{1}{f_0} \kappa_{\text{pert,c}} = \frac{16\phi_0}{225} \left| \frac{\gamma_1}{K_0} \right|^{16/15} |\bar{p}|^{-14/15} \quad \text{(III).} \quad (4.56)$$

Since the compressibility is the second derivative of the free energy with respect to pressure, it is also the pressure derivative of the elastic order parameter, $\epsilon = \partial_p \mathcal{F}$. Close to the endpoint, the order parameter scales as $\epsilon \sim \bar{p}^{1/\delta}$, from which the scaling of the compressibility follows as $\kappa \sim \bar{p}^{(1-\delta)/\delta}$. Thus, we can identify the critical exponent $\delta = 15$ in agreement with the Ising universality class.

In contrast, the non-perturbative calculation determines the compressibility at the critical temperature as

$$\frac{K_0^2}{f_0 \gamma_1^2} \kappa_{\text{non}} = \left(\frac{2}{9\bar{p}^2 u(t)} \right)^{1/3} + \frac{K(t)}{3} \left(\frac{4}{3\bar{p}^4 u(t)^2} \right)^{1/3} \quad \text{in (c).} \quad (4.57)$$

This implies a mean field exponent $\delta = 3$ as it was already shown in Sec. 4.3.2.

4.5 Experimental Relevance

So far, we discussed the elastically coupled Mott transition on theoretical and quite general grounds. In this section, we will now turn to specific experimental consequences and want to connect the theory to actual physical situations. Of particular importance is the extent of the elastic Landau critical region in the phase diagram, i.e., over which pressure and temperature range the elastic coupling induces mean field behavior for the Mott transition.

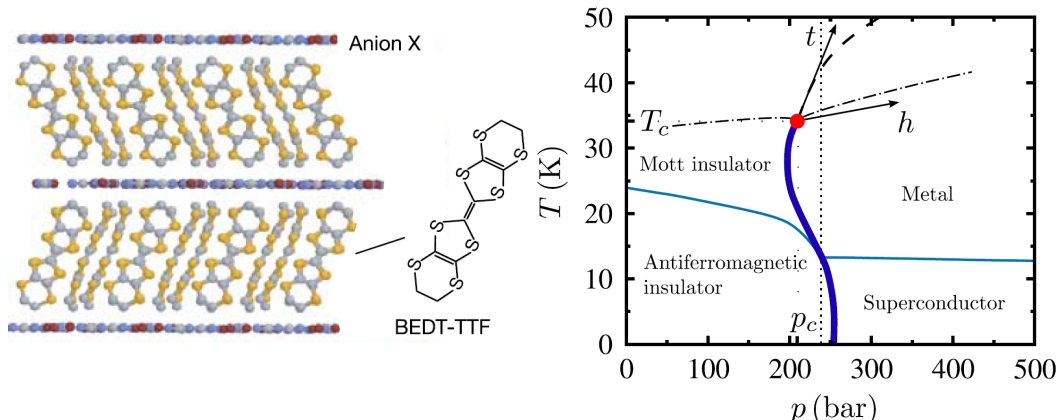


Fig. 4.10: Left: Structure of the organic salt κ -(BEDT-TTF) $_2$ X (taken from Ref. [55]). The quasi-2D conduction layers of BEDT-TTF are separated by insulating anion layers. Right: Schematic phase diagram of κ -(BEDT-TTF) $_2$ Cu[N(CN) $_2$]Cl under pressure (taken from Ref. [2]). At lowest temperatures, it is antiferromagnetic which is turned into a superconductor upon applying pressure. Above the Néel temperature, the compound has a paramagnetic insulating phase at small pressures which is separated from a metallic phase by a first order transition line. It terminates in a second order endpoint at $T_c \sim 30$ K. Above this critical temperature the transition is a smooth crossover. The dotted line corresponds to the position of *d8-Br*. Also, the local coordinate system (t, h) at the critical endpoint is added.

As mentioned already in Sec. 4.3 there are in principle two possible situations depicted in Fig. 4.6. Either, the elastic coupling is sufficiently weak, such that the system develops Mott Ising critical behavior and only at smaller distances from the critical endpoint exhibits a crossover to the elastic mean field regime. This situation was the premise of our analysis so far as we used the Ising critical theory. For large elastic couplings, on the other hand, the elastic Landau regime extends over a much larger region of the phase diagram, such that the system has a direct crossover from the Mott-Landau to the elastic Landau region. In this case, the thermodynamic signatures of Ising criticality will not develop. In this section, we will investigate two different examples of compounds, mentioned already in Sec. 4.1.2, showing a pressure tuned Mott transition. One is the family of organic salts κ -(BEDT-TTF) $_2$ X whereas the other is chromium doped V_2O_3 . Both are experimentally very well studied in the literature, giving us the opportunity to estimate the extent of the elastic Ising regime. In particular, we will argue, that κ -(BEDT-TTF) $_2$ X is an example for the crossover from the Ising critical to the elastic Landau regime, whereas V_2O_3 does not enter the Ising critical regime at all.

4.5.1 The κ -(BEDT-TTF) $_2$ X Family

One of the best studied examples for a pressure tuned Mott transition is the series of organic salts κ -(BEDT-TTF) $_2$ X, where X stands for a variety of monovalent anions. The abbreviation BEDT-TTF denotes bis(ethylenedithio)tetrathiafulvalene

and is often further abbreviated to ET. A variation where the protons of the terminal ethylene groups are replaced by deuterium is called *d8-ET* and accordingly there also exists a hydrogenated variant called *h8-ET*. The salts have a layered structure, as depicted on the right hand side of Fig. 4.10, and are, thus, quasi-two dimensional. On the right hand side of Fig. 4.10, the phase diagram of κ -(*d8-ET*)₂X with X=Cu[N(CN)₂]]Cl is depicted which is the prototypical compound as it shows all phases of the family. Other members of the family are subject to chemical pressure meaning that, depending on the kind of anion and whether it is the pure, deuterated or hydrogenated variant of ET, ambient pressures for them corresponds to a finite pressure to the prototypical compound. For example, the fully deuterated salt with X=Cu[N(CN)₂]]Br, also called *d8-Br*, is at ambient pressure located at $p \approx 240$ bar (dotted line) in this phase diagram.

Ultrasonic measurements of longitudinal waves propagating perpendicular to the layers revealed a huge dip in the relative velocity (about 20 %, Ref. [63]) close to the critical endpoint corresponding to a very pronounced softening of the elastic mode C_{22} . A further lattice anomaly was found by de Souza et al. [1], by measuring the thermal expansion in *d8-Br*. This compound is at ambient pressure slightly above the critical pressure, $p - p_c \approx 50$ bar and could be fitted by a critical Ising theory [2], i.e., assuming a perturbative coupling to the elastic degrees of freedom.

Also, the conductivity measurements of Kagawa et al. [55] together with their later interpretation in Ref. [56] showed strong indications that the pressure tuned Mott transition of this compound belongs to the Ising universality class. These results give reason to assume that the Ising critical regime is realized in these compounds, i.e., the scenario on the left hand side of Fig. 4.6 is realized.

However, we have to estimate the extend of this regime in order to identify whether the κ -(BEDT-TTF)₂X family is a good candidate to experimentally find elastic Landau criticality. This would, for instance, not be the case if the pressure scale is too small to be experimentally accessible. Also, the difference between the Ising critical and the Ising mean field properties may be so small that they are not resolvable, convicting the discussion above to an interesting, yet academic problem for this series. The aforementioned analysis of the thermal expansion data [1] by Bartosch et al. [2] gives us the opportunity of having an estimate of the physical parameters of this compound.

First of all, we have to identify the theoretical parameters with the physical ones. The parameter t is the tangent of the line of first order transitions on the right of Fig. 4.10 at the critical endpoint. Thus, the temperature-like variable has a small linear pressure admixture, and, similar, the pressure-like variable has a small temperature admixture

$$t = \frac{T - T_{c,0} - \zeta(p - p_c)}{T_{c,0}}, \quad h = \frac{p - p_c - \lambda(T - T_{c,0})}{p_0}. \quad (4.58)$$

Here, we used the freedom of scaling to measure t in units of $T_{c,0} \approx 30$ K which is the critical temperature deduced in the perturbative regime. The parameters ζ and λ govern the admixtures which lead to the slopes of the h - and t - axis in the (p, T) -diagram on the right hand side of Fig. 4.10 and are assumed to be small. Up to order λ^0 and ζ^0 , the thermal expansion as derived from the perturbative analysis reads as

$$\alpha(T, p) \approx \frac{f_0}{p_0 T_{c,0}} \partial_t \partial_h f_{\text{sing}}(t, h) \quad (4.59)$$

$$= \frac{f_0}{p_0 T_{c,0}} \text{sgn}(h) h^{-7/15} \Psi_\alpha \left(\frac{t}{h^{8/15}} \right), \quad (4.60)$$

where we introduced the function $\Psi_\alpha(x) = \frac{8}{15}(\Phi'(x) - x \Phi''(x))$. In Ref. [2], the data was fitted by the function

$$\alpha(T, p) = A \text{sgn } h |p_0 h|^{-7/15} \Psi_\alpha \left(\frac{BT_{c,0}}{p_0^{8/15}} \frac{t}{|h|^{8/15}} \right) + C + D T_{c,0} t, \quad (4.61)$$

leading to the identification $B = p_0^{8/15}/T_{c,0}$ and $A = f_0/(T_{c,0}^2 B)$. The coefficients C and D account for a non-singular background contribution and, as such, will be of no importance for our following considerations. The best fit for the parameter set to the experimental data was obtained by Bartosch et al. [2] as

$$\begin{aligned} (p - p_c)/\lambda &= 26.7K & , & & T_{c,0} + \zeta(p - p_c) &= 27.5K \\ B\lambda^{-8/15} &= 3.88K^{-7/15} & , & & A\lambda^{-7/15} &= 874 \cdot 10^{-6} K^{-8/15}. \end{aligned}$$

Now, we have to translate these numbers into the notation used in the previous sections, especially the values for the coupling constants γ_1 and γ_2 . From the fitting parameters we can directly obtain $f_0 = 5.7$ bar. For the other parameters, we have to compare the definitions of t and h given in Eq. (4.58) with the arguments of the Ising part of the free energy in Eq. (4.20). In the perturbative regime, where $E = p/K_0$, these were

$$t = \tau + p_c \frac{\gamma_2}{K_0} + \frac{\gamma_2}{K_0} (p - p_c), \quad (4.62)$$

$$h = h_0 + p_c \frac{\gamma_1}{K_0} + \frac{\gamma_1}{K_0} (p - p_c), \quad (4.63)$$

which we have to compare to the definitions given in Eq. (4.58).

$$\tau + p_c \frac{\gamma_2}{K_0} + \frac{\gamma_2}{K_0} (p - p_c) \hat{=} \frac{T - T_{c,0}}{T_{c,0}} - \frac{\zeta(p - p_c)}{T_{c,0}} \quad (4.64)$$

$$h_0 + p_c \frac{\gamma_1}{K_0} + \frac{\gamma_1}{K_0} (p - p_c) \hat{=} \frac{p - p_c}{p_0} - \lambda \frac{T - T_{c,0}}{p_0}. \quad (4.65)$$

Following Ref. [64], we estimate the bulk modulus as $K_0 = 122\,000$ bar and infer $\tau + \gamma_2 p_c/K_0 = (T - T_{c,0})/T_{c,0}$ as well as $h_0 + p_c \gamma_1/K_0 = -0.004(T - T_{c,0})/T_{c,0}$. For the elastic coupling constants, γ_1 and γ_2 , we obtain $\gamma_1/K_0 = 1/p_0 = 7 \cdot 10^{-5}$ and $\gamma_2/K_0 = -\zeta/T_{c,0} = -1.7 \cdot 10^{-3} \text{ bar}^{-1}$. However, as the exact critical temperature is

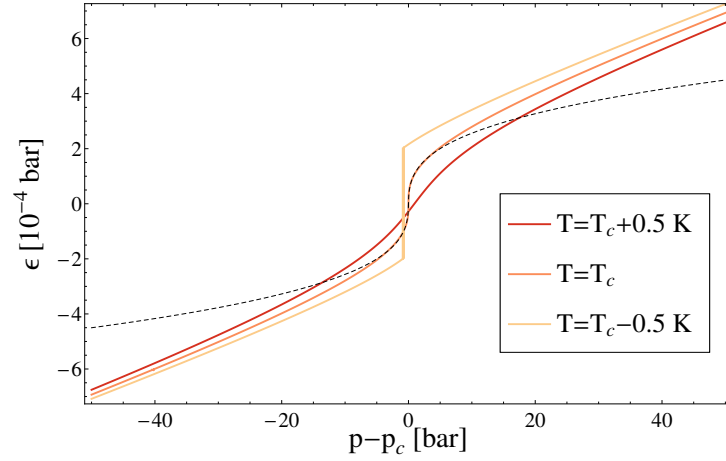


Fig. 4.11: Pressure dependence of the strain close to the critical temperature T_c for the parameters obtained from the $d8$ -Br compound measured in Ref. [1, 2]. For large pressures the strain follows Hooke's law of a linear stress-strain relation, whereas close to the critical point it becomes non-linear. The dashed asymptotic behavior at the critical temperature is given by $\epsilon \sim (p - p_c)^{1/\delta}$ with the mean field exponent $\delta = 3$.

not known, the estimate for ζ and, thus, for γ_2 is not reliable. Because of this, we may set for convenience $\gamma_2 = 0$ in the following analysis, neglecting only sub-leading corrections.

Now, to estimate the deviation of the critical temperature from the perturbatively calculated one, $\delta T_c = T_c - T_{c,0}$, we have to evaluate where the renormalized bulk modulus vanishes which happens at

$$\delta T_c = T_{c,0} \left(\frac{2 f_0 c_1 \gamma_1^2}{K_0} \right)^{4/7} \approx 2.5 \text{ K}. \quad (4.66)$$

This deviation is quite large as it corresponds to a relative deviation of about 8% compared to $T_{c,0}$.

The pressure range of the elastic Landau critical region, \bar{p}^* , is estimated by the value at which the perturbatively calculated strain equals the non-perturbative solution, $\bar{p}^*/K_0 = (6\bar{p}^*/u(t_c))^{1/3}$. It follows

$$\delta p^* = \left(\frac{K_0^3 (\delta T_c / T_{c,0})^{22/4}}{4 \gamma_1^4 c_2 f_0} \right)^{1/2} \approx 44 \text{ bar}. \quad (4.67)$$

Thus, the non-perturbative region is large enough to be experimentally accessible and resolvable. In fact, as the deviation for the $d8$ -Br compound from the critical pressure was estimated as $p - p_c \approx 50$ bar, it is already within the crossover regime to the elastic Landau critical region.

With the obtained parameters of the κ -family, we can for instance plot the lattice strain, ϵ , as a function of pressure. This is done using the full form of f_{sing} in Fig. 4.11

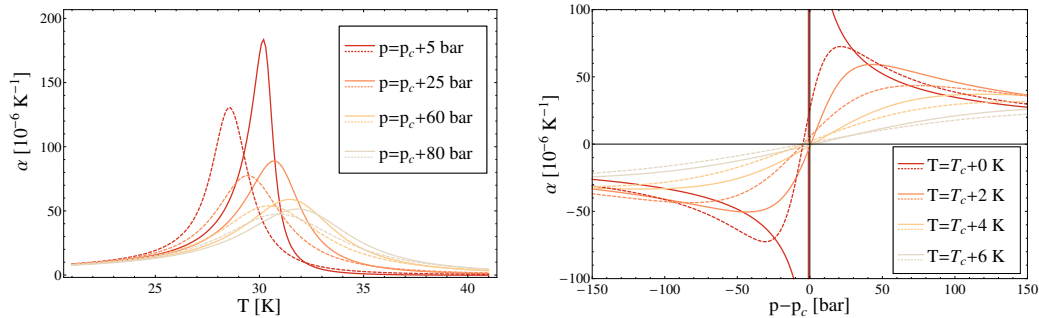


Fig. 4.12: Thermal expansion, α , evaluated for the parameters obtained in Ref. [1, 2] for the $d8\text{-Br}$ compound. It is shown as function of temperature (left) and pressure (right) close to the critical point (T_c, p_c) . Outside the elastic Landau regime, i.e., for $p - p_c \gg \bar{p}^*$ and $T - T_c \gg \delta T_c$, the perturbative (dashed) and the non-perturbative (solid) result coincide very well. Approaching the critical point this changes drastically. For instance, the peak position on the left hand side which indicates the position of the critical endpoint is noticeably shifted.

for three different temperatures. As one can see, right at the critical temperature close to the critical pressure the strain obeys a power law, $\epsilon \sim (p - p_c)^{1/\delta}$, with the mean field exponent $\delta = 3$ signaling the breakdown of Hooke's law. For larger pressures, the strain approaches a linear pressure dependence as expected from the perturbative analysis. Above T_c , the non-linearity is suppressed, whereas for smaller temperatures the strain jumps at the first order transition line.

In Fig. 4.12, we plotted the non-perturbative calculated thermal expansion (solid lines) in comparison to the result obtained by a perturbative calculation in the Ising critical region. On the left hand side, the temperature dependence of the thermal expansion for different pressures is shown close to the critical point. Importantly, the central peak which signals the critical endpoint is shifted to lower temperatures for the perturbative solution and the deviation is approximately given by δT_c . On the right hand side, we plotted the pressure dependence of the thermal expansion for different temperatures. Here, we also see a strong deviation from the perturbatively calculated Ising critical behavior, though one has to be careful how to compare the two results. Since the perturbative calculation results in a critical temperature which is $T_{c,0} = T_c - \delta T_c$, corresponding curves have different distances from the critical point.

As discussed in Sec. 4.1.2, the conductivity σ was interpreted in Ref. [56] as the energy density of the Ising model which scales as $\sigma \sim \partial_t f_{\text{sing}}(t, h)$. Thus, the above analysis suggests also a crossover of the conductivity when entering the elastic Landau region i.e., for $T - T_c \ll \delta T_c$ and $p - p_c \ll \bar{p}^*$. The measurements performed on $\kappa\text{-(BEDT-TTF)}_2\text{Cu[N(CN)}_2\text{)]Cl}$ by Kagawa et al. [55] indeed show a crossover in the temperature dependence of both, the conductivity and its pressure derivative, at $T - T_c \approx 1$ K.

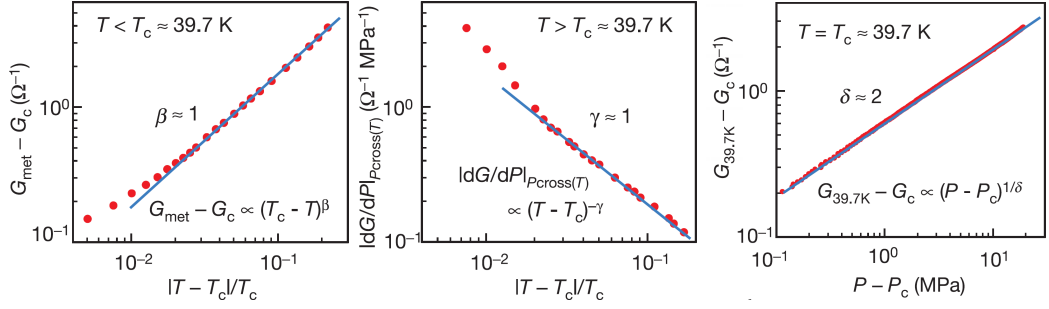


Fig. 4.13: Measurements of the conductivity by Kagawa et al. [55]. Close to the critical endpoint at $T - T_c \approx 0.03T_c \approx 1$ K, a crossover is seen in β and γ . This is the estimated order of magnitude, where elastic mean field behavior is expected. However, as discussed in the main text, the deviations are not completely consistent with mean field exponents, though the number of measured points is not sufficient.

Denoting the measured exponents with the subscript σ , we see in Fig. 4.13 that the exponent β_σ becomes smaller than 1 and the exponent γ_σ becomes larger than 1. According to Ref. [56], β_σ is related to the actual critical exponents by $\beta_\sigma = 1 - \alpha$. Following this line of thought, the increase of β would imply a change of the specific heat exponent α to finite positive values. However, in mean field theory as well as for the 2D Ising universality class this exponent should be $\alpha = 0$. On the other hand, the coupling to the lattice also induces an interlayer coupling such that the system is no longer effectively two-dimensional. Therefore, the change in the critical exponents may also be related to 3D Ising exponents, where indeed $\alpha \approx 0.11$. In conclusion, although we see a change in these two critical exponents at the predicted temperature scale, the data is not completely consistent with the theory.

Also, the pressure dependence seems to show no sign of a crossover up to lowest pressures. The corresponding measured exponent is related to the critical exponents by $\delta_\sigma = \delta\beta/(1 - \alpha)$ [56] and equals $15/8$ in the Ising critical region. Applying the same formula to the mean field exponents and substituting $1 - \alpha = \beta_\sigma$ would yield an exponent $\delta_\sigma = 3/(2\beta_\sigma)$. If indeed $\beta_\sigma < 1$, it may be that the effects cancel each other such that the crossover cannot be resolved in such a conductivity measurement.

However, based on this data no firm statement can be made about the regime of critical elasticity. First of all, the number of data points below 1 K is too few to yield a sound result and secondly, the above analysis suggests that there may be also other mechanisms at work. Finally, there is an additional uncertainty in the exact value of the critical temperature, T_c .

To check the validity of our theory, further experimental analysis is needed, for example detailed dilatometric or ultrasonic studies. Since our estimates find an experimentally well accessible extent of the elastic mean field regime, the κ -(BEDT-TTF)₂X family seems to be a good candidate for such further studies of the elastic Mott transition.

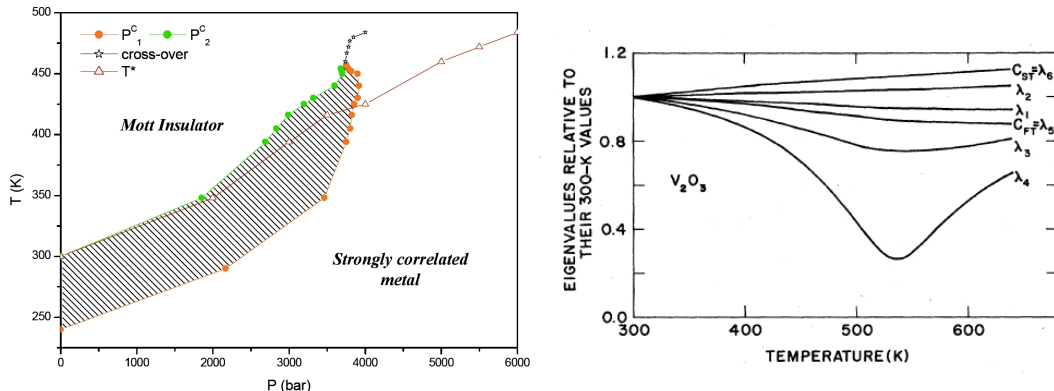


Fig. 4.14: Left: Close-up of the region around the critical endpoint of chromium doped V_2O_3 (taken from Ref. [69]). The hatched region denotes the coexistence regime of both phases. The critical endpoint is located at $(P_c, T_c) \approx (3738 \text{ bar}, 457.5 \text{ K})$.

Right: Temperature dependence of the eigenvalues of the elastic tensor for pure V_2O_3 at ambient pressure (taken from Ref. [70]). The mode λ_4 shows a significant drop at temperatures of the order of the critical temperature.

4.5.2 Vanadium Sesquioxide V_2O_3

The transition metal oxide V_2O_3 is one of the best studied examples of Mott metal-insulator transitions. Its phase diagram was already shown in Fig. 4.4 as a paradigm for a generic Mott metal-insulator transition. In its pure form it is a metal, which turns to an antiferromagnet below a Néel temperature of $T_N \sim 160 \text{ K}$. Substituting vanadium with small amounts of chromium, one obtains a first order transition at room temperature to a non-magnetic insulator.

The studies yielding the full phase diagram were published in the early seventies in a series of papers by McWhan et al. [48, 65–68]. They also discovered that 1% chromium doping corresponds to an applied pressure of $p \approx -4 \text{ kbar}$. Even then, it was noticed that the Mott transition is accompanied by an isostructural volume change, and it was termed a solid-solid transition, although at the same time an analogy to the liquid-gas transition was assumed [67].

About a decade later, Nichols et al. [70] performed detailed ultrasonic measurements on pure V_2O_3 determining the whole set of elastic constants and their temperature dependence between 300 K and 640 K. As V_2O_3 has the trigonal crystal symmetry class $R\bar{3}c$, it has 6 independent elastic moduli constants. Plotting the temperature dependence of the eigenvalues of the elastic constant matrix, as shown on the left of Fig. 4.14, one obtains a strong decrease of $\lambda_4 = \frac{1}{2}(C_{11} + C_{12} + C_{33}) - \frac{1}{2}\sqrt{(C_{11} + C_{12} - C_{33})^2 + 8C_{13}^2}$. This decrease goes down to about 26% of its value at 300 K and occurs at temperatures of the order of the critical endpoint. For the doped compound located at the critical endpoint of the Mott transition, we, therefore, expect the elastic modulus of this mode to vanish which corresponds to the condition $(C_{11} + C_{12})C_{33} - 2C_{13}^2 = 0$. The other eigenvalues, on the other hand, seem to be only slightly temperature dependent.

The corresponding strain is a superposition of longitudinal strains in the basal plane ($e_1 + e_2$) and along the c-axis (e_3). The ratio of the two contributions is given by $(e_1 + e_2)/e_3 = -2C_{13}/(\lambda_4 - C_{33})$ which also goes through a minimum. Notably, this mode is not associated with a breaking of the crystal symmetry as $e_1 + e_2$ and e_3 are invariant under all $\bar{3}m$ crystal symmetry operations. This agrees with our prediction of an isostructural instability close to the Mott transition. Also, the pronounced softening of only a single mode fits to our assumption, that the most important coupling should be bilinear as explained in Sec. 3.1.

In Fig. 4.15, we show the conductivity data obtained by Limelette et al. [54]. They found mean field behavior over at least two decades in temperature and pressure. Only for pressures of the order of $p - p_c \sim 10^{-3} p_c \approx 4$ bar, i.e., in the immediate vicinity of the critical endpoint, deviations were seen. Comparison with the pressure range of $p - p_c \approx 4000$ bar, on which the crystal softening is already very pronounced, this should be deep within the regime of elastic criticality. Therefore, we conclude that the elastic Landau regime is larger than the Ising critical regime and, thus, there is only a crossover from the Mott Landau regime to the elastic Landau regime.

Recently, also ultrasonic measurements of transversal and longitudinal waves propagating along the c-axis of $(V_{1-x}Cr_x)_2O_3$ with $x = 0.11$ were performed [71]. The velocity changes of these two acoustic waves give access to the pressure dependence of the two elastic moduli C_{33} and C_{44} , respectively. The first one shows a pronounced softening, whereas the latter shows no sign of critical behavior which coincides with the measurements of the pure compound [70]. Unfortunately, the constants C_{11} and C_{12} were not accessible, which showed a much stronger decrease in the pure compound.

In future experiments, it would be instructive to obtain the pressure dependence of the elastic constant λ_4 close to the critical point. Most interesting would be a direct measurement of the order parameter of the transition, which is the corresponding strain, $E = e_1 + e_2 + ae_3$. The coefficient a close to the endpoint can be estimated from Ref. [70] as $a = 2C_{13}/C_{33} \approx 0.8$. Such a measurement of the lattice constants can be achieved by Lamor diffraction experiments as, for instance, done for MnSi in Ref. [72].

4.6 Summary and Discussion

In this chapter, the influence of the elastic lattice on the Mott metal-insulator transition was investigated as an example for an electronic finite temperature phase transition. It turned out that the non-perturbative bilinear coupling has a strong influence on the transition and even changes the universality class of its critical end-

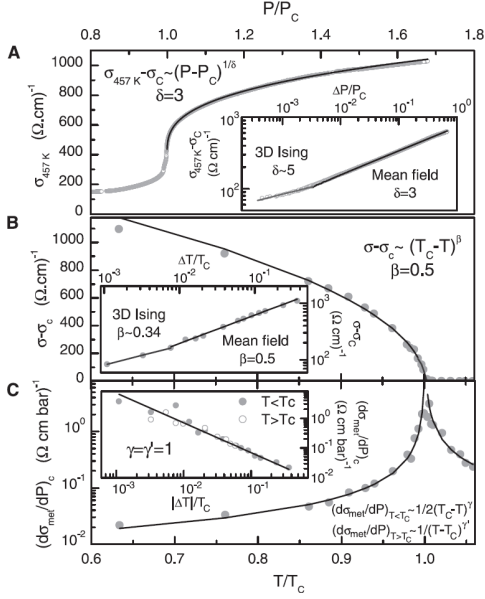


Fig. 4.15: Measurements of the critical exponents for V_2O_3 by [54]. Over large temperature and pressure ranges mean field behavior is obtained. Only very close to the endpoint a deviation can be seen which the authors of this study interpreted as 3D Ising critical behavior. It sets in at pressures of the order of $p - p_c \sim 10^{-3} p_c \approx 4$ bar and temperatures around $T - T_c \sim 10^{-2} T_c \approx 457.5$ K

point. The expected Ising critical behavior turns into a mean field elastic endpoint upon approaching the endpoint.

The size of the region of elastic criticality distinguishes two different scenarios as shown in Fig. 4.6. Far away from the critical endpoint where fluctuations are weak the system exhibits Mott Landau mean field behavior. For small elastic couplings, the system first exhibits upon approaching the endpoint a crossover to the Ising critical behavior of the Mott transition. Eventually, the elastic coupling becomes strong enough and by a second crossover the elastic mean field region is entered. On the other hand, for large couplings, the elastic Landau regime may be comparable or even larger than the Ising critical regime of the Mott transition. Thus, the system directly crosses from a Mott Landau into an elastic Landau regime.

Starting from the assumption that the system does exhibit a finite regime of Ising criticality, we derived the critical free energy for the elastically coupled Mott transition and deduced the critical thermodynamics. The most important feature to identify critical elasticity is the breakdown of Hooke's law, i.e., a non-linear stress-strain relation close to the critical endpoint. This is the smoking gun criterion to detect the elastic Landau regime.

Another important feature is the behavior of the specific heat which upon approaching the critical endpoint does not diverge. Instead, the specific heat coefficient exhibits a mean field jump of $\Delta\gamma \approx 0.63 f_0 / T_0^2$, where T_0 and f_0 are some non-universal temperature and energy scales. Strikingly, the height of the jump does not depend on the strength of the coupling. The thermal expansion and the compressibility follow a mean field behavior, as the asymptotics can be described by the Ising mean field exponents $\beta = 1/2$ and $\delta = 3$.

Two well studied examples of the Mott transition are κ -(BEDT-TTF) $_2$ X and chromium doped V_2O_3 . We argued, that the former realizes the scenario with two

crossovers, exhibiting an Ising critical regime. Based on thermal expansion data [1, 2], we estimated the extent of the elastic Landau regime as $\Delta T^* \approx 2.5$ K and $\Delta p^* \approx 50$ bar. The conductivity measurements by Kagawa et al. [55] indicate indeed a crossover at a temperature scale of the order of ΔT^* . However, the available data does not conclusively support a crossover to mean field exponents and further experimental investigations are needed. Since the compound of Ref. [1] is at ambient pressures already above or at the crossover to the Ising critical regime, it would be, in particular, instructive to investigate a member of the κ -(BEDT-TTF)₂X family with a lower chemical pressure.

In V₂O₃, we argued that the crossover to the Ising critical regime is preempted by the elastic Landau regime and, thus, Ising critical behavior is not obtained. A comparison of elastic measurements in the pure material with conductivity measurements in the chromium doped compound close to the endpoint, suggests that one of the elastic constants gets critical long before a deviation from mean field behavior is observed. Since the elastic mode which gets soft at the transition could be identified, it would be interesting to obtain its actual pressure dependence close to the endpoint. Thereby, the regime of critical elasticity could be detected directly by the breakdown of Hooke's law.

Chapter 5

Quantum Critical Metamagnets

In the last chapter, we discussed the effects of an elastic coupling to a finite temperature phase transition. Here, we consider the situation of a transition at zero temperature, a quantum phase transition (QPT), which arises when the ground state of a system changes in response to a non-thermal control parameter. This field of condensed matter theory was pioneered by Hertz [73] in 1976 and since then attracted much attention. For reviews see, e.g., Refs. [74–76].

Although there is, in principle, a large variety of non-thermal control parameters, many of them have conceptual or experimental disadvantages. Applying chemical pressure by doping introduces crystal defects, disorder and, in particular, cannot be varied continuously. Therefore, sweeps through the quantum critical point are not possible. Applying physical pressure, on the other hand, although continuously variable, causes difficulties in measuring some thermodynamic quantities due to the experimental setup in a pressure cell. Using a magnetic field as a tuning parameter inherently breaks the spatial symmetry of the system. Thus, many phase transitions induced by a finite magnetic field are first-order transitions which do not yield diverging susceptibilities.

However, there are different examples where a field-driven transition is of second order as, for instance, the Bose-Einstein condensation of magnons, see Ref. [77, 78]. In other materials, a phase transition between a low-magnetization state to a high-magnetization state occurs at a finite applied magnetic field $H_c > 0$. Such so-called metamagnetic systems provide another way to magnetic field driven quantum critical points. The possibility of metamagnetic quantum criticality was introduced by Grigera et al. [79] when analyzing the layered perovskite $\text{Sr}_3\text{Ru}_2\text{O}_7$. They found that the endpoint of the first-order metamagnetic transition could be driven to lower temperatures and eventually to zero. Thus, they concluded that the system exhibits a so-called quantum critical endpoint (QCEP) which differs from usual quantum critical points by the absence of a spontaneous symmetry breaking. Recently, it was suggested that a metamagnetic QCEP might even be a generic feature for materials

with an itinerant ferromagnetic phase when applying pressure [3] which increased the interest in quantum critical metamagnetism even further.

In this chapter, we focus on the bare metamagnetic QCEP and follow essentially our work as described in Ref. [80], whereas the discussion of elastic effects is postponed to the next chapter. In the following, we review the mean-field theory of metamagnetism and the experimental findings concerning metamagnetic criticality in Sec. 5.1. Thereafter, we introduce the spin-fluctuation theory of metamagnetism (Sec. 5.2) from which we obtain the effective potential of the theory. In Sec. 5.3, we derive the magnetization and the free energy from which the thermodynamics follow as function of applied field and temperature discussed in Sec. 5.4.

5.1 Metamagnetism

Metamagnetism is a phenomenological term for a super-linear rise of the magnetization at a finite magnetic field, H . In some systems it may even jump at a first-order transition. Since no symmetry is broken at a metamagnetic transition, the line of first-order transitions in a (H, T) diagram terminates in a critical endpoint, (H^*, T^*) , where the transition is of second order and above which the magnetization increases rapidly but smoothly. If by tuning of a third control parameter this endpoint can be driven to zero temperature, one obtains a QCEP. In the following, we briefly discuss the theoretical background of metamagnetism and subsequently give an overview of experimental evidence of a QCEP.

5.1.1 Mean-Field Theory

To introduce the basic principle behind metamagnetism, we follow Ref. [81] and consider the simplest model of the magnetization, \mathbf{M} , in a magnetic field, \mathbf{H} . Since the field breaks rotational invariance, we can focus on the component of the magnetization parallel to the field, $M = \mathbf{M} \cdot \hat{\mathbf{H}}$, and expand the free energy in it. In absence of a magnetic field the system has an Ising symmetry, therefore, this expansion can only contain even powers of the magnetization and reads as

$$F(M) = -g\mu_B H M + \frac{a}{2} M^2 + \frac{u}{4} M^4 + \frac{v}{6} M^6. \quad (5.1)$$

This approach of course neglects the effects of thermal and quantum fluctuations, but it will suffice to get an understanding of the metamagnetic transition. To obtain a second minimum of the free energy, we need $a > 0$, $u < 0$ and of course $v > 0$ to stabilize the potential. Upon rescaling $M = m\sqrt{|u|/v}$ and $g\mu_B H = \tilde{H}\sqrt{|u|^5/v^3}$, Eq. (5.1) takes the form

$$F(M) = \frac{|u|^3}{v^2} \left(-\tilde{H}m + \frac{\alpha}{2}m^2 - \frac{1}{4}m^4 + \frac{1}{6}m^6 \right), \quad (5.2)$$

where $\alpha = av/u^2$ is the only free coefficient of the system.

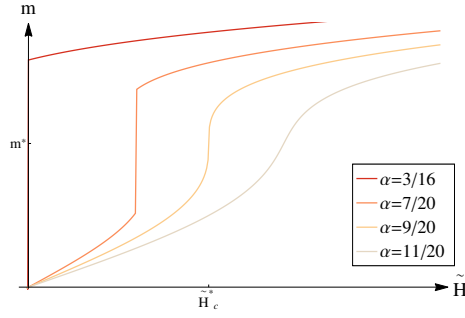


Fig. 5.1: Magnetization for different values for α . The metamagnetic transition happens for $\frac{3}{16} \leq \alpha \leq \frac{9}{20}$. For larger values we only get a metamagnetic crossover, whereas for lower values the system is a ferromagnet.

In contrast to the ferromagnetic transition, a metamagnetic phase transition is characterized by the fact that the second minimum, $m \neq 0$, is a local minimum at zero field and only becomes a global minimum for finite fields. This happens exactly for $\alpha = 3/16$. On the other hand, we obtain a jump of the magnetization at a finite field \tilde{H}^* only if the free energy at zero field has an inflection point, which yields $\alpha_c \leq 9/20$. Above this value one gets no longer a phase transition but only a crossover from a low-magnetization to a high-magnetization region.

Exactly at α_c , one obtains the second-order critical endpoint, where the slope of the magnetization curve diverges as a function of applied field. The critical field, \tilde{H}_c^* , and magnetization, m^* , are given by

$$\tilde{H}_c^* = \sqrt{\frac{3}{10}} \left(\alpha_c - \frac{21}{100} \right) \quad , \quad m^* = \sqrt{\frac{3}{10}}. \quad (5.3)$$

Expanding the potential in $\phi = m - m^*$ and setting $h = \tilde{H} - \tilde{H}^*$ we obtain up to constants the Landau functional to be

$$\frac{v^2}{|u^3|} F(\phi) = -h\phi + \frac{1}{2} \left(\alpha - \frac{9}{20} \right) \phi^2 + \frac{1}{2} \phi^4 + \sqrt{\frac{3}{10}} \phi^5 + \frac{1}{6} \phi^6, \quad (5.4)$$

Thus, the quadratic term vanishes at the critical point, $\alpha_c = 9/20 = 0$ and we obtain a second-order transition at $h = 0$.

The potential has no specific symmetry and contains, in principle, all powers of the field, ϕ . Due to the definition of ϕ , the cubic term vanishes and in the limit of negligible quintic and higher coupling the model has an emergent Ising symmetry. However, taking fluctuations into account will, in principle, lead to a cubic term in the effective theory. We will address this issue in our analysis in Sec. 5.2.

In Fig. 5.1, the magnetization as a function of magnetic field is depicted for some values of α . For values of $\alpha < 3/16$ we see jump of the magnetization at $h = 0$, i.e., a ferromagnetic transition. Upon further increasing α the magnetization rises smoothly at small fields,. However, for $3/16 \leq \alpha \leq 9/20$ the magnetization exhibits

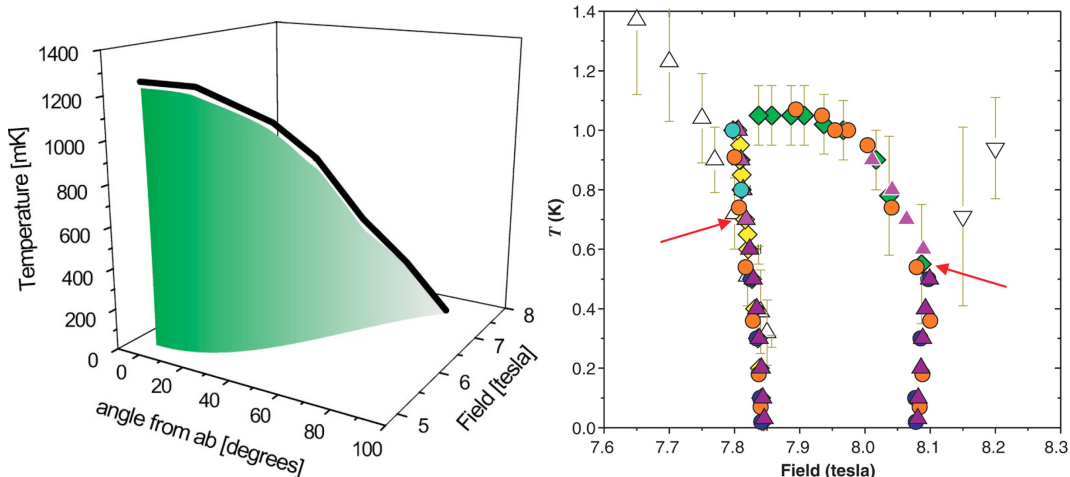


Fig. 5.2: Left panel: Phase diagram of $\text{Sr}_3\text{Ru}_2\text{O}_7$ taken from Ref. [85]. The shaded surface depicts the area of first-order metamagnetic transitions. It is bounded by a solid line of second-order critical endpoints, which shows a strong angular dependence. Tilting the magnetic field from the ab -plane into the direction of the c -axis reduces the critical temperature to nearly $T = 0$.

Right panel: Experimental phase diagram of $\text{Sr}_3\text{Ru}_2\text{O}_7$ for fields applied in the c -direction taken from Ref. [86]. Close to the putative QCEP at $H_c \approx 7.8$ T, a phase with nematic electronic characteristics is entered. The red arrows indicate endpoints, where for higher temperatures the transition is of second order, whereas it is of first-order for lower temperatures.

a jump at some finite field, \tilde{H}_c , whereas for higher values the super-linear rise of the magnetization is continuous. For $\alpha = 9/20$, the slope of the magnetization diverges indicating the second-order endpoint.

5.1.2 Experiments

The scenario of metamagnetic quantum critical endpoints in real materials was first addressed by Millis et al. [82]. Based on data of Perry et al. [83], they suggested that the bilayer ruthenate $\text{Sr}_3\text{Ru}_2\text{O}_7$ is a candidate material close to such a QCEP at ambient pressures. Resistivity measurements at low temperatures by Grigera et al. [79, 84] on this perovskite compound indeed showed strong indications of metamagnetic quantum criticality at a rather small field of about 7.8 T applied parallel to the c -axis.

Further studies [85] revealed a dependence on the angle of the applied field with respect to the c -axis. Applying the field in the ab -plane, the endpoint lies at approximately $T_c = 1.25$ K, whereas it could be tuned below 50 mK for fields having a 10° angle with the c -axis. Thus, an easy-to-handle second tuning parameter was found showing the critical point to be indeed an endpoint of a first-order transition line. The corresponding phase diagram is shown on the left side of Fig. 5.2.

However, in ultra-pure samples the metamagnetic transition was shown to split at lowest temperatures into two first-order transitions [87, 88]. As it turned out,

the quantum critical endpoint was preempted by the formation of a novel phase which has electronic nematic features [86]. Resistivity measurements showed that the fourfold symmetry of the RuO₂ planes was reduced to a twofold symmetry giving rise to the idea of a *d*-wave Pomeranchuk instability of the Fermi surface. Electron-lattice coupling also induces an crystal anisotropy which was confirmed by thermal expansion measurements [89]. However, it is not clear yet what is actually the driving force of the formation of the nematic phase. A current review of the nematic phase in Sr₃Ru₂O₇ can be found in Ref. [90].

Applying hydrostatic pressure also decreases the critical temperature, as shown in Ref. [91], where the magnetic field was applied in the *ab*-plane. The QCEP was determined to be at $p_c \approx 13.6$ kbar and, importantly, no evidence of a nematic phase masking the QCEP was found. However, pressure tuning yields experimental difficulties for some measurements due to the required pressure cell and also increases the transition field from $H^* \approx 5$ T to $H^* \approx 9$ T. To further investigate the metamagnetic quantum critical point also the magnetoelastic coupling in the related single layer ruthenate SrRuO₄ doped with calcium was investigated [92].

Metamagnetism was also investigated in antiferromagnetic heavy-fermion compounds, some of which may also have a metamagnetic QCEP. More than twenty years ago, a metamagnetic transition in CeRu₂Si₂ at lowest temperatures was found [93–96]. It turned out that the putative metamagnetic quantum endpoint is located at negative pressures in the phase diagram of CeRu₂Si₂. Such negative pressures can be achieved by doping with lanthanum [97] which yields a volume expansion. Also CeRh₂Si₂ [98], UPt₃ [99] as well as MnSi [100] show metamagnetic behavior. However, up to now a metamagnetic QCEP is found in none of those compounds yet.

Recently, Belitz et al. [3] suggested that a metamagnetic quantum endpoint might even be a generic feature of itinerant ferromagnets. When applying pressure to ferromagnets, neighboring sites get closer together, and the overlap of the wavefunction increases yielding a larger spin-spin coupling constant and a decreasing Curie temperature. Non-analytic corrections in Fermi liquid theory yield a non-analytic long-range interaction of the order parameter. This interaction leads to the termination of the second-order transition line in a tricritical point, where the ferromagnetic transition becomes first-order. From the tricritical point wings of first-order metamagnetic transition surfaces emerge in the (T, H, p) space, see Fig. 5.3. The boundary of these wings is a line of second-order critical endpoints which may also be tuned to zero by further increasing the pressure.

This scenario could explain previously found metamagnetic features in ZrZn₂ [101] and UGe₂ [102] close to the critical pressure, where the Curie temperature goes to zero. Further measurements on the boundary of the metamagnetic first-order transition in UGe₂ [5, 6] estimated $(H_c, p_c) = (17-19 \text{ T}, 3.5-3.6 \text{ GPa})$ for the

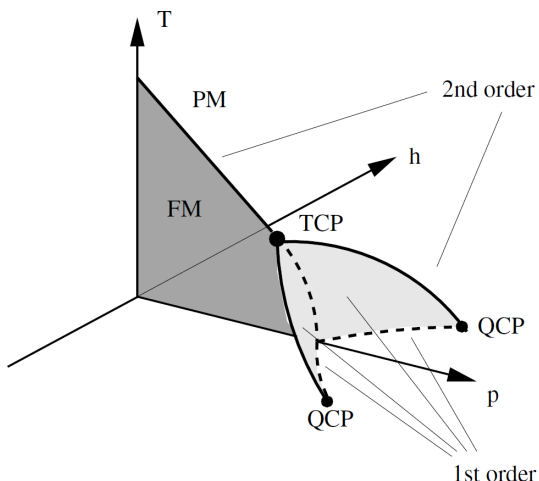


Fig. 5.3: Generic phase diagram of an itinerant ferromagnet (FM) proposed in Ref. [3]. Applying pressure decreases the Curie temperature of the ferromagnetic transition. The line of second-order phase transitions terminates at a tricritical point (TCP), where the transition becomes first-order. For finite fields, two wings of first-order metamagnetic transitions emerge which are bounded by line of second-order endpoints. Increasing pressure and field the critical temperature decreases eventually ending in a quantum critical point (QCP).

QCEP by extrapolation. Finally, Aoki et al. [4] reported evidence for a metamagnetic QCEP of UCoAl at a critical pressure of $p_c \approx 1.5$ GPa and an applied magnetic field of $H_c \approx 7$ T.

5.2 Spin-Fluctuation Theory

As shown in Sec. 5.1, close to the metamagnetic instability the longitudinal part of the magnetization, M , becomes critical, fluctuating around a mean value M^* . The classical potential for the deviations was given in Eq. (5.4) as

$$\mathcal{V}_0(\phi) = -h_0\phi(\mathbf{r}) + \frac{r_0}{2}\phi(\mathbf{r})^2 + \frac{u_{30}}{3!}\phi(\mathbf{r})^3 + \frac{u_{40}}{4!}\phi(\mathbf{r})^4 + \frac{u_{50}}{5!}\phi(\mathbf{r})^5 \quad (5.5)$$

where we allowed for spatial fluctuations of the magnetization. As the Ising symmetry is broken by the applied magnetic field, the resulting potential, in principle, contains all powers of ϕ .

Additionally, the effective action of the quantum theory contains a fluctuation part which follows from spin-fluctuation theory by Millis et al. [82]:

$$\mathcal{S}_{\text{fl}}[\phi] = \frac{1}{2} \sum_{\mathbf{k}, \omega_n} \Delta(\mathbf{k}, \omega_n) \phi_{\mathbf{k}, \omega_n} \phi_{-\mathbf{k}, \omega_n}, \quad (5.6)$$

$$\Delta(\mathbf{k}, \omega_n) = \mathbf{k}^2 + \frac{|\omega_n|}{|\mathbf{k}|}. \quad (5.7)$$

The dynamic part, $|\omega_n|/|\mathbf{k}|$, is a Landau-damping term originating from particle-hole excitations in the metal, determining the critical exponent $z = 3$. Since we will consider dimensions $d = 2, 3$, the effective dimension defined as $D = d + z$ is well above the upper critical dimension, $d^+ = 4$. Note that we rescaled variables, where length and energy are measured in dimensionless units. The resulting effective action then takes the following form:

$$\mathcal{S}[\phi] = \frac{1}{2} \sum_{\mathbf{k}, \omega_n} \phi_{\mathbf{k}, \omega_n} \Delta(\mathbf{k}, \omega_n) \phi_{-\mathbf{k}, \omega_n} + \int d\tau \int d\mathbf{r} \mathcal{V}_0(\phi(\mathbf{r}, \tau)), \quad (5.8)$$

with $\mathcal{V}_0(\phi)$ given in Eq. (5.5). Here, h_0 and r_0 measure the distance to the critical point and are assumed to be small.

Concerning the validity of the spin-fluctuation theory there are two general assumptions. First, the Taylor expansion of the bare potential, Eq. (5.5), has to exist, and, second, the static susceptibility has to be an analytic function of momenta such that indeed $\Delta(k, 0) = k^2$. As the coefficients depend on the derivatives of the density of states, it has to be sufficiently smooth at the Fermi energy. Van-Hove singularities at the Fermi energy, for example, would spoil the possibility of this expansion.

Also non-analytic corrections to the correlation functions in Fermi liquid theory can be induced by interaction effects. As already mentioned, in particular for ferromagnetic quantum phase transitions interactions between fermions and the long-wavelength bosonic modes induce non-analyticities in the static spin susceptibility as well as in the Landau potential, see Refs. [103–105]. Long-range interactions of the order parameter fluctuations mediated by virtual particle-hole pairs may even render the ferromagnetic transition first-order [3].

However, for a metamagnetic instability the Pauli susceptibility and the magnetic field have already a finite value. Thus, spin-flip processes are frozen out, and the Ising order parameter couples to the relative density fluctuations of the spin-majority and spin-minority Fermi surfaces. This leads then to the fact that in contrast to the SU(2) case the non-analytic contributions cancel out, and the static spin susceptibility is indeed analytic, $\chi^{-1} \sim k^2$ as shown in Ref. [104]. Therefore, the model given in Eq. (5.8) is applicable to the metamagnetic transition provided that there is no van-Hove singularity at the Fermi level.

In principle, all parameters of the action are functions of applied magnetic field, pressure and temperature and can be obtained from microscopic calculations, see Ref. [106]. However, in the following this dependence is assumed to be small. In particular, the couplings u_i and the mass r_0 are treated as constant with respect to temperature whereas for the field h_0 we assume that it has an implicit Fermi liquid-like temperature dependence proportional to T^2 ,

$$h_0(H, p, T) \approx h_0(H, p) + h_T T^2 \quad (5.9)$$

$$r_0(H, p, T) \approx r_0(H, p). \quad (5.10)$$

Although h_T is irrelevant in the RG sense, it yields important corrections to thermodynamics, and its effects will be discussed in Sec. 5.4 below.

5.2.1 Wegner-Houghton Equation

Rather than treating the fluctuations close to the metamagnetic endpoint perturbatively, we will in the following consider their effects in a systematic self-consistent way. This is done by means of the renormalization group (RG) in the spirit of Wegner and Houghton (see Ref. [107] for details). They derived the so-called Wegner-Houghton equation which is a formally exact functional differential equation describing the flow of the effective action upon infinitesimally decreasing the cutoff Λ . This captures all momentum-dependent interactions in a infinite hierarchy of functional RG equations.

Integrating out an infinitesimal high-energy/high-momentum shell, $[\Lambda e^{-l}, \Lambda]$ with $l \ll 1$, of the Gaussian part of the action adds the re-exponentiated propagator to the potential, $\tilde{\mathcal{V}}(\phi) = \mathcal{V}(\phi) + f(T, r_0)$, where the function f is given by

$$\begin{aligned} f(T, r_0) &= \frac{1}{2} \frac{\partial}{\partial \ln \Lambda} \ln \det G(r_0, \mathbf{k}, \omega_n) \\ &= \frac{1}{2} \Lambda \frac{\partial}{\partial \Lambda} \int_0^\Lambda \frac{d^d \mathbf{k}}{(2\pi)^d} \frac{1}{\beta} \sum_{\omega_n} \ln G(r_0, \mathbf{k}, \omega_n). \end{aligned} \quad (5.11)$$

Here, in the second line we assumed a scalar propagator, G , and the summation over Matsubara frequencies has to be understood as regularized by the cutoff Λ^z . In the usual spirit of the RG approach, we rescale the residual action to the original cutoff Λ , yielding a renormalization of the bare parameters according to their engineering dimensions, i.e., $r_0 \rightarrow r_0 e^{2l}$ and $T \rightarrow T e^{z l}$. The full mass term of the renormalized action is now given by the second derivative of the potential $\tilde{\mathcal{V}}$ with respect to the field ϕ instead of the bare mass, r_0 . Iterating this procedure corresponds to an integration along a trajectory of the RG flow and the effective potential at an RG scale λ is given by

$$\mathcal{V}_\lambda(\phi) = \mathcal{V}_0(\phi) + \int_0^\lambda dl e^{-Dl} f(T e^{zl}, \mathcal{V}_l''(\phi) e^{2l}). \quad (5.12)$$

Thus, in the limit $\lambda \rightarrow \infty$ we get a self-consistent equation for the effective potential, $\mathcal{V}(\phi)$, for the macroscopic magnetization summing up the effects of the fluctuation in the additional integral to infinite order.

Having a closer look at the function $f(T, R)$, we see that we can split it in two parts $f(T, R) = f_0(R) + f_\infty(T, R)$ which are of different nature. The first one is given by an analytic expansion of $f(0, R)$ to second order in the mass,

$$f_0(R) = f(0, 0) + f^{(0,1)}(0, 0) R + \frac{1}{2} f^{(0,2)}(0, 0) R^2. \quad (5.13)$$

Its contribution to the RG flow, Eq. (5.12) is exponentially suppressed by at least a factor of $e^{-(d-4)l}$ and thus yields a significant correction only at the beginning of the flow. Because of this, we can conveniently absorb its effect into a renormalization of

the bare parameters of the potential given in Eq. (5.5), as the new starting values of the remaining RG flow,

$$\begin{aligned}\mathcal{V}_{\text{ren}}(\phi) &= \mathcal{V}_0(\phi) + \int_0^\infty dl e^{-Dl} f_0(\mathcal{V}_0''(\phi)e^{2l}) \\ &\equiv -h\phi + \frac{r}{2!}\phi^2 + \frac{u}{4!}\phi^4 + \frac{u_5}{5!}\phi^5 + \dots\end{aligned}\quad (5.14)$$

In the last line we skipped an unimportant constant and, furthermore, used the freedom to shift the field ϕ to eliminate the cubic term. For a negligible quintic term the potential gains an emergent Ising symmetry, however, note that the quintic term will lead to renormalizations as specified below.

The remaining contribution, $f_\infty(T, R)$, is most important at the final stage of the RG flow and captures the universal fluctuation corrections. Substituting in the integral $l = \mu + \ln(\Lambda T^{-1/z})$ we obtain the fluctuation function

$$T^{D/z} \mathcal{A}_d(R T^{-2/z}) = T^{D/z} \int_{-\ln \Lambda T^{-1/z}}^\infty d\mu e^{-D\mu} \Lambda^{-D} f_\infty(\Lambda^z e^{z\mu}, \Lambda^2 R T^{-2/z} e^{2\mu}), \quad (5.15)$$

where the subscript d accounts for the spatial dimensionality. Thus, the effective potential for the macroscopic magnetization is given by

$$\mathcal{V}(\phi) = \mathcal{V}_{\text{ren}}(\phi) + T^{D/z} \mathcal{A}_d(\mathcal{V}''(\phi) T^{-2/z}), \quad (5.16)$$

which is a self-consistent differential equation and usually hard to solve. However, it turns out that it can be solved perturbatively for small temperatures and the asymptotic behavior can be determined.

5.2.2 Effective Metamagnetic Potential

For the metamagnetic action, Eq. (5.8), replacing the Matsubara summation by an integral along the branch cut singularity and employing a hard cutoff regularization, the integration kernel, f , is given by

$$\begin{aligned}f(T, R) &= \frac{K_d}{2} \Lambda \frac{\partial}{\partial \Lambda} \int_0^\Lambda dk k^{d-1} \int_{-\Lambda^z}^{\Lambda^z} \frac{d\omega}{2\pi i} \coth \frac{\omega}{2T} \ln(r + \mathbf{k}^2 - i \frac{\omega}{|\mathbf{k}|}) \\ &= K_d \Lambda \frac{\partial}{\partial \Lambda} \int_0^\Lambda dk k^{d-1} \int_0^{\Lambda^z} \frac{d\omega}{2\pi} \coth \frac{\omega}{2T} \text{Im}\{\ln(R + k^2 - i \frac{\omega}{k})\} \\ &= -\frac{K_d}{2\pi} \Lambda \frac{\partial}{\partial \Lambda} \int_0^\Lambda dk k^{d-1} \int_0^{\Lambda^z} d\omega \coth \frac{\omega}{2T} \arctan \frac{\omega}{k(R + k^2)},\end{aligned}\quad (5.17)$$

where the d -dimensional angular integration yields the factor $K_d = \left[2^{d-1} \pi^{\frac{d}{2}} \Gamma(\frac{d}{2})\right]^{-1}$. The derivative with respect to the cutoff gives, in principle, two terms corresponding to the two integrals. However, as the derivative with respect to the energy integration

only leads to sub-leading contributions, we will omit it. With this simplification and substituting $\epsilon = \omega/(2T)$, the function $\mathcal{A}_d(x)$ reads

$$\mathcal{A}_d(x) = \mathcal{A}_{d,0}(x) - \frac{K_d}{2\pi} \int_0^{\Lambda^z} d\epsilon (\coth \epsilon - 1) \int_{-\ln \Lambda T^{-1/z}}^{\infty} d\mu e^{-d\mu} 2 \arctan \frac{2e^{z\mu}\epsilon}{xe^{2\mu} + 1}, \quad (5.18)$$

where the term $\mathcal{A}_{d,0}(x)$ accounts for the zero-temperature part of the function $f_\infty(T, R)$. It can be evaluated exactly, whereas for the rest we can calculate the asymptotic behavior for small and large arguments. This asymptotics are given in $d = 3$ dimensions to leading order by

$$\mathcal{A}_3(x) = \begin{cases} -\mathbf{b}_1 \log \frac{\Lambda^3}{T} - \mathbf{b}_0 + \mathbf{b}_2 x - \mathbf{b}_3 x^{\frac{3}{2}} & , x \ll 1 \\ \bar{\mathbf{b}}_1 x^3 \log \frac{\Lambda^3}{Tx^{3/2}} + \bar{\mathbf{b}}_0 x^3 - \bar{\mathbf{b}}_2 \log \frac{\Lambda^3}{Tx^{3/2}} + \bar{\mathbf{b}}_3 x^{-3} \log x & , \frac{\Lambda^2}{T^{2/3}} \gg x \gg 1, \end{cases} \quad (5.19)$$

which has a remaining dependence on the non-universal cutoff Λ . The coefficients \mathbf{b}_0 and $\bar{\mathbf{b}}_0$ can be absorbed in the non-universal logarithmic dependence of the leading behavior, and both are omitted in the following. The other coefficients are

$$\begin{aligned} \mathbf{b}_1 &= \frac{1}{36\pi}, & \mathbf{b}_2 &= \frac{1}{6\sqrt{3}\pi^2} \Gamma(4/3) \zeta(4/3), & \mathbf{b}_3 &= \frac{1}{12\pi}, \\ \bar{\mathbf{b}}_1 &= \frac{1}{72\pi^3}, & \bar{\mathbf{b}}_2 &= \frac{1}{36\pi}, & \bar{\mathbf{b}}_3 &= \frac{\pi}{60}. \end{aligned} \quad (5.20)$$

For $d = 2$ dimensions we obtain

$$\mathcal{A}_2(x) = \begin{cases} -\mathbf{c}_1 + \mathbf{c}_3 x \log \frac{1}{x} & , x \ll 1 \\ \bar{\mathbf{c}}_1 x^{\frac{5}{2}} - \bar{\mathbf{c}}_2 x^{-\frac{1}{2}} + \bar{\mathbf{c}}_3 x^{-2} & , x \gg 1 \end{cases}, \quad (5.21)$$

which is universal in the limit $\Lambda/T^{1/3} \rightarrow \infty$, i.e., independent of the cutoff, Λ . The coefficients are given as

$$\mathbf{c}_1 = \frac{1}{4\pi} \Gamma(5/3) \zeta(5/3), \quad \mathbf{c}_3 = \frac{1}{8\pi}, \quad \bar{\mathbf{c}}_1 = \frac{1}{30\pi}, \quad \bar{\mathbf{c}}_2 = \frac{\pi}{24}, \quad \bar{\mathbf{c}}_3 = \frac{1}{4\pi} \zeta(3). \quad (5.22)$$

The limiting behaviors for $d = 2, 3$ can be summarized as

$$\mathcal{A}_d(x) = \begin{cases} -\mathbf{a}_1 + \mathbf{a}_2 x - \mathbf{a}_3 x^{\frac{d}{2}} & , x \ll 1 \\ x^{\frac{D}{2}} \left(\bar{\mathbf{a}}_1 - \bar{\mathbf{a}}_2 x^{-z} + \bar{\mathbf{a}}_3 x^{-\frac{z(d-z+4)}{2}} \right) & , x \gg 1 \end{cases}, \quad (5.23)$$

where the coefficients are positive up to logarithms.

The term proportional to $\bar{\mathbf{a}}_1$ stems from the zero-temperature part, $\mathcal{A}_{d,0}(x)$, whereas the non-analytic term with coefficient \mathbf{a}_3 originates from the zero Matsubara mode. The term with the coefficient $\bar{\mathbf{a}}_3$ will give rise to non-analytic Fermi liquid corrections.

In the following, we will only consider situations, where all coupling constants in Eq. (5.14) are positive. This includes, in particular, $r > 0$, implying that we will approach the critical endpoint, $r = 0$, from above, and we will not discuss the first-order transition occurring for negative r .

5.3 Free Energy

The effective dimension is well above the upper critical dimension, $D > d^+ = 4$, and, hence, the quartic and quintic coupling as well as even higher terms are irrelevant in the RG sense. However, the fourth-order term is needed to stabilize the potential and therefore we have to keep it. The influence of the quintic term, u_5 , will be addressed only when it is necessary.

Omitting the quintic term, the potential obtains an emergent Ising symmetry, i.e., it is invariant under the transformation $(h, \phi) \rightarrow (-h, -\phi)$. Hence, we can immediately conclude that for lowest temperatures the critical free energy density, \mathcal{F}_{cr} , has to be an even function of the field h . As in Chap. 4, we obtain the free energy by minimizing the effective potential, Eq. (5.16).

Just as for the Mott-transition in Chap. 4, the most relevant operator is h , which is proportional to the deviation from the metamagnetic field, $h \sim H - H^*$. Due to the linear coupling to the magnetization, ϕ , it acts as a force driving it out of its zero-field equilibrium value $\phi = 0$. The finite-field equilibrium configuration is reached when the potential built by the quadratic and quartic term cancel this force. The magnitude of the magnetization depends, thus, on the stiffness of the potential. In the following, we distinguish a linear regime with a stiff potential and a non-linear regime, where the potential is soft.

5.3.1 Linear Regime

In the linear regime, the minimizing configuration, $\bar{\phi}$, is close to zero, and we may simply expand the effective potential, Eq. (5.16), in ϕ . Thereby, the parameters of the effective theory become temperature-dependent and are defined by the value of the respective derivative of the effective potential at $\phi = 0$. The potential stiffness, $R(T) = \mathcal{V}^{(2)}(0)$, is to leading order in the temperature given as

$$R(T) = r + uT^{(D-2)/z} \mathcal{A}'_d \left(RT^{-2/z} \right). \quad (5.24)$$

Furthermore, we obtain also a renormalization of the magnetic field due to existence of the quintic term

$$H(T) = h - U_3 T^{(D-2)/z} \mathcal{A}'_d \left(RT^{-2/z} \right) \quad (5.25)$$

$$U_3(T) = u_5 T^{(D-2)/z} \mathcal{A}'_d \left(RT^{-2/z} \right) \quad (5.26)$$

The renormalization of higher terms is skipped as they are already irrelevant operators. All renormalizations are given by the first derivative of the function \mathcal{A}_d and have asymptotically the behavior

$$T^{(D-2)/z} \mathcal{A}'_d \left(R T^{-2/z} \right) \approx \begin{cases} \mathfrak{r}_d T^{(d+1)/3} & , R \ll T^{2/3} \\ \bar{\mathfrak{r}}_{d,0} r^{(d+1)/2} + \bar{\mathfrak{r}}_d T^2 r^{(d-5)/2} & , R \gg T^{2/3} \end{cases}, \quad (5.27)$$

The temperature-independent term in the low-temperature limit yields only a constant shift for the parameters. Especially, for the potential stiffness, $R(T)$, it yields a renormalization of the bare mass which is given by $\delta r \sim r^{(d+1)/2} \ll r$ for small r and is, thus, negligible. Therefore, we will skip it in the remainder of this chapter. The other coefficients in Eq. (5.27) for dimensions $d = 2, 3$ are given as

$$\mathfrak{r}_2 = \mathfrak{c}_3 \ln \frac{T^{2/3}}{R}, \quad \bar{\mathfrak{r}}_2 = \frac{1}{2} \bar{\mathfrak{c}}_2, \quad \mathfrak{r}_3 = \mathfrak{b}_2, \quad \bar{\mathfrak{r}}_3 = \frac{3}{2} \bar{\mathfrak{b}}_2, \quad (5.28)$$

in terms of the parameters of Eq. (5.20) and Eq. (5.22), respectively. Approaching the QCEP, the temperature dependence of the potential stiffness

$$R(T) = r + u \begin{cases} \mathfrak{r}_d T^{(d+1)/3} & , R \ll T^{2/3} \\ \bar{\mathfrak{r}}_d T^2 r^{(d-5)/2} & , R \gg T^{2/3} \end{cases}, \quad (5.29)$$

is extremely important since the bare mass, r , is tuned to zero. However, finite temperatures increase the stiffness of the potential. For higher temperatures, the zero Matsubara mode, i.e., the term with coefficient \mathfrak{a}_3 , yields a contribution linear in temperature. In $d = 3$, this contribution is sub-leading, whereas in $d = 2$ it is logarithmically enhanced. On the other hand, for lowest temperatures, $R \ll T^{2/z}$, thermal fluctuations lead to a Fermi-liquid-like temperature correction, T^2 .

For the renormalization of the magnetic field, H , one could expect that similar arguments concerning its importance hold. This is, however, not the case since its renormalization is a second-order effect

$$H(T) - h \approx -u_5 \begin{cases} \mathfrak{r}_d^2 T^{2(d+1)/3} & , R \ll T^{2/3} \\ \bar{\mathfrak{r}}_d^2 T^4 r^{(d-5)} & , R \gg T^{2/3} \end{cases}. \quad (5.30)$$

for high and low temperatures, respectively.

Thus, the corrections are at least of order $\mathcal{O}(T^2 \ln^2 T)$ in $d = 2$ and of order $\mathcal{O}(T^{8/3})$ in $d = 3$. Disregarding the logarithmic enhancement in two dimensions, these corrections are of the same or even of higher order than the intrinsic temperature dependence of h , resulting from Fermi liquid theory. Thus, they are in any case sub-leading and we need not to consider them in the following, substituting therefore $H(T)$ by h .

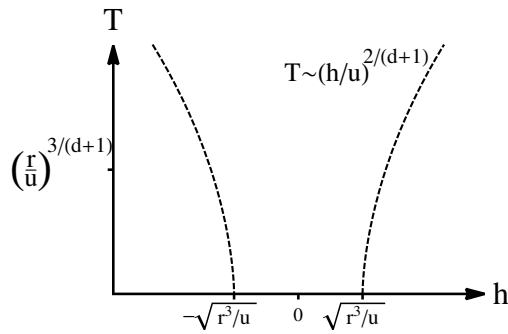


Fig. 5.4: Crossover lines between the linear regime at small fields, h , and the non-linear regime at larger fields for a finite tuning parameter r . They are determined by the condition $R^3 \sim uh^2$ and bend outwards from the center. At zero temperature they start vertical, as the effective mass equals the bare mass, $R \sim r$. At a scale $T \sim (r/u)^{3/(d+1)}$ the temperature dependence dominates R , and the crossover lines follow asymptotically a power law in h .

In the linear regime, we demand a stiff potential which requires a large quadratic term. In comparison with the cubic term, this implies $R^2 \gg U_3 h$. As U_3 goes to zero for lowest temperatures this can for finite r be always obeyed. Thus, we may skip the cubic term from the beginning, and we only compare the mass to the quartic term, yielding $R^3 \gg uh^2$. These crossover lines are depicted in Fig. 5.4. In the limit $r \ll uT^{(D-2)/z}$, the potential stiffness, R , is dominated by thermal fluctuations, and the boundaries follow $T \sim (h/u)^{2/(d+1)}$. Below a crossover temperature $T \sim (r/u)^{3/(d+1)}$, thermal fluctuations become less important, and the stiffness is determined by the constant value of r . Therefore, the boundaries start to repel each other, hitting the zero-temperature axis with an infinite slope at $h \sim \pm\sqrt{r^3/u}$. Neglecting the temperature-dependent cubic term, the effective potential is given by

$$\mathcal{V}(\phi) = \mathcal{V}(0) - h\phi + \frac{R(T)}{2!}\phi^2 + \frac{u}{4!}\phi^4, \quad (5.31)$$

and the minimizing field configuration, thus, reads

$$\bar{\phi} = \frac{h}{R}, \quad R^3 \gg uh^2. \quad (5.32)$$

Corrections due to U_3 or renormalizations of the magnetic field are negligible, Thus, the effective potential indeed obtains the emergent Ising symmetry of Eq. (5.31).

Taking the effective potential at the minimum, $\mathcal{V}(\bar{\phi})$, we obtain the free energy density. To lowest order in the magnetic field, h , we get

$$\mathcal{F}_{\text{cr}} = T^{D/z} \mathcal{A}_d(RT^{-2/z}) - \frac{h^2}{2R}, \quad \text{for } R^3 \gg uh^2. \quad (5.33)$$

The second term is just the energy stored in the potential which is quadratic in h in the linear regime and temperature dependent due to the thermal renormaliza-

tion of the stiffness. The first term accounts for the energy arising from Gaussian fluctuations around the minimizing field configuration.

5.3.2 Non-Linear Regime

In the non-linear regime, the potential stiffness is small, $R^3 \ll uh^2$, and the second derivative is dominated by $\mathcal{V}'' \approx u\phi^2/2$, i.e., the field itself. Thus, we have to minimize the potential

$$\mathcal{V}(\phi) \approx -h\phi + \frac{u}{4!}\phi^4 + T^{D/z}\mathcal{A}_d\left(\frac{u}{2}\phi^2T^{-2/z}\right). \quad (5.34)$$

Here, we neglected the quintic term which is only valid for fields smaller than a certain threshold field $|h| < h_5$. By rescaling $\phi \rightarrow (h/u)^{1/3}\tilde{\phi}$ in Eq. (5.14) we obtain this threshold to be $h_5 = u^4/u_5^3$, above which the emergent Ising symmetry is lost.

At zero temperature, the force applied by the magnetic field has to be balanced by the quartic term. This gives the classical field configuration

$$\bar{\phi} = \text{sgn } h \left(\frac{6|h|}{u}\right)^{1/3}, \quad R^3 \ll h^2u \quad (5.35)$$

The exponent of the magnetization equals the mean field exponent $\delta = 3$ as we are above the upper critical dimension. Now, turning on the temperature, we may expand the field configuration around this mean field result $\phi = \bar{\phi} + \delta\phi$, where $\delta\phi$ is assumed to be a small temperature correction. Expanding the potential in this deviation and keeping only the leading-order temperature dependencies, we obtain

$$\mathcal{V}(\phi) \approx \mathcal{V}(\bar{\phi}) + \bar{\phi} \left[r + uT^{(D-2)/z}\mathcal{A}'_d\left(\frac{u}{2}\bar{\phi}^2T^{-2/z}\right) \right] \delta\phi + \frac{u}{4}\bar{\phi}^2\delta\phi^2 \quad (5.36)$$

Minimization simply yields $\delta\phi = 2f/(u\bar{\phi})$, where we identified the temperature-dependent force as

$$f = - \left[r + uT^{(D-2)/z}\mathcal{A}'_d\left(\frac{u}{2}\bar{\phi}^2T^{-2/z}\right) \right]. \quad (5.37)$$

The temperature dependence of the solution can be obtained from Eq. (5.27), where in the low-temperature regime one has to substitute r by $u\bar{\phi}^2/2$. In particular, the effect of the correction of the magnetization on the critical free energy is an extra term proportional to the square the force, f^2 . Its temperature dependence is the same as the temperature dependence of the renormalization of the magnetic field in the linear regime, Eq. (5.30). Therefore this correction exceeds the current level of accuracy and is, thus, sub-leading. Neglecting this correction, the critical part of the free energy is given by

$$\mathcal{F}_{\text{cr}} = T^{D/z}\mathcal{A}_d \left[\left(\frac{9uh^2}{2T^2}\right)^{1/3} \right] - \frac{3}{4} \left(\frac{6h^4}{u}\right)^{1/3}. \quad (5.38)$$

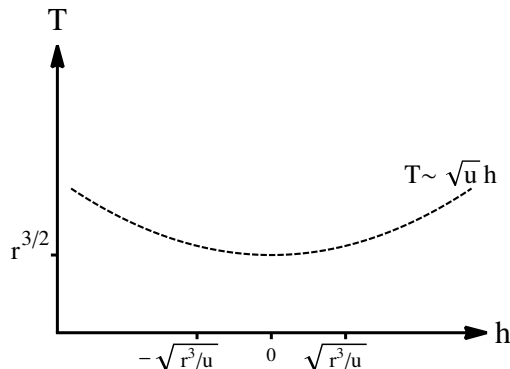


Fig. 5.5: Crossover between the Fermi liquid regime at low temperatures and the quantum critical regime at high temperatures. It is defined by the argument of the fluctuation function \mathcal{A}_d as $T^{2/z} \sim \mathcal{V}''(\bar{\phi})$. In the limit $r \rightarrow 0$, i.e., for the QCEP, the crossover line goes to zero at $h = 0$. For large fields the crossover boundary increases linearly with h .

The term proportional to $|h|^{4/3}$ reflects the non-linear nature of the restoring force, and it is temperature independent in the non-linear regime, whereas the first term captures the Gaussian fluctuations.

5.3.3 Free Energy Density

The free energy in the linear regime, Eq. (5.33), and in the non-linear regime, Eq. (5.38) has a mean field component due to the classical field configuration, and a fluctuation term given by the function \mathcal{A}_d . Importantly, the nature of the fluctuation term changes when its argument is of the order of one. Thus the temperature scale $T^{2/3} \sim \mathcal{V}''(\bar{\phi})$ determines a second important crossover.

For low temperatures, $T^{2/3} \ll \mathcal{V}''(\bar{\phi})$, we obtain from the limiting behavior of the function \mathcal{A}_d , Eq. (5.23), that the temperature dependence of the free energy is quadratic, $\mathcal{F} = \mathcal{F}_0(h) - (T/T_0)^2$, showing Fermi liquid behavior. Hence, when calculating thermodynamics, we will obtain the signatures of a conventional metal. In contrast, if the curvature of the potential is small, fluctuations lead to much larger deviations from the equilibrium field configuration and are much more important. Therefore, in the limit $\mathcal{V}''(\bar{\phi}) \ll T^{2/z}$, thermal fluctuations induce non-analyticities which lead to quantum critical behavior. The crossover line between this Fermi liquid and quantum critical regime is shown in Fig. 5.5.

In the linear regime, the curvature of the potential is given by the stiffness, $R(T)$, and the crossover line intersects the zero-field axis at $T \sim r^{3/2}$. This is of course only true close enough to the critical endpoint, when $r^{d+1} \ll r^2/u^2$, i.e., when the stiffness at the Fermi liquid crossover is dominated by the bare mass, r . In the non-linear regime the curvature depends on the magnetization itself and thereby on the applied magnetic field, $\mathcal{V}''(\bar{\phi}) \sim h^{2/3}u^{1/3}$. Accordingly, the crossover temperature will asymptotically scale linear with the applied field, $T \sim h\sqrt{u}$.

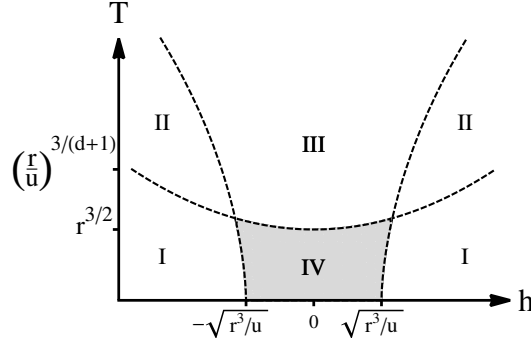


Fig. 5.6: The two crossover lines of Figs. 5.4 and 5.5 divide the phase diagram for a finite distance to the QCEP, r , into four different regimes. Critical divergences are cut off in regime IV. In the limit $r \rightarrow 0$, regime IV ceases to exist as both crossover lines approach the zero temperature axis at $h = 0$, converging to the QCEP.

The two crossover lines define four different regimes, depicted in Fig. 5.6, each with a different behavior of the critical free energy. Additionally, there is a third crossover temperature, $T \sim (r/u)^{3/(d+1)}$ in regime III, below which the stiffness becomes approximately temperature independent. Importantly, for finite r the divergences arising from the fluctuation term are cut off upon entering regime IV. In the limit of $r \rightarrow 0$ regime IV disappears since all crossover lines hit the zero-temperature axis at $h = 0$, defining the QCEP.

The critical free energy follows from Eqs. (5.33), (5.38) and (5.23), and to leading order takes the following form:

$$\mathcal{F}_{\text{cr}} = \begin{cases} -\bar{f}_2 T^2 \left(\frac{9h^2 u}{2} \right)^{\frac{d-3}{6}} - \frac{3}{4} \left(\frac{6h^4}{u} \right)^{1/3} & \text{I} \\ -\bar{f}_1 T^{\frac{d}{3}+1} + \bar{f}_2 T^{\frac{d+1}{3}} \frac{u}{2} \left(\frac{9h^2 u}{2} \right)^{1/3} - \frac{3}{4} \left(\frac{6h^4}{u} \right)^{1/3} & \text{II} \\ -\bar{f}_1 T^{\frac{d}{3}+1} - \frac{h^2}{2R} & \text{III} \\ -\bar{f}_4 T^2 r^{\frac{d-3}{2}} - \frac{h^2}{2R} & \text{IV} \end{cases} \quad (5.39)$$

where we set explicitly $z = 3$ and the coefficients f_i in spatial dimension $d = 2$ (upper row) and $d = 3$ (lower row) are given by

$$\bar{f}_2 = \begin{cases} \bar{c}_2 \\ \bar{b}_2 \ln \frac{\Lambda^3}{u^{1/2}|h|} \end{cases}, \quad \bar{f}_1 = \begin{cases} c_1 \\ b_1 \ln \frac{\Lambda^3}{T} \end{cases}, \quad \bar{f}_2 = \begin{cases} c_3 \ln \frac{T^{2/3}}{(uh^2)^{1/3}} \\ b_2 \end{cases}, \quad \bar{f}_4 = \begin{cases} \bar{c}_2 \\ \bar{b}_2 \ln \frac{\Lambda^3}{r^{3/2}} \end{cases}$$

in terms of the parameters of Eq. (5.20) and Eq. (5.22).

5.4 Thermodynamics

From the critical free energy, Eq. (5.39), one can obtain the thermodynamics of the quantum critical metamagnetic system, i.e., the response to a variation of temperature, pressure or magnetic field. Due to the fluctuations, the free energy has an explicit dependence on temperature, whereas the other parameters enter only through the dependence of the tuning parameters r and h . The temperature dependence of these parameters was already discussed in Sec. 5.2 and is assumed to be negligible for $r = r(p, H)$ and of Fermi liquid type for the scaling field $h = h_0(p, H) + h_T T^2$. However, this latter temperature dependence yields for most quantities sub-leading correction and is, hence, neglected where possible.

In the following, we will mainly focus on the pressure and field dependence of h , since it is the most relevant parameter of the theory. The influence of variations of the mass due to field or pressure tuning is only mentioned briefly when necessary, otherwise r is treated as a constant. However, the influence of the renormalized mass, R , is most important as its temperature dependence leads to strong thermodynamic signatures in the vicinity of the metamagnetic transition. Furthermore, we assume $h \sim H - H_m(p)$ and, as we are close to the critical point, we may expand $H(p)$ such that the critical magnetic field depends linearly on pressure $\partial_p H_m(p) = \text{const.}$ Thus, the free energy is a function

$$\mathcal{F}(H, p, T) = \mathcal{F}(H - H_m(p), T) \quad (5.40)$$

In the following, we consider several thermodynamic quantities which are partially related to each other due to the assumptions made above. This is because a derivative with respect to the magnetic field, H , and a derivative with respect to pressure are essentially the same,

$$\frac{\partial \mathcal{F}}{\partial p} = -\frac{\partial H_m(p)}{\partial p} \frac{\partial \mathcal{F}}{\partial H} \propto \frac{\partial \mathcal{F}}{\partial H}. \quad (5.41)$$

This proportionality is on the other hand an experimentally verifiable criterion for the assumptions made above. First of all, we will consider the specific heat coefficient, $\gamma = -\partial_T^2 \mathcal{F}$, measuring the change of entropy with temperature. The thermal expansion, α , which is defined as $\alpha = \frac{1}{V} \partial_T V|_p = \frac{1}{V} \partial_T \partial_p \mathcal{F}$ has, thus, the same behavior as the temperature derivative of the magnetization, $\partial_T M = -\partial_T \partial_H \mathcal{F}$. Furthermore, the compressibility, defined as $\kappa = -\frac{1}{V} \partial_p V|_T = -\frac{1}{V} \partial_p^2 \mathcal{F}$, and the magnetic susceptibility, $\chi = -\partial_H^2 \mathcal{F}$, are equivalent, as well as the magnetostriction which is a mixed derivative with respect to pressure and magnetic field, $\lambda = \frac{1}{V} \partial_H V = -\frac{1}{V} \partial_H \partial_p \mathcal{F}$. We will also discuss the Grüneisen ratio, $\Gamma = \alpha/C$, and accordingly its magnetic analogue, $\Gamma_H = -\partial_T M/C$, where $C = \gamma T$ is the specific heat.

Neglecting the dependencies of the parameter r and assuming h to be linear in magnetic field and temperature independent has another, directly observable consequence. As the theory has an emergent Ising symmetry close to the critical point, the free energy Eq. (5.39) is symmetric with respect to $h = 0$. This implies that it has to be also symmetric with respect to the metamagnetic field $H_m(p)$

$$\mathcal{F}_{\text{cr}}(H - H_m(p), T) = \mathcal{F}_{\text{cr}}(H_m(p) - H, T). \quad (5.42)$$

Thus, the specific heat and the susceptibility will be even functions of the field $H - H_m$, whereas the thermal expansion will be odd, as it involves a single derivative with respect to H .

This symmetry is of course spoiled by a variation of the mass r upon changing the magnetic field and also by the sub-leading Fermi liquid like temperature dependence of h . The effect on the different thermodynamic quantities will also be discussed below. Furthermore, we just consider the critical metamagnetic part of the free energy, although there may also be a non-critical background.

In the following, we will discuss the cricketal thermodynamics close to the QCEP qualitatively on the basis of the asymptotic behavior of the free energy, given in Eq. (5.39), which is correct up to logarithmic corrections. Additionally, we confirmed our results numerically with good agreement. Therefore, we numerically calculated the function \mathcal{A}'_d and with this iteratively solved the self-consistent equation for the effective mass, Eq. (5.24). The free energy was then evaluated by taking the potential at the exact classical solution, $\bar{\phi}$, substituting the effective mass for the bare one, $r \rightarrow R(T)$, and adding the fluctuation term where we set $\mathcal{V}''\phi = R(T) + \frac{u}{2}\bar{\phi}^2$.

5.4.1 Susceptibility, Magnetostriction and Compressibility

The most important thermodynamic quantity for the metamagnetic system is, of course, the magnetic susceptibility χ , as its divergence at the field H_m is the hallmark of the metamagnetic instability. Under the assumptions made above it is proportional to $\partial_h^2 \mathcal{F}_{\text{cr}}$ and, thus, an even function of the applied field with respect to the metamagnetic field, $\chi(H - H_m) = \chi(H_m - H)$.

In Fig. 5.7, the temperature dependence for small (upper panel) and large fields (lower panel) is shown, respectively. On the left hand side, the qualitative behavior is sketched, whereas the right hand side shows the numerical calculation for four different field values in $d = 3$.

Within the linear regime, the susceptibility increases monotonously with decreasing temperature, as it is given by the inverse stiffness,

$$\chi \propto \frac{1}{R(T)} \quad \text{in III, IV}, \quad (5.43)$$

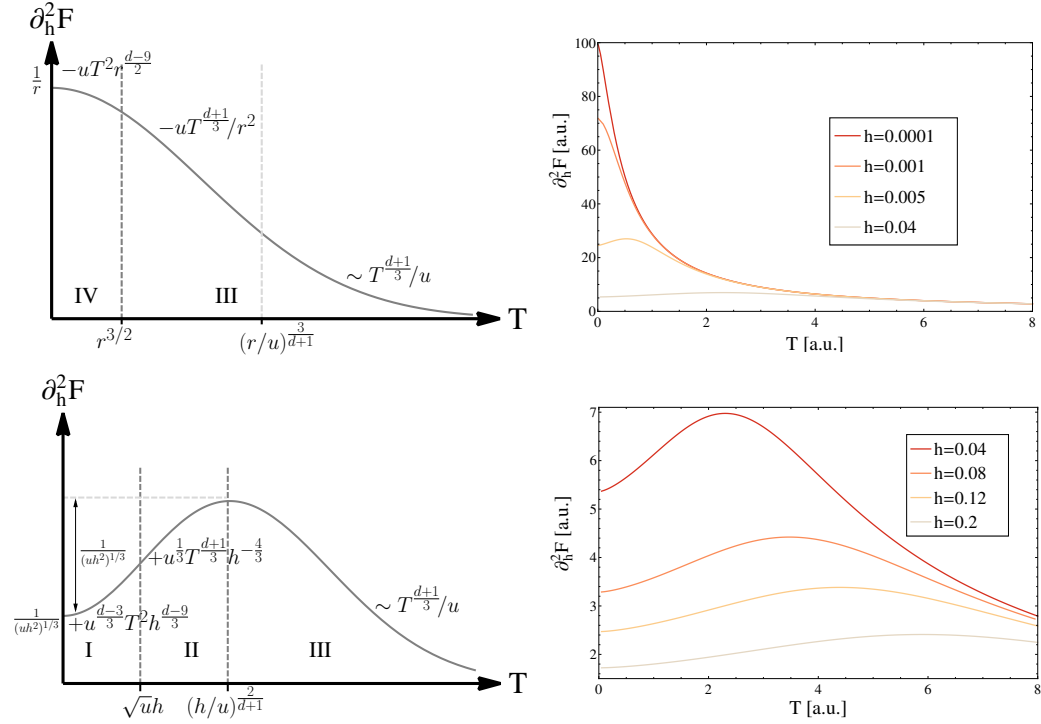


Fig. 5.7: Temperature dependence of the susceptibility for low (upper panels) and high fields h (lower panels). On the left hand side, the asymptotic behavior is sketched, and the roman numbers label the regimes depicted in Fig. 5.6. On the right hand side the numerical results for $r = 0.01$ and $u = 1$ in $d = 3$ are shown. With these parameters, the crossover from the linear to the non-linear regime at zero temperatures is approximately at $|h| \sim \sqrt{r^3/u} = 0.001$.

thus, for $T = 0$ it is $\chi|_{T=0} = 1/r$. This behavior for lowest fields is also seen in the numerical plot in the upper panel of Fig. 5.7. Importantly, this implies that approaching the QCEP the susceptibility diverges as $\chi \sim T^{-(d+1)/3}$ down to lowest temperatures which is stronger than for free spins.

At higher fields, the susceptibility develops a characteristic peak at the crossover from regime III to II, which was measured in $\text{Sr}_2\text{Ru}_3\text{O}_7$ [108] and already discussed in Ref. [82]. Upon lowering the temperature, the Fermi liquid regime is entered at $T < h$, where it obtains an T^2 .

In the Fermi liquid regime the susceptibility is obtained as

$$\chi = \left(\frac{2}{9uh^2} \right)^{1/3} + \frac{(d-3)(d-6)}{9} u^{(d-3)/6} h^{(d-9)/3} T^2 \quad \text{in I.} \quad (5.44)$$

The difference between the height of the peak and the saturation value at $T = 0$ increases as the metamagnetic field is approached according to $h^{-2/3}$. Corrections due to the pressure and field dependence of the bare mass, r , are suppressed by a factor of h in the linear regime and do not arise to the present order of accuracy in the non-linear regime.

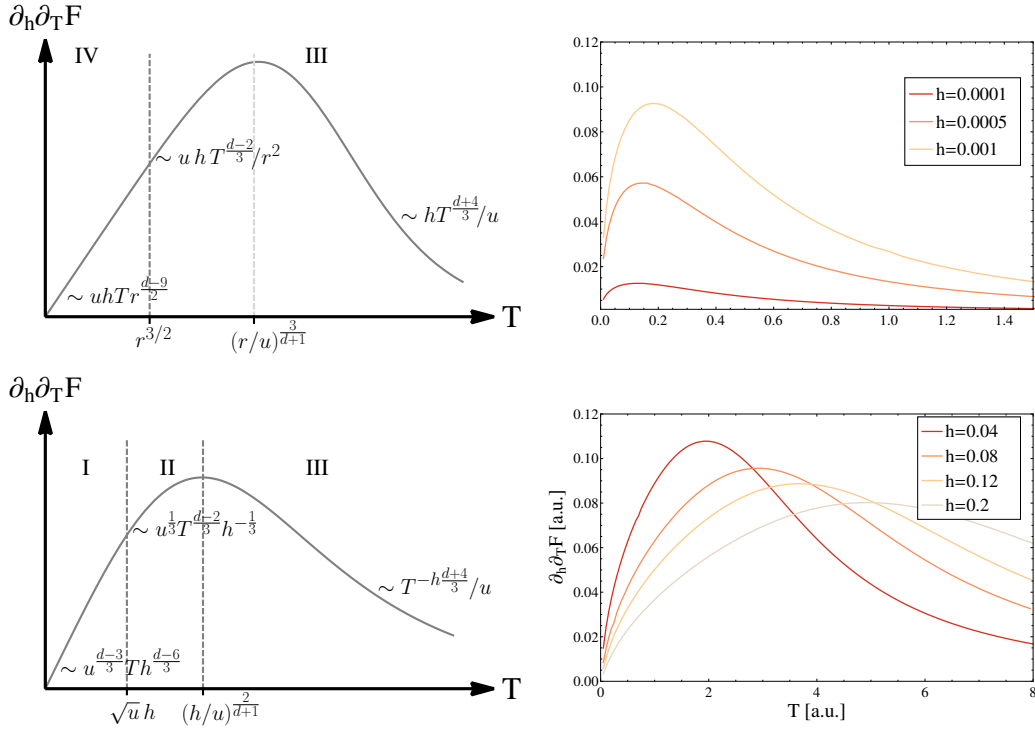


Fig. 5.8: Temperature dependence of the mixed derivative $\partial_h \partial_T \mathcal{F}_{\text{cr}}$ corresponding to the thermal expansion, α . On the left hand side, the qualitative behavior is sketched and on the right hand side it the numerical calculation for $r = 0.01$ and $u = 1$ in $d = 3$ is shown. Neglecting sub-leading terms in the free energy, it is an odd function of h , going through zero at $h = 0$. It has a characteristic maximum which close to the transition field, i.e., in the linear regime (upper panels), increases with increasing field. For high fields, $|h| \gg \sqrt{r^3/u}$, (lower panels) it shows the opposite behavior.

Since the susceptibility is the derivative of the magnetization with respect to the magnetic field, $\chi \sim \partial_h M$, it relates to the critical exponent δ as $\chi \sim h^{\frac{1}{\delta}-1}$. Therefore, we can read off the mean field value $\delta = 3$.

As mentioned earlier, in presence of a magnetoelastic coupling the magnetic susceptibility is close to the metamagnetic field asymptotically proportional to the magnetostriction and the compressibility. Since the susceptibility diverges upon approaching the QCEP, so does the compressibility, leading to a critical correction to some elastic moduli. This softening of the crystal, as already discussed in Ref. [27], indicates that the QCEP is unstable with respect to structural transitions. The detailed discussion of the implications is postponed to Chap. 6.

5.4.2 Thermal Expansion, Temperature Derivative of the Magnetization

The mixed derivative $\partial_h \partial_T \mathcal{F}_{\text{cr}}$ is proportional to the thermal expansion, α , as well as to the temperature derivative of the magnetization. It is an odd function of

the field h and, thus, has a sign change, which is a generic behavior at quantum critical points, as discussed in Ref. [109]. For field-tuned quantum critical points, for instance, the temperature derivative of the magnetization is the derivative of the entropy, $S = \partial_T \mathcal{F}_{\text{cr}}$, with respect to the magnetic field. Exactly at the QCP, the entropy will have a maximum since the system has two different ground states which leads to frustration. Therefore, the derivative of the entropy has a sign change at the critical field.

Fig. 5.8 shows the thermal expansion as function of temperature, for high and low fields. Close to the metamagnetic field it is given by

$$\alpha \propto h \frac{R'(T)}{R(T)^2} \quad \text{in III, IV.} \quad (5.45)$$

proportional to the field h . At high temperatures it decreases with increasing T as $\alpha \sim T^{-(d+4)/3}$. At the scale, where the temperature dependence of the mass ceases to dominate, the thermal expansion has a maximum and goes linear to zero. The position and the height of the maximum is defined by the saturation of $R(T)$. Hence, for the QCEP the thermal expansion will at a finite field diverge as function of temperature. This divergence is cut off when the Fermi liquid regime at lowest temperatures is reached.

Upon entering the non-linear regime, $|h| > \sqrt{r^3/u}$, the thermal expansion has qualitatively the same features, but the maximum is defined by the crossover temperature between regime III and II. Hence, it is shifted to higher temperatures as the field increases. The asymptotic behavior in the non-linear regime is given by

$$\alpha \propto T^{(d-2)/3} u^{1/3} h^{-1/3} \quad \text{in II} \quad (5.46)$$

$$\alpha \propto T u^{(d-3)/6} h^{(d-6)/3} \quad \text{in I.} \quad (5.47)$$

Thus, the maximum decreases with increasing magnetic field, in contrast to the behavior in the linear regime.

The behavior of the thermal expansion was already discussed in Ref. [110] with respect to measurements on $\text{Sr}_3\text{Ru}_2\text{O}_7$ and in Ref. [111] in the context of CeRu_2Si_2 . Both measurements showed an asymmetry of the thermal expansion with respect to h . However, it is the emergent Ising symmetry of the theory which constrains the sign change to happen at the metamagnetic field, $H = H_m$. As already mentioned, the Ising symmetry is broken by the temperature-dependent part, h_T , of the scaling field and also by the pressure and field dependence of the bare mass $r(p, H)$. Both effects yield, in principle, only sub-leading corrections. However, whenever the leading-order contribution vanishes, these corrections become important. Asymmetries in the thermal expansion are, thus, a measure of the strength of sub-leading corrections.

To discuss the most important contributions, we can limit ourselves to the regimes III and IV in the phase diagram, Fig. 5.6, as the shift in the thermal expansion will be small. The critical free energy is given by $\mathcal{F}_{\text{cr}} = -h^2/(2R)$ and the thermal expansion follows as

$$\frac{\partial \mathcal{F}}{\partial p \partial T} = \frac{\partial \mathcal{F}}{\partial h \partial T} \partial_p h_0 + \frac{\partial \mathcal{F}}{\partial r \partial T} \partial_p r + 2h_T T \left(\frac{\partial \mathcal{F}}{\partial h \partial h} \partial_p h_0 + \frac{\partial \mathcal{F}}{\partial r \partial h} \partial_p r \right). \quad (5.48)$$

On the right hand side, the temperature derivative acts on the explicit temperature dependence of \mathcal{F} and on $R(T)$ only. The first term yields the thermal expansion calculated above, whereas the other terms are corrections to the leading order behavior. Most important is the twofold derivative with respect to the field, h , since it is the only term independent of h and, thus, accountable for a finite thermal expansion at $h = 0$. It yields

$$\delta \alpha|_{h=0} = 2Th_T \frac{\partial \mathcal{F}}{\partial h \partial h} = \frac{2h_T T}{R(T)} = 2h_T \begin{cases} \frac{1}{v_d u} T^{-(d-2)/3} & T \gg \left(\frac{r}{u}\right)^{2/(d+1)} \\ \frac{1}{r} & T \ll \left(\frac{r}{u}\right)^{2/(d+1)} \end{cases} \quad (5.49)$$

and close to the QCEP, $r = 0$, the upper limit is realized. Therefore, the residual thermal expansion increases with decreasing temperatures.

On the other hand, we can calculate the field at which the thermal expansion vanishes, or equivalently, where the maxima of the entropy are located in the (H, T) diagram. For a nearly pressure independent mass, r we find the field correction

$$(H - H_m)|_{\alpha=0} = 2h_T T \frac{R}{R'(T)} - h_T T^2 \approx \frac{5-d}{d+1} h_T T^2 \quad (5.50)$$

where the approximations holds for $T \gg (r/u)^{3/(d+1)}$, i.e., close to the QCEP. For experiments, this implies that subtracting this contribution from the data, one should recover the Ising symmetry, provided $h(p)$ and $r(p)$ vary sufficiently weak.

5.4.3 Specific Heat Coefficient

Like the susceptibility, the specific heat is in the Ising symmetric limit an even function of magnetic field h . In Fig. 5.9 the field dependence of the specific heat coefficient is plotted. For lowest temperatures in the Fermi liquid regime I, it increases upon lowering the field as

$$\gamma = 2\bar{f}_2 \left(\frac{9}{2} u h^2 \right)^{(d-3)/6} \quad \text{in I,} \quad (5.51)$$

which becomes logarithmic in three dimensions. Upon entering the regime IV, the specific heat coefficient saturates to a value of

$$\gamma = 2\bar{f}_4 r^{(d-3)/2} \quad \text{in IV.} \quad (5.52)$$

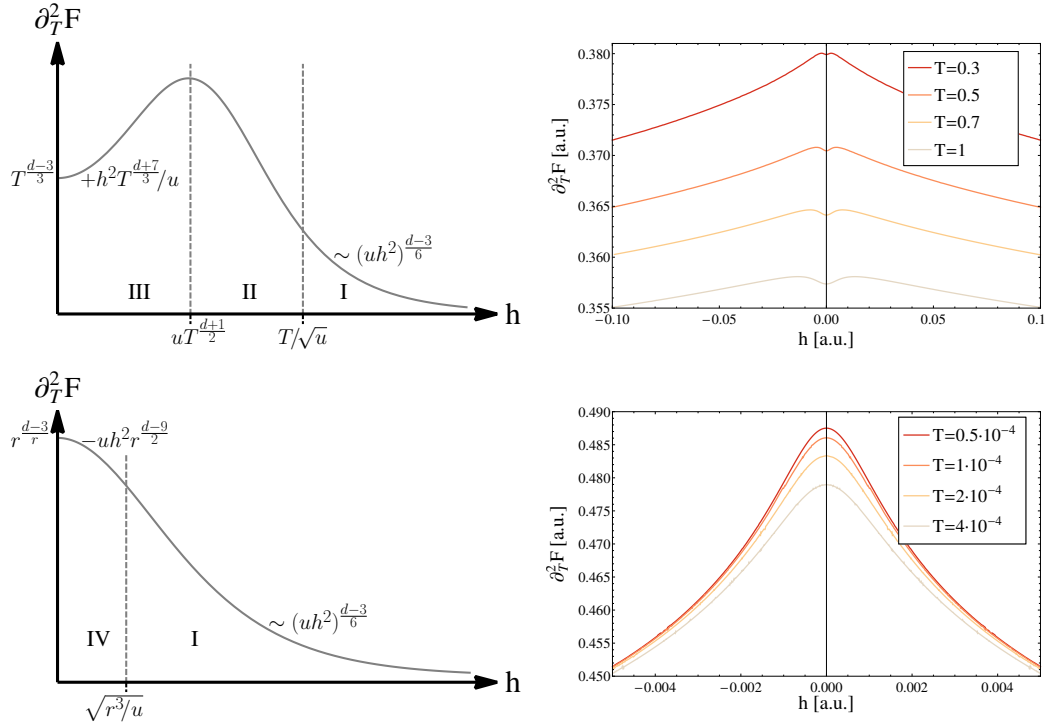


Fig. 5.9: Field dependence of the critical specific heat coefficient. The qualitative behavior is sketched on the left side, whereas the right hand side shows the numerical evaluation for the parameter set $r = 0.01$, $u = 1$ in $d = 3$. Neglecting sub-leading terms in the free energy, it is an even function of h .

For high temperatures (upper panel), the specific heat shows a peak at the crossover from the linear (III) to the non-linear regime (II). The shift in the absolute value of the specific heat is due to the field independent term in Eq. (5.53). For lowest temperatures (lower panel), we are in the Fermi liquid regime where this peak is absent.

In the linear quantum critical regime III, the specific heat coefficient is sensitive to the additional crossover line as it is given by

$$\gamma = \frac{d}{3} \left(\frac{d+3}{3} \right) f_1 T^{(d-3)/3} + \frac{h^2}{2R} \left(2 \frac{R'}{R^2} - \frac{R''}{R} \right) \quad \text{in III.} \quad (5.53)$$

Thus, for small fields and high temperatures, $T \gg (r/u)^{3/(d+1)}$, the effective mass is temperature dominated implying $R' \sim R/T$, and the field dependent term yields a positive correction. When entering regime II, the specific heat is given by

$$\gamma = \frac{d}{3} \left(\frac{d+3}{3} \right) f_1 T^{(d-3)/3} - f_2 \frac{(d+1)(d-2)}{3} T^{(d-5)/3} \left(\frac{u h^2}{6} \right)^{1/3} \quad \text{in II,} \quad (5.54)$$

having a negative correction to the leading term. Hence, the specific heat has a characteristic maximum at the crossover from III to II as seen in the upper panels of Fig. 5.9. For intermediate temperatures, $r^{3/2} < T < (r/u)^{3/(d+1)}$, the correction in regime III becomes negative, such that the maximum disappears.

The characteristic double-peak structure close to the critical field was also seen in CeRu₂Si₂ [112]. In Ref. [111] it was shown to be a generic feature whenever the susceptibility has a positive curvature with respect to temperature. The reason is that the curvature of the specific heat with respect to the magnetic field, h , and the curvature of the susceptibility with respect to the temperature are basically the same close to the metamagnetic field, $\partial_h^2 \gamma \sim \partial_h^2 \partial_T^2 \mathcal{F} \sim \partial_T^2 \chi$. Thus, a positive curvature of the susceptibility at lowest fields together with the symmetry and the asymptotic decrease implies two maxima around $H = H_m$ of the specific heat.

Taking into account the Fermi liquid temperature correction of the scaling field h , we see that the specific heat gets three additional contributions

$$\begin{aligned} \gamma &= -\partial_T^2 \mathcal{F} - 2h_T \partial_h \mathcal{F} - 4h_T T \partial_T \partial_h \mathcal{F} - 2h_T \partial_h^2 \mathcal{F} \\ &= \gamma_0 + 2h_T M - 4h_T T \alpha_0 + 2h_T T^2 \chi_0 \end{aligned} \quad (5.55)$$

where the index indicates that the respective quantity at $h_T = 0$ is meant.

In the Fermi liquid regime (I and IV) all these corrections are sub-leading and, thus, negligible. In the linear quantum critical regime (III), terms linear in the field h are added by the magnetization and by the thermal expansion which, however, are both sub-leading due to the inverse stiffness. For large fields h and temperatures, i.e., in regime II, all contributions are sub-leading, though the magnetization yields an additional contribution, important at intermediate scales.

5.4.4 Grüneisen Parameters

For pressure-tuned quantum critical points the Grüneisen ratio, $\Gamma = \alpha/C_p$, is an interesting quantity to look at. As discussed in Ref. [113], the critical Grüneisen ratio, $\Gamma_{\text{cr}} = \alpha_{\text{cr}}/(T\gamma_{\text{cr}})$ necessarily diverges near a QCP, in contrast to a classical critical point, where it is in general constant. As long as scaling applies, the exponents of the divergence and even the prefactor are fully determined by the critical exponents of the universality class of the transition. The analogous consideration holds in case of magnetic field driven quantum critical points for the magnetic Grüneisen ratio, $\Gamma_H = -\partial_T M/C_H$. Within our approximation, the volumetric Grüneisen parameter and the magnetic Grüneisen ratio are proportional to each other, $\Gamma \propto \Gamma_H \propto \partial_h \partial_T \mathcal{F}_{\text{cr}}/(T\partial_T^2 \mathcal{F}_{\text{cr}})$.

Due to the Ising symmetry, the thermal expansion vanishes at $H = H_m$ and this feature is passed on to the Grüneisen parameter. For small but finite fields (regime III) and high temperatures, $T \gg (r/u)$, the Grüneisen ratio is

$$\Gamma_H = \frac{3(d+1)}{d(d+3)} \frac{h}{f_1 \tau_d u} T^{-\frac{2(d+2)}{3}} \quad \text{in III for } T \gg \left(\frac{r}{u}\right)^{\frac{3}{d+1}}. \quad (5.56)$$

Upon lowering the temperatures, the temperature dependence of the effective mass, $R(T)$, is negligible and the Grüneisen parameter becomes

$$\Gamma_H = \frac{3(d+1)}{d(d+3)} \frac{\tau_d}{f_1} \frac{hu}{r^2} T^{-2/3} \quad \text{in III for } T \ll \left(\frac{r}{u}\right)^{\frac{3}{d+1}}. \quad (5.57)$$

Taking into account the logarithmic correction hidden in the factor τ_2 , one obtains $\Gamma_H \sim h T^{-2/z} \ln 1/T$, whereas in $d = 3$ the factor f_1 depends logarithmically on temperature yielding $\Gamma_H \sim h(T^{2/z} \ln 1/T)^{-1}$. This is the same temperature dependence as deduced in Ref. [113]. However, the additional factor h yields a suppression of the Grüneisen parameter.

In regime I, the Grüneisen parameter is in two dimensions simply proportional to the inverse of the tuning parameter,

$$\Gamma_H = \frac{3-d}{3} \frac{1}{H-H_m} \quad \text{in I } (d=2) \quad (5.58)$$

which also agrees to the general scaling arguments presented in [113]. In $d = 3$, due to the logarithmic dependence of the free energy on h , we obtain also a logarithmic correction to the Grüneisen parameter

$$\Gamma_H = \frac{1}{(H-H_m) \log \frac{\Lambda^3}{\sqrt{u|h}}} \quad \text{in I } (d=3). \quad (5.59)$$

Notably, the prefactor differs in both dimensions from the scaling predictions. This is on the one hand side due to the fact that the system is above the upper critical dimension. On the other hand, a strict scaling form can only be obtained for 2 relevant parameters. However, in the situation at hand we have three relevant parameters namely T , r and h , thus the Grüneisen parameter has to be less universal.

5.5 Summary

In this chapter, we discussed the critical thermodynamics of an itinerant metamagnetic quantum critical endpoint. This metamagnetic endpoint is defined by the divergence of the differential susceptibility at a finite field H^* . Close to the endpoint the theory develops an emergent Ising symmetry. We studied the metamagnetism in the framework of spin-fluctuation theory as proposed by Millis et al. [82] based on works by Moriya [114] and Yamada [115]. The dynamics of the spin fluctuations are dominated by Landau-damping yielding a critical dynamical exponent $z = 3$.

We applied functional renormalization group techniques which yields a self-consistent equation, Eq. (5.16), for the effective potential. This equation was the starting point of our analysis and yielded the asymptotic temperature dependence of the effective potential.

The phase diagram for the metamagnet close to a quantum critical endpoint consists of two crossover lines. First, there is a crossover line from a linear field dependence of the magnetization for small deviations from the metamagnetic field, $h \sim H - H^*$, to a non-linear regime for higher fields. Second, we obtain a crossover from a quantum critical regime at high temperatures to a Fermi-liquid like regime. These lines both terminate in the quantum critical endpoint giving rise to three different regimes. For systems which are not yet critical, but exhibit only a metamagnetic crossover, a fourth regime is obtained which has a linear magnetization, but is Fermi-liquid like otherwise.

We obtained the critical free energy as a function of temperature and magnetic field in these different regimes, from which we could derive the critical thermodynamics of the metamagnetic instability. Assuming a linear pressure dependence of the metamagnetic transition field, $H_m(p)$, we obtained the susceptibility, the thermal expansion, the specific heat coefficient and the Grüneisen parameter.

The thermal expansion exhibits a sign change at the transition field, $H_m(p)$, which corresponds to a maximum of the entropy. To leading order, the thermal expansion is odd in the field h due to the emergent Ising symmetry. However, sub-leading temperature dependent contributions of h spoil the Ising symmetry and result in a shift of the region of entropy accumulation from $H = H_m$ which is quadratic in temperature.

The specific heat as function of the applied magnetic field shows a characteristic double peak structure resulting in a minimum at the critical field. Right at the critical field, $h = 0$, it diverges as $T^{(d-3)/3}$, a behavior which is cut off away from the critical point, i.e., for finite r . The (magnetic) Grüneisen parameter also diverges for finite fields, but as it is linear in the field it vanishes in the zero-field limit.

These results are especially important for the scenario of itinerant ferromagnets with a zero-field tricritical point. Here, wings of metamagnetic transitions, emerging from the tricritical point, terminate in a QCEP which should show the thermodynamic signatures obtained above. The systems UCoAl [4] and UGe₂ [5, 6] are promising candidates for a quantitative test of spin-fluctuation theory for critical metamagnetism based on the results obtained above.

Importantly, susceptibility, magnetostriction, and compressibility should show similar behavior which implies a divergence of the compressibility upon approaching the metamagnetic instability. Therefore, the elastic moduli get renormalized and one expects a pronounced crystal softening. As for the finite temperature Mott transition (Chap. 4) we, thus, find the metamagnetic QCEP to be unstable in presence of a magnetoelastic coupling, since the spin fluctuations will destabilize the crystal lattice. Since no symmetry is broken at the metamagnetic transition, one expects an isostructural transition preempting the quantum critical endpoint, which is the subject of the next chapter.

Chapter 6

Compressible Quantum Critical Metamagnetism

As discussed in the previous chapter, the metamagnetic fluctuations yield a diverging compressibility. Thus, the quantum critical endpoint is inherently unstable with respect to elastic deformations of the crystal, and the critical endpoint will be preempted by an isostructural transition.

In the following, we will investigate the elastic coupling of a quantum critical metamagnetic system. After having specified, how the elastic degrees of freedom are coupled to the metamagnetic fluctuations (Sec. 6.1), we investigate, in particular, the influence of the phonons in Sec. 6.2. We will show, that, for instance, the neutron scattering intensity pattern, by which the magnetic structure is investigated, crucially changes.

On the other hand, the influence of the phonons on the critical thermodynamics is shown to be negligible. Due to the finite shear moduli, the phonons remain non-critical in the event of a vanishing eigenvalue of the elastic constant matrix. Therefore, they will only yield a renormalization of the physical parameters. The analysis is carried out along the same lines as in Chap. 5, i.e., obtaining a self-consistent equation for the effective potential by means of functional RG.

We deduce the free energy and the crossover lines in the phase diagram for the finite temperature endpoint of the first order transition in Sec. 6.3.1 and, especially, focus on the fine-tuned situation of a quantum endpoint in Sec. 6.3.2.

From the free energy, we derive the critical thermodynamics, i.e., the specific heat coefficient, thermal expansion and the compressibility as well as the Grüneisen parameter (Sec. 6.4). We show that the elastic coupling yields a suppression of some of the critical divergences, for instance of the specific heat, at lowest temperatures. On the other hand, the Grüneisen parameter diverges with an unusual high power law. Furthermore, we estimate a temperature scale on which the elastic effects should be observable on the example of $\text{Sr}_3\text{Ru}_2\text{O}_7$ in Sec. 6.5.

6.1 Elastic Coupling

Analogous to Sec. 5.2, we describe the metamagnetic system within spin-fluctuation theory for the longitudinal fluctuations of the Pauli magnetization, ϕ , around its mean value. Within this theory, the action of the metamagnons is given by Eq. (5.8). For later convenience, we introduce the magnon propagator, $g_0^{-1}(\mathbf{q}, \omega_n)$, and rewrite this action as

$$\mathcal{S}_{\text{mm}}^0[\phi] = \frac{1}{2} \sum_{\mathbf{q}, \omega_n} \phi_{\mathbf{q}, n} g_0^{-1}(\mathbf{q}, \omega_n) \phi_{\mathbf{q}, n} + \int \left(\frac{v_{30}}{3!} \phi^3 + \frac{v_{40}}{4!} \phi^4 + \frac{v_{50}}{5!} \phi^5 - h_0 \phi \right) d\mathbf{x} d\tau.$$

Here we introduced for later convenience the propagator

$$g_0^{-1}(\mathbf{q}, \omega_n) = r_0 + q^2 + \gamma_m \frac{|\omega_n|}{q}. \quad (6.1)$$

The dynamics of the metamagnetic action is governed by Landau damping due to particle-hole excitations, giving rise to a dynamical exponent $z_{>} = 3$. The damping term is only active if the energy-momentum ratio is small, $\omega_n/q \ll 1$, since otherwise there is no phase space to scatter into. Anticipating the different scaling of the phonons and the energy rescaling within the RG-procedure, we also introduce the constant γ_m .

Concerning the lattice degrees of freedom, we describe them in the continuum limit as we are interested in low energy physics. Splitting the strain tensor, \tilde{u} , into the local displacement, \mathbf{u} , and the macroscopic volume change, E , as discussed in Sec. 2.2.4, the action for the elastic system in the harmonic approximation is given according to Sec. 2.3 by

$$\mathcal{S}_{\text{el,p}}[u] = \frac{1}{2} \sum_{\mathbf{q} \neq 0, \omega_n} u_i(\mathbf{q}, \omega_n) D_{im}(\mathbf{q}, \omega_n) u_m(\mathbf{q}, \omega_n), \quad (6.2)$$

$$\mathcal{S}_{\text{el,E}}[E] = \frac{1}{2} E_{ij} C_{ijlm} E_{lm}. \quad (6.3)$$

The phonon propagator, D is in terms of the elastic constant matrix, C_{ijlm} , given by

$$D_{im}(\mathbf{q}, \omega_n) = \delta_{im} \rho \omega_n^2 + C_{ijlm} q_j q_l, \quad (6.4)$$

where, ρ is the mass density. The acoustic phonons are ballistic modes, having a dynamical exponent $z_{<} = 1$, therefore, as already mentioned, we have a system with two different dynamical exponents. The dynamics of the macroscopic modes, E_{ij} , are not considered since they yield only a non-extensive contribution to the free energy, i.e., the number of modes does not increase with the volume. Thus, concerning the thermodynamics of the system, they can be neglected.

As the metamagnetic endpoint is located at a finite magnetic field, H^* , time reversal invariance is broken and, hence, a bilinear coupling between metamagnetic and elastic degrees of freedom is allowed. The coupling splits into a phonon contribution, $\mathcal{S}_{c,p}$, and a macroscopic contribution $\mathcal{S}_{c,E}$, which are given by

$$\mathcal{S}_{c,p}[\phi, u] = - \int \phi(\mathbf{r}, \tau) \lambda_{ij} u_{ij}(\mathbf{r}, \tau) d\mathbf{r} d\tau, \quad (6.5)$$

$$\mathcal{S}_{c,E}[\phi, E] = -\phi_{\mathbf{q}=0} \lambda_{ij} E_{ij}. \quad (6.6)$$

Due to symmetry, only singlets of the irreducible representation of the crystal group can couple to the metamagnetic fluctuations. In the following, we will consider only an isotropic coupling, $\lambda_{ij} = \lambda \delta_{ij}$, such that only the longitudinal phonons and the trace of the macroscopic strain E are coupled. Importantly, this does not imply that we can integrate out all other elastic modes as they are coupled to each other via the elastic tensor. Introducing the short hand notation $\psi_{\mathbf{q},n} = (\phi, \mathbf{u})_{\mathbf{q},n}$ and $\psi_0 = (\phi_0, \mathbf{E})$, where \mathbf{E} is given in Voigt notation, the full action of the elastically coupled metamagnetic system reads as

$$\begin{aligned} \mathcal{S}[\phi, u, E] = & \frac{1}{2} \psi_0^\dagger G_0^{-1} \psi_0 + \frac{1}{2} \sum_{\mathbf{q} \neq 0, \omega_n} \psi_{\mathbf{q},n}^\dagger G^{-1}(\mathbf{q}, \omega_n) \psi_{\mathbf{q},n} \\ & + \int \left(\frac{v_{30}}{3!} \phi^3 + \frac{v_{40}}{4!} \phi^4 + \frac{v_{50}}{5!} \phi^5 - h_0 \phi \right) d\mathbf{r} d\tau, \end{aligned} \quad (6.7)$$

where the propagators for the finite and zero momentum modes are defined by

$$G^{-1}(\mathbf{q}, \omega_n) = \begin{pmatrix} g^{-1}(\mathbf{q}, \omega_n) & i\lambda \mathbf{q}^T \\ -i\lambda \mathbf{q} & D(\mathbf{q}, \omega_n) \end{pmatrix} \quad (6.8)$$

$$G_0^{-1} = \begin{pmatrix} r_0 & -\lambda(1, 1, 1, 0, 0, 0) \\ -\lambda(1, 1, 1, 0, 0, 0)^T & C \end{pmatrix}. \quad (6.9)$$

Note, that G^{-1} is a four-by-four matrix for the magnetization and the phonons, whereas there are six elastic zero momentum modes and, thus, G_0^{-1} is a seven-by-seven matrix.

6.2 Phonons

The longitudinal phonons are linearly coupled to the finite momentum modes of the magnetization, ϕ . Thus, any quantity directly related to the fluctuations of the magnetization is strongly affected by the elastic coupling. For instance, elastic neutron scattering experiments probe these fluctuations and, thus, the intensity pattern of such an experiment is sensitive to the phonon coupling. Therefore, we will investigate in the following how such a pattern is qualitatively changed.

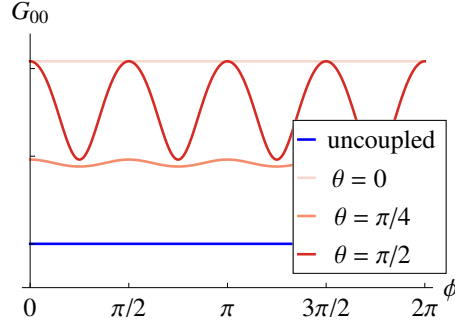


Fig. 6.1: Calculated quasi-elastic neutron scattering intensity for different polar angles, θ , in the limit $\mathbf{q} \rightarrow 0$. In comparison to the bare metamagnetic system (blue), the elastic coupling yields a shift to higher intensities. Importantly, one observes a modulation according to $\cos(4\phi)$ reflecting the fourfold symmetry of the cubic lattice. The parameters were chosen as $r = 2$, $\lambda = 1$, $C_{11} = 1.7$, $C_{12} = 0.3$ and $C_{44} = 2.1$.

Furthermore, in the remainder of this chapter, we want to analyze the elastically coupled metamagnetism along the same lines as in Chap. 5. The functional RG analysis is based on the successive integration over the high momentum modes, thus, the phonon interaction will enter this procedure. We carefully have to analyze their impact to obtain an analogous self-consistent equation for the effective potential of the macroscopic magnetization.

6.2.1 Neutron Scattering Intensity

Elastic neutron scattering probes the magnetic structure of the metamagnetic system at a finite wave vector. Since these modes are coupled linearly to the phonons, such an experiment will show direct consequences of the elastic coupling as Cowley [116] pointed out. The scattered neutron intensity for a transferred wave-vector \mathbf{k} at an energy ω is given by

$$S(\mathbf{k}, \omega) = \frac{NT}{\pi\omega} |F(\mathbf{k})|^2 \text{Im} G_{11}(\mathbf{q}, \omega), \quad (6.10)$$

where, due to momentum conservation, the magnon momentum, \mathbf{q} , equals the difference of the transferred wave-vector and a reciprocal lattice vector, $\mathbf{q} = \mathbf{G} - \mathbf{k}$. The function $F(\mathbf{k})$ denotes the structure factor of the magnetic fluctuations which will not be considered any further in order to focus on the more general mechanism. Most important is the response function, $G_{11}(\mathbf{q}, \omega) = \langle \phi_{\mathbf{q}, \omega} \phi_{-\mathbf{q}, -\omega} \rangle$, which is determined to lowest order by inverting the propagator matrix, Eq. (6.8).

For the bare metamagnetic system, i.e., in the limit $\lambda \rightarrow 0$, it is simply given by $G_{11}(\mathbf{q}, \omega^+) = g(\mathbf{q}, -i\omega) = (r + q^2 - i\gamma_m\omega/|\mathbf{q}|)^{-1}$ and, thus, isotropic up to order q^2 with respect to the magnon momentum. In higher orders, there may be anisotropic effects which, for small momenta, are less relevant.

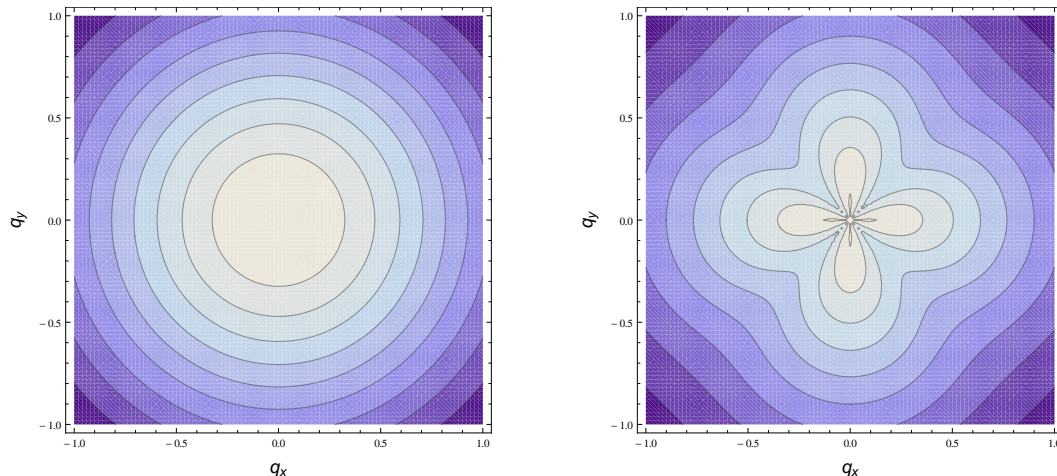


Fig. 6.2: Calculated quasi-elastic neutron scattering intensity in the (q_x, q_y) -plane in the limit $\mathbf{q} \rightarrow 0$. On the left hand side, the bare metamagnetic system is shown which yields an isotropic intensity pattern. On the right hand side, the elastic coupling is turned on, resulting in a scattering pattern with a fourfold symmetry which reflects the cubic lattice symmetry. The chosen parameters are the same as for Fig. 6.1.

However, turning on the phonon-interaction this is no longer true. On the contrary, since the phonons carry information about the underlying lattice structure, the scattering amplitude also acquires a similar structure. First of all, we have to calculate the inverse of the full propagator matrix. The magnon-magnon correlation function is given by

$$G_{11}(\mathbf{q}, \omega) = \frac{\det D(\mathbf{q}, \omega)}{\det G^{-1}(\mathbf{q}, \omega)} = \left(-i\gamma_m \frac{\omega}{q} + r + q^2 - \frac{\lambda^2 q^2}{\det D(\mathbf{q}, \omega)} \right)^{-1}. \quad (6.11)$$

The full scattering intensity for a given wave vector, \mathbf{q} is obtained by integrating over all energies,

$$\int_{-\infty}^{\infty} d\omega \frac{\text{Im} G_{11}(\mathbf{q}, \omega)}{\omega} = \int_{-\infty}^{\infty} d\omega \frac{\gamma_m}{q} \left[\left(\frac{\gamma_m \omega}{q} \right)^2 + \left(r + q^2 - \frac{\lambda^2 q^2}{\det D(\mathbf{q}, \omega)} \right)^2 \right]^{-1}.$$

As we integrate slightly above the real axis, the denominator has two poles, one in the upper complex plane and one in the lower plane. Thus, closing the integration contour by a semicircle at complex infinity in the upper complex plane, we obtain

$$S(\mathbf{k}) = NT |F(\mathbf{k})|^2 G_{11}(\mathbf{q}, 0). \quad (6.12)$$

For simplicity, let us consider the example of a cubic lattice for which the elastic modulus tensor has only three independent components, C_{11} , C_{12} and C_{44} , see Chap. 2. In this case, the magnon-magnon correlation function may be written as

$$G_{11}(\mathbf{q}, 0) = \left[(r + q^2) - \frac{\lambda^2}{C_{11}} \frac{1 + \frac{2A_1 C_{11}}{C_{11} + C_{12}} + \frac{3A_2 C_{11}}{C_{11} + 2C_{12} + C_{44}}}{1 + A_1 + A_2} \right]^{-1}, \quad (6.13)$$

where A_1 and A_2 are functions of the polar (θ) and azimuthal (ϕ) angle of the momentum \mathbf{q} and read as

$$A_1 = \frac{(C_{11} - C_{12} - 2C_{44})(C_{11} + C_{12})}{8C_{11}C_{44}} [2 \sin^2(2\theta) + (1 - \cos 4\phi) \sin^4 \theta],$$

$$A_2 = \frac{(C_{11} - C_{12} - 2C_{44})^2(C_{11} + 2C_{12} + C_{44})}{32C_{11}C_{44}^2} (1 - \cos 4\phi) \sin^2(2\theta) \sin^2 \theta.$$

Hence, we find a $\cos(4\phi)$ -modulation, which is depicted in Fig. 6.1, reflecting the fourfold symmetry of the cubic lattice. Additionally to this modulation, the amplitude of the oscillation as well as the mean value of the intensity depend on the polar angle, θ . Importantly, the anisotropy is independent of the modulus of \mathbf{q} , i.e., the zero momentum limit depends on the direction, $\hat{\mathbf{q}}$, from which it is approached. Note that in the fine-tuned isotropic limit, $C_{11} - C_{12} = 2C_{44}$, the angle dependence of the scattering amplitude vanishes and the coupling results in a constant shift of the scattering amplitude, $G_{11}^{\text{iso}} = (r + q^2 - \lambda^2/C_{11})^{-1}$.

In Fig. 6.2, we show a density plot of the correlation function in the (q_x, q_y) -plane for the uncoupled and the coupled system, respectively. Again, we see that the formerly isotropic scattering pattern obtains a modulation reflecting the symmetry of the lattice structure. For larger momenta, this modulation is washed out, as the isotropic part in Eq. (6.13) dominates over the angle dependence originating from the elastic coupling.

6.2.2 Parameter Renormalization Due To Phonons

Let us again consider, the full action given in Eq. (6.7). In order to obtain the focus on the important mechanisms at work, we will make a couple of simplifications. If we again consider a cubic lattice, with its three different elastic constants, C_{11} , C_{12} and C_{44} , in particular, the macroscopic shear modes, E_{ij} for $i \neq j$, are decoupled from the diagonal strain elements and can be integrated out. Therefore, the action for a cubic lattice reads as

$$\begin{aligned} \mathcal{S}[\phi, \mathbf{u}, \mathbf{E}] = & \frac{1}{2} \sum_{\mathbf{q} \neq 0, \omega_n} \begin{pmatrix} \phi \\ \mathbf{u} \end{pmatrix}_{\mathbf{q}, n}^\dagger \begin{pmatrix} g^{-1}(\mathbf{q}, \omega_n) & i\lambda \mathbf{q}^T \\ -i\lambda \mathbf{q} & D(\mathbf{q}, \omega_n) \end{pmatrix} \begin{pmatrix} \phi \\ \mathbf{u} \end{pmatrix}_{\mathbf{q}, n} \\ & + \frac{1}{2} \begin{pmatrix} \phi_0 \\ \mathbf{E} \end{pmatrix}^\dagger \begin{pmatrix} r_0 & -\lambda(1, 1, 1) \\ -\lambda(1, 1, 1)^T & \tilde{C} \end{pmatrix} \begin{pmatrix} \phi_0 \\ \mathbf{E} \end{pmatrix} \\ & + \int \left(\frac{v_{30}}{3!} \phi^3 + \frac{v_{40}}{4!} \phi^4 + \frac{v_{50}}{5!} \phi^5 - h_0 \phi \right) d\mathbf{r} d\tau, \end{aligned} \quad (6.14)$$

where the components of the vector \mathbf{E} are given by the diagonal elements of the tensor of macroscopic distortions ($\mathbf{E}_i = E_{ii}$) and the matrix \tilde{C} is given by $\tilde{C}_{ij} = C_{iijj}$. Notably, Landau damping is absent for the zero momentum magnetic mode, due to the lack of phase space, as discussed above, and higher order terms in ω are neglected.

Since only the longitudinal phonons couple to the order parameter, we switch to a longitudinal-transversal basis, $\mathbf{u} = (u_L, u_1, u_2)$, in which the dynamic matrix splits into an isotropic and an anisotropic part, $D = D_{\text{iso}} + \delta D_{\text{an}}$. The anisotropy parameter, $\delta = C_{11} - C_{12} - 2C_{44}$, vanishes for elastically isotropic crystals. The isotropic part is given by $D_{\text{iso}} = \omega^2 \mathbb{1} + |\mathbf{q}|^2 \text{diag}(C_{11}, C_{44}, C_{44})$, whereas D_{an} has momentum dependent off-diagonal elements and is given in Eq. (2.75).

$$E = E_{xx} + E_{yy} + E_{zz}, \quad E_1 = E_{xx} - E_{zz} \quad \text{and}, \quad E_2 = E_{xx} - 2E_{yy} + E_{zz}.$$

in which the interaction tensor, \tilde{C} , of the macroscopic modes is diagonal,

$$\tilde{C} = \begin{pmatrix} C_{11} - \frac{4}{3}C_{44} - \frac{2}{3}\delta & 0 & 0 \\ 0 & C_{44} - \frac{\delta}{2} & 0 \\ 0 & 0 & C_{44} - \frac{\delta}{2} \end{pmatrix}. \quad (6.15)$$

As E_1 and E_2 appear only quadratic in the action they can be integrated out.

Importantly, the criteria for stability under elastic fluctuations demand $C_{11} > 0$ and $C_{11}^2 > C_{12}^2$ which implies $C_{11} > C_{12}$. Substituting δ in Eq. (6.15), the modulus governing the macroscopic volume change, E , reads as $K = C_{11} - \frac{2}{3}(C_{11} - C_{12})$ and is, thus, always smaller than C_{11} which governs the longitudinal phonons. Therefore, when the magneto-elastic coupling drives the macroscopic modes critical, the phonons will still be non-critical. In the following, we will, for simplicity, analyze the system in the isotropic limit, i.e., for $\delta = 0$, in which case the longitudinal and the transversal phonons are decoupled. Therefore, we can also integrate out the latter reducing the action to

$$\begin{aligned} \mathcal{S}[\phi, u_L, E] = & \frac{1}{2} \sum_{\mathbf{q} \neq 0, \omega_n} \begin{pmatrix} \phi \\ u_L \end{pmatrix}_{\mathbf{q}, n}^\dagger \begin{pmatrix} g^{-1}(\mathbf{q}, \omega_n) & i \lambda q \\ -i \lambda q & \rho \omega_n^2 + q^2 C_{11} \end{pmatrix} \begin{pmatrix} \phi \\ u_L \end{pmatrix}_{\mathbf{q}, n} \\ & + \int \left(\frac{v_{30}}{3!} \phi^3 + \frac{v_{40}}{4!} \phi^4 + \frac{v_{50}}{5!} \phi^5 - h_0 \phi \right) \mathbf{d}\mathbf{r} \, d\tau \end{aligned} \quad (6.16)$$

$$+ \frac{1}{2} \begin{pmatrix} \phi_0 \\ E \end{pmatrix}^\dagger \begin{pmatrix} r_0 & -\lambda \\ -\lambda & K \end{pmatrix} \begin{pmatrix} \phi_0 \\ E \end{pmatrix} \quad (6.17)$$

The corrections due to anisotropy could then, in principle, be treated in a perturbative approach. However, concerning thermodynamics a small anisotropy will only yield subleading corrections. To simplify notations, we will drop the subscript, L , further on, denoting the longitudinal phonons with u . This is our starting point for the analysis of the quantum endpoint of compressible metamagnetic systems.

The self-consistent functional RG equation, Eq. (5.12), defines the effective macroscopic potential of the coupled magneto-elastic system by the evolution of

the microscopic potential along a RG trajectory. In the coupled theory, we have not only to consider the second derivative of the action, $\mathcal{S}[\phi, u]$, with respect to the metamagnons, ϕ , but also the second derivative with respect to the longitudinal phonons, u , and the mixed derivative. Thus, the effective macroscopic potential is obtained by

$$\mathcal{V} = \mathcal{V}_0 + \int_0^\mu d\mu' e^{-(d+z)\mu'} f_{\mu'} \left(\frac{\delta^2 \mathcal{S}_{\mu'}}{\delta \phi^2}, \frac{\delta^2 \mathcal{S}_{\mu'}}{\delta \phi \delta u}, \frac{\delta^2 \mathcal{S}_{\mu'}}{\delta u^2} \right). \quad (6.18)$$

The subscript μ' denotes that the parameters are rescaled according to their respective engineering dimensions. Importantly, phonons and metamagnons are governed by different dynamics. The phonons have a dynamical exponent $z_< = 1$, whereas we obtain $z_> = 3$ for the metamagnons. In the rescaling step of the RG procedure, we, therefore, leave the general frequency exponent, z , unspecified and rescale the mass density of the atoms, ρ , and the previously introduced parameter γ_m accordingly, as done in Ref. [117]:

$$\begin{aligned} r &\rightarrow r e^{2\mu}, & \gamma_m &\rightarrow \gamma_m e^{-(z-z_>)\mu}, & \lambda &\rightarrow \lambda e^\mu, \\ \rho &\rightarrow \rho e^{-2(z-z_<)\mu}, & T &\rightarrow T e^{z\mu}, & C_{11} &\rightarrow C_{11}. \end{aligned} \quad (6.19)$$

The function f is again the re-exponentiated contribution of a high energy shell integration of the Gaussian part of the action,

$$f = -\Lambda \frac{\partial}{\partial \Lambda} \frac{1}{2} \int_0^\Lambda \frac{d\mathbf{q}}{(2\pi)^d} \frac{1}{\beta} \sum_{\omega_n} \log [\det G^{-1}], \quad (6.20)$$

where the matrix G^{-1} is given by the Hessian of the action

$$G^{-1} = \begin{pmatrix} \mathcal{S}_{\phi,\phi} & \mathcal{S}_{u,\phi^\dagger} \\ \mathcal{S}_{u,\phi} & \mathcal{S}_{u,u} \end{pmatrix}. \quad (6.21)$$

Here, we introduced the shorthand notation for the functional derivatives of the action $\mathcal{S}_{\alpha,\beta} = \delta^2 \mathcal{S} / (\delta \alpha \delta \beta)$.

Because of the bilinear coupling and the lack of anharmonic phonon terms, only $\mathcal{S}_{\phi,\phi}$ depends self-consistently on the potential, $R = \mathcal{V}''(\phi)$, and we obtain

$$\det G^{-1} = \left(R + q^2 + \gamma_m \frac{|\omega_n|}{q} \right) \left(\rho \omega_n^2 + C_{11} q^2 \right) - \lambda^2 q^2. \quad (6.22)$$

As it turns out, the function f splits into two terms. One describes phonons with a renormalized energy, $\omega_1 < v\Lambda$ and a damping term-, and the other describes a metamagnetic system, with a renormalized mass, $R_{\text{ph}} < R$, which is given by $R_{\text{ph}} = R - \lambda^2 / C_{11}$. As we will see in the following, the preemptive structural transition occurs at $R = \lambda^2 / K$. Importantly, the bulk modulus, K , is smaller than

C_{11} and, therefore, the phonon-renormalized mass is always larger than zero above the transition, implying non-critical fluctuations.

The integration over the RG-flow yields, first of all, a renormalization of the bare parameters, due to zero temperature contributions which only act at the initial stage of the RG flow. Apart from that, we obtain two fluctuation terms, \mathcal{A}_d and \mathcal{B}_d , for the metamagnetic and the phonon fluctuations, respectively, and the effective potential reads as

$$\begin{aligned} \mathcal{V}(E, \phi) = & \frac{K}{2} E^2 - pE - \lambda \phi E - h\phi + \frac{r}{2!} \phi^2 + \frac{u}{4!} \phi^4 \\ & + T^{\frac{D}{z} >} \mathcal{A}_d \left(\mathcal{V}_{\text{ph}}''(\phi) T^{-\frac{2}{z}} \right) + T^{\frac{D}{z} <} \mathcal{B}_d \left(\mathcal{V}_{\text{ph}}''(\phi) T^{-\frac{2}{z}}, \mathcal{V}''(\phi) T^{-\frac{2}{z}} \right). \end{aligned} \quad (6.23)$$

The function $\mathcal{A}_d(x)$ is the same as in Chap. 5 since it stems from the renormalized metamagnetic theory. However, its argument is not the bare metamagnetic potential stiffness but the renormalized one $\mathcal{V}_{\text{ph}}''(\phi) = \mathcal{V}''(\phi) - \lambda^2/C_{11}$.

Concerning the phonon part, $\mathcal{B}_d(x, y)$, it is $\mathcal{V}''(\phi) \gg T^2$ as well as $\mathcal{V}_{\text{ph}}''(\phi) \gg T^2$ close to the quantum endpoint. In this limit and for $\Lambda \gg T$, the asymptotic behavior is given by

$$T^{D < / z <} \mathcal{B}_d \left(\mathcal{V}_{\text{ph}}''(\phi) T^{-\frac{2}{z}}, \mathcal{V}''(\phi) T^{-\frac{2}{z}} \right) = T^{d+1} \mathfrak{b}_d \left(v^2 \frac{\mathcal{V}_{\text{ph}}''(\phi)}{\mathcal{V}''(\phi)} \right)^{d/2}. \quad (6.24)$$

Comparison with $T^{D > / z >} \mathcal{A}_d \left(\mathcal{V}_{\text{ph}}''(\phi) T^{-\frac{2}{z}} \right)$ shows that this contribution is always sub-leading at low temperatures, i.e., in the vicinity of the quantum critical endpoint. Therefore, we may neglect the phonon contribution in the following.

This splitting is of course not at all obvious and is related to the different dynamics of the phonons and the magnons. For the details of the tedious and technical derivation of this equation and the exact form of the two fluctuation function, \mathcal{B}_d , the reader may be referred to App. C.

6.3 Free Energy

The elastic part of the effective potential, Eq. (6.23) reads as

$$\mathcal{V}_{\text{el}}(E) = \frac{K}{2} E^2 - pE - \lambda \phi E \quad (6.25)$$

where we added the second term to account for an applied pressure, p . The strain, E , is obtained by minimizing $\mathcal{V}_{\text{el}}(E)$ yielding $E = (p + \lambda \phi)/K$. Thus, the strain follows directly the behavior of the magnetization. Substituting this in Eq. (6.23) leads to the following effective metamagnetic potential

$$\mathcal{V}(\phi) = -\frac{p^2}{2K} - \left(h + \frac{\lambda p}{K} \right) \phi + \frac{r - \lambda^2/K}{2!} \phi^2 + \frac{u}{4!} \phi^4 + T^{D > / z >} \mathcal{A}_d \left(\mathcal{V}_{\text{ph}}''(\phi) T^{-2/z} \right). \quad (6.26)$$

The constant first term is irrelevant with respect to minimization of the potential, therefore, we will skip it in the following. However, it will give rise to an extra contribution $1/K$ to the compressibility of the system, which we discuss in Sec. 6.4.

Apart from the fluctuation function, Eq. (6.26) resembles the metamagnetic potential discussed in Chap. 5 with a shifted magnetic field, $h_{\text{el}} = h + \lambda p/K$, and a renormalized bare mass, $r_{\text{el}} = r - \lambda^2/K$. Therefore, large parts of the discussion of the bare theory also apply to this case. In particular, the negligence of terms higher than fourth order in the magnetization, ϕ , is equally well justified. It, again, leads to an emergent Ising symmetry, though, in this case with respect to $h_c = -\lambda p/K$ rather than to $h_c = 0$.

The main difference to the bare system is that the quadratic term of the potential may become negative. Therefore, we obtain a first order phase transition at $h_{\text{el}} = 0$ terminating in a second order endpoint, which is determined by $\mathcal{V}''(0) - \lambda^2/K = 0$. Importantly, the argument of the fluctuation term, \mathcal{A}_d , depends on the phonon-renormalized potential, $\mathcal{V}''(0) - \lambda^2/C_{11}$. As $K > C_{11}$ the argument is positive at the endpoint and, therefore, the system exhibits no critical fluctuations.

Since we analyze the system along the same lines as in Chap. 5, we will not be as explicit in the following as before. To begin with, we will consider the first order transition with a finite temperature endpoint at T_c and, thereafter, investigate the fine-tuned limit $T_c \rightarrow 0$, i.e., the quantum endpoint.

6.3.1 First Order Transition

If the mass becomes negative, $r < \lambda^2/K$, the elastically coupled metamagnetic system exhibits a first order isostructural transition at low temperatures. At a finite temperature, T_c , the line of these first order transitions terminates in a second order endpoint. The behavior around the endpoint is similar to the finite temperature endpoint of the Mott transition on compressible lattices as both have an emergent Ising symmetry. However, since we start the analysis here from the magnetic sector, rather than from the effective elastic potential as done in Chap. 4, it is still instructive to look at this case again. Starting from the more general phase diagram of this situation, we investigate then the emergence of the quantum critical endpoint.

As before, we can distinguish two different regimes by the strength of the fluctuations. In the so-called linear regime, the potential experienced by the fluctuations, $\mathcal{V}_{\text{ph}}(\phi)$, is rather stiff and we can simply expand the fluctuation function, $\mathcal{A}_d(\mathcal{V}_{\text{ph}}''(\phi)T^{-2/z})$, in the magnetization, ϕ . In contrast, the fluctuations become very strong, if the phonon-renormalized potential becomes very soft. In this case, the curvature of the potential is given by the magnetization itself, $\mathcal{V}''(\phi) \approx \frac{u}{2}\phi^2$. The two regimes are separated by a crossover line determined by the mean magnetization, $\bar{\phi}$, as $\frac{u}{2}\bar{\phi}^2 \sim \mathcal{V}_{\text{ph}}''(0)$.

Linear Regime

Expanding the full potential, $\mathcal{V}(\phi)$, in the magnetization, we obtain

$$\mathcal{V}(\phi) = \mathcal{V}(0) - h_{\text{el}}\phi + \frac{R_{\text{el}}}{2}\phi^2 + \frac{u}{4!}\phi^4, \quad (6.27)$$

in leading order of the temperature. The discussion of sub-leading temperature corrections, for example to the field h_{el} , is analogous to the one already given in Chap. 5. The temperature dependent effective mass is obtained as $R_{\text{el}} = \mathcal{V}''(0)$ and reads as

$$R_{\text{el}} = \begin{cases} r_{\text{el}} + \tau_d u T^{(d+1)/3} & \text{for } R_{\text{ph}} \ll T^{2/3} \\ \bar{r}_{\text{el}} + \bar{\tau}_d u T^2 r_{\text{ph}}^{(d-5)/2} & \text{for } R_{\text{ph}} \gg T^{2/3} \end{cases}, \quad (6.28)$$

where the coefficients are the same as in Eq. (5.28). Note, that the fluctuation corrections to the potential stiffness, R_{el} , are not determined by itself, but by the phonon-renormalized mass, r_{ph} . The low temperature regime is, therefore, reached even for vanishing r_{el} . For this reason, we have to keep the temperature independent term in the low temperature regime, which was absorbed in another renormalization, of the mass, $\bar{r}_{\text{el}} = r_{\text{el}} + u T^{(D>-2)/z>} \mathcal{A}'_d (R_{\text{ph}} T^{-2/z>}) \big|_{T=0}$.

The critical temperature is determined by the condition of a vanishing quadratic term, $R_{\text{el}}(T_c) = 0$ which leads for sufficiently large $|r_{\text{el}}|$ to

$$T_c = \left(\frac{|r_{\text{el}}|}{\tau_d u} \right)^{3/(d+1)}. \quad (6.29)$$

For positive masses, $R_{\text{el}} > 0$, we have, effectively, a similar situation as in the uncoupled case and for $R_{\text{el}}^3 \gg h_{\text{el}}^2 u$, the potential, Eq. (6.27), is minimized by

$$\bar{\phi}_1 = \frac{h_{\text{el}}}{R_{\text{el}}}. \quad (6.30)$$

On the other hand, in the opposite case, for large fields, we obtain

$$\bar{\phi}_2 = \text{sgn}(h_{\text{el}}) \left[\left(\frac{6|h_{\text{el}}|}{u} \right)^{1/3} - R_{\text{el}} \left(\frac{4}{3|h_{\text{el}}|u^2} \right)^{1/3} \right]. \quad (6.31)$$

If the mass becomes negative, $R_{\text{el}} < 0$, and fields are large, Eq. (6.31) is still the minimizing configuration. In contrast, for $|R_{\text{el}}|^3 \gg h_{\text{el}}^2 u$, the solution is given by

$$\bar{\phi}_3 = \text{sgn}(h_{\text{el}}) \sqrt{\frac{6|R_{\text{el}}|}{u}} + \frac{h_{\text{el}}}{2|R_{\text{el}}|}. \quad (6.32)$$

As expected, we obtain a strain-induced first order phase transition at $h_{\text{el}} = 0$, where the magnetization jumps about $\Delta\phi = 2\sqrt{6|R_{\text{el}}|/u}$. The field configuration having

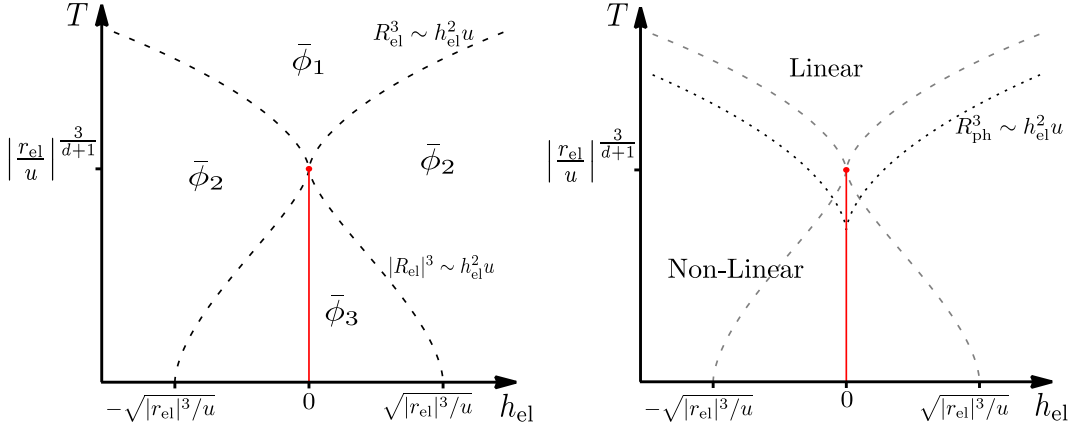


Fig. 6.3: Left: The first order transition (red line) terminates in a second order endpoint where $R_{\text{el}}(T_c) = 0$. From this endpoint the crossover lines emerge at which the magnetization $\bar{\phi}$ changes its field dependence.

Right: The crossover from the linear to the non-linear regime (black, dotted) for large fields h_{el} asymptotically matches the magnetization crossover. However, close to the endpoint it deviates, terminating at zero field at lower temperatures than the second order endpoint.

the opposite sign in the first term corresponds to the metastable second minimum of the potential, coexisting with the global minimum and giving rise to hysteresis effects. The line of first order transitions terminates in a critical endpoint which is defined by $R_{\text{el}}(T_c) = 0$. Since $R_{\text{el}}(T)$ is monotonically increasing, the quantum endpoint is obtained for $\bar{r}_{\text{el}} = 0$.

The crossover lines for the different field configurations is depicted on the left hand side of Fig. 6.3. The free energy in these regimes takes the form

$$\mathcal{F} = T^{D>/z>} \mathcal{A}_d \left(R_{\text{ph}} T^{-2/z>} \right) \quad (6.33)$$

$$+ \begin{cases} -\frac{h_{\text{el}}^2}{2R_{\text{el}}} & , |R_{\text{el}}|^3 \gg uh_{\text{el}}^2, R_{\text{el}} > 0 \\ -\frac{3R_{\text{el}}^2}{2u} - \sqrt{\frac{6|R_{\text{el}}|}{u}} |h_{\text{el}}| - \frac{h_{\text{el}}^2}{4|R_{\text{el}}|} & , |R_{\text{el}}|^3 \gg uh_{\text{el}}^2, R_{\text{el}} < 0 . \\ -\frac{3}{4} \left(\frac{6|h_{\text{el}}|^4}{u} \right)^{1/3} + R_{\text{el}} \left(\frac{9|h_{\text{el}}|^2}{2u^2} \right)^{1/3} & , |R_{\text{el}}|^3 \ll uh_{\text{el}}^2 \end{cases}$$

Non-Linear Regime

The crossover from the linear to the non-linear regime is given by $R_{\text{ph}} \sim \frac{u}{2} \bar{\phi}_i^2$, since the fluctuations are determined by the phonon-renormalized potential, and is depicted on the right hand side of Fig. 6.3. For small magnetic fields and positive stiffness, $R_{\text{el}}^3 \ll uh_{\text{el}}^2$, the crossover condition translates to $R_{\text{ph}}^3 \sim uh_{\text{el}}^2$. However, since $R_{\text{ph}} > R_{\text{el}}$, this criterion can never be met.

For negative R_{el} and small fields, $|R_{\text{el}}|^3 \ll uh_{\text{el}}^2$, we are in the coexistence regime with a second, metastable minimum of the potential. Here, the crossover line between the linear and the non-linear regime is given by $R_{\text{ph}} \sim -3R_{\text{el}}$ which implies that $R_{\text{el}} \sim \lambda^2(K - C_{11})/(KC_{11})$. Since the shear modulus, $\mu \sim C_{11} - K$, is, in general, smaller but of the same order than the bulk modulus, the crossover temperature is smaller than the critical temperature, however, it is in the same parametric region.

For much smaller temperatures than the crossover temperature, we can approximate $R_{\text{el}} \approx r_{\text{el}}$ and the fluctuations yield terms of the order $\mathcal{O}(\phi^{D>})$ are sub-leading. Therefore, the potential is minimized by $\bar{\phi}_3$ yielding the free energy

$$\mathcal{F} = T^{D>/z>} \mathcal{A}_d \left[\left(\sqrt{3|r_{\text{el}}|} + \sqrt{\frac{u}{2} \frac{|h_{\text{el}}|}{|r_{\text{el}}|}} \right)^2 T^{-2/z>} \right] - \frac{3r_{\text{el}}^2}{2u} - \sqrt{\frac{6|r_{\text{el}}|}{u}} |h_{\text{el}}| - \frac{h_{\text{el}}^2}{4|r_{\text{el}}|}.$$

In contrast to the linear regime, the fluctuation term does now also depend on the elastically renormalized mass, r_{el} . We may further expand the fluctuation term in the magnetic field, h_{el} , yielding

$$\begin{aligned} \mathcal{F} = T^{D>/z>} \mathcal{A}_d \left(3|r_{\text{el}}| T^{-2/z>} \right) + T^{(D>-2)/z>} \mathcal{A}'_d \left(3|r_{\text{el}}| T^{-2/z>} \right) \sqrt{\frac{3u}{2|r_{\text{el}}|}} |h_{\text{el}}| \\ - \frac{3r_{\text{el}}^2}{2u} - \sqrt{\frac{6|r_{\text{el}}|}{u}} |h_{\text{el}}| - \frac{h_{\text{el}}^2}{4|r_{\text{el}}|}. \end{aligned} \quad (6.34)$$

For large fields, the crossover is determined by the condition $|R_{\text{ph}}|^3 \sim h_{\text{el}}^2 u$ which corresponds to temperatures $T \sim (h_{\text{el}}/u)^{2/(d+1)}$. This matches asymptotically the condition $|R_{\text{el}}|^3 \ll h_{\text{el}}^2 u$ where the crossover from the configuration $\bar{\phi}_2$ to $\bar{\phi}_1$ takes place. This implies that no parametrically large linear regime with a field configuration $\bar{\phi}_2$ exists. However, closer to the endpoint the two crossover lines deviate from one another, giving rise for such a crossover. Approaching the endpoint at T_c , one, thus, ends up in a regime where the potential is soft, but the fluctuation term is smooth due to its argument, $R_{\text{ph}} T^{-2/z>}$, being finite. The field configuration is still given by $\bar{\phi}_1$ and the resulting free energy reads as

$$\mathcal{F} = T^{D/z} \mathcal{A}_d \left[\left(\frac{9h_{\text{el}}^2 u}{2T^2} \right)^{1/3} \right] - \frac{3}{4} \left[\frac{6h_{\text{el}}^4}{u} \right]^{1/3} + R_{\text{el}} \left[\frac{9h_{\text{el}}^2}{2u^2} \right]^{1/3}. \quad (6.35)$$

Fermi Liquid Regime

Finally, at lowest temperatures, there is a crossover to the Fermi liquid regime where the fluctuations change their nature and the free energy density becomes quadratic in temperature, $\mathcal{F} = F_0(h_{\text{el}}) - (T/T_0)^2$. This crossover is determined by the condition $\mathcal{V}_{ph}''(\phi) \sim T^{-2/3}$. At zero field, neglecting the temperature dependence of R_{ph} , this

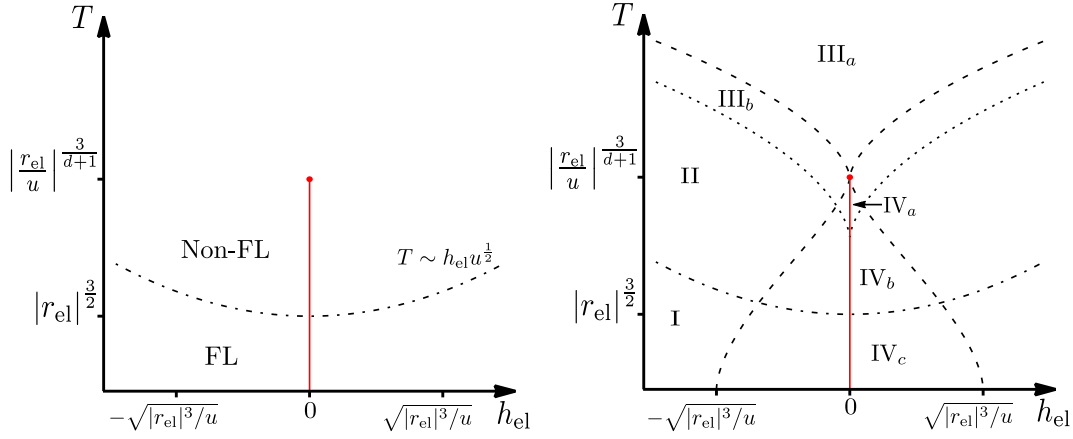


Fig. 6.4: A third crossover happens when the fluctuations change their nature, giving rise to Fermi-liquid like behavior. This crossover line is depicted in the left panel. On the right hand side, the phase diagram is summarized and the seven different regimes are labeled as in Eq. (6.36).

translates to $r_{\text{ph}} + 3|r_{\text{el}}| \sim T^{-2/3}$. In case that both masses are of the same order, $r_{\text{ph}} \sim r_{\text{ph}}$, the crossover temperature follows as $T \sim |r_{\text{el}}|^{3/2}$. This is fair below the temperature of the second order endpoint, which is at $T_c \sim (|r_{\text{el}}|/u)^{3/(d+1)}$

For large fields, the fluctuation function changes at a temperature $T \sim h_{\text{el}}\sqrt{u}$ similar to the inelastic case. The crossover line to the Fermi liquid regime is depicted on the left hand side of Fig. 6.4.

Free Energy

The three different crossovers give rise to seven different regimes in the phase diagram, as depicted on the right hand side of Fig. 6.4. For high temperatures, the relative difference of the bare and the elastically renormalized stiffness, $(R_{\text{el}} - R)/R$, becomes negligible and, hence, the elastic coupling has only a small influence on macroscopic observables. Indeed, the free energy in region III_a resembles the free energy of the bare metamagnet in region III with a renormalized magnetic field, h_{el} . Similarly, for large fields, the finite magnetization dominates the phonon-renormalized effective mass, and, therefore, the free energies of the elastically coupled and the bare metamagnetic system coincide also in the regions I and II.

Approaching the critical region, the elastic coupling starts to change the behavior of the system yielding, first and foremost, a shift in the critical temperature. In particular for $r = 0$, the bare metamagnetic theory predicts a quantum critical endpoint. Instead, the endpoint is lifted to a finite temperature endpoint below which we obtain a line of first order transitions.

In connection with the finite temperature endpoint, for high temperatures, the parametrically small regime III_b with magnetization-independent fluctuations and, more important, the coexistence regime, IV arises. In the latter the metamagnetic

potential has a second metastable minimum, since the elastic mass, R_{el} , is large and negative. The coexistence regime is split into three parts, namely the linear regime, IV_a , the non-linear regime, IV_b , and the Fermi liquid regime, IV_c .

For $r = 0$ and in this case of a small phonon-renormalized mass, r_{ph} , the free energy can be written as

$$\mathcal{F} = \begin{cases} -\bar{f}_2 T^2 \left[\frac{9uh_{\text{el}}^2}{2} \right]^{\frac{d-3}{6}} - \frac{3}{4} \left[\frac{6h_{\text{el}}^4}{u} \right]^{\frac{1}{3}} & \text{I} \\ -f_1 T^{\frac{d}{3}+1} + f_2 T^{\frac{d+1}{3}} \left[\frac{9uh_{\text{el}}^2}{2} \right]^{\frac{1}{3}} - \frac{3}{4} \left[\frac{6h_{\text{el}}^4}{u} \right]^{\frac{1}{3}} & \text{II} \\ -f_1 T^{\frac{d}{3}+1} - \frac{h_{\text{el}}^2}{2R_{\text{el}}} & \text{III}_a \\ -f_1 T^{\frac{d}{3}+1} - \frac{3}{4} \left[\frac{6h_{\text{el}}^4}{u} \right]^{\frac{1}{3}} + R_{\text{el}} \left[\frac{9h_{\text{el}}^2}{2u^2} \right]^{\frac{1}{3}} & \text{III}_b \\ -f_1 T^{\frac{d}{3}+1} - \frac{3R_{\text{el}}^2}{2u} - |h_{\text{el}}| \sqrt{\frac{6|R_{\text{el}}|}{u}} - \frac{h_{\text{el}}^2}{4|R_{\text{el}}|} & \text{IV}_a \\ -f_1 T^{\frac{d}{3}+1} + f_2 T^{\frac{d+1}{3}} \left[\sqrt{3|r_{\text{el}}|} + \frac{1}{2} \sqrt{\frac{h_{\text{el}}^2 u}{2r_{\text{el}}^2}} \right]^2 - \frac{3r_{\text{el}}^2}{2u} - \sqrt{\frac{6h_{\text{el}}^2|r_{\text{el}}|}{u}} - \frac{h_{\text{el}}^2}{4|r_{\text{el}}|} & \text{IV}_b \\ -\bar{f}_4 T^2 \left[\sqrt{3|\bar{r}_{\text{el}}|} + \frac{1}{2} \sqrt{\frac{h_{\text{el}}^2 u}{2\bar{r}_{\text{el}}^2}} \right]^{d-3} - \frac{3\bar{r}_{\text{el}}^2}{2u} - \sqrt{\frac{6h_{\text{el}}^2|\bar{r}_{\text{el}}|}{u}} - \frac{h_{\text{el}}^2}{4|\bar{r}_{\text{el}}|} & \text{IV}_c \end{cases} \quad (6.36)$$

6.3.2 Quantum Endpoint

The end-point of the first order transition is driven to zero temperature, i.e., a quantum endpoint emerges, when $R_{\text{el}}(T = 0) = 0$, which implies a vanishing \bar{r}_{el} . Since $R_{\text{el}} \geq 0$, the regions IV_a , IV_b and IV_c of the phase diagram in Fig. 6.4 are not realized in this case. The crossover between the two possible field configuration, $\bar{\phi}_1$ and $\bar{\phi}_2$, still occurs at $R_{\text{el}} \sim uh_{\text{el}}^2$ terminating in the quantum endpoint. The crossover from the linear to the non-linear regime, given by $R_{\text{ph}} \sim (9uh_{\text{el}}^2/2)^{1/3}$, takes for low temperatures place at a constant field of $h_{\text{el}} \sim \sqrt{r_{\text{ph}}^3/u}$. As the temperature increases, thermal corrections get stronger and the crossover lines start to deviate asymptotically as $T \sim (uh_{\text{el}}^2)^{1/(d+1)}$.

Most interesting, is the crossover to the Fermi liquid regime, determined by the condition $\mathcal{V}_{\text{ph}}''(\bar{\phi}) = R_{\text{ph}} + \frac{u}{2}\bar{\phi}^2 \sim T^{2/3}$. For large fields, this yields the same behavior as for the finite temperature endpoint, being determined by $T \sim \sqrt{uh_{\text{el}}}$. As the field is lowered, the relative magnetization, $\bar{\phi}$, goes to zero. Importantly, for any finite r_{ph} , the Fermi liquid crossover line is not driven to zero temperature. Instead, it continues into regime III_a .

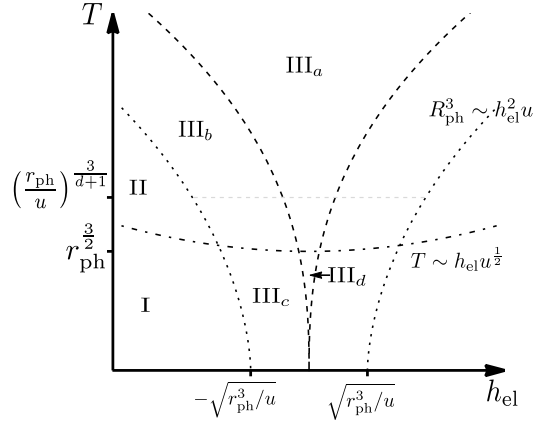


Fig. 6.5: Phase diagram of the quantum endpoint scenario, $\bar{r}_{\text{el}} = 0$. The magnetization crossover line (dashed) stays unchanged. The crossover from the linear to the non-linear regime (dotted) ends at zero temperature at a finite field determined by the phonon-renormalized mass. Strikingly, the Fermi liquid crossover (dashed-dotted) stays even at zero field at a finite temperature $T \sim r_{\text{ph}}^{3/2}$. Thus, critical fluctuations associated with a quantum critical endpoint get cut off at this temperature scale, giving rise to mean field like behavior.

Thus, upon approaching the quantum endpoint by lowering the temperature at $h_{\text{el}} = 0$, one inevitably enters the Fermi liquid regime, yielding the regimes III_c and III_d. The crossover scale is to leading order given by

$$T_{FL} \sim r_{\text{ph}}^{3/2}. \quad (6.37)$$

At this scale, critical fluctuations associated with the quantum endpoint are cut off and mean field like behavior is recovered, as it will be discussed in Sec. 6.4. The phase diagram of the quantum endpoint is depicted in Fig. 6.5 the free energy is given by

$$\mathcal{F} = \begin{cases} -\bar{f}_2 T^2 \left[\frac{9uh_{\text{el}}^2}{2} \right]^{\frac{d-3}{6}} - \frac{3}{4} \left[\frac{6h_{\text{el}}^4}{u} \right]^{\frac{1}{3}} & \text{I} \\ -\bar{f}_1 T^{\frac{d}{3}+1} + \bar{f}_2 T^{\frac{d+1}{3}} \left[\frac{9uh_{\text{el}}^2}{2} \right]^{\frac{1}{3}} - \frac{3}{4} \left[\frac{6h_{\text{el}}^4}{u} \right]^{\frac{1}{3}} & \text{II} \\ -\bar{f}_1 T^{\frac{d}{3}+1} - \frac{h_{\text{el}}^2}{2R_{\text{el}}} & \text{III}_a \\ -\bar{f}_1 T^{\frac{d}{3}+1} - \frac{3}{4} \left[\frac{6h_{\text{el}}^4}{u} \right]^{\frac{1}{3}} + R_{\text{el}} \left[\frac{9h_{\text{el}}^2}{2u^2} \right]^{\frac{1}{3}} & \text{III}_b \\ -\bar{f}_2 r_{\text{ph}}^{\frac{d-3}{2}} T^2 - \frac{3}{4} \left[\frac{6h_{\text{el}}^4}{u} \right]^{\frac{1}{3}} + R_{\text{el}} \left[\frac{9h_{\text{el}}^2}{2u^2} \right]^{\frac{1}{3}} & \text{III}_c \\ -\bar{f}_2 r_{\text{ph}}^{\frac{d-3}{2}} T^2 - \frac{h_{\text{el}}^2}{2R_{\text{el}}} & \text{III}_d \end{cases}. \quad (6.38)$$

Notably, the potential stiffness, $R_{\text{el}}(T)$, has no term independent of temperature as it is fine-tuned to zero to obtain the quantum endpoint. For high temperatures, it scales as $R_{\text{el}} \sim T^{\frac{d+1}{3}}$, whereas for lowest temperatures it goes as $R_{\text{el}} \sim T^2$. According to Eq. (6.28), the crossover is determined by the condition $R_{\text{ph}} \approx r_{\text{ph}} \sim T^{2/3}$ which is the Fermi liquid crossover temperature.

6.4 Thermodynamics

From the asymptotic analytic expressions for the free energy density, Eq. (6.38) and Eq. (6.36), we can, similar to Sec. 5.4, derive the response of the elastically coupled metamagnetic system to changes of temperature, magnetic field or pressure. Since the pressure only shift the magnetic field linearly, derivatives with respect to field and pressure are proportional to each other,

$$\frac{\partial F}{\partial p} = \frac{\lambda}{K} \frac{\partial F}{\partial h} \propto \frac{\partial F}{\partial H}. \quad (6.39)$$

Therefore, as already emphasized in Sec. 5.4, many thermodynamic quantities show the same critical behavior. For instance, the thermal expansion, $\alpha = \frac{1}{V} \partial_T \partial_p F$, is equivalent to the temperature derivative of the magnetization, $\partial_T M = \partial_T \partial_H F$. Likewise, the magnetostriction, $\lambda = -\frac{1}{V} \partial_H \partial_p F$, and the differential magnetic susceptibility, $\chi = -\partial_H^2 F$, have the same critical behavior. In principle, the compressibility, $\chi = -\frac{1}{V} \partial_p^2 F$, also follows the same behavior, however, as already mentioned in Sec. 6.3, due to the quadratic pressure term in the potential, Eq. (6.26), it has an additional non-critical contribution, $\delta\kappa = 1/K$.

Furthermore, we will also consider the specific heat coefficient, $\gamma = -\partial_T^2 F$, as well as the Grüneisen parameter, $\Gamma = \alpha/(T\gamma)$, which coincides with its magnetic analogue, $\Gamma_H = -\partial_T M/(T\gamma)$.

As already seen, far away from the endpoint in the regimes I, II and III_a, the influence of the elastic coupling is small, and the thermodynamic quantities are the same as for the bare metamagnetic system. However, close to the endpoint, the elastic coupling will be responsible for deviations from the critical behavior. In the following, we derive the analytic expressions from Eq. (6.38) and Eq. (6.36), and, additionally, show numerical plots, which were calculated within the same scheme as in Chap. 5.

6.4.1 Susceptibility, Compressibility and Magnetostriction

Susceptibility, χ , and magnetostriction, λ , are proportional to each other, as well as the critical part, κ_{crit} , of the compressibility, $\kappa = K^{-1} + \kappa_{\text{crit}}$. Since the metamagnetic transition is associated with an isostructural transition, the compressibility has to diverge upon approaching the endpoint.

Finite Temperature Endpoint

Sweeping the magnetic field through the endpoint at T_c , the susceptibility will diverge as

$$\chi = \left(\frac{2}{9u}\right)^{\frac{1}{3}} |h_{\text{el}}|^{-\frac{2}{3}} \text{sgn } h_{\text{el}} \quad \text{in II and III}_b, \quad (6.40)$$

thus, it is not sensitive to the crossover from II to III_b. Similarly, upon lowering the temperature at the metamagnetic field, $h_{\text{el}} = 0$, we find for temperatures $T > T_c$

$$\chi = \frac{1}{R_{\text{el}}} = \frac{1}{r_{\text{el}} + \mathbf{r}_d u T^{\frac{d+1}{3}}} \quad \text{in III}_a. \quad (6.41)$$

The divergence is proportional to $\chi \sim (T - T_c)^{-\gamma}$, from which we deduce by linearization of $R_{\text{el}} \sim T - T_c$ the critical exponent, $\gamma = 1$. This equals the mean field value which was also obtained for the finite temperature endpoint of the Mott transition. Below the critical endpoint, this behavior is qualitatively continued

$$\chi = \frac{1}{2|R_{\text{el}}|} \quad \text{in IV}_a, \quad (6.42)$$

and the relative prefactor of $\chi_{\text{III}_a}/\chi_{\text{IV}_a} = 2$ is also an indication for Ising mean field behavior. Upon lowering the temperature further, we end up in regime IV_b, where the susceptibility is given by

$$\chi = \frac{1}{2|r_{\text{el}}|} - \frac{1}{2} \mathbf{f}_2 u T^{\frac{d+1}{3}} \left(\frac{1}{r_{\text{el}}^2}\right) \quad \text{in IV}_b, \quad (6.43)$$

which is the low temperature expansion of χ in IV_a.

Quantum Endpoint

In case of a quantum endpoint, the behavior does not change much. For lowest temperatures the field dependence is also given by

$$\chi = \text{sgn } h_{\text{el}} \left[\left(\frac{2}{9u}\right)^{\frac{1}{3}} |h_{\text{el}}|^{-\frac{2}{3}} + R_{\text{el}} \left(\frac{2}{9u}\right)^{\frac{2}{3}} |h_{\text{el}}|^{-\frac{4}{3}} \right] \quad \text{in I and III}_c \quad (6.44)$$

and, thus, diverges exactly as in the elastically uncoupled case. This divergence is cut off when entering III_d, where the susceptibility will saturate. In terms of critical exponents, it is $\chi \sim h_{\text{el}}^{-1+1/\delta}$, hence, we obtain the mean field value $\delta = 3$.

For zero field, $h_{\text{el}} = 0$, the susceptibility has the general form $\chi = R_{\text{el}}^{-1}$. However, the behavior of the elastically renormalized mass depends on the phonon-renormalized mass, R_{ph} . Therefore, it changes its behavior at the same temperature scale where the crossover temperature to the Fermi liquid regime is reached to a

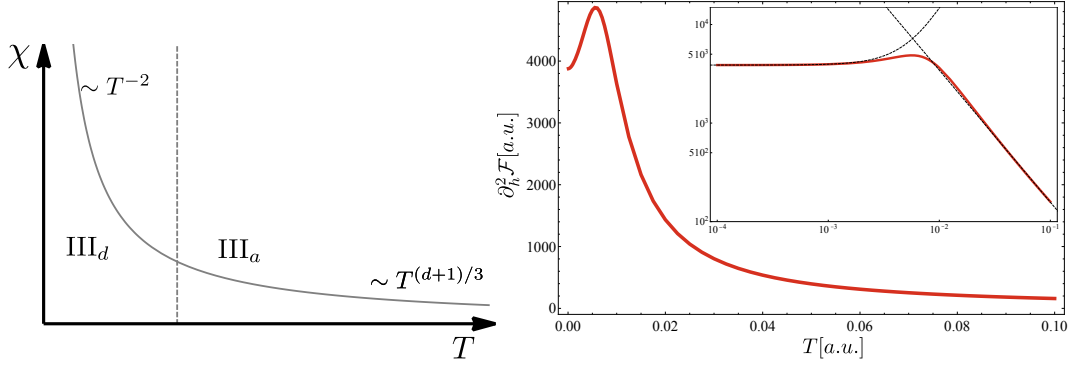


Fig. 6.6: Left: Sketch of the temperature dependence of the susceptibility above the QCEP. Right: Numerical evaluation for $d = 2$ at a magnetic field of $h = 2 \times 10^{-6}$ with the parameters $r_{\text{ph}} = 0.05$, $u = 1$, and $\Lambda = 1000$. A power law fit, $\chi \sim T^x$ yields for high temperatures an exponent of approximately $x \approx -1.3$, consistent with the analytic result (see also double-logarithmic inset). At small temperatures, however, we obtain $\chi \approx c_1 + c_2 T^2$ with positive constants c_1 and c_2 , which suggests that regime I or III_c are already reached.

Fermi liquid-like T^2 -dependence. Thus, the susceptibility has, upon lowering the temperature, the asymptotic behavior,

$$\chi = (\mathbf{r}_d u)^{-1} T^{-\frac{d+1}{3}} \quad \text{in } \text{III}_a \quad (6.45)$$

$$\chi = (\bar{\mathbf{r}}_d u)^{-1} r_{\text{ph}}^{\frac{d-5}{2}} T^{-2} \quad \text{in } \text{III}_d \quad (6.46)$$

The susceptibility diverges quadratically upon approaching the zero temperature axis which implies a critical exponent $\gamma = 2$. However, for any finite field, there will eventually be a second crossover to regime III_c where this divergence becomes cut off, and the susceptibility saturates.

On the left hand side of Fig. 6.6, we sketched the temperature dependence of the susceptibility upon approaching the QCEP given in Eq. (6.45). The numerical calculation for two dimensions, however, differs from the analytics as depicted on the right hand side of Fig. 6.6. At high temperatures, we obtain approximately a power law behavior, $\chi \sim T^x$, with an exponent, $x = -4/3$. This is between the two asymptotic values, $x = -1$ and $x = -2$ obtained in Eq. (6.45). Therefore, we conclude, that we this is within the crossover region of the phase diagram, where the two asymptotics merge, i.e., the asymptotics of regime III_d are not yet dominating.

Upon lowering the temperature, however, the susceptibility has a maximum and thereafter quadratically approaches a constant at $T = 0$. This is exactly the behavior of the regimes I and III_c , therefore the regime III_d is probably left again, before the asymptotics could fully develop. To obtain the T^{-2} behavior of the linear Fermi liquid regime III_d , we, therefore, would have to consider smaller fields, h_{el} . This, however, is numerically not easy. Perhaps also the choice of other parameter combinations would also yield a better numerical accessibility of the regime III_d .

6.4.2 Thermal Expansion, Temperature Derivative of the Magnetization

As mentioned before, the thermal expansion has the same behavior as the temperature derivative of the magnetization. Neglecting the inherent quadratic temperature dependence of h , both are odd functions of the field h_{el} due to the emergent Ising symmetry at the endpoint. Deviations from this symmetry were discussed in Chap. 5, and carry over to the elastically coupled system, thus, we will not discuss them here.

Finite Temperature Endpoint

Approaching the critical endpoint by varying the magnetic field, we obtain the thermal expansion to be

$$\alpha = \frac{2(d+1)}{9} \mathfrak{f}_2 u T^{\frac{d-2}{3}} \left(\frac{9}{2u^2} \right)^{\frac{1}{3}} |h_{\text{el}}|^{-\frac{1}{3}} \text{sgn } h_{\text{el}} \quad \text{in II.} \quad (6.47)$$

Upon the crossover to regime III_c, the thermal expansion does not change qualitatively and will diverge further as

$$\alpha = \frac{2(d+1)}{9} \mathfrak{r}_d u T^{\frac{d-2}{3}} \left(\frac{9}{2u^2} \right)^{\frac{1}{3}} |h_{\text{el}}|^{-\frac{1}{3}} \text{sgn } h_{\text{el}} \quad \text{in III}_b. \quad (6.48)$$

More interesting, however, is the behavior upon temperature tuning through the critical endpoint. For high temperatures and zero field h_{el} , the thermal expansion has to vanish exactly, due to the Ising symmetry. However, for small but finite magnetic fields, it is

$$\alpha = \frac{h_{\text{el}}}{R_{\text{el}}^2} R'_{\text{el}} \quad \text{in III}_a. \quad (6.49)$$

Below the critical temperature, in the coexistence regime, the thermal expansion is even at zero field finite and reads as

$$\alpha = \sqrt{\frac{3}{2u}} \frac{R'_{\text{el}}}{\sqrt{R_{\text{el}}}} + \frac{h_{\text{el}}}{R_{\text{el}}^2} R'_{\text{el}} \quad \text{in IV}_a \quad (6.50)$$

Since the thermal expansion is proportional to the temperature derivative of the order parameter of the structural transition, $\alpha \sim \partial_T(\partial_p \mathcal{F})$, it is related to the critical exponent β as $\alpha \sim |T - T_c|^{\beta-1}$. Therefore, with $|R_{\text{el}}(T)| \sim |T - T_c|$, we find the mean field exponent $\beta = 1/2$. Lowering the temperature further, we enter regime IV_b, where the thermal expansion takes the form

$$\alpha = \frac{2(d+1)}{3} \mathfrak{f}_2 u T^{\frac{d-2}{3}} \sqrt{\frac{u}{2r_{\text{el}}^2}} \quad \text{in IV}_b, \quad (6.51)$$

which, as for the susceptibility, equals the low temperature expansion of the thermal expansion in regime IV_a.

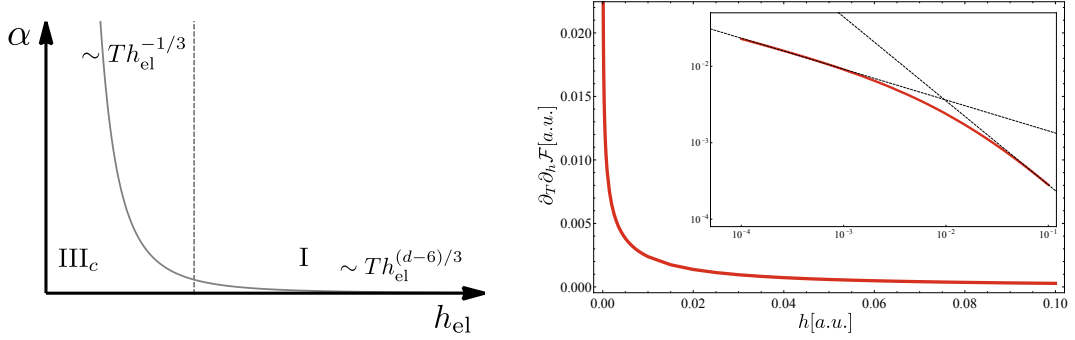


Fig. 6.7: Thermal expansion at lowest temperatures as a function of magnetic fields. On the left hand side, the analytic result is sketched, whereas the right hand side displays the numerical calculation in $d = 2$. The parameter values were chosen as $T = 2 \times 10^{-4}$, $r_{\text{ph}} = 0.05$, $u = 0.1$, and $\Lambda = 1000$. A power law fit, $\alpha \sim |h_{\text{el}}|^x$, for high temperatures yields an exponent $x \approx -1.1$, whereas we find $x \approx -0.4$ for small temperatures (see also double-logarithmic inset).

Quantum Endpoint

For $\bar{r}_{\text{el}} = 0$, the thermal expansion at lowest temperatures reads as

$$\alpha = \frac{2(3-d)\bar{\tau}_2}{3} \left(\frac{9u}{2}\right)^{\frac{d-3}{6}} T |h_{\text{el}}|^{\frac{d-6}{3}} \text{sgn } h_{\text{el}} \quad \text{in I,} \quad (6.52)$$

resembling the bare metamagnetic system as the elastic coupling affects the critical behavior only close to the endpoint. Entering regime III_c , we obtain in leading order

$$\alpha = \frac{4}{3} \bar{\tau}_d \left(\frac{9u}{2}\right)^{1/3} r_{\text{ph}}^{\frac{d-5}{2}} T |h_{\text{el}}|^{-\frac{1}{3}} \text{sgn } h_{\text{el}} \quad \text{in III}_c. \quad (6.53)$$

Therefore, the exponent field dependence is the same as for the finite temperature endpoint. Since the thermal expansion vanishes for $h_{\text{el}} = 0$ due to the Ising symmetry, the divergence is cut off when the regime III_a is entered.

The behavior of the thermal expansion upon tuning the magnetic field at lowest temperatures is sketched on the right hand side of Fig. 6.7. On the left hand side, we, again, depicted the numerically obtained data. A exponential fit yields exponents which are in fair agreement with the asymptotic behavior for small and large applied fields, i.e., in the regimes III_c and I, respectively.

For sufficiently small fields, we may observe the crossover from regime III_a to the Fermi liquid regime, III_d as a function of temperature. The thermal expansion then has the following limiting behaviors

$$\alpha = \frac{d+1}{3} \frac{h_{\text{el}}}{\bar{\tau}_d u} T^{-\frac{(d+4)}{3}} \quad \text{in III}_a, \quad (6.54)$$

$$\alpha = 2 \frac{h_{\text{el}}}{\bar{\tau}_d u} r_{\text{ph}}^{\frac{5-d}{2}} T^{-3} \quad \text{in III}_d. \quad (6.55)$$

Although the thermal expansion is suppressed by a factor of h_{el} , it diverges with a very high power of temperature when approaching the quantum endpoint. However, for any finite field, there will, eventually, be a second crossover to the regime III_c where this divergence is cut off, and, finally, the thermal expansion will scale linearly to zero.

6.4.3 Specific Heat Coefficient

The specific heat coefficient shows the strongest influence of the elastic coupling, since it stems from the fluctuation term only. Thus, it is very sensitive to the absence of critical fluctuations in the elastically coupled case.

Finite Temperature Endpoint

As already seen in Chap. 4 for the finite temperature endpoint of the Mott transition, the specific heat coefficient does not show any divergence upon sweeping through the endpoint with the magnetic field. Instead, we obtain

$$\gamma = \frac{d(d+3)}{9} \bar{f}_1 T^{\frac{d}{3}-1} - R''_{\text{el}} \left(\frac{9 h_{\text{el}}^2}{2u^2} \right)^{1/3} \quad \text{for II and III}_b. \quad (6.56)$$

If we lower the temperature at zero field, the specific heat coefficient increases according to

$$\gamma = \frac{d(d+3)}{9} \bar{f}_1 T^{\frac{d}{3}-1} \quad \text{for III}_a. \quad (6.57)$$

However, since the endpoint is at a temperature $T_c > 0$, it does not diverge, and below the crossover the specific heat coefficient is given as

$$\gamma = \frac{d(d+3)}{9} \bar{f}_1 T^{\frac{d}{3}-1} + \frac{3R_{\text{el}}'^2}{u} + \frac{3R_{\text{el}}R_{\text{el}}''}{2u} \quad \text{for IV}_a. \quad (6.58)$$

As in Chap. 4, we obtain a mean field jump of the specific heat which is of the order of $\Delta\gamma \sim T_c^{2(d-2)/3}/u$.

Quantum Endpoint

For the quantum endpoint, varying the magnetic field at lowest temperatures the specific heat will first resemble the behavior of the bare metamagnetic system

$$\gamma = 2 \bar{f}_2 \left(\frac{9 u h_{\text{el}}^2}{2} \right)^{\frac{d-3}{6}} \quad \text{in I.} \quad (6.59)$$

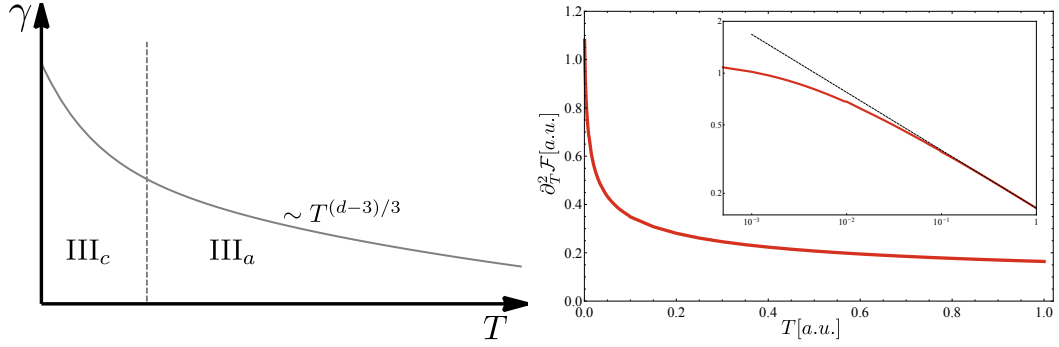


Fig. 6.8: Temperature dependence of the specific heat at zero field, $h_{\text{el}} = 0$. At the crossover to the Fermi liquid regime III_c , the divergence is cut off, and the specific heat approaches a constant value, as shown in the sketch on the left hand side. The numerical calculation in $d = 2$ for the parameters $r_{\text{ph}} = 0.05$, $u = 0.1$, and $\Lambda = 1000$. A power law fit, $\gamma \sim T^x$, for high temperatures results in an exponent of approximately $x \approx -0.34$. At small temperatures, the specific heat approaches a constant value.

Upon entering regime III_c , the elastic renormalization becomes important and the behavior of the specific heat coefficient changes to

$$\gamma = 2\bar{f}_2 r_{\text{ph}}^{\frac{d-3}{2}} + 2\bar{v}_d r_{\text{ph}}^{\frac{d-5}{2}} \left(\frac{9u}{2}\right)^{\frac{1}{3}} |h_{\text{el}}|^{\frac{2}{3}} \text{sgn } h_{\text{el}} \quad \text{in } \text{III}_c. \quad (6.60)$$

Thus, the specific heat saturates at a constant value, determined by the phonon-renormalized mass, r_{ph} .

Similarly, approaching the quantum endpoint at zero field by lowering the temperature, we obtain

$$\gamma = \bar{f}_1 \frac{d(d+3)}{9} T^{\frac{d}{3}-1} \quad \text{in } \text{III}_a, \quad (6.61)$$

diverging at least logarithmically, due to the critical fluctuations. When entering the Fermi liquid regime III_d , this divergence is cut off, and the specific heat, again, saturates to

$$\gamma = 2\bar{f}_2 r_{\text{ph}}^{\frac{d-3}{2}} \quad \text{in } \text{III}_d. \quad (6.62)$$

This behavior is sketched on the left panel of Fig. 6.8. A power law fit, $\gamma \sim T^x$ of the numerically obtained data, depicted on the right panel, yields for high temperatures the exponent $x = -0.4 \approx -\frac{1}{3}$ in agreement with Eq. (6.61). For lowest temperatures the specific heat approaches a constant, as seen in the double-logarithmic inset.

For the critical exponent α , defined by $C = T\gamma \sim T^{-\alpha}$, this implies a change from $\alpha = -\frac{d}{3}$ for relatively high temperatures to $\alpha = -1$ for lowest temperatures. For $d = 3$, this effect is only a logarithmic correction, and may, thus, experimentally not be detectable.

6.4.4 Grüneisen Parameters

The Grüneisen parameter, defined as the ratio between the thermal expansion and the specific heat, $\Gamma = \alpha/(T\gamma)$, is an particularly interesting quantity at a quantum critical point. In contrast to a finite temperature critical point, where it remains constant, the Grüneisen ratio diverges at a quantum critical point. If scaling applies, the divergence is determined by the critical exponents as shown in Ref. [113]. However, as we have seen above, the metamagnetic system on a compressible lattice does not have a real quantum *critical* endpoint, but rather a quantum mean field endpoint, hence, we also expect unusual exponents for the Grüneisen parameter.

Far from the QCEP, at large fields, the Grüneisen parameter diverges as

$$\Gamma = \frac{3-d}{3} h_{\text{el}}^{-1} \quad \text{in I,} \quad (6.63)$$

which is, except for prefactors, in agreement with general scaling arguments, as discussed in Sec. 5.4.4. However, when entering regime III_c, it becomes

$$\Gamma = \frac{2}{3} \frac{\bar{\tau}_d}{\bar{f}_2} \left(\frac{9u}{2} \right)^{\frac{1}{3}} r_{\text{ph}}^{-1} |h_{\text{el}}|^{-\frac{1}{3}} \text{sgn } h_{\text{el}} \quad \text{in III}_c, \quad (6.64)$$

diverging with the unusual weak power law of $|h_{\text{el}}|^{-1/3}$. Approaching the quantum endpoint by lowering the temperature at small but finite magnetic fields, we obtain

$$\Gamma = \frac{3(d+1)}{3d(d+3)} \frac{h_{\text{el}}}{\bar{f}_1 \bar{\tau}_d u} T^{-\frac{2(d+2)}{3}} \quad \text{in III}_a, \quad (6.65)$$

like in the bare metamagnetic system. The crossover to the Fermi liquid regime yields a change in the behavior of the Grüneisen parameter

$$\Gamma = \frac{h_{\text{el}}}{\bar{f}_2 \bar{\tau}_d u} r_{\text{ph}}^{4-d} T^{-4} \quad \text{in III}_d, \quad (6.66)$$

Thus, in contrast, to the field dependence, it shows a very high divergence with temperature and differs from the usual quantum critical behavior discussed in Ref. [113]. However, one has to take into account that the Grüneisen parameter is suppressed by a factor of h_{el} , therefore, at some finite temperature it will reach the crossover to regime III_c where it saturates to a constant.

6.5 Estimate for Sr₃Ru₂O₇

In this section, we want to estimate the temperature scale on which effects of the elastic coupling may be observed in real systems. This is achieved with help of thermal expansion measurements performed by Gegenwart et al. [110] for Sr₃Ru₂O₇.

As discussed in Sec. 5.1.2, Sr₃Ru₂O₇ is a quasi-2 dimensional system which develops towards a metamagnetic quantum endpoint at a magnetic field of 7.8 T applied parallel to the *c*-axis. Although the quantum endpoint in this system is preempted by the formation of an electronic nematic phase, the compound may, nevertheless, serve us as an exemplary system of a metamagnetic quantum endpoint.

In the following, we calculate the temperature shift of the second order endpoint for $r = 0$, i.e., in the scenario, where the bare system would exhibit a quantum critical point. Although this is not an experimental accessible quantity, it will serve us as an estimate of the temperature scale on which elasticity affects the critical properties.

In terms of the microscopic parameters, the critical temperature is given in Eq. (6.29) as $T_c = (|r_{\text{el}}|/(\mathfrak{r}_d u))^{3/(d+1)}$. For $r = 0$, the shift of the quantum critical endpoint to finite temperatures in the quasi-2 dimensional Sr₃Ru₂O₇ follows as

$$T_c = \frac{\lambda^2/K}{\mathfrak{r}_2 u}. \quad (6.67)$$

From magnetoresistance measurements under pressure, Ref. [118], we can determine the pressure dependence of the critical magnetic field as

$$\frac{\partial \mu_0 H_c}{\partial p} = \frac{\partial h_{\text{el}}}{\partial p} = \frac{\lambda}{K} \approx 5.6 \frac{\text{T}}{\text{GPa}}. \quad (6.68)$$

Furthermore, in the linear regime, III_a, the free energy can be written, up to field-independent terms, as $F = -\frac{1}{2}\chi |\mu_0(H - H_c)|^2$, where the susceptibility at $r = 0$ is given by $\chi = (\mathfrak{r}_2 u T - \lambda^2/K)^{-1} \approx (\mathfrak{r}_2 u T)^{-1}$. The thermal expansion follows from this form of the free energy density as

$$\begin{aligned} \alpha &= \frac{\partial^2 F}{\partial(\mu_0 H_c) \partial T} \frac{\partial \mu_0 H_c}{\partial p} = \frac{\partial \chi}{\partial T} \frac{\partial \mu_0 H_c}{\partial p} (\mu_0(H - H_c)) \\ &= \frac{1}{\mathfrak{r}_2 u} \frac{\lambda}{K} \frac{\mu_0(H - H_c)}{T^2}, \\ \Rightarrow \frac{\lambda^2/K}{\mathfrak{r}_2 u} &= K \frac{\partial \mu_0 H_c}{\partial p} \frac{\alpha T^2}{\mu_0(H - H_c)}. \end{aligned} \quad (6.69)$$

The previously mentioned thermal expansion measurements of Gegenwart et al. [110], are depicted in form of a scaling plot in Fig. 6.9 and show a linear behavior in the scaling region for $H < H_c$ (left) as well as for $H > H_c$ (right). Unfortunately, the measurements in these two regimes do not collapse onto one curve as the Ising symmetry would predict. As discussed in Sec. 5.4.2, the temperature dependence of h yields deviations from the Ising-symmetric results, thus, our analysis will yield two different critical temperatures. However, as this temperature is itself not a measurable quantity it anyhow serves as a benchmark for the temperature regime in which the elastic effects occur.

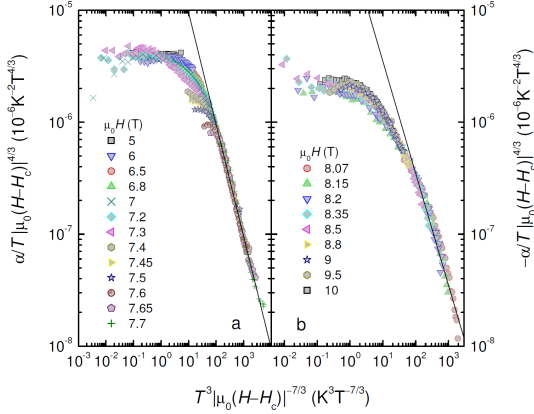


Fig. 6.9: Scaling plot of thermal expansion measurements on $\text{Sr}_3\text{Ru}_2\text{O}_7$ performed by Gegenwart et al. [110] on a double-logarithmic scale. Below (left) as well as above (right) the critical field, $H_c \approx \text{K}$, the data collapses to a single scaling function which yields the behavior $\alpha \sim |\mu_0(H - H_c)| T^{-2}$.

The linear behavior of the scaling plot, using the unitless parameters $t = T/K$ and $h = H/\text{Tesla}$, translates to

$$\alpha = A t^{1-3m} h^{(7m-4)/3} 10^{-4} K^{-1} \quad (6.70)$$

The fitted straight lines have parameters $(m, A) \approx (1, 0.95)$ for high fields, $H < H_c$, and $(m, A) \approx (1, 0.35)$ for low fields, $H > H_c$. Unfortunately, to our knowledge, no explicit values of the bulk modulus, K , for $\text{Sr}_3\text{Ru}_2\text{O}_7$ are available. However, assuming a typical value of the order of $K \approx 200$ GPa, we obtain a critical temperature of

$$T_c = \begin{cases} 0.1 \text{ K}, & H < H_c \\ 0.03 \text{ K}, & H > H_c \end{cases} \quad (6.71)$$

Although these are very small numbers, they are still well in the milli-Kelvin regime, which, in principal, is experimentally accessible. However, for the special case of $\text{Sr}_3\text{Ru}_2\text{O}_7$ this temperature scale deep within the nematic phase which is entered at about $T_n \approx 1$ K.

6.6 Summary

In this chapter, we investigated the influence of the elastic degrees of freedom on the metamagnetic quantum critical endpoint. In particular, we considered in detail the effect of the phonons which, so far, were treated on the basis of qualitative arguments. The actual impact of the phonons depends on what quantity one is interested.

On the one hand side, the coupling of the metamagnons to the phonons crucially changes the intensity pattern of neutron scattering experiments when measuring the magnetic structure. Whereas the bare itinerant metamagnetic system shows an isotropic intensity pattern, the elastic coupling yields an anisotropic modulation,

reflecting the symmetry of the underlying lattice. For the special case of a cubic lattice, we obtained an intensity modulation according to $I(\phi) \sim \cos(4\phi)$.

On the other hand, phonons play only a minor role for the critical thermodynamics of the quantum endpoint due to the different dynamics of the phonons and the metamagnons. Whereas the phonons have a dynamical critical exponent of $z_{<} = 1$, the metamagnons are governed by an exponent $z_{>} = 3$. Because of these different energy scales, the system basically splits into a phonon and a magnon system, with renormalized parameters such as the phonon velocity, $v_m < v$, and a renormalized magnon mass, $R_{\text{ph}} < R$.

However, the macroscopic modes are strongly affecting the metamagnetic system. The quantum critical endpoint is preempted by an isostructural first order transition, similar to the finite temperature Mott endpoint, discussed in Chap. 4. This first order transition terminates in an endpoint which, again, shows elastic Landau mean field behavior. The bilinear elastic coupling also yields a linear pressure dependence of the critical metamagnetic field, $H_c(p) = H_{c,0} + p/K$, which was assumed in Chap. 5.

However, fine tuning the parameters of the theory by an additional control parameter, e.g., the angle between the magnetic field and the ab -plane in $\text{Sr}_3\text{Ru}_2\text{O}_7$, one can still drive the critical temperature of the endpoint to zero and, thus, obtain a quantum endpoint. Importantly, approaching this quantum endpoint exactly at the critical field, the system still exhibits a crossover to the Fermi liquid regime at a finite temperature, $T_{FL} > 0$.

The thermodynamics in this regime are quite peculiar, as, for instance, the thermal expansion shows at small but finite fields a strong divergence according to $\alpha \sim h_{\text{el}} T^{-3}$. On the other hand, the divergence of the specific heat coefficient at zero field is cut off upon entering the Fermi liquid regime. Both effects conspire in the behavior of the (magnetic) Grüneisen parameter which diverges with an unusual high power of temperature according to $\Gamma \sim h_{\text{el}} T^{-4}$ at small but finite fields.

Finally, we considered the layered compound $\text{Sr}_3\text{Ru}_2\text{O}_7$ as an exemplary system close to a metamagnetic quantum endpoint. As a benchmark of the strength of the elastic coupling, we estimated the temperature of the endpoint for the case that the system develops a quantum critical point in the uncoupled case. This temperature is of the order of 100 mK and, thus, very small, however, it may be still in the experimentally accessible regime. Also, for other compounds, the parameters may be more convenient such that the temperature range on which the elastic coupling manifests itself is larger.

Chapter 7

Summary

In this Thesis, we studied the coupling of the critical degrees of freedom at a solid state phase transition to the underlying lattice. In particular, we considered the finite temperature phase transition from a Mott insulator to a metal and the metamagnetic quantum endpoint.

After a general introduction to the theory of crystal elasticity we reviewed the preceding work on classical phase transitions on compressible lattices. Due to the peculiar difference between the macroscopic strain and its spatial fluctuations, i.e., the elastic waves, a long ranged interaction is induced which may change the nature of the phase transition. In particular, due to the absence of soft modes at the critical point, the system becomes mean field like and critical behavior of the thermodynamics is suppressed.

In the following, this mechanism was studied for the Mott metal-insulator transition. The nature of this phase transition and its universality class was discussed for over thirty years [49] and is still under debate. Starting from the theoretically expected Ising critical behavior, we showed that the interplay with elastic degrees of freedom will render the behavior mean field like, in the vicinity of the endpoint. The smoking gun criterion to detect the elastic mean field regime is the breakdown of Hooke's law, i.e., a non-linear stress-strain relation close to the critical endpoint. Also the specific heat coefficient exhibits a finite mean field jump instead of a divergence.

Depending on the relative magnitude of the elastic coupling, Ising critical behavior may either still be preserved at a finite distance from the critical point, or it is completely suppressed. We argued, that the organic salt κ -(BEDT-TTF)₂X is an example for the former scenario and could, based on thermal expansion data [1, 2], estimate the elastic Landau regime as $\Delta T^* \approx 2.5$ K and $\Delta p^* \approx 50$ bar. On the other hand, we argue that Ising critical behavior is absent in the chromium doped V₂O₃, since one of the elastic constants becomes critical long before a deviation from mean field behavior is observed.

The following chapters, were devoted to the zero temperature critical endpoint in itinerant metamagnets and its critical thermodynamics. Such a metamagnetic quantum phase transition was recently suggested of being a generic feature for itinerant ferromagnets [3] and was found in UCoAl [4] and UGe₂ [5, 6].

Starting from spin-fluctuation theory, we derived an effective potential for the macroscopic magnetization by means of functional renormalization group techniques, which takes fluctuations self-consistently into account. This potential enabled us, to derive the asymptotic appearance of the free energy and, subsequently, of thermodynamic quantities such as, specific heat, thermal expansion and susceptibility. The obtained characteristics compare qualitatively well to existing experimental measurements.

Importantly, the compressibility shows the same behavior as the susceptibility which necessarily diverges at the transition. Thus, we expect a crystal softening which results in an isostructural transition preempting the metamagnetic QCEP. We investigated this mechanism by including elastic degrees of freedom, i.e., the macroscopic strain and the phonons, in the functional RG approach used for the bare metamagnetic system. For simplicity, we restricted ourselves to isotropic crystals.

The influence of the phonons on the system is, as shown, crucial for quantities sensitive to finite momentum metamagnons. It changes, for instance, the neutron scattering intensity pattern when measuring the magnetic structure which inherits the symmetry of the underlying lattice. However, concerning the critical thermodynamics, the phonons yield only sub-leading contributions. Due to the different dynamics of the metamagnons and the phonons, the system can be described as two renormalized but decoupled sub-systems.

However, the macroscopic elastic modes yield, as expected, an isostructural first order transition, similar to the finite temperature Mott transition, preempting the quantum critical endpoint. The resulting finite temperature second order endpoint, again, shows elastic Landau mean field behavior.

When tuning this endpoint to zero temperature, we obtain a quantum endpoint which, however, shows a very interesting behavior. Most important, upon lowering the temperature at the critical field, the system will, inevitably, enter a Fermi liquid regime at a finite temperature, $T_{FL} > 0$. This results in unusual power laws of the critical thermodynamics. Whereas the thermal expansion diverges strongly with temperature above the quantum critical endpoint, the usual specific heat divergence is cut off. As a consequence, the (magnetic) Grüneisen parameter diverges with an unusual high power of temperature, $\Gamma \sim h_{el} T^{-4}$.

As a benchmark of the strength of the elastic coupling in metamagnetic systems, we estimated the temperature shift of the quantum critical endpoint for Sr₃Ru₂O₇. It was found to be of the order of 100 mK, which is still within an experimentally accessible regime though it is within the nematic phase in this specific material.

Appendix A

Symmetry Classes of the Elastic Constant Matrix

The elastic constant matrix, C , has in general 21 independent components. However, if the lattice has certain symmetries, all quantities describing it have to be also symmetric in that respect. Thus, the symmetries of the lattice reduce the number of independent components as they yield further constraints. Here, following Ref. [7], we determine the elastic constant matrix for all of the 32 crystallographic point groups. As it turns out, there are 9 different symmetry groups of the elastic constant matrix, one for each lattice system and two more for trigonal and tetragonal systems with higher symmetries.

A.1 Triclinic System

In the two triclinic systems, 1, $\bar{1}$, all 21 components of the elastic constant matrix are independent. If every atom is a center of inversion symmetry, Cauchy's relation applies $C_{ijkl} = C_{ikjl}$ and only 15 of the elastic constants are independent. The resulting elastic constant matrix reads as

$$C = \left(\begin{array}{ccc|ccc} C_{11} & C_{12} & C_{13} & C_{14} & C_{15} & C_{16} \\ C_{12} & C_{22} & C_{23} & C_{24} & C_{25} & C_{26} \\ C_{13} & C_{23} & C_{33} & C_{34} & C_{35} & C_{36} \\ \hline C_{14} & C_{24} & C_{34} & C_{23} & C_{16} & C_{25} \\ C_{15} & C_{25} & C_{35} & C_{16} & C_{13} & C_{14} \\ C_{16} & C_{26} & C_{36} & C_{25} & C_{14} & C_{12} \end{array} \right). \quad (\text{A.1})$$

Since we have to choose a coordinate system which depends on three angles relative to the body, it can be chosen such that it imposes three additional conditions. Such the triclinic system has in general 18 independent elastic moduli and 12 if Cauchy's relations apply.

A.2 Monoclinic System

The point groups 2 , m and $\frac{2}{m}$ belong to the monoclinic system. Taking, for instance, a crystal in which the xy -plane is a mirror plane (m), a reflection translates to the transformation $x \rightarrow x$, $y \rightarrow y$ and $z \rightarrow -z$. The components of the elastic modulus tensor transform as the product of the corresponding coordinates, thus, components with an odd number of z 's appearing in the index change their sign, while the others stay constant. As the crystal is symmetric with respect to such a transformation, the elastic constant matrix has also to obey this symmetry. Thus, the components which change their sign have to be zero and the elastic constant matrix reads as

$$C = \left(\begin{array}{ccc|ccc} C_{11} & C_{12} & C_{13} & 0 & 0 & C_{16} \\ C_{12} & C_{22} & C_{23} & 0 & 0 & C_{26} \\ C_{13} & C_{23} & C_{33} & 0 & 0 & C_{36} \\ \hline 0 & 0 & 0 & C_{44} & C_{45} & 0 \\ 0 & 0 & 0 & C_{45} & C_{55} & 0 \\ C_{16} & C_{26} & C_{36} & 0 & 0 & C_{66} \end{array} \right), \quad (\text{A.2})$$

with 13 independent elastic constants. The freedom to rotate the arbitrarily chosen coordinate system around the fixed z -axis can be used to eliminate another component, leaving a total number of 12 elastic constants. Similar considerations for the two other point groups yield the same matrix for the z -axis being the twofold rotation axis.

A.3 Orthorhombic System

The orthorhombic system consists of the point groups $2mm$, 222 and $\frac{2}{m}\frac{2}{m}\frac{2}{m}$. Let us consider, for instance, a crystal with three mirror planes, i.e., $\frac{2}{m}\frac{2}{m}\frac{2}{m}$. A reflection on one of these planes translates to a transformation where two of the coordinates stay constant whereas the third one exhibits a sign change. Therefore, all entries with an odd number of any of the coordinates appearing in the index have to vanish and the elastic constant matrix reads as

$$C = \left(\begin{array}{ccc|ccc} C_{11} & C_{12} & C_{13} & 0 & 0 & 0 \\ C_{12} & C_{22} & C_{23} & 0 & 0 & 0 \\ C_{13} & C_{23} & C_{33} & 0 & 0 & 0 \\ \hline 0 & 0 & 0 & C_{44} & 0 & 0 \\ 0 & 0 & 0 & 0 & C_{55} & 0 \\ 0 & 0 & 0 & 0 & 0 & C_{66} \end{array} \right), \quad (\text{A.3})$$

leaving a total number of 9 independent elastic constants.

A.4 Trigonal System

Crystals of the the trigonal class have a threefold axis of proper or improper rotation and consist of the point groups $\bar{3}$, 3 , $3m$, 32 and $\bar{3}\frac{3}{m}$. Choosing the coordinate system such that the z -axis is parallel to the threefold axis, we make a coordinate transformation in the xy -plane to the complex coordinates $\xi = x + iy$ and $\eta = x - iy$. In this coordinate system, a rotation around the z -axis about $2\pi/3$ is described by the transformation $\xi \rightarrow \xi e^{2\pi/3}$, $\eta \rightarrow \eta e^{-2\pi/3}$. As the crystal symmetry demands no change in the elastic tensor under this rotation, in the new coordinate system only components of the elastic tensor, with indices where η and ξ appear the same number of times or one of them appears three times are non-vanishing.

The strain tensor transforms like the products of the coordinates of its indices. For instance, it is $\xi^2 = x^2 + 2ixy - y^2$ from which follows $u_{\xi\xi} = u_{xx} + 2iu_{xy} - u_{yy}$. Therefore, we obtain for the free energy,

$$\begin{aligned}
\mathcal{F} &= \mathcal{F}_0 + \frac{1}{2}C_{zzzz}u_{zz}u_{zz} + 4C_{z\xi z\eta}u_{z\xi}u_{z\eta} + 2C_{zz\xi\eta}u_{zz}u_{\xi\eta} + 2C_{\xi\eta\xi\eta}u_{\xi\eta}u_{\xi\eta} \\
&\quad + C_{\xi\xi\eta\eta}u_{\xi\xi}u_{\eta\eta} + 4C_{z\eta\eta\eta}u_{z\eta}u_{\eta\eta} + 4C_{z\xi\xi\xi}u_{z\xi}u_{\xi\xi\xi} \\
&= \mathcal{F}_0 + \frac{1}{2}C_{zzzz}u_{zz}u_{zz} + 4C_{z\xi z\eta}(u_{zx}^2 + u_{zy}^2) + 2C_{zz\xi\eta}(u_{xx} + u_{yy})u_{zz} \\
&\quad + 2C_{\xi\eta\xi\eta}(u_{xx} + u_{yy})^2 + C_{\xi\xi\eta\eta}((u_{xx} - u_{yy})^2 + 4u_{xy}^2) \\
&\quad + 4C_{z\eta\eta\eta}(u_{zx}(u_{xx} - u_{yy}) - 2u_{xy}u_{zy} - i(2u_{xy}u_{zx} + u_{zy}(u_{xx} - u_{yy}))) \\
&\quad + 4C_{z\xi\xi\xi}(u_{zx}(u_{xx} - u_{yy}) - 2u_{xy}u_{zy} + i(2u_{xy}u_{zx} + u_{zy}(u_{xx} - u_{yy}))) \quad (\text{A.4})
\end{aligned}$$

Collecting the prefactors of identical strain terms, we obtain the elastic constant matrix with 7 independent elastic constants in Voigt notation

$$C = \left(\begin{array}{ccc|ccc} C_{11} & C_{12} & C_{13} & C_{14} & -C_{25} & 0 \\ C_{12} & C_{11} & C_{13} & -C_{14} & C_{25} & 0 \\ C_{13} & C_{13} & C_{33} & 0 & 0 & 0 \\ \hline C_{14} & -C_{14} & 0 & C_{44} & 0 & C_{25} \\ -C_{25} & C_{25} & 0 & 0 & C_{44} & C_{14} \\ 0 & 0 & 0 & C_{25} & C_{14} & \frac{1}{2}(C_{11} - C_{12}) \end{array} \right). \quad (\text{A.5})$$

If we have an additional symmetry, as in the classes $3m$, 32 and $\bar{3}\frac{3}{m}$, the elastic constant matrix can be reduced even further. Let us consider, for instance, the point group $3m$, which has an additional mirror plane, and we can choose the coordinate system such that the x -axis is perpendicular to this plane. Then, a reflection translates to $x \rightarrow -x$ and invariance requires $C_{yyxz} = C_{25} = 0$. Similar considerations for the other two groups yield the same result, and the elastic constant matrix reduces to 6 independent elastic constants.

A.5 Tetragonal System

Crystals of the tetragonal class have a fourfold axis of proper or improper rotation and it consists of the point groups $\bar{4}$, 4 , $\frac{4}{m}$, $\bar{4}2m$, $4mm$, 422 and $\frac{4}{m}\frac{2}{m}\frac{2}{m}$. We choose the coordinate system such that the z -axis is parallel to the fourfold axis. Since a this axis is, of course also a twofold axis, we start from the monoclinic elastic constant matrix. A rotation of $\pi/2$ results in the transformation $x \rightarrow y$, $y \rightarrow -x$ and $z \rightarrow z$ and, therefore, all elastic constants having only one x or y index have to vanish due to the minus sign, i.e., $C_{36} = 0$ and $C_{45} = 0$. Furthermore, the x and y direction are exchangeable which means that $C_{11} = C_{22}$, $C_{13} = C_{23}$, $C_{44} = C_{55}$ and $C_{16} = -C_{26}$. Taken together, the elastic constant matrix reads as

$$C = \left(\begin{array}{ccc|ccc} C_{11} & C_{12} & C_{13} & 0 & 0 & C_{16} \\ C_{12} & C_{11} & C_{13} & 0 & 0 & -C_{16} \\ C_{13} & C_{13} & C_{33} & 0 & 0 & 0 \\ \hline 0 & 0 & 0 & C_{44} & 0 & 0 \\ 0 & 0 & 0 & 0 & C_{44} & 0 \\ C_{16} & -C_{16} & 0 & 0 & 0 & C_{66} \end{array} \right) \quad (\text{A.6})$$

having 7 independent elastic constants. If we have an additional twofold rotation axis or a mirror plane in another plane than the xy plane, as in the classes $\bar{4}2m$, $4mm$, 422 , $\frac{4}{m}\frac{2}{m}\frac{2}{m}$, the off-diagonal blocks become zero,

$$C_{16} = 0 \quad (\text{A.7})$$

These tetragonal classes have 6 independent elastic constants.

A.6 Hexagonal System

Hexagonal systems have a sixfold axis of proper or improper rotation and this class consists of the point groups 6 , $\bar{6}$, $\frac{6}{m}$, $6mm$, $\bar{6}m2$, 622 , and $\frac{6}{m}\frac{2}{m}\frac{2}{m}$. The derivation of the elastic constant matrix is analogous to the trigonal case, with the further constraints $C_{z\xi\xi\xi} = 0 = C_{z\eta\eta\eta}$, as the angles do not add up to 2π anymore. Therefore, we have 5 independent elastic moduli and the tensor reads as

$$C = \left(\begin{array}{ccc|ccc} C_{11} & C_{12} & C_{13} & 0 & 0 & 0 \\ C_{12} & C_{11} & C_{13} & 0 & 0 & 0 \\ C_{13} & C_{13} & C_{33} & 0 & 0 & 0 \\ \hline 0 & 0 & 0 & C_{44} & 0 & 0 \\ 0 & 0 & 0 & 0 & C_{44} & 0 \\ 0 & 0 & 0 & 0 & 0 & \frac{1}{2}(C_{11} - C_{12}) \end{array} \right) \quad (\text{A.8})$$

A.7 Cubic System

The cubic class consists of the point groups 23 , $\frac{2}{m}\bar{3}$, $\bar{4}3m$, 432 , $\frac{4}{m}\bar{3}\frac{2}{m}$. Choosing the axes of the coordinate system along the fourth order axes of the crystal, we have the same symmetries as in the high hexagonal case, Eq. A.6, with the additional constraint $C_{16} = 0$. Furthermore, rotation of the crystal through $\pi/2$ around the x and y axis give the additional constraints $C_{33} = C_{11}$, $C_{13} = C_{12}$, $C_{66} = C_{44}$ yielding

$$C = \left(\begin{array}{ccc|ccc} C_{11} & C_{12} & C_{12} & 0 & 0 & 0 \\ C_{12} & C_{11} & C_{12} & 0 & 0 & 0 \\ C_{12} & C_{12} & C_{11} & 0 & 0 & 0 \\ \hline 0 & 0 & 0 & C_{44} & 0 & 0 \\ 0 & 0 & 0 & 0 & C_{44} & 0 \\ 0 & 0 & 0 & 0 & 0 & C_{44} \end{array} \right), \quad (\text{A.9})$$

Thus, cubic crystals have 3 independent elastic constants.

Appendix B

Irreducible Representations of the Strain Tensor

Each of the 32 crystal point groups can be split into irreducible representations. Accordingly, we can classify the eigenvectors of the elastic constant matrix, i.e., the strain components, by the irreducible representation they belong to. In the following table (taken from Cowley [21]), this classification is shown. The coordinate system is chosen analogous to App. A.

The notation follows Ref. [23], namely T denotes three dimensional representations (triplets), E denotes two dimensional representations (doublets) and A and B denote one dimensional representations (singlets). The singlets B are antisymmetric and the singlets A are symmetric under the highest symmetry operation, i.e., proper or improper rotation around the principal axis or reflection through the xy -plane. If there is more than one irreducible representation denoted by the same letter, which differ in a secondary symmetry operation, the one being symmetric with respect to this lower symmetry operation carries the index 1.

In the third column of the table, the stability criterion for the respective irreducible representations is listed, i.e., the combination of the elastic moduli which has to remain positive to prevent structural instability.

As discussed in the main text, there may be acoustic waves whose velocity depends only on the eigenvalues of the elastic constant matrix, thus, getting soft at a structural transition. If those phonons are not allowed, we denote this representation as type 0. For type I, such phonons exist on a one dimensional manifold in momentum space, whereas for type II representations, there exist is a whole plane of propagation vectors, which satisfy this condition. This classification is denoted in the next to last column, where we also listed the vectors of propagation, \mathbf{q} , of the soft phonons and the respective vectors of polarization, \mathbf{u} . The last column denotes whether symmetry allows for a cubic invariant of the strain, in which case a structural phase transition is of first order.

Appendix B. Irreducible Representations of the Strain Tensor

Rep.	Strain	Stability	Phonons	Cubic Inv.
Triclinic classes				
6 A	$u_{xx}; u_{yy}; u_{zz}; u_{xy}; u_{xz}; u_{yz}$	$\det C_{ij}$	0	no
Monoclinic classes				
4 A	$u_{xx}; u_{yy}; u_{zz}; u_{xy}$	$\det C_{ij}, i, j \in \{1, 2, 3, 6\}$	0	yes
2 B	$u_{xz}; u_{yz}$	$C_{44}C_{55} - C_{45}^2$	0	no
Orthorhombic classes				
3 A ₁	$u_{xx}; u_{yy}; u_{zz}$	$\det C_{ij}, i, j \leq 3$	0	yes
B ₁	u_{xy}	C_{66}	I $\mathbf{q} \parallel [010], [100]$ $\mathbf{u} \parallel [100], [010]$	no
B ₂	u_{xz}	C_{55}	I $\mathbf{q} \parallel [100], [001]$ $\mathbf{u} \parallel [001], [100]$	no
B ₃	u_{yz}	C_{44}	I $\mathbf{q} \parallel [001], [010]$ $\mathbf{u} \parallel [010], [001]$	no
Trigonal classes $3, \bar{3}$				
2 A	$u_{xx} + u_{yy}; u_{zz}$	$(C_{11} + C_{12})C_{33} - 2C_{13}^2$	0	yes
2 E	$u_{xx} - u_{yy}, u_{xy}; u_{xz}, u_{yz}$	$(C_{11} - C_{12})C_{44} - 2C_{14}^2 - 2C_{25}^2$	0	yes
Trigonal classes $32, \bar{3}m, 3m$				
2 A ₁	$u_{xx} + u_{yy}; u_{zz}$	$(C_{11} + C_{12})C_{33} - 2C_{13}^2$	0	yes
2E	$u_{xx} - u_{yy}, u_{xy}; u_{xz}, u_{yz}$	$(C_{11} - C_{12})C_{44} - 2C_{14}^2$	0	yes
Tetragonal classes $4, \bar{4}, \frac{4}{m}$				
2 A	$u_{xx} + u_{yy}; u_{zz}$	$(C_{11} + C_{12})C_{33} - 2C_{13}^2$	0	yes
2 B	$u_{xx} - u_{yy}; u_{xy}$	$(C_{11} + C_{12})C_{66} - 2C_{16}^2$	0	no
E	u_{xz}, u_{yz}	C_{44}	II $\mathbf{q} \perp [001], [001]$ $\mathbf{u} \parallel [001]$	no
Tetragonal classes $4mm, \bar{4}2m, 422, \frac{4}{m} \frac{2}{m} \frac{2}{m}$				
2 A ₁	$u_{xx} + u_{yy}; u_{zz}$	$(C_{11} + C_{12})C_{33} - 2C_{13}^2$	0	yes
B ₁	$u_{xx} - u_{yy}$	$C_{11} - C_{12}$	I $\mathbf{q} \parallel [110]$ $\mathbf{u} \parallel [1\bar{1}0]$	no
B ₂	u_{xy}	C_{66}	I $\mathbf{q} \parallel [100]$ $\mathbf{u} \parallel [010]$	no
E	u_{xz}, u_{yz}	C_{44}	II $\mathbf{q} \perp [001]$ $\mathbf{u} \parallel [001]$	no
Hexagonal classes				
2 A ₁	$u_{xx} + u_{yy}; u_{zz}$	$(C_{11} + C_{12})C_{33} - 2C_{13}^2$	0	yes
E ₁	$u_{xx} - u_{yy}, u_{xy}$	$C_{11} - C_{12}$	II $\mathbf{q} \perp [001]$ $\mathbf{u} \perp [001]$ and \mathbf{q}	yes
E ₂	u_{xz}, u_{yz}	C_{44}	II $\mathbf{q} \perp [001]$ $\mathbf{u} \parallel [001]$	yes
Cubic classes				
A ₁	$u_{xx} + u_{yy} + u_{zz}$	$C_{11} + 2C_{12}$	0	yes
E	$u_{xx} - u_{yy}, 2u_{zz} - u_{xx} - u_{yy}$	$C_{11} - C_{12}$	I $\mathbf{q} \parallel [110]$ $\mathbf{u} \parallel [1\bar{1}0]$	yes
T ₂	u_{xy}, u_{xz}, u_{yz}	C_{44}	II $\mathbf{q} \perp [100]$ $\mathbf{u} \parallel [100]$	yes
Isotropic classes				
L=0	$u_{xx} + u_{yy} + u_{zz}$	$3C_{12} + 2C_{44}$	0	yes
L=2	$u_{xx} - u_{yy}, 2u_{zz} - u_{xx} - u_{yy}$ u_{xy}, u_{xz}, u_{yz}	C_{44}	II $\mathbf{u} \perp \mathbf{q}$	yes

Appendix C

Effective Action due to Phonons

The Wegner-Houghton equation for the evolution of the microscopic potential along a RG trajectory reads as

$$\mathcal{V} = \mathcal{V}^0 + \int_0^\mu d\mu' e^{-(d+z)\mu'} f_{\mu'} \left(\frac{\delta^2 \mathcal{S}_{\mu'}}{\delta \phi^2}, \frac{\delta^2 \mathcal{S}_{\mu'}}{\delta \phi \delta u}, \frac{\delta^2 \mathcal{S}_{\mu'}}{\delta u^2}, T_{\mu'} \right). \quad (\text{C.1})$$

The subscript μ' denotes that all parameters are rescaled according to their engineering dimensions

$$\begin{aligned} r &\rightarrow r e^{2\mu}, & \gamma_m &\rightarrow \gamma_m e^{-(z-z_>)\mu}, & \lambda &\rightarrow \lambda e^\mu, \\ \rho &\rightarrow \rho e^{-2(z-z_<)\mu}, & T &\rightarrow T e^{z\mu}, & C_{11} &\rightarrow C_{11}. \end{aligned} \quad (\text{C.2})$$

The dynamical exponent, z , is left unspecified, whereas $z_< = 1$ and $z_> = 3$ are the dynamical exponents of the bare phonon and magnon system, respectively. The function f is the re-exponentiated contribution of a high energy shell integration of the Gaussian part of the action (6.16), which is given by

$$f = -\Lambda \frac{\partial}{\partial \Lambda} \frac{1}{2} \int_0^\Lambda \frac{d\mathbf{k}}{(2\pi)^d} \frac{1}{\beta} \sum_{\omega_n} \log [\det G^{-1}], \quad (\text{C.3})$$

Denoting $\mathcal{S}_{\lambda,\mu} = \delta^2 \mathcal{S} / (\delta \lambda \delta \mu)$, the matrix G^{-1} is given by

$$G^{-1} = \begin{pmatrix} \mathcal{S}_{\phi,\phi} & \mathcal{S}_{u,\phi^\dagger} \\ \mathcal{S}_{u,\phi} & \mathcal{S}_{u,u} \end{pmatrix}. \quad (\text{C.4})$$

Due to the linear coupling and the lack of anharmonic phonon terms, only $\mathcal{S}_{\phi,\phi}$ depends on the field ϕ . Denoting $R = \mathcal{V}_{\phi,\phi}|_{\phi_{\min}}$ the determinant yields

$$\det G^{-1}(\omega_n) = \rho \left(R + k^2 + \gamma_m \frac{|\omega_n|}{k} \right) \left(\omega_n^2 + v^2 k^2 \right) - \lambda^2 k^2. \quad (\text{C.5})$$

Here, we introduced the phonon velocity $v^2 = C_{11}/\rho$.

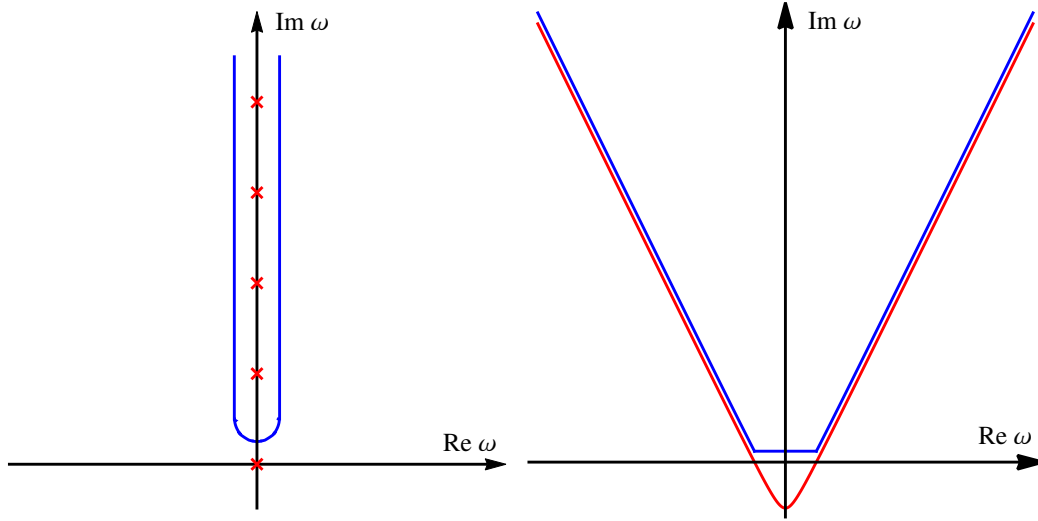


Fig. C.1: The Matsubara summation is converted into a integral over the contour \mathcal{C} enclosing the positive imaginary axis, depicted in blue on the left hand side. On the right hand side, the branch cut of the logarithm is depicted in red, and the contour is deformed as seen in blue.

The derivative with respect to the cutoff in Eq. (C.3) acts on the momentum integral which, therefore, yields a factor Λ^d/K_d where K_d is the d -dimensional solid angle divided by $(2\pi)^d$.

Concerning the Matsubara summation we may separate the Matsubara zero mode and sum twice over positive Matsubara frequencies only, thus, getting rid of the modulus, $|\omega_n|$.

$$f = -\frac{K_d}{2}\Lambda^d \left\{ \log \det G^{-1}(0) + \frac{2}{\beta} \sum_{\omega_n > 0} \log \det G^{-1}(\omega_n) \right\}. \quad (\text{C.6})$$

For finite temperatures, the summation over bosonic Matsubara frequencies may then be rewriting as a contour integral enclosing the poles of the hyperbolic cotangent,

$$\frac{2}{\beta} \sum_{\omega_n > 0} \log \det G^{-1}(\omega_n) = \int_{\mathcal{C}} \frac{d\omega}{2\pi i} \left(\coth \frac{\omega}{2T} - 1 \right) \log \det G^{-1}(-i\omega), \quad (\text{C.7})$$

where \mathcal{C} is the contour depicted on the left of Fig. C.1 and we subtracted the zero temperature contribution.

The logarithm has a branch cut in the complex ω -plane when the imaginary part of its argument vanishes and the real part becomes negative. Denoting $\omega = x + iy$, the argument reads as

$$\det G^{-1}(-i\omega) = \rho \left(R + \Lambda^2 + \gamma_m \frac{y - ix}{\Lambda} \right) \left(v^2 \Lambda^2 - x^2 + y^2 - 2ixy \right) - \lambda^2 \Lambda^2. \quad (\text{C.8})$$

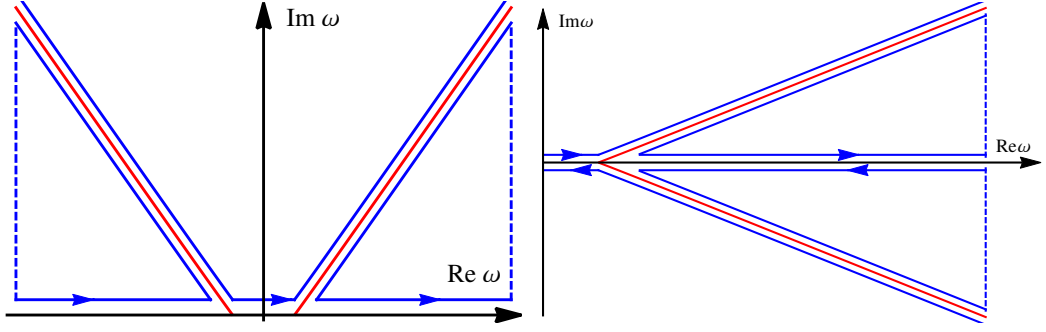


Fig. C.2: For the calculation, two triangular integration contours (blue) below the branch cut (red) as depicted on the left side were added. A substitution $\text{Re } \omega \rightarrow -\text{Re } \omega$ in the left quadrant of the complex ω -plane yields the integration contours depicted on the right hand side. In red again the branch cut z (upper) and \bar{z} (lower) are shown.

We see that it is real for $x = 0$ or along a curve $z(x) = x + iy(x)$, defined by

$$y(x) = -\frac{1}{3} \frac{\Lambda}{\gamma_m} (R + \Lambda^2) \pm \sqrt{\frac{1}{9} \frac{\Lambda^2}{\gamma_m^2} (R + \Lambda^2)^2 + \frac{1}{3} (x^2 - V^2 \Lambda^2)}. \quad (\text{C.9})$$

which is depicted in the right of Fig. C.1. Thus, the ω -integration in Eq. (C.7) can be written as

$$\int_{\mathcal{C}} \frac{d\omega}{2\pi i} \left(\coth \frac{\omega}{2T} - 1 \right) \log \det G^{-1}(-i\omega) \quad (\text{C.10})$$

$$= \int_{-v\Lambda}^{v\Lambda} \frac{dx}{2\pi i} \left(\coth \frac{x}{2T} - 1 \right) \log \det G^{-1}(x^+) \\ + \left(\int_{-\infty}^{-v\Lambda} + \int_{v\Lambda}^{\infty} \right) \frac{dx}{2\pi i} \frac{\partial z(x)}{\partial x} \left(\coth \frac{z(x)}{2T} - 1 \right) \log \det G^{-1}(z^+(x)), \quad (\text{C.11})$$

where the superscript denotes an infinitesimally shift $x^+ = x + i\epsilon$.

Next, we add the two closed contours depicted on the left of Fig. C.2 which yield no extra contribution as no pole is enclosed by it. The dashed, line is located at complex infinity and, thus, gives no contribution. Transforming $x \rightarrow -x$ for the negative integration regime, yields $z^+(-x) = -\bar{z} + i\epsilon$, thus, we end up with the integration contours depicted on the right of Fig. C.2. For the integration over the real axis we notice that $\det G^{-1}(x^+) \rightarrow \det \overline{G^{-1}}(x^+)$, and therefore, we obtain

$$f(T) - f(0) \propto \left(\int_0^{v\Lambda} + \int_{v\Lambda}^{\infty} \right) \frac{dx}{2\pi i} \left(\coth \frac{x}{2T} - 1 \right) \text{Im} \{ \log \det G^{-1}(x^+) \} \\ + \left(\oint_{z^+} - \oint_{z^-} \right) \frac{dz}{2\pi i} \left(\coth \frac{z}{2T} - 1 \right) \log \det G^{-1}(z) \\ + \left(\oint_{\bar{z}^+} - \oint_{\bar{z}^-} \right) \frac{dz}{2\pi i} \left(\coth \frac{-z}{2T} - 1 \right) \log \det G^{-1}(-z), \quad (\text{C.12})$$

where z , and, \bar{z} denote the branch cuts depicted in red in Fig. C.2.

Across the branch cuts, the imaginary part of $\det G^{-1}(z)$ and $\det G^{-1}(-z)$ has a sign change. Thus, the integration infinitesimally above and below the branch cut just yields the imaginary part of the integrand which can be simplified to

$$\begin{aligned}
 f(T) - f(0) \propto & \left(\int_0^{v\Lambda} + \int_{v\Lambda}^{\infty} \right) \frac{dx}{\pi} \left(\coth \frac{x}{2T} - 1 \right) \text{Im} \{ \log \det G^{-1}(x^+) \} \\
 & + \oint_z \frac{dz}{\pi} \left(\coth \frac{z}{2T} - 1 \right) \text{Im} \{ \log \det G^{-1}(z^+) \} \\
 & + \oint_{\bar{z}} \frac{dz}{\pi} \left(\coth \frac{-z}{2T} - 1 \right) \text{Im} \{ \log \det G^{-1}(-z^-) \}. \quad (\text{C.13})
 \end{aligned}$$

Concerning the integrals along the real axis, we have to evaluate the imaginary part of $\log \det G^{-1}(\omega^+)$. In the first integral we have $\text{Re} \det G^{-1} < 0$ and $\text{Im} \det G^{-1} > 0$. In the integration regime of the second integral the imaginary part is always negative $\text{Im} \det G^{-1} < 0$, whereas the real part changes its sign at a renormalized phonon energy $\omega_1 = v_1 \Lambda$ with the renormalized phonon velocity

$$v_1 = v \sqrt{1 - \frac{\lambda^2/C_{11}}{R + \Lambda^2}} = v \sqrt{\frac{R_{\text{ph}} + \Lambda^2}{R + \Lambda^2}}, \quad (\text{C.14})$$

$$R_{\text{ph}} = R - \frac{\lambda^2}{C_{11}}. \quad (\text{C.15})$$

The velocity, v_1 , is well defined, since the renormalized mass, R_{ph} , is positive above the transition temperature. Thus, the imaginary part of the logarithm yields

$$\arctan \left[\frac{\text{Im} \det G^{-1}(\omega^+)}{\text{Re} \det G^{-1}(\omega^+)} \right] + \begin{cases} 0 & , \omega < \omega_1 \\ -\pi & , \omega_1 < \omega < v\Lambda \\ \pi & , \omega > v\Lambda. \end{cases}$$

Note that this function is discontinuous only at the bare phonon pole but continuous at the renormalized phonon energy, ω_1 . A partial integration finally yields.

$$\begin{aligned}
 -\mathcal{P} \int_0^{\Gamma} 2T \left(\log \left[\sinh \frac{\omega}{2T} \right] - \frac{\omega}{2T} \right) \frac{\partial}{\partial \omega} \arctan \left[\frac{\text{Im} \det G^{-1}(\omega)}{\text{Re} \det G^{-1}(\omega)} \right] \frac{d\omega}{\pi} \\
 - 4T \left(\log \left[\sinh \frac{v\Lambda}{2T} \right] - \frac{v\Lambda}{2T} \right) + T \left(\log \left[\sinh \frac{\Gamma}{2T} \right] - \frac{\Gamma}{2T} \right), \quad (\text{C.16})
 \end{aligned}$$

where the principal value is taken at the bare phonon pole, $\omega = v\Lambda$.

For the integration along the branch cuts the imaginary part of the determinant is $\text{Im} \det G^{-1}(z^+(x)) = -\epsilon$, therefore, we find for the logarithm

$$\text{Im} \left[\log \det G^{-1}(z^+(x)) \right] = \arctan \left(\frac{-\epsilon}{\text{Re} \det G^{-1}(x)} \right) - \pi.$$

A partial integration yields a derivative with respect to x of the arc tangent, which for vanishing ϵ becomes the delta function, $\pi\delta(\text{Re det } G^{-1}(x))$. As the real part of the determinant is strictly smaller zero we are left with the boundary terms only. Thus, the integration over the branch cut yields

$$4T \left(\log \sinh \frac{v\Lambda}{2T} - \frac{v\Lambda}{2T} \right) - 4T \left(\text{Re} \left[\log \sinh \frac{z(\Gamma)}{2T} \right] + \frac{z(\Gamma)}{2T} \right). \quad (\text{C.17})$$

Gathering the contributions of the integration along the real axes, Eq. (C.16), and along the branch cut, Eq. (C.17), and taking the limit $\Gamma \rightarrow \infty$, we end up with

$$f(T) - f(0) = -\frac{K_d}{2\pi} \Lambda^d \left\{ \mathcal{P} \int_0^\infty \frac{d\omega}{\pi} 2T \left(\log \left[2 \sinh \frac{\omega}{2T} \right] - \frac{\omega}{2T} \right) Q(\omega) \right\}. \quad (\text{C.18})$$

The function $Q(\omega)$ denotes the derivative of the arctan in Eq. (C.16) and separates into two parts which can be written as

$$Q(\omega) = -\frac{\gamma_m}{\Lambda} \frac{R(\omega) + \Lambda^2}{(R(\omega) + \Lambda^2)^2 + \left(\frac{\gamma_m}{\Lambda}\omega\right)^2} - A(\omega) \frac{\sigma(\omega)}{(\omega - \omega_1)^2 + \sigma(\omega)^2}. \quad (\text{C.19})$$

The first term resembles the bare metamagnetic contribution with an energy dependent mass which is given by

$$R(\omega) = R_{\text{ph}} - \frac{\lambda^2}{C_{11}} \frac{\omega^2/(v\Lambda)^2}{1 - \omega^2/(v\Lambda)^2}. \quad (\text{C.20})$$

Since the magnons scale according to $z_{>} = 3$, whereas the phonons scale according to $z_{<} = 1$, we have to consider both scalings to analyze the renormalization effect. In the former case we have $\omega \sim \Lambda^3$ and, the mass correction scales as

$$\frac{\omega^2/(v\Lambda)^2}{1 - \omega^2/(v\Lambda)^2} \sim \frac{\Lambda^4}{1 - \Lambda^4}. \quad (\text{C.21})$$

On the RG-trajectory, the cutoff decreases exponentially and, thus, the correction is irrelevant in the final RG-flow. The integrand has to be analyzed for $R_{\text{ph}} \ll \Lambda^2 \ll 1$, thus, the first term in Eq. (C.19) scales with $z_{>} = 3$ asymptotically as

$$-\frac{\gamma_m}{\Lambda} \frac{R(\omega) + \Lambda^2}{(R(\omega) + \Lambda^2)^2 + \left(\frac{\gamma_m}{\Lambda}\omega\right)^2} \sim -\frac{\gamma_m}{\Lambda} \frac{\Lambda^2}{\Lambda^4}, \quad (\text{C.22})$$

and is thus divergent up to at a scale $\Lambda \sim \sqrt{R_{\text{ph}}}$.

If, on the other, hand we apply $z_{<} = 1$ scaling, we obtain that R_{ph} scales to the bare mass R , however, the integrand scales as

$$-\frac{\gamma_m}{\Lambda} \frac{R(\omega) + \Lambda^2}{(R(\omega) + \Lambda^2)^2 + \left(\frac{\gamma_m}{\Lambda}\omega\right)^2} \sim -\frac{\gamma_m}{\Lambda} \frac{\Lambda^2}{\gamma_m}, \quad (\text{C.23})$$

and, thus, does not contribute to the asymptotic RG-flow. The divergence of $R(\omega)$ at the bare phonon pole, $\omega = v\Lambda$, is, on the one hand, excluded due to the principal value and, on the other hand, the integrand decreases close to the divergence as

$$-\frac{\gamma_m}{\Lambda} \frac{R(\omega) + \Lambda^2}{(R(\omega) + \Lambda^2)^2 + \left(\frac{\gamma_m}{\Lambda}\omega\right)^2} \sim -\frac{\gamma_m}{\Lambda} \frac{1}{R(\omega)}. \quad (\text{C.24})$$

From this analysis, we conclude that we can set $R(\omega) = R_{\text{ph}}$ recovering the bare magnon contribution with a renormalized mass.

The second term of the function $Q(\omega)$, Eq. (C.19), resembles the phonon part of the theory. Bare phonons would yield just a single delta peak at the phonon energy $\omega = v\Lambda$. Here, we have written the second term to resemble a Lorentzian with an energy dependent width, $\sigma(\omega)$, and weight, $A(\omega)$. The peak position is given by the renormalized phonon energy, $\omega_1 = v_1\Lambda$, and the scale dependent parameters are given as

$$A(\omega) = \pi \frac{2\omega (v^2\Lambda^2 - \omega_1^2)}{(\omega + \omega_1)(v^2\Lambda^2 - \omega^2)}, \quad (\text{C.25})$$

$$\sigma(\omega) = \frac{\gamma}{\Lambda} \frac{\omega (v^2\Lambda^2 - \omega^2)}{(\omega + \omega_1)(R + \Lambda^2)}. \quad (\text{C.26})$$

Again we analyze the behavior of this term upon scaling according to the two different dynamical exponents, $z_< = 1$ and $z_> = 3$. In the former case, we can set $\omega = \omega_1$, and, keeping in mind that the bare mass, R , is finite, we find the two parameters scale as

$$A(\omega_1) = \pi \quad \text{and} \quad \sigma(\omega_1) = \frac{\gamma}{\Lambda} \frac{v^2\Lambda^2\lambda^2/C_{11}}{2(R + \Lambda^2)^2} \sim \Lambda. \quad (\text{C.27})$$

Upon the asymptotic RG flow, the width becomes exponentially small, i.e., the Lorentzian peak gets sharper. Since the prefactor equals the normalization factor π , we, indeed, obtain a Dirac delta function which is peaked at the renormalized phonon energy.

In contrast, if we scale according to $z = 3$ we obtain

$$A(\omega) \sim \frac{\omega v^2\Lambda^2}{\omega_1 v^2\Lambda^2} \sim \Lambda^2 \quad \text{and} \quad \sigma(\omega) \sim \frac{1}{\Lambda} \frac{\omega v^2\Lambda^2}{\omega_1 R} \sim \Lambda^3. \quad (\text{C.28})$$

Still the width is decreasing, however, likewise the weight vanishes. Taking a look at the scaling of the second part of Eq. (C.19), we see that

$$A(\omega) \frac{\sigma(\omega)}{(\omega - \omega_1)^2 + \sigma(\omega)^2} \sim \Lambda^2 \frac{\Lambda^3}{\omega_1^2 + \Lambda^6} \sim \Lambda^3 \quad (\text{C.29})$$

and, hence, it vanishes for the asymptotic RG-flow.

In conclusion, the second part of the function $Q(\omega)$, Eq. (C.19), resembles the single delta peak of phonons with a renormalized phonon energy ω_1 . Taking all together, we can approximation Eq. (C.18) as

$$f(T) - f(0) = \frac{K_d}{2\pi} \Lambda^d \left\{ 2T\pi \log \left[2 \sinh \frac{\omega_1}{2T} \right] - \pi\omega_1 \right. \\ \left. + 2T \mathcal{P} \int_0^\Gamma d\omega \left(\log \left[\sinh \frac{\omega}{2T} \right] - \frac{\omega}{2T} \right) \frac{R_{\text{ph}} + \Lambda^2}{\left(\frac{\gamma_m}{\Lambda} \omega \right)^2 + (R_{\text{ph}} + \Lambda^2)^2} \right\}. \quad (\text{C.30})$$

where the first line is the phonon contribution of energy ω_1 , whereas the second line is the metamagnetic contribution having a mass R_{ph} . Thus, the coupled system resembles the two bare systems with renormalized parameters. As seen in the analysis above, this is due to the fact that the dynamics and, in particular, the dynamical exponents for phonons and magnons are different. Thus, the characteristic energies at a given momentum, Λ , differ strongly so that energy and momentum conservation prohibit most decay processes.

For zero temperatures, the Matsubara frequencies become continuous and the summation in Eq. (C.6) goes over in an integral $T \sum_n \rightarrow \int \frac{d\omega}{2\pi}$ with some cutoff Γ . By partial integration, we obtain apart from a cutoff dependent boundary term

$$f(T=0) = \frac{K_d}{2\pi} \Lambda^d \int_0^\infty d\omega \omega \left(\frac{\gamma_m}{\Lambda} \frac{1}{R(\omega) + \Lambda^2 + \frac{\gamma_m}{\Lambda} \omega} + \frac{2\omega}{\omega^2 + v(\omega)^2 \Lambda^2} \right), \quad (\text{C.31})$$

which, again, separates into two contributions. The first term in parentheses resembles the zero temperature contribution of bare phonons with a frequency-dependent velocity $v(\omega)$. Similarly, the second part resembles the bare metamagnetic theory with a frequency-dependent effective mass $R(\omega)$. These effective parameters are

$$R(\omega) = R_{\text{ph}} + \frac{\lambda^2}{C_{11}} \frac{\omega^2 / (v\Lambda)^2}{1 + \omega^2 / (v\Lambda)^2}, \quad (\text{C.32})$$

$$v(\omega) = v \left(1 - \frac{\lambda^2}{C_{11}} \frac{1}{R + \Lambda^2 + \gamma_m \omega / \Lambda} \right)^{1/2}. \quad (\text{C.33})$$

A similar scaling analysis as in the finite temperature case shows that the energy dependence can be replaced by the static renormalization of the mass and the velocity and, again, the system splits into the two subsystems. Integrating out the phonon part, we end up with

$$f(T=0) = \frac{K_d}{2\pi} \Lambda^d \left\{ \Gamma \left[\log \left(\rho \left(\Gamma^2 + \Lambda^2 v^2 \right) \right) - 2 \right] + \pi\omega_1 \right. \\ \left. + \Gamma \log \left[R - \frac{\lambda^2}{C_{11} \left(\frac{\Gamma^2 \Lambda^2}{v^2} + 1 \right)} + \Lambda^2 + \frac{\gamma_m \Gamma}{\Lambda} \right] - \int_0^\infty d\omega \frac{\frac{\gamma_m}{\Lambda} \omega}{R_{\text{ph}} + \Lambda^2 + \frac{\gamma_m}{\Lambda} \omega} \right\}. \quad (\text{C.34})$$

Since the zero temperature as well as the finite temperature contributions can be decomposed into a magnon and a phonon part, we can split the function f into these two contributions, $f(T) = m(T) + p(T)$.

An expansion to second order in R_{ph} , of the zero temperature magnon contribution yields

$$m_0(R_{\text{ph}}) = m(0, 0) + m^{(0,1)}(0, 0) R_{\text{ph}} + \frac{1}{2} m^{(0,2)}(0, 0) R_{\text{ph}}^2. \quad (\text{C.35})$$

All terms are exponentially suppressed upon the final RG-flow, hence, we can absorb them in a renormalization of the bare parameters of the potential.

Considering the phonons, the zero temperature contribution apart from cutoff dependent terms given by $v_1\Lambda/2$ where the renormalized phonon velocity was defined in Eq. (C.14). On the RG-trajectory, the velocity flows as $v \rightarrow v_\mu = ve^{-(z<-z)\mu}$, and Eq. (C.1) yields for the zero temperature phonon contribution

$$K_d \Lambda^d \int_0^\infty d\mu' e^{-d\mu'} \left\{ \frac{ve^{-\mu}\Lambda}{2} \sqrt{\frac{R_{\text{ph}}e^{2\mu} + \Lambda^2}{Re^{2\mu} + \Lambda^2}} + \frac{\Gamma}{\pi} \left[\frac{1}{2} \log(\rho(e^{-2z}\Gamma^2 + \Lambda^2v^2)) - 1 \right] \right\}.$$

which also vanishes also for the asymptotic RG-flow. Therefore, we we can also absorb it in a renormalization of the bare parameters. Taking both renormalizations together we define

$$\begin{aligned} \mathcal{V}_{\text{ren}} &= \mathcal{V}^0 + \int_0^\infty d\mu e^{-(d+z)\mu'} \left\{ m_{0,\mu}(\mathcal{V}_{\text{ph},0}''e^{2\mu}) + p_{0,\mu}(ve^{-(z<-z)\mu}, \mathcal{V}_{\text{mm},0}''e^{2\mu}) \right\} \\ &= -h\phi_0 + \frac{r}{2!}\phi_0^2 + \frac{u}{4!}\phi_0^4 - \lambda\phi_0 E + \frac{K}{2}E^2 \end{aligned} \quad (\text{C.36})$$

where we set $\mathcal{V}_{\text{ph},0}(\phi) = \mathcal{V}_0(\phi) - \lambda^2/C_{11}$ and used the freedom of shifting ϕ_0 , to eliminate the cubic term. Also, we neglected a unimportant constant. The remaining RG-integration for the magnetic contribution is analogous to the bare metamagnetic system, covered in Chap. 5, yielding the fluctuation term $T^{D>/z>} \mathcal{A}_d(\mathcal{V}_{\text{ph}}''(\phi)T^{-2/z>})$. Using $\log(2 \sinh x) - x = \log(1 - e^{2x})$, the integration of the phonon part reads as

$$\begin{aligned} T^{D</z<} \mathcal{B}_d &= \int_0^\infty d\mu e^{-D\mu} K_d \Lambda^d T e^{z\mu} \log \left[1 - \exp \left(\frac{ve^{(z-z<)\mu}\Lambda}{Te^{z\mu}} \sqrt{\frac{R_{\text{ph}}e^{2\mu} + \Lambda^2}{Re^{2\mu} + \Lambda^2}} \right) \right] \\ &= T^{D</z<} K_d \int_{-\log \Lambda T^{-1/z<}}^\infty d\mu e^{-d\mu} \log \left[1 - \exp \left(ve^{-\mu} \sqrt{\frac{T^{-1/z<} R_{\text{ph}} + e^{-2\mu}}{T^{-1/z<} R + e^{-2\mu}}} \right) \right] \end{aligned}$$

where in the second line we shifted the integration variable $\mu \rightarrow \mu + \log \Lambda T^{-1/z<}$.

Close to the quantum endpoint, both, the bare and the renormalized mass are large compared to the temperature, $R_{\text{ph}}, R \gg T^2$, such that we can replace the square root by the constant $\sqrt{R_{\text{ph}}/R}$. In this limit, defining the magnetically renormalized velocity $v_m = v\sqrt{R_{\text{ph}}/R}$, the function B_d has the asymptotic behavior

$$T^{D</z<} \mathcal{B}_d = T^{D</z<} K_d v_m^{-d} \int_{-\log v_m \Lambda T^{-1/z<}}^{\infty} d\mu e^{-d\mu} \log [1 - \exp(e^{-\mu})] \quad (\text{C.37})$$

$$= \mathfrak{b}_d T^{d+1} \left(v^2 \frac{R_{\text{ph}}}{R} \right)^{d/2} \quad (\text{C.38})$$

where in the last line we assumed the limit $v_m \Lambda \gg T$.

Bibliography

- [1] M. de Souza, A. Brühl, C. Strack, B. Wolf, D. Schweitzer, and M. Lang, *Phys. Rev. Lett.* **99**, 037003 (2007).
- [2] L. Bartosch, M. de Souza, and M. Lang, *Phys. Rev. Lett.* **104**, 245701 (2010).
- [3] D. Belitz, T. R. Kirkpatrick, and J. Rollbühler, *Phys. Rev. Lett.* **94**, 247205 (2005).
- [4] D. Aoki, T. Combier, V. Taufour, T. D. Matsuda, G. Knebel, H. Kotegawa, and J. Flouquet, *Journal of the Physical Society of Japan* **80**, 094711 (2011).
- [5] V. Taufour, D. Aoki, G. Knebel, and J. Flouquet, *Phys. Rev. Lett.* **105**, 217201 (2010).
- [6] H. Kotegawa, V. Taufour, D. Aoki, G. Knebel, and J. Flouquet, *Journal of the Physical Society of Japan* **80**, 083703 (2011).
- [7] L. D. Landau and E. M. Lifshitz, *Theory of Elasticity* (Pergamon Press, 1959), ISBN 9780750626330.
- [8] H. B. Huntington, *The Elastic Constants of Crystals*, no. Bd. 7 in *Solid State Reprints* (Academic Press, 1958), ISBN 9780521004541.
- [9] H. Kleinert, *Gauge Fields in Condensed Matter: Stresses and defects*, Bd. 2 (World Scientific, 1989), ISBN 9789971502102.
- [10] J. Sòlyom, *Fundamentals of the Physics of Solids*, Vol. 1 (Springer, 2007), ISBN 9783540725992.
- [11] R. Truell, C. Elbaum, and B. Chick, *Ultrasonic Methods in Solid State Physics* (Acad. Press, 1969).
- [12] B. Lüthi, *Physical Acoustics in the Solid State*, no. Bd. 15 in *Springer Series in Solid-State Sciences* (Springer, 2007), ISBN 9783540721932.
- [13] W. Voigt, *Lehrbuch der Kristallphysik: (mit Ausschluss der Kristalloptik)*, B.G. Teubners Sammlung von Lehrbüchern auf dem Gebiete der mathematischen Wissenschaften mit Einschluss ihrer Anwendungen (B.G. Teubner, 1910).

- [14] P. Helnwein, *Computer Methods in Applied Mechanics and Engineering* **190**, 2753 (2001), ISSN 0045-7825.
- [15] M. Born and K. Huang, *Dynamical theory of crystal lattices*, International Series of Monographs on Physics (Clarendon Press, 1962), ISBN 0198512481.
- [16] A. Abrikosov, L. Gor'kov, and I. Dzyaloshinskii, *Quantum Field Theoretical Methods in Statistical Physics*, International series of monographs in natural philosophy (Pergamon Press, 1965).
- [17] W. Rehwald, *Advances in Physics* **22**, 721 (1973).
- [18] R. Cowley, *Advances in Physics* **29**, 1 (1980).
- [19] A. I. Larkin and S. A. Pikin, *Sov. Phys. JETP* **29**, 891 (1969).
- [20] B. Dünweg, *Habilitation* (2000).
- [21] R. A. Cowley, *Phys. Rev. B* **13**, 4877 (1976).
- [22] L. Landau, *Phys. Z. Sowjet* **11**, 26 (1937).
- [23] V. Heine, *Group Theory in Quantum Mechanics: An Introduction to Present Usage*, vol. 9 of *International Series of Monographs in Pure and Applied Mathematics* (Pergamon Press, 1960).
- [24] O. K. Rice, *J. Chem. Phys.* **22**, 1535 (1954).
- [25] C. Domb, *J. Chem. Phys.* **25**, 783 (1956).
- [26] D. C. Mattis and T. D. Schultz, *Phys. Rev.* **129**, 175 (1963).
- [27] F. Anfuso, M. Garst, A. Rosch, O. Heyer, T. Lorenz, C. Rüegg, and K. Krämer, *Phys. Rev. B* **77**, 235113 (2008).
- [28] M. E. Fisher, *Phys. Rev.* **176**, 257 (1968).
- [29] S. Pikin, *Physica A: Statistical Mechanics and its Applications* **194**, 352 (1993).
- [30] J. Sak, *Phys. Rev. B* **10**, 3957 (1974).
- [31] J. Bruno and J. Sak, *Phys. Rev. B* **22**, 3302 (1980).
- [32] J. Bruno and J. Sak, *Phys. Rev. B* **22**, 3319 (1980).
- [33] D. J. Bergman and B. I. Halperin, *Phys. Rev. B* **13**, 2145 (1976).
- [34] A. P. Levanyuk and A. A. Sobyenin, *ZhETF Pis. Red.* **11**, 540 (1970).

- [35] J. Villain, *Solid State Communications* **8**, 295 (1970).
- [36] H. Wagner and H. Horner, *Advances in Physics* **23**, 587 (1974).
- [37] M. Zacharias, L. Bartosch, and M. Garst, *Phys. Rev. Lett.* **109**, 176401 (2012).
- [38] F. Bloch, *Zeitschrift für Physik* **57**, 545 (1929), ISSN 0044-3328.
- [39] J. H. de Boer and E. J. W. Verwey, *Proceedings of the Physical Society* **49**, 59 (1937).
- [40] N. F. Mott, *Proc. R. Soc. Lond. A* **62**, 416 (1949).
- [41] M. Imada, A. Fujimori, and Y. Tokura, *Rev. Mod. Phys.* **70**, 1039 (1998).
- [42] J. Hubbard, *Proc. R. Soc. Lond. A* **276**, 238 (1963).
- [43] A. Altland and B. Simons, *Condensed Matter Field Theory* (Cambridge Univ. Press, Cambridge, 2010).
- [44] M. J. Rozenberg, X. Y. Zhang, and G. Kotliar, *Phys. Rev. Lett.* **69**, 1236 (1992).
- [45] A. Georges and W. Krauth, *Phys. Rev. Lett.* **69**, 1240 (1992).
- [46] A. Georges and W. Krauth, *Phys. Rev. B* **48**, 7167 (1993).
- [47] A. Georges, G. Kotliar, W. Krauth, and M. J. Rozenberg, *Rev. Mod. Phys.* **68**, 13 (1996).
- [48] D. B. McWhan, A. M. andj. P. Remeika, W. F. Brinckman, and T. M. Rice, *Phys Rev. B* **7**, 1920 (1973).
- [49] C. Castellani, C. D. Castro, D. Feinberg, and J. Ranninger, *Phys. Rev. Lett.* **43**, 1957 (1979).
- [50] M. Blume, V. J. Emery, and R. B. Griffiths, *Phys. Rev. A* **4**, 1071 (1971).
- [51] G. Kotliar, E. Lange, and M. J. Rozenberg, *Phys. Rev. Lett.* **84**, 5180 (2000).
- [52] S. Onoda and M. Imada, *Phys. Rev. B* **67**, 161102 (2003).
- [53] S. Moukouri and E. Eidelstein, *Phys. Rev. B* **86**, 155112 (2012).
- [54] P. Limelette, A. Georges, D. Jérôme, P. Wzietek, P. Metcalf, and J. M. Honig, *Science* **302**, 89 (2003).
- [55] F. Kagawa, K. Miyagawa, and K. Kanoda, *Nature* **436**, 534 (2005).

BIBLIOGRAPHY

- [56] S. Papanikolaou, R. M. Fernandes, E. Fradkin, P. W. Phillips, J. Schmalian, and R. Sknepnek, *Phys. Rev. Lett.* **100**, 026408 (2008).
- [57] A. Pelissetto and E. Vicari, *Physics Reports* **368**, 549 (2002).
- [58] A. A. Belavin, A. M. Polyakov, and A. Zamolodchikov, *Nucl. Phys. B* **241**, 333 (1984).
- [59] A. A. Belavin, A. M. Polyakov, and A. Zamolodchikov, *J. Stat. Phys* **34**, 763 (1984).
- [60] D. Chelkak and S. Smirnov, *Invent. math.* **189**, 515 (2012).
- [61] P. Fonseca and A. Zamolodchikov, *J. Stat. Phys.* **110** (2003).
- [62] P. Majumdar and H. R. Krishnamurthy, *Phys. Rev. Lett.* **73**, 1525 (1994).
- [63] D. Fournier, M. Poirier, M. Castonguay, and K. D. Truong, *Phys Rev. Lett.* **90**, 127002 (2003).
- [64] S. R. Hassan, A. Georges, and H. R. Krishnamurthy, *Phys. Rev. Lett.* **94**, 036402 (2005).
- [65] D. B. McWhan, T. M. Rice, and J. P. Remeika, *Phys. Rev. Lett.* **23**, 1384 (1969).
- [66] D. B. McWhan and J. P. Remeika, *Phys. Rev. B* **2**, 3734 (1970).
- [67] A. Jayaraman, D. B. McWhan, J. P. Remeika, and P. D. Dernier, *Phys. Rev. B* **2**, 3751 (1970).
- [68] D. B. McWhan, J. P. Remeika, T. M. Rice, W. F. Brinkman, J. P. Maita, and A. Menth, *Phys. Rev. Lett.* **27**, 941 (1971).
- [69] P. Limelette, Ph.D. thesis, l'université Paris Sud (Paris XI) (2003).
- [70] D. N. Nichols, R. J. Sladek, and H. R. Harrison, *Phys. Rev. B* **24**, 3025 (1981).
- [71] S. Populoh, P. Wzietek, R. Gohier, and P. Metcalf, *Phys. Rev. B* **84**, 075158 (2011).
- [72] C. Pfleiderer, P. Böni, T. Keller, U. K. Rößler, and A. Rosch, *Science* **316**, 1871 (2007).
- [73] J. A. Hertz, *Phys. Rev. B* **14**, 1165 (1976).
- [74] S. Sachdev, *Quantum Phase Transitions* (University Press, 2001), ISBN 9780521004541.

-
- [75] T. Vojta, *Annalen der Physik* **9** (2000), ISSN 1521-3889.
- [76] M. Vojta, *Reports on Progress in Physics* **66**, 2069 (2003).
- [77] T. Nikuni, M. Oshikawa, A. Oosawa, and H. Tanaka, *Phys. Rev. Lett.* **84**, 5868 (2000).
- [78] T. Radu, H. Wilhelm, V. Yushankhai, D. Kovrizhin, R. Coldea, Z. Tylczynski, T. Lühmann, and F. Steglich, *Phys. Rev. Lett.* **95**, 127202 (2005).
- [79] S. A. Grigera, R. S. Perry, A. J. Schofield, M. Chiao, S. R. Julian, G. G. Lonzarich, S. I. Ikeda, Y. Maeno, A. J. Millis, and A. P. Mackenzie, *Science* **294**, 329 (2001).
- [80] M. Zacharias and M. Garst, *Phys. Rev. B* **87**, 075119 (2013).
- [81] A. Schofield, A. Millis, S. Grigera, and G. Lonzarich, in *Ruthenate and Rutheno-Cuprate Materials*, edited by C. Noce, A. Vecchione, M. Cuoco, and A. Romano (2002), vol. 603 of *Lecture Notes in Physics*, pp. 271–289, ISBN 978-3-540-44275-2.
- [82] A. J. Millis, A. J. Schofield, G. G. Lonzarich, and S. A. Grigera, *Phys. Rev. Lett.* **88**, 217204 (2002).
- [83] R. S. Perry, L. M. Galvin, S. A. Grigera, L. Capogna, A. J. Schofield, A. P. Mackenzie, M. Chiao, S. R. Julian, S. I. Ikeda, S. Nakatsuji, et al., *Phys. Rev. Lett.* **86**, 2661 (2001).
- [84] S. Grigera, A. Mackenzie, A. Schofield, S. Julian, and G. Lonzarich, *Int. J. Mod. Phys. B* **16**, 3258 (2002).
- [85] S. A. Grigera, R. A. Borzi, A. P. Mackenzie, S. R. Julian, R. S. Perry, and Y. Maeno, *Phys. Rev. B* **67**, 214427 (2003).
- [86] S. A. Grigera, P. Gegenwart, R. A. Borzi, F. Weickert, A. J. Schofield, R. S. Perry, T. Tayama, T. Sakakibara, Y. Maeno, A. G. Green, et al., *Science* **306**, 1154 (2004).
- [87] R. S. Perry, K. Kitagawa, S. A. Grigera, R. A. Borzi, A. P. Mackenzie, K. Ishida, and Y. Maeno, *Phys. Rev. Lett.* **92**, 166602 (2004).
- [88] A. G. Green, S. A. Grigera, R. A. Borzi, A. P. Mackenzie, R. S. Perry, and B. D. Simons, *Phys. Rev. Lett.* **95**, 086402 (2005).
- [89] C. Stingl, R. S. Perry, Y. Maeno, and P. Gegenwart, *Phys. Rev. Lett.* **107**, 026404 (2011).

- [90] A. Mackenzie, J. Bruin, R. Borzi, and A. R. S. Grigera (2013).
- [91] W. Wu, A. McCollam, S. A. Grigera, R. S. Perry, A. P. Mackenzie, and S. R. Julian, *Phys. Rev. B* **83**, 045106 (2011).
- [92] J. Baier, P. Steffens, O. Schumann, M. Kriener, S. Stark, H. Hartmann, O. Friedt, A. Revcolevschi, P. Radaelli, S. Nakatsuji, et al., *Journal of Low Temperature Physics* **147**, 405 (2007).
- [93] P. Haen, J. Flouquet, F. Lapierre, P. Lejay, and G. Remenyi, *Journal of Low Temperature Physics* **67**, 391 (1987), ISSN 0022-2291.
- [94] C. Paulsen, A. Lacerda, L. Puech, P. Haen, P. Lejay, J. Tholence, J. Flouquet, and A. Visser, *Journal of Low Temperature Physics* **81**, 317 (1990).
- [95] H. Aoki, S. Uji, A. K. Albessard, and Y. Onuki, *Phys. Rev. Lett.* **71**, 2110 (1993).
- [96] J. Flouquet, S. Kambe, L. Regnault, P. Haen, J. Brison, F. Lapierre, and P. Lejay, *Physica B: Condensed Matter* **215**, 77 (1995), ISSN 0921-4526.
- [97] D. Aoki, C. Paulsen, T. D. Matsuda, L. Malone, G. Knebel, P. Haen, P. Lejay, R. Settai, Y. Ōnuki, and J. Flouquet, *Journal of the Physical Society of Japan* **80**, 053702 (2011).
- [98] T. Hamamoto, K. Kindo, T. Kobayashi, Y. Uwatoko, S. Araki, R. Settai, and Y. Onuki, *Physica B: Condensed Matter* **281-282**, 64 (2000), ISSN 0921-4526.
- [99] M. B. Suvasini, G. Y. Guo, W. M. Temmerman, and G. A. Gehring, *Phys. Rev. Lett.* **71**, 2983 (1993).
- [100] C. Thessieu, C. Pfleiderer, A. N. Stepanov, and J. Flouquet, *Journal of Physics: Condensed Matter* **9**, 6677 (1997).
- [101] M. Uhlarz, C. Pfleiderer, and S. M. Hayden, *Phys. Rev. Lett.* **93**, 256404 (2004).
- [102] A. Huxley, I. Sheikin, and D. Braithwaite, *Physica B: Condensed Matter* **284-288, Part 2**, 1277 1278 (2000), ISSN 0921-4526.
- [103] D. Belitz, T. R. Kirkpatrick, and T. Vojta, *Phys. Rev. B* **55**, 9452 (1997).
- [104] J. Rech, C. Pépin, and A. V. Chubukov, *Phys. Rev. B* **74**, 195126 (2006).
- [105] D. L. Maslov and A. V. Chubukov, *Phys. Rev. B* **79**, 075112 (2009).
- [106] B. Binz and M. Sigrist, *EPL (Europhysics Letters)* **65**, 816 (2004).

- [107] F. J. Wegner and A. Houghton, Phys. Rev. A **8**, 401 (1973).
- [108] S.-I. Ikeda, Y. Maeno, S. Nakatsuji, M. Kosaka, and Y. Uwatoko, Phys. Rev. B **62**, R6089 (2000).
- [109] M. Garst and A. Rosch, Phys. Rev. B **72**, 205129 (2005).
- [110] P. Gegenwart, F. Weickert, M. Garst, R. S. Perry, and Y. Maeno, Phys. Rev. Lett. **96**, 136402 (2006).
- [111] F. Weickert, M. Brando, F. Steglich, P. Gegenwart, and M. Garst, Phys. Rev. B **81**, 134438 (2010).
- [112] Y. Aoki, T. Matsuda, H. Sugawara, H. Sato, H. Ohkuni, R. Settai, Y. O⁻nuki, E. Yamamoto, Y. Haga, A. Andreev, et al., Journal of Magnetism and Magnetic Materials **177-181**, Part 1, 271 (1998).
- [113] L. Zhu, M. Garst, A. Rosch, and Q. Si, Phys. Rev. Lett. **91**, 066404 (2003).
- [114] T. Moriya, Journal of the Physical Society of Japan **55**, 357 (1986).
- [115] H. Yamada, Phys. Rev. B **47**, 11211 (1993).
- [116] R. A. Cowley, Phys. Rev. Lett. **36**, 744 (1976).
- [117] M. Zacharias, P. Wölfle, and M. Garst, Phys. Rev. B **80**, 165116 (2009).
- [118] M. Chiao, C. Pfleiderer, S. Julian, G. Lonzarich, R. Perry, A. Mackenzie, and Y. Maeno, Physica B: Condensed Matter **312-313**, 698 (2002).

Acknowledgments

Zu allererst möchte ich mich bei Dr. Markus Garst für seine Betreuung während meiner Doktorarbeit bedanken. Seine Anleitung und Unterstützung haben diese Arbeit durch unschätzbare Diskussionen, Erklärungen und, wenn es sein musste, Geduld erst ermöglicht. Nicht minder dankbar bin ich Prof. Dr. Achim Rosch, dessen Ideen und lebendige Faszination für die Physik mich immer wieder fesselte. Zudem hat er eine Gruppenatmosphäre geschaffen, die gleichermaßen anregend wie freundschaftlich ist. Natürlich gilt ihm mein Dank auch nicht zuletzt dafür, dass er mir die Möglichkeit gab, diese Arbeit zu schreiben. Bezüglich des letzten Punktes möchte ich mich auch bei der Bonn-Cologne Graduate School of Physics and Astronomy (BCGS) bedanken; zum einen für ihre finanzielle Unterstützung aber auch dafür, dass sie mir die Möglichkeit gab äußerst interessante Seminare und Workshops zu besuchen.

Es war ein Vergnügen, hier in Köln in dieser Gruppe zu arbeiten, und nicht geringen Anteil habe daran natürlich auch meine heutigen und ehemaligen Kollegen. Die oben erwähnte, offene Atmosphäre wurde natürlich sehr von ihnen befördert. Ob bei fachlichen Fragen unkompliziert und engagiert weitergeholfen wurde, oder beim Feierabendbier zusammengesessen wurde, stets hatte man einen freundschaftlichen Umgang miteinander. Viele von ihnen sind in der Tat längst keine Kollegen mehr, sondern Freunde geworden, mit denen ich schon so manchen schönen Abend (gerne auch länger) verbracht habe.

Zunächst möchte ich mich bei meinen Bürokollegen bedanken, die mir mit Rat und Tat zur Seite standen, meine dümmsten Fragen beantworteten und meine eigenen Arten und Marotten ertrugen (keine Angst, die Kästen kommen irgendwann weg). Daher einen großen Dank an Fabrizio Anfuso, Akos Rapp, Benjamin Buldman, Jonathan Lux, Michael Becker, Tobias Meng und Matthias Sitte. Letzterem zusammen mit Karin Everschor-Sitte möchte ich noch insbesondere für ihre Hilfe beim redigieren und ihre moralische Unterstützung während der letzten Zeit danken. Alles Gute euch dreien in den US'n'A.

Für eine schöne Zeit in den letzten Jahre zeichnen sich neben den oben genannten verantwortlich Lucas Hollender, Stephan Mandt, Alex Wollny, Etienne Gärtner, Carolin Küppersbusch, Heidi Weber, Johannes Waizner, Lars Fritz, David Rasch, Ste-

fan Burhand, Christoph Schütte, Maximilian Genske, Robert Bamler, Pascal Krautscheidt, Eran Sela, Karen Rodriguez, Ralf Bulla, Adel Benlagra, Ricardo Doretto, Andrew Mitchell, Simon Trebst, Mascha Baedorf, Stefan Bittihn, Peter Bröcker, Max Gerlach, Johannes Helmes, Maria Hermanns und Matthias Vojta.

Zum Abschluss dieser Aufzählung müssen noch unbedingt die hochwohlgeborenen Mitglieder des geheimen und verschwiegenen Ordens erwähnt werden, der hier nicht genannt werden soll. Sie haben mit Witz und Poesie, Feuer und Flamme und allerlei Unseriösitäten diese Zeit zu einer unvergesslichen gemacht. Carpe Noctem, Brüder, Schwestern und Ladyboys.

Aber auch außerhalb unseres Institutes möchte ich mich bedanken, und bleibe zunächst einmal bei der Physik. Es war immer wieder schön und erfrischend mit unseren netten Kollegen der experimentellen Festkörperphysik zusammen zu sein. Auch dank des Doktorandenseminars des SFB 608 durfte ich sie als hilfsbereite Menschen kennenlernen, die man im Falle von "Experimental"-Problemen immer um Rat fragen konnte. Auch die netten (feucht)-fröhlichen Abende, die wir miteinander hatte, werden mir stets in guter Erinnerung bleiben.

Des weiteren bedanke ich bei allen meinen Freunden. Für die schönen, die tollen und die langen Tage. Für die, die nie wiederkommen, und für die Erinnerungen, die guten wie die schlechten.

Oder eben auch nicht, denn steter Tropfen höhlt den Kopf. Dahingehend sei vor allem noch Tobias Stangier erwähnt, der mich quasi an den Toren Kölns willkommen heißen hat. Ich dank dir für die schöne Zeit beim Spabieren, bei unserer Lesereise und bei allen anderen Gelegenheiten. Und ich dank dir für die Aufnahme des Düsseldorfers, der ich zwar immer noch voller Stolz bin, der aber Köln auch deinetwegen sehr missen würde. Du bist ein echter Freund...Dein Wort hält Wort, lass alle Schatten fort.

Zu guter Letzt geht mein Dank an meine Freundin, Andrea Schäfer, die es trotz größtmöglicher lokalpatriotisch-moralischer Skrupel und meiner manchmal anstrengenden Art mit mir aushält. Vor allem die letzten Wochen hielten schwerste körperlichen und geistige Entbehrungen bereit, die sie (fast) ohne zu klagen erduldet. Ich werde versuchen, das in nächster Zukunft wieder gut zu machen. Ich danke dir für deine Unterstützung, deine Motivation, deinen Witz, natürlich auch für deine Hartnäckigkeit und deine Liebe. Ich freue mich auf unsere gemeinsame Zukunft. Ich liebe dich.

Erklärung

Ich versichere, dass ich die von mir vorgelegte Dissertation selbständig angefertigt, die benutzten Quellen und Hilfsmittel vollständig angegeben und die Stellen der Arbeit - einschließlich Tabellen, Karten und Abbildungen-, die anderen Werken im Wortlaut oder dem Sinn nach entnommen sind, in jedem Einzelfall als Entlehnung kenntlich gemacht habe; dass diese Dissertation noch keiner anderen Fakultät oder Universität zur Prüfung vorgelegen hat; dass sie - abgesehen von unten angegebenen Teilpublikationen - noch nicht veröffentlicht worden ist sowie, dass ich eine solche Veröffentlichung vor Abschluss des Promotionsverfahrens nicht vornehmen werde. Die Bestimmungen der Promotionsordnung sind mir bekannt. Die von mir vorgelegte Dissertation ist von Prof. Dr. Achim Rosch betreut worden.

Köln, 04. Mai 2013

Mario Zacharias

Teilpublikationen

- Mario Zacharias, Lorenz Bartosch and Markus Garst, *Mott Metal-Insulator Transition On Compressible Lattices*, Phys. Rev. Lett. **109**, 176401 (2012)
- Mario Zacharias and Markus Garst, *Quantum Criticality In Itinerant Metamagnets*, Phys. Rev. B **87**, 075119 (2013)

Lebenslauf

Dipl.-Phys.

Mario Zacharias

12. März 2014

Persönliche Daten:

Anschrift: Severinstr. 149
50678 Köln
Telefon: 0221 / 7162694
E-mail: M.zacharias@web.de

Geburtsdatum und -ort: 15.05.1983 in Bochum

Staatsangehörigkeit: deutsch

Familienstand: ledig

Studium:

02/2009 - 07/2013 Promotion an der Universität zu Köln
Doktorvater: Prof. Dr. Achim Rosch

10/2003 - 02/2009 Universität zu Köln
Studienfach Theoretische Festkörperphysik
Diplomarbeit bei Prof. Dr. Achim Rosch (1,1):
*The Quadrupolar Pomeranchuk Instability:
Interplay of Multiple Critical Modes with Different Dynamics*

Wehrdienst:

06/2002 - 08/2003 Grundwehrdienst
Tätigkeit als Fernmeldesoldat in Drabenderhöhe

Schulische Ausbildung:

08/1993 - 06/2002 Gymnasium Hochdahl in Erkrath
Abschluss: Abitur (1,4)

02/1991 - 06/1993 Grundschule Unterfeldhaus in Erkrath

08/1989 - 02/1991 Grundschule Bad Driburg

Auszeichnungen/Stipendien:

10/2009 - 07/2013 Stipendiat der Bonn-Cologne Graduate School

Publikationen:

Multiscale Quantum Criticality: Pomeranchuk Instability In Isotropic Metals

Mario Zacharias, Peter Wölfle and Markus Garst, Phys. Rev. B **80**, 165116 (2009),
ausgewählt als Editor's Suggestion

Mott Metal-Insulator Transition On Compressible Lattices

Mario Zacharias, Lorenz Bartosch and Markus Garst, Phys. Rev. Lett. **109**, 176401 (2012)

Quantum Criticality In Itinerant Metamagnets

Mario Zacharias and Markus Garst, Phys. Rev. B **87**, 075119 (2013)